Acoustic remote sensing of Arctic Sea Ice from long term soundscape measurements

Bazile Kinda

UNIVERSITÉ DE GRENOBLE

THÈSE

Pour obtenir le grade de

DOCTEUR DE L'UNIVERSITÉ DE GRENOBLE

Spécialité : **Océan, Atmosphère, Hydrologie**

Arrêté ministériel : 7 août 2006

Présentée par

Gnouregma Bazile KINDA

Thèse dirigée par **Jérôme I. MARS**
et codirigée par **Cédric GERVAISE**
et par **Yann STEPHAN**

préparée au sein du
Laboratoire Grenoble, Image, Parole, Signal, Automatique (GIPSA-Lab) et du **Laboratoire des Sciences et Techniques de l'Information, de la Communication et de la Connaissance (Lab-STICC)**
dans **l'école doctorale Terre, Univers, Environnement (TUE)**

Acoustic remote sensing of Arctic Sea Ice from long term soundscape measurements

Thèse soutenue publiquement le **29 novembre 2013**,
devant le jury composé de :

Mr Michel FILY
Professeur, Laboratoire LGGE (UMR 5183), Président
Mr Jean-Yves ROYER
DR CNRS, Laboratoire Domaine Océanique (LDO UMR 6538), Rapporteur
Mr Sergio JESUS
Professeur, SiPLAB, FCT, Rapporteur
Mr Yvan SIMARD
DR Chercheur, Institut Maurice-Lamontagne, Institut des sciences de la mer de Rimouski, Examinateur
Mme Carole NAHUM
ICT IIIA, PhD , Direction Générale de l'Armement (DGA), Direction Scientifique, Examinatrice
Mr Jérôme I. MARS
Professeur, GIPSA-Lab, Grenoble INP, Directeur de thèse
Mr Cédric GERVAISE
Chercheur SC, HDR, Chaire Chorus, Grenoble INP, Co-Directeur de thèse
Mr Yann STEPHAN
Chercheur, HDR, SHOM, Co-Directeur de thèse

UNIVERSITE DE GRENOBLE
ÉCOLE DOCTORALE TUE
Terre Univers Environnement

N° attribué par la bibliothèque

_____

THESE

pour obtenir le grade de

DOCTEUR EN SCIENCE
de l'Université de Grenoble

Mention : Océan, Atmosphère, Hydrologie

présentée et soutenue publiquement

par

Gnouregma Bazile KINDA

le 29 Novembre 2013

préparée aux
Laboratoire Grenoble, Image, Parole, Signal, Automatique (GIPSA-Lab)
Laboratoire des Sciences et Techniques de l'Information, de la Communication et de la Connaissance (Lab-STICC)

ACOUSTIC REMOTE SENSING OF ARCTIC SEA ICE FROM LONG TERM SOUNDSCAPE MEASUREMENTS

Directeurs de thèse : J. I. MARS, C. GERVAISE et Y. STÉPHAN

JURY

Président	:	Monsieur Michel FILY	- Laboratoire LGGE (UMR 5183)
Rapporteurs	:	Monsieur Jean-Yves ROYER	- DR CNRS, LDO (UMR 6538)
		Monsieur Sergio JESUS	- SiPLAB, FCT
Examinateurs	:	Monsieur Yvan SIMARD	- Institut Maurice-Lamontagne, ISMER/UQAR
		Madame Carole NAHUM	- Direction Générale de l'Armement (DGA)
Directeur	:	Monsieur Jérôme I. MARS	- GIPSA-Lab, Grenoble INP
Co-Directeurs	:	Monsieur Cédric GERVAISE	- Chaire Chorus, Grenoble INP
		Monsieur Yann STEPHAN	- SHOM, Brest

A mon père,
A ma mère;

Remerciements

Un proverbe burkinabé stipule que ***si la chèvre mange du karité, elle le doit à son bienfaiteur le vent***. En effet, du sahel africain à l'Arctique Canadien, il n'y a pas qu'un pas! Je saisis donc l'occasion ici pour présenter mes remerciements à toutes celles et à tous ceux qui ont contribué d'une manière ou d'une autre à la réalisation de ce travail.

Je voudrais tout d'abord exprimer ma reconnaissance envers mes directeurs de thèse J. I. Mars, C. Gervaise et Y. Stéphan pour m'avoir accueilli et mis à disposition les moyens matériels pour l'accomplissement de ce travail. Je remercie C. Gervaise pour m'avoir accueilli et fait découvrir le monde sous-marin qui m'était jusqu'alors inconnu. Cédric, je te remercie aussi pour m'avoir fait découvrir le monde de la recherche, j'ai beaucoup appris au-delà de la science. Je remercie Y. Stéphan pour ces années de collaboration, de discussions, et pour sa disponibilité. Mr Stéphan, je te remercie également pour m'avoir donné l'occasion de participer à ma première campagne en mer, qui fut pour moi une grande expérience. Je remercie J.I. Mars pour avoir accepté d'encadrer cette thèse. JIM, je te remercie pour ta disponibilité, tes conseils précieux qui m'ont accompagné tout au long de ces trois années, et particulièrement ton soutien inconditionnel pour cette dernière année décisive. A tous les trois j'exprime ma gratitude pour m'avoir permis d'aller à la découverte d'autres mondes.

De toute évidence, ce travail n'aurait pas été le même sans le concours précieux du Pr. Yvan Simard du ministère Pêches et Océans du Canada. Mr Simard, je te remercie pour avoir accepté de m'accueillir dans ton équipe pendant treize mois. Au-delà de m'avoir permis de travailler sur des données rares, je te remercie pour ta disponibilité, ton sens d'écoute et pour la qualité de toutes ces discussions constructives que nous avons pu avoir. Je te remercie pour m'avoir fait découvrir ce monde sous-marin Arctique, dont je connais aujourd'hui les vocalises des mammifères plus que les chants des oiseaux de ma savane natale. Mr Simard, je te réitère ma reconnaissance d'avoir presque transformé le sahélien que je suis en un presque marin en me donnant l'occasion de participer à plusieurs campagnes de mesures en mer. Ce fut l'occasion pour moi de découvrir ces fabuleux animaux de la mer disparus ...du sahel il y a fort bien longtemps!

Je tiens à remercier Mr. Sergio Jesus et Jean-Yves Royer, qui ont bien voulu rapporter ma thèse. Je vous remercie pour le travail accompli et pour vos remarques pertinentes. Je renouvelle mes remerciements à Mr. Michel Fily pour avoir accepté de présider ma soutenance de thèse. Un grand merci à Mr. Y. Simard et à Mme. C. Nahum pour avoir accepté de participer à mon jury de thèse en qualité d'examinateurs.

J'exprime ma reconnaissance amicale envers mes collègues de l'ENSTA-Bretagne, avec qui j'ai partagé toutes ces années. Mes remerciements vont à J. Bonnel (De Bonnel, quand on habite dans un manoir), pour sa disponibilité et son soutien désintéressé, ses conseils et ses encouragements. Je remercie F-X Socheleau pour nos discussions scientifiques très enrichissantes autour des estimateurs. Je remercie également F. Le Courtois, dit Docteur Touré (l'homme pour qui rien n'est impossible!) et Y. Le Gall (Mr l'invariant, qui varie quand même!), pour les moments de discussions et leur disponibilité. Je ne puis m'empêcher de faire référence à la *ap runwalk team, alias les chiens mouillés*, pour les moments de courses à pieds, de préférence sous la pluie. Je remercie le Greco-Belge, *Ker* Korakas, ses connaissances approfondies de LaTex m'ont été fort utiles! Je remercie O. Le Bot avec qui j'ai partagé le même bureau sur deux

continents différents! Je n'oublie pas ces longues randonnées à la recherche des orignaux! Je n'oublie pas les informaticiens, J. Champeau et son équipe. Un clin d'œil à Bruno qui a veillé à ce qu'il ne manque pas de café! Mes remerciements vont également à P. Dhaussy pour avoir contribué à me ramener de mes promenades chez nos cousins québécois. Je n'oublie évidemment pas le GIPSA-Lab, en particulier l'équipe SigmaPhy. A ce titre, je remercie JIM, N. Barbara. Je remercie également D. Mathias, D. Rock, et toutes les personnes avec qui j'ai eu l'occasion de discuter soit autour d'un café soit autour d'un verre. Un clin d'œil particulier à F. Aulanier avec qui j'ai partagé ces moments inoubliables de la phase de rédaction du manuscrit.

C'est également l'occasion pour moi de remercier toutes les personnes avec qui j'ai pu passer de bons moments pendant ces années d'aventure. Un grand merci tout particulier à Jean-Guy Nistad pour son hospitalité. Je te suis sincèrement reconnaissant. Un grand merci à Nathalie Roy pour ces promenades en fin de journée pendant ces missions en mer. Mes remerciements vont également à Manuela Conversano, à Maude Audet, à Delphine Benoit pour les moments de partage lors de mon passage au Québec. Je me souviendrai de ces soirées d'hiver autour d'un jus mais aussi ces danses interminables au Baro! Ahah ce Baro!! Merci à mon frère Sylvain Gautier, à Erwan et à toute la bande pour leur sens de faire la fête.

Je ne saurai terminer cette page de remerciements sans un retour au bercail, là où tout a commencé. Ce qui semble évident ne l'est pas toujours. A ce titre, je remercie mes parents pour m'avoir donné cette chance de départ. Je remercie mes grands frères Emmanuel, Thomas, mon petit frère Sakré et ses petits frères pour leur soutien de toujours. Papa Wendemy (je préfère ce prénom à Valentin), trouvez ici toute ma reconnaissance pour votre soutien. Je fais également un clin d'œil au trio de l'Université d'Ouagadougou. Je pense notamment à Bassan Balé Jacques et à Pascal Bado.

Le mot de fin revient à Virginie Katleen pour m'avoir accompagné et supporté pendant ces trois années d'aventure humaine, avec ses moments parfois difficiles. Je te suis reconnaissant et te remercie du fond du coeur. Une petite pensée pour mon fils Emery, arrivé juste à temps pour me tenir en éveil pendant la période de rédaction de mon manuscrit.

Je m'excuse auprès de tous ceux dont le nom n'a pu être cité. Je les porte également dans mon cœur.

Je termine cette page de remerciement par cette citation de Louis Guilloux ***Si on ne se met pas en question, si on ne court pas une vraie aventure, au bout de laquelle on sera vainqueur ou vaincu avec le risque de se casser la gueule, alors ça n'a aucun intérêt***. L'aventure continue...

Contents

En science, on trouve d'abord et on cherche ensuite. Il n'y a pas de fait en soi mais des faits observés.

Saint-John Perse

Chapter 1

Résumé

Contents

Les océans occupent 71% de la surface de la terre. En tenant compte de ses formes liquide (océans, lacs, rivières, végétations humides) et solide (neige, glace terrestre et de mer), l'eau représente jusqu'à 85% de la surface terrestre. Les océans régulent le climat et constituent la principale réserve de protéine de la terre ; ils jouent donc un rôle primordial dans l'équilibre du système global. Les océans regorgent également d'importantes ressources minières et énergétiques (pétrole, gaz, etc.). Le développement de l'industrie marine (trafic maritime, industrie offshore, etc.) a entrainé une augmentation significative des niveaux sonores du bruit océanique dans les océans des moyennes latitudes qui deviennent préoccupant pour la communauté scientifique [Tasker10, Boyd11].

L'Arctique et les mers des régions polaires sont dépourvus d'activité industrielle significative et on peut encore y mesurer le bruit océanique produit par les sources naturelles d'origines physiques et biologiques. Les travaux effectués au cours de cette thèse visent à explorer le bruit océanique dans la mer de Beaufort et dans la Baie d'Hudson sous deux aspects. D'une part, on veut évaluer les conséquences naturelles du changement climatique sur les paysages acoustiques des régions polaires. Pour ce faire, on se fixe pour objectif de caractériser les variations saisonnières, en comparant les différences du paysage acoustique lorsque la surface océanique des régions où sont effectuées les mesures est libre de glace et lorsque celle-ci est couverte de glace. D'autre part, on veut évaluer le potentiel de l'acoustique passive (PAM), comme moyen de monitorage de la banquise. On étudiera alors le paysage acoustique lorsque les régions où sont effectuées les mesures sont couvertes de glace.

Les travaux présentés dans cette thèse ont été réalisés en collaboration entre le GIPSA_Lab (Grenoble, Image, Parole, Signal, Automatique), l'ENSTA Bretagne (Ecole Nationale Supérieure des Techniques Avancées), le SHOM (Service Hydrographique et Océanique de la Marine) et l'ISMER-UQAR (Institut des Sciences de la Mer à l'Université du Québec à Rimouski). Les données acoustiques utilisées ont été mises à disposition par le Pr. Yvan Simard, titulaire de la Chaire de recherche du ministère des Pêches et des Océans Canada en Acoustique Marine Appliquée à la recherche sur l'écosystème et les mammifères marins. Le Pr. Simard est également membre des réseaux de recherche Québec-Océan et Réseau de Centres Excellence (RCE) ArcticNet, dans le cadre duquel les données acoustiques ont été acquises. Le réseau ArcticNet regroupe en effet des scientifiques de disciplines diverses, qui travaillent depuis 2003, pour comprendre l'impact du changement climatique dans les régions nordiques du Canada et formuler des recommandations pour les décideurs politiques, économiques, et écologiques. Cette collaboration m'a notamment permis d'effectuer un séjour de 13 mois au sein de l'ISMER-UQAR, dont 6 mois en 2011 et 7 mois en 2012.

Le présent chapitre résume les principaux résultats de mes travaux. Il est organisé comme suit. La première section présente l'océan Arctique et les changements déjà observés dans le contexte du réchauffement climatique. La section 1.2 aborde les méthodes PAM comme moyen de surveillance de l'environnement marin en général, puis son utilisation dans le contexte de l'Arctique et des mers subarctiques. La section 1.3 rappelle les objectifs de mes travaux, avec un récapitulatif des données utilisées ainsi que le protocole de traitement mis en œuvre, et enfin une synthèse des principaux résultats est proposée. Ce chapitre se termine avec une conclusion, suivie de perspectives et la liste des contributions scientifiques.

1.1 L'Arctique et les changements climatiques

1.1.1 L'océan Arctique

L'océan Arctique est le plus petit des cinq océans de notre planète avec une superficie de 9.4×10^6 km^2 [Jones01], soit $\sim$3% de la surface terrestre. L'Arctique se compose de quatre bassins océaniques (Bassins du Canada, de Markarov, d'Amundsen, de Nansen) entourés de sept mers (Beaufort, Chukchi, Sibérie, Laptev, Kara, Barents, Groenland, Norvège) (Fig. 1.1) [Dickson08]. Les mers entourant les bassins de l'océan Arctique sont essentiellement des plateaux continentaux d'une profondeur <100 m et représentent $\sim$1/3 de la surface totale de l'Arctique, faisant de celui-ci l'océan le moins profond des cinq régions océaniques, avec une profondeur moyenne de 1800 m [Thomas10].

L'Arctique présente la particularité d'être entièrement couvert de glace pendant la majeure partie de l'année. Au milieu de l'hiver boréal, la couverture de glace de mer dans les régions arctiques atteint son maximum et couvre une superficie de $\sim15.5\times10^6$ km^2, s'étendant du pôle nord jusqu'au 44°N dans la mer du Japon [Thomas10]. La couverture minimale est observée en septembre de chaque année où la couverture de glace est alors réduite à $\sim6\times10^6$ km^2.

La circulation océanique dans l'océan Arctique est une donnée importante pour ce travail. Dans l'Arctique, la circulation océanique est la résultante de quatre forces majeures [Rotschky11] : les vents, la pression atmosphérique, l'apport d'eau douce des rivières, la circulation thermohaline totale. Deux principales circulations dominent la circulation de l'Arctique : la Gyre de Beaufort et la dérive transpolaire (Fig. 1.2). La Gyre de Beaufort (Fig. 1.2, BG) centrée à (80 °N, 155 °W) dans le Bassin Canadien [Barry93] est traditionnellement une circulation anti-cyclonique et constitue le principal réservoir d'eau de faible salinité (eau douce) dans l'océan Arctique, soit $\sim$45 000 km^3 [Proshutinsky02, Proshutinsky05]. Cette réserve d'eau est principalement alimentée par la décharge des rivières et des fleuves [Proshutinsky02, Dickson08]. Les eaux douces de la Gyre de Beaufort sont séparées de la couche supérieure plus salée du Bassin Eurasien (Bassin de Nansen et d'Amundsen, Fig. 1.1) par un principal front qui définit la structure barocline de la dérive transpolaire (Fig. 1.2, TPD) [Dickson08].

En dehors de la banquise rattachée aux côtes pendant l'hiver boréal, le couvert de la glace arctique est en perpétuel mouvement sous l'influence de ces deux régimes de circulation océanique. Si la Gyre de Beaufort piège les blocs de glace en son sein pendant plusieurs années, la dérive transpolaire pousse la glace contre les côtes du Groenland et de l'Archipel Canadien, engendrant par des processus de compression et de déformation en crêtes, les glaces les plus épaisses de l'Arctique dans cette région [Kwok06].

De plus, les échanges de l'Arctique avec le Pacifique se font à travers la mer et le détroit de Bering, tandis que deux principaux chenaux le relient à l'Atlantique. On a d'une part les mers du Groenland et du Norvège, via le détroit de Fram (chenal profond, 2500 m) et la mer de Barents (petit fond, 50–500 m) à l'Est, et d'autre part la Baie de Baffin au Sud-Est du Groenland via un réseau de chenaux à travers l'Archipel Canadien [Jones01, Zhang03]. Ainsi, la glace de l'Arctique s'exporte principalement par le détroit de Fram, et par les réseaux secondaires de l'archipel canadien (les détroits du Golfe d'Amundsen, de M'Clure et des îles de la Reine Elizabeth) [Kwok06, Tsukernik10, Smedsrud11].

Les océans contrôlent les fluctuations climatiques, en raison de leur haute capacité de transport de la chaleur d'un point à un autre, principalement de l'équateur aux pôles. La circu-

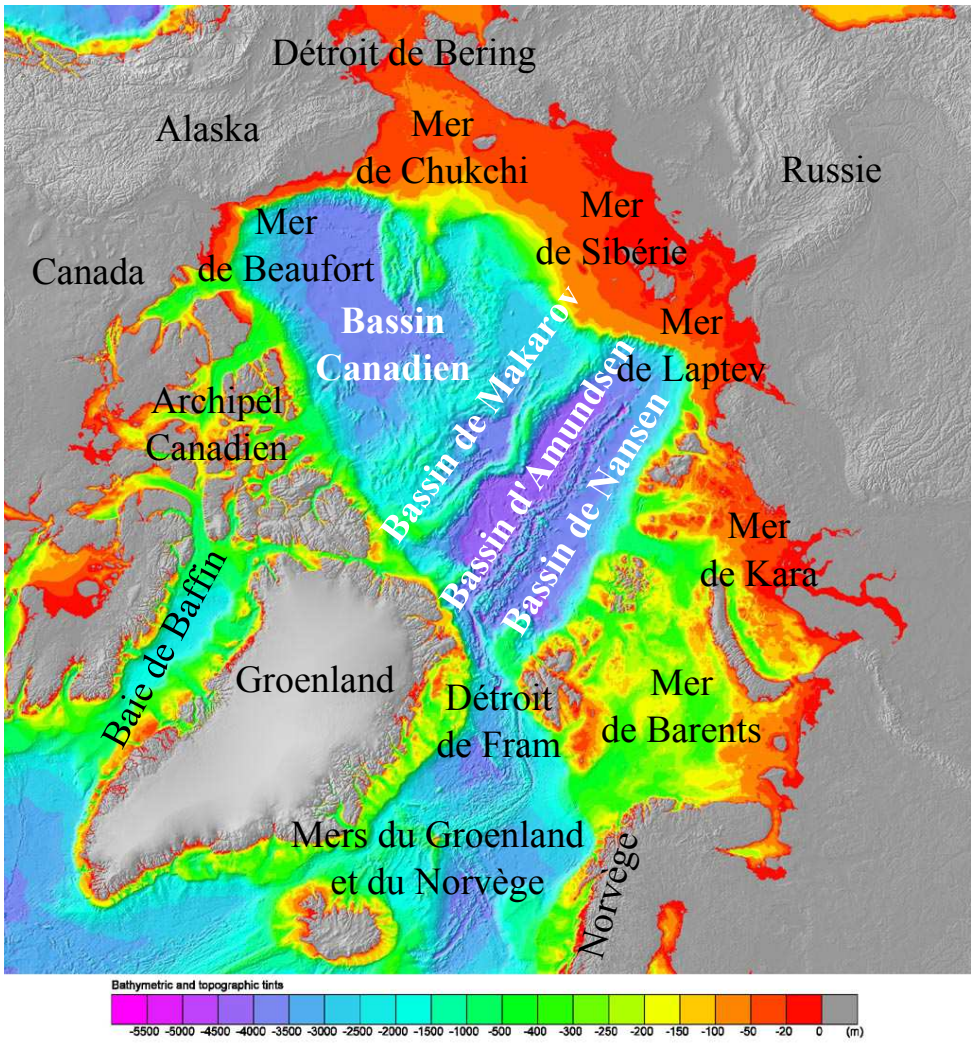

Figure 1.1: Bathymétrie et bassins océaniques de l'océan Arctique (source : [Dickson08]). Source de la carte de fond (http://www.ngdc.noaa.gov/mgg/bathymetry/arctic).

lation thermohaline est une composante majeure de ces échanges [Siedler01, Clark02, Dickson08, Srokosz12]. C'est un processus complexe résultant de l'interaction océan-atmosphère. En effet les eaux denses produites dans les régions polaires, grâce à la combinaison de la perte de chaleur de la surface de l'océan et du rejet de sel pendant la congélation, forment une part importante de cette circulation [Thomas10, Goosse99]. Dans l'Atlantique Nord, l'intensité de cette circulation dépend de la formation de ces eaux denses qui s'écoulent en profondeur par advection dans la mer du Labrador [Dickson08]. Cet équilibre millénaire pourrait être menacé par les changements récents liés au réchauffement climatique.

1.1.2 Les changements climatiques dans l'Arctique

La température moyenne de la terre a augmenté de 0.6°C ces 100 dernières années. Au cours de ce millénaire l'augmentation de la température à partir de 1976 est la plus importante. Dans les régions arctiques, la hausse de température est deux fois plus importante que

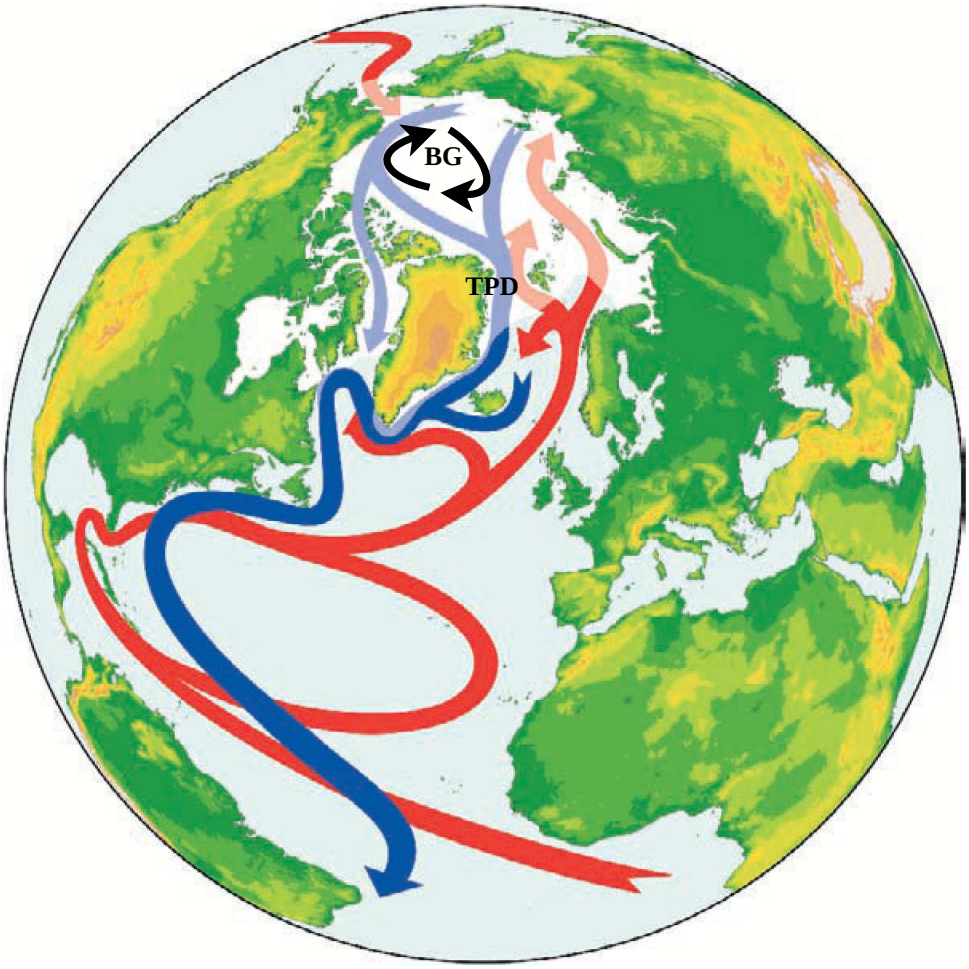

Figure 1.2: Circulation océanique globale simplifiée; On y voit les échanges entre le Pacifique, l'Arctique, et l'Atlantique. Les courants rouges sont les entrées d'eau chaude dans l'Arctique, alors que les courants bleues sont les courants de profondeur constitués d'eau dense produite par l'Arctique, en direction du sud (adapté de [Dickson08], p.386). Les flèches noires dans le bassin canadien symbolisent la Gyre de Beaufort.

partout ailleurs sur le globe. Dans les années 1950, l'Arctique était entièrement couvert de glace toute l'année. La glace de mer joue un rôle prépondérant dans les échanges de chaleurs océan-atmosphère car elle réfléchit 50–80% de l'énergie solaire en fonction des saisons, contribuant ainsi au maintien d'un climat froid dans les hautes latitudes [Stroeve12a]. Du fait de sa faible épaisseur, (1.89 m en moyenne en 2008), la glace arctique est très sensible aux perturbations du couple océan-atmosphère, et est considérée comme une sentinelle pour la surveillance des changements climatiques [Haas10a].

Depuis l'avènement des satellites modernes à micro-ondes passifs à partir de 1979 [Stroeve07] qui ont permis un suivi continu de la couverture de glace, l'Arctique a perdu plus de 35% de sa couverture de glace en été à raison de -11% par décennie. Pendant la même période, la glace arctique a perdu ∼48% de son épaisseur, passant de 3.64 m en moyenne en 1980 à 1.89 m en 2008 [Kwok09b]. Les modèles climatiques prédisent que l'Arctique pourrait être dépourvu de glace en été au cours de ce siècle, entre 2040 et 2100 [Stroeve12b, Wadhams12].

Or l'Arctique joue un rôle important dans le climat global, du fait de sa contribution en eau douce (de faible salinité) dans l'Atlantique Nord qui est un facteur déterminant pour la stabilité de la circulation thermohaline (Fig. 1.2). Les conséquences à long terme de la disparition totale de la glace en Arctique restent mal connues, en raison de la complexité des interactions océan-atmosphère et du système global du climat. Les modèles numériques de dynamique océanique montrent cependant que la circulation thermohaline est très sensible à une perturbation de l'eau douce dans l'Atlantique Nord de l'ordre de 10^6 $m^3.s^{-1}$ [Clark01, Clark02]. Proshutinsky *et al.* [Proshutinsky05] notent que le déversement de 5% du contenu de la réserve d'eau douce de la Gyre de Beaufort suffit pour provoquer des anomalies de salinité dans l'Atlantique comme il a déjà été observé dans les années 1970. En outre, des mesures récentes montrent que la réserve d'eau douce de la Gyre de Beaufort (bassins du Canada et du Makarov) a augmenté de ∼8 500 km^3 ces dernières années [McPhee09]. Cette augmentation pourrait affecter la structure de la dynamique de surface et modifier ainsi la structure des courants de surface [McPhee09] et par conséquent le transport d'eau douce dans la Gyre de Beaufort.

Aussi la fonte progressive de la glace de mer est susceptible d'augmenter la quantité d'eau de faible salinité disponible dans l'Arctique, avec une possible décharge dans l'Atlantique. Vellinga *et al.* [Vellinga02] ont montré que l'effondrement de la circulation thermohaline globale, suite à une introduction brusque d'une quantité importante d'eau douce dans l'Atlantique Nord, aura des conséquences à l'échelle de la planète, parmi lesquelles une baisse de la température de l'ordre de 8°C en Atlantique, de 1 à 3°C en Europe et jusqu'à 2°C en Amérique et en Asie. Ces changements s'accompagneront incessamment d'une redistribution globale des vents, des précipitations, de l'évaporation et de l'humidité des sols.

Outre ces modèles de prédictions numériques, des preuves scientifiques des effets du changement climatique existent déjà à tous les niveaux (océanique, terrestre, sociétale et économique) particulièrement dans les hautes latitudes de l'hémisphère nord. Bien évidemment, la diminution continuelle et spectaculaire de la glace de mer dans l'océan Arctique est le signe le plus visible du réchauffement climatique au cours du 20^e siècle. Ce changement altère radicalement les écosystèmes de l'océan Arctique. En effet, l'augmentation de la température de l'océan et l'allongement de la durée de l'été, c'est-à-dire l'exposition de la surface d'eau libre de glace, influencent la dynamique de la chaine alimentaire, de sa base (les organismes microscopiques) au niveau trophique supérieur [Archambault10]. Un déplacement de la distribution des poissons vers le nord a déjà été observé dans la mer de Bering [Archambault10].

Les écosystèmes des cours d'eau douce (lacs, fleuves, rivières, estuaires, etc) dans les régions arctiques qui dépendent des conditions environnementales et des caractéristiques propres de chaque cours d'eau [Prowse06], ne sont pas à l'abri du réchauffement climatique. Des changements de structures physiques (stratification, température, oxygénation) et biologiques (production primaire, arrivée d'espèces invasives, distributions des espèces, etc) sont à prévoir avec les hausses de température [Prowse06, Wrona06, Vincent12] dans cette partie du monde.

L'impact majeur du changement climatique au niveau des écosystèmes terrestres des régions arctiques est la détérioration et la distribution spatiale du pergélisol [Hinzman05] (cette couche de sol perpétuellement gelée qui couvre 20 à 25% la surface des sols dans les régions froides [Serreze00]). Le pergélisol contrôle les processus hydrographiques locaux des régions polaires, en maintenant les sols humides [Hinzman05]. Il contribue aussi à piéger le carbone et à réduire la production du méthane [Jorgenson01]. La disparition du pergélisol pourrait alors entraîner l'assèchement des sols accompagné d'une réorganisation des écosystèmes, d'une augmentation de la fréquence des feux de forêt, et d'un changement des flux de chaleur [Walther02, Hinzman05,

Soja07, Henry12]. D'importants changements au niveau de la végétation à l'échelle régionale sont déjà observés dans les régions arctiques, avec une augmentation de la croissance des plantes [Serreze00, Henry12]. Il en découle une modification de l'abondance, de la persistance et de la distribution des animaux terrestres [Henry12, Hinzman05].

Les changements environnementaux dans les régions arctiques ont aussi un impact direct sur les communautés nordiques. La principale inconnue est de loin l'impact du réchauffement climatique sur la santé des communautés autochtones des régions arctiques. La hausse des températures est favorable à la prolifération de maladies infectieuses d'origine alimentaire (gastro-entérite, intoxication par les mollusques) ou d'origine animale transmise à l'Homme [Epstein05, Parkinson05, Parkinson09]. Les communautés autochtones doivent également faire face au réchauffement climatique en adaptant leur mode de vie. Les changements de la distribution des animaux terrestres et marins, ainsi que l'amincissement de la banquise nécessitent de nouveaux modes de transport, de chasse et de pêche [Ford04, Hinzman05, Ford06]. En outre, les changements futurs vont altérer les routes de glace à travers les lacs pour le transport industriel, les pipelines, et les modes de construction pour faire face à l'augmentation potentielle de tempêtes de forte intensité [Berkes02, Ford04, Hinzman05].

Les fontes de la glace de l'Arctique présentent aussi deux opportunités économiques majeures. D'une part, d'importantes réserves d'énergies fossiles (gaz naturel, pétrole) se trouvent au-delà du cercle polaire dans les régions arctiques, notamment au niveau des plateaux continentaux [Nassichuk83, Kontorovich10, Gautier09, Grantz12]. A cela, s'ajoutent les ressources minières [Safonov10, Dobretsov10] : nickel, platine, uranium, chrome, diamant, manganèse, or, antimoine, tungstène, cuivre, étain, métaux rares, etc. D'autre part, les pays de l'hémisphère nord voient dans la fonte de glace un raccourci pour la navigation commerciale, via le passage du Nord-Ouest, à travers l'Archipel Canadien. Cette route maritime, déjà ouverte en 2007 [Field12, Stroeve12a], rapproche par exemple la Chine de l'Union Européenne de 4000 miles nautiques [Hong12].

Comme on l'a vu, l'importance de l'Arctique dans le système global lui vaut une attention particulière nécessitant un monitorage long terme de son évolution. L'océan dans son ensemble est alors scruté avec des moyens multiformes, notamment par des satellites d'observation et des mesures *in-situ*. Les méthodes de surveillance par PAM s'inscrivent dans ce cadre comme moyen supplémentaire de monitorage de l'environnement arctique.

1.2 Observation de l'environnement par acoustique passive (PAM)

1.2.1 Les paysages acoustiques sous-marins

Le concept de "'soundscape"' a été introduit en écologie pour décrire les relations entre un paysage et la composition de sa production sonore. Par définition, un soundscape ou paysage acoustique, est une combinaison complexe de la contribution de multiples sources sonores que l'on peut regrouper en trois catégories [Pijanowski11a, Pijanowski11b] : la biophonie (production biologique), l'anthropophonie (activité humaine) et la géophonie (activité géophysique, météorologique). Le paysage acoustique possède donc des variations spatio-temporelles.

L'océan est un excellent support pour la propagation des ondes acoustiques, et le bruit océanique est par conséquent une propriété spatio-temporelle de l'environnement marin. Le

paysage acoustique sous-marin peut être décrit par la Fig. 1.3 :

- La biophonie : c'est la production sonore des organismes marins, des invertébrés (bivalves, crustacés, etc) aux vertébrés (poissons, mammifères marins).
- La géophonie : c'est la production sonore issue de processus météorologiques (vents, précipitations), de l'activité géologique (tremblements de terre, volcans) et de la dynamique de la glace de mer (dérive, déformation, fractures) dans les régions polaires.
- L'anthropophonie : c'est l'ensemble des sources sonores liées à l'activité humaine. On retrouve les sources permanentes (trafic maritime, industrie offshore, etc.) et les sources impulsionnelles (sonars militaires et civils, prospection pétrolière, battage, etc.). A ces sources s'ajoutent les motoneiges et les brise-glaces rencontrés dans les régions polaires.

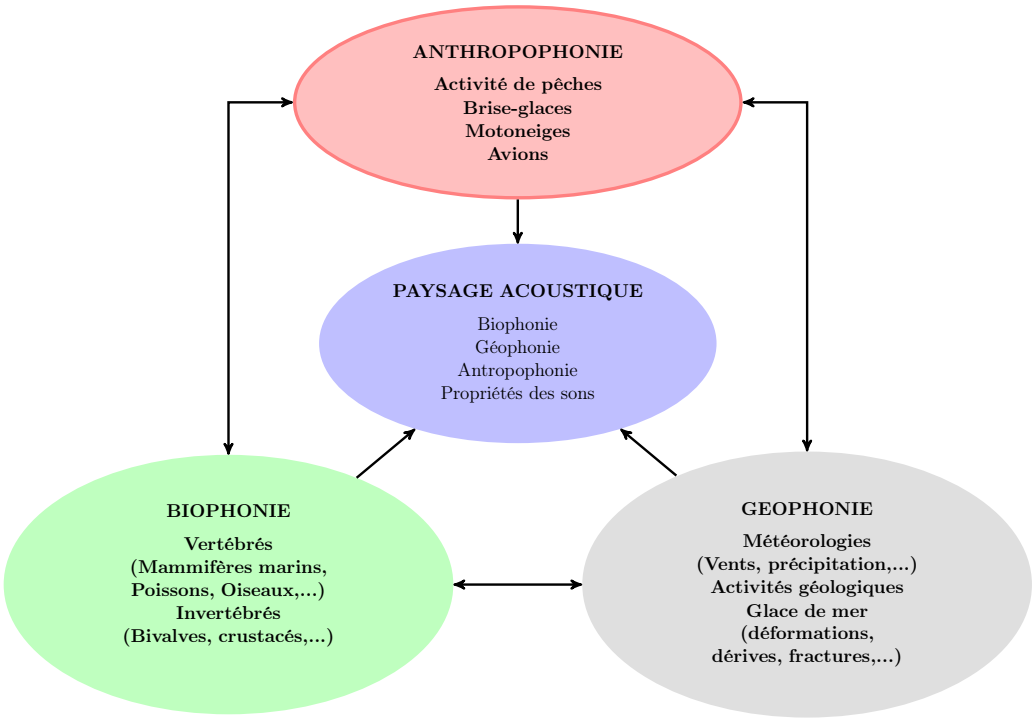

Figure 1.3: Paysage acoustique sous-marin (source : Chaire CHORUS L. Di Iorio & C. Gervaise), montrant les contributions des trois catégories de sources sonores.

Suivant les caractéristiques des sources (puissance sonore, impulsionnelles, etc.) et leur distribution spatio-temporelle dans l'environnement, la mesure d'un paysage sonore révèle donc deux composantes. Le bruit ambiant qui provient des sources lointaines ou permanentes, et les transitoires issus d'événements occasionnels comme représenté sur la Fig. 1.4 [Gervaise13]

Depuis les travaux de Wenz [Wenz62], il est communément admis que le spectre du bruit ambiant peut se découper en trois bandes de fréquences caractéristiques de trois phénomènes indépendants dans l'océan (Fig. 1.5). Ainsi le bruit de turbulence océanique domine la bande infrasonique (<10 Hz), le bruit du trafic maritime est concentré sur les basses fréquences (10–1000 Hz) et le bruit d'agitation de la surface océanique couvre une large bande fréquentielle (0.2 kHz–100 kHz). A ces sources s'ajoutent des transitoires occasionnels de forte puissance. Ainsi, les explosions et les tremblements de terre, lorsqu'ils existent, dominent les ultra basses fréquences (1–100 Hz), tandis que les précipitations dominent localement le bruit d'agitation de

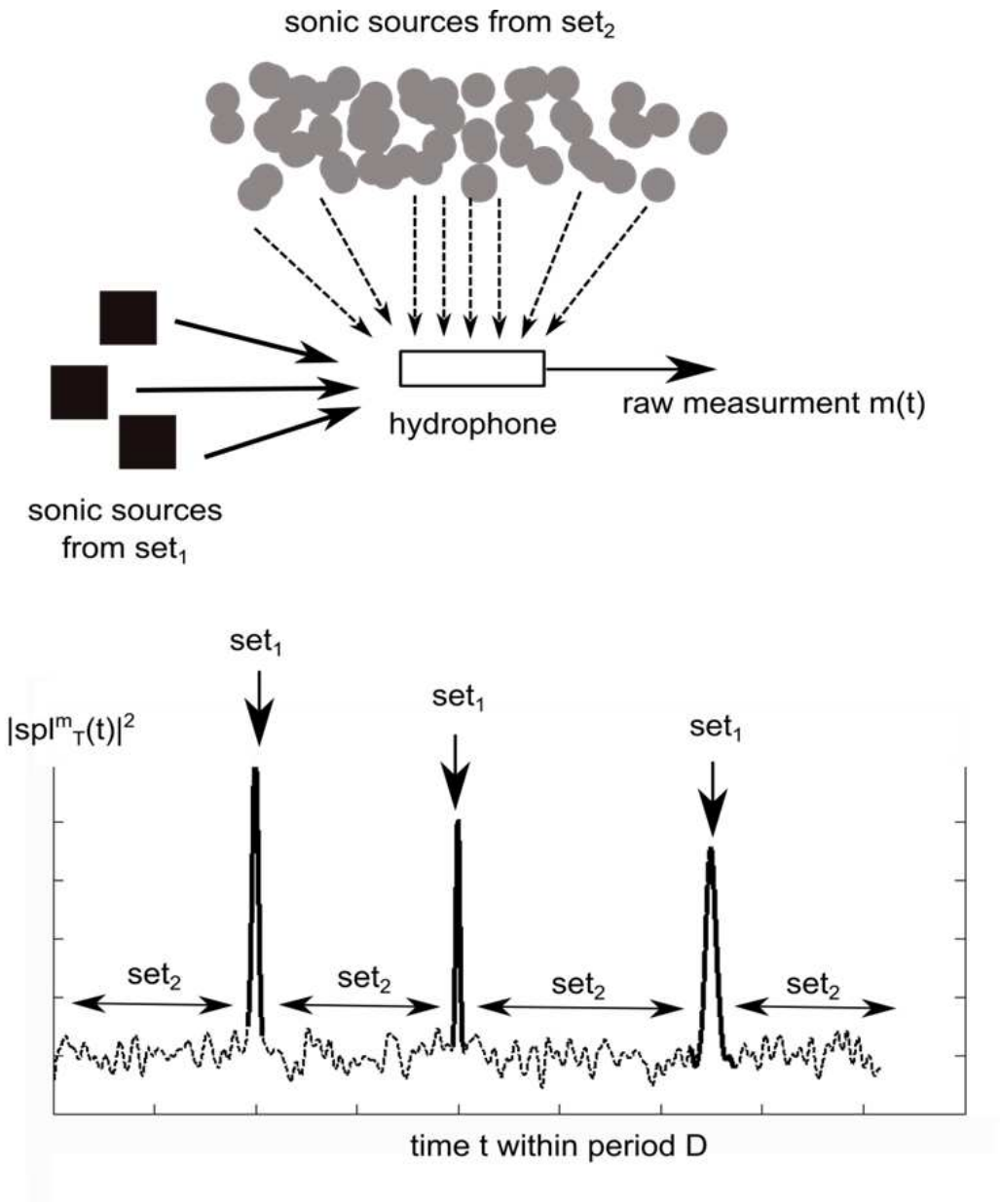

Figure 1.4: Représentation d'un paysage acoustique [Gervaise13]. Le bruit ambiant (set_2) provient des sources lointaines. Les segments (set_1) sont des événements occasionnels de forte puissance.

la surface dans la bande fréquentielle 1 kHz–20 kHz. La production sonore des animaux marins couvrent un large spectre fréquentiel (5 Hz–>100 kHz) et les contributions de la glace de mer au bruit océanique se rencontrent dans la bande fréquentielle 10 Hz–20 kHz.

Le trafic maritime a été identifié comme le principal contributeur du bruit ambiant dans les basses fréquences dont les niveaux dans les océans des moyennes latitudes a doublé tous les 10 ans depuis les années 1960 dans certains sites [Andrew02, Hildebrand04, McDonald06, Hildebrand09, Andrew11] pour atteindre des niveaux préoccupants pour la communauté scientifique. Cette situation risque de se dégrader du fait de la croissance soutenue du trafic maritime, considéré

comme moyen de transport à faible empreinte carbone.

L'étude des effets des perturbations sonores anthropiques fait l'objet de nombreux travaux de recherche et des règlementations commencent à émerger. Ainsi, la Directive Cadre Stratégie pour le Milieu Marin (DCSMM) impose aux états européens de garantir dans les eaux européennes un "bon état sonore" à l'horizon 2020. Le bon état sonore est définit comme un état ne nuisant pas aux espèces marines et sera évalué à partir des niveaux de bruits ambiants dans les gammes de fréquence du trafic maritime et des quantités de signaux impulsifs émis dans le milieu [Dekeling13].

Parmi les méthodologies mises en œuvre dans les observatoires océaniques, l'océanographie acoustique passive consiste à inférer l'état du milieu marin en écoutant uniquement les sons que produisent ses hôtes naturels ou anthropiques. L'analyse de ce chorus sonore permet d'évaluer des paramètres océaniques (température de l'eau, nature des fonds, dynamiques des processus, profil de célérité, etc.) ou des indicateurs (présence et densité d'espèces, densité de bateaux, volume d'activité sismique, volumes de perturbations sonores, etc.) qui peuvent être interprétés et exploités par la communauté scientifique.

1.2.2 Contexte de l'Arctique canadien

Les eaux canadiennes contiennent ∼25% des 17 750 espèces microscopiques, végétales et animales du Canada[Archambault10]. Comme discuté dans la section précédente, les régions arctiques sont celles qui sont ou seront les plus affectées par le réchauffement climatique. Afin de comprendre l'impact de ce changement et de formuler des recommandations pour les décideurs politiques, économiques et écologiques, un Réseau de Centre d'Excellence du Canada, RCE ArcticNet, a vu le jour en 2003. Ce réseau regroupe des scientifiques de diverses disciplines et des gestionnaires travaillant en collaboration avec les communautés inuites et nordiques. Les recherches menées dans le Haut Arctique canadien, l'Arctique de l'Est canadien et la Baie d'Hudson ont pour but de comprendre, d'interpréter, de prévoir l'évolution et de surveiller l'état écologique des environnements terrestres, côtiers et marins afin de réagir aux éventuelles dégradations.

La plupart des animaux marins et surtout les mammifères marins se servent de l'acoustique comme moyen de communication, de reconnaissance de leur environnement et de prédation. Du fait des vocalises spécifiques à chaque espèce de mammifères, leur présence ou absence peut être déterminée par l'acoustique passive (PAM). L'efficacité du PAM et celle des systèmes acoustiques des animaux marins (écholocation, communication, évitement de prédateur) dépend de l'environnement sonore où évoluent ces animaux. Aussi l'impact des sources sonores d'origine humaine ou physique, qu'elles soient impulsives (sonars militaires ou civils, les explosions sismiques, l'industrie offshore) ou chroniques (bruit du trafic maritime) sur la vie marine, des poissons aux mammifères marins, commence à être bien documenté.

La réponse des animaux face à une exposition du bruit est très complexe, et dépend de la configuration spatiale animal-émetteur, du niveau de la source à l'émission, de la sensibilité du système de réception, de la durée et de la répétition du signal. Les effets de l'activité humaine peuvent varier de la simple gène [Southall08] à la perte partielle ou totale de l'appareil auditif [Southall08, Popper03, Codarin09, Halvorsen13, NRC03] en passant par le stress [Smith04, Rolland12] et le masquage des signaux de communication ou la réduction des portées [Clark09, Gervaise12b]. Les effets à long terme du bruit chronique, le trafic maritime par exemple, sont très difficiles à mesurer, d'où la nécessité de déterminer des seuils pour les différentes espèces

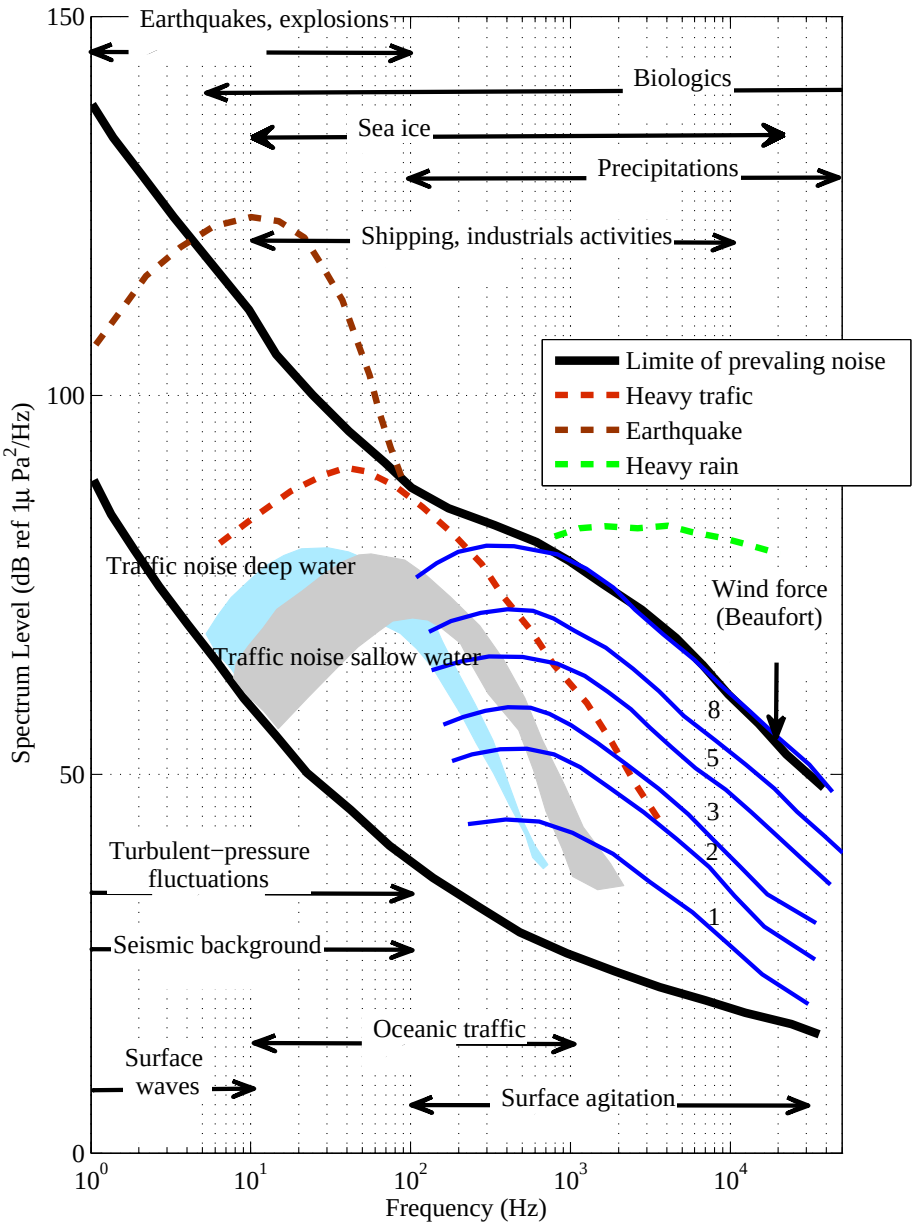

Figure 1.5: Spectres de Wenz du bruit océanique (source: [Wenz62]). Les trois principaux contributeurs au bruit ambiant sont le bruit de turbulence océanique (Surface waves), le trafic maritime (Oceanic traffic) et l'agitation de la surface océanique (Surface agitation). A ce bruit ambiant s'ajoutent des transitoires d'origine physique(tremblement de terre, glace de mer) et biologique.

pour des positions géographiques différentes [Boyd11].

Dans les eaux canadiennes (incluant l'Arctique canadien), on retrouve 52 des 125 espèces de mammifères marins [Archambault10], dont certaines sont endémiques de l'Arctique, et d'autres saisonnières. La connaissance de la distribution des espèces en Arctique était par le passé basée sur des observations directes et sur des prises de chasse. Aussi, les conditions climatiques particulièrement rudes en hiver rendaient ces informations discontinues, parcellaires et incomplètes. La disparition de la glace a augmenté la surface d'eau libre estivale de 1.5-2.0$\times 10^6 \mathrm{km}^2$ depuis 1980 et la durée de l'été s'est allongée de 3 semaines pour la même période (6.9 jours par décennie). Ces changements s'accompagnent d'une augmentation de la production primaire et d'une redistribution spatio-temporelle des animaux marins résidents et/ou migrateurs.

L'Arctique canadien était dépourvu de navigations commerciales significatives jusqu'à ces dernières années qui ont vu l'ouverture du passage du Nord-Ouest en 2007 [Field12, Stroeve12a]. Les premières études décrivant le paysage acoustique de l'Arctique remontent aux années 1960, avec les travaux de Milne et Ganton [Milne64, Milne66, Milne67]. Sous la glace, les principales sources du bruit océanique sont les craquements de la glace sous l'influence des fluctuations de la température de l'air. En absence d'activité significative de la glace, le bruit ambiant peut être très faible, jusqu'à 20–25 dB ($re\ 1\mu Pa$) en dessous des niveaux mesurés pour un état de mer zéro en environnement ouvert [Macpherson62, Milne64, Carey11]. A ce bruit ambiant s'ajoutent des transitoires acoustiques de forte puissance crées par la dynamique de la glace (les fractures, l'empilement, le cisaillement, etc). Il est à noter que ces études étaient basées sur des enregistrements de courte durée (1–24 jours) et dédiées à des objectifs spécifiques.

Nous avons vu plus haut que l'Arctique est une zone importante pour le climat terrestre dans son rôle sur la circulation thermohaline générale. Cette zone est très sensible au réchauffement climatique, dont un des effets sera la fonte de la glace avec un impact climatique important. De plus, cette fonte de la glace aura l'effet pervers de permettre l'industrialisation des régions arctiques (recherche de matières premières et leur exploitation, construction de ports, trafic maritime, etc.). A l'impact climatique s'ajoute donc un impact écologique majeur, d'où la nécessité de surveiller l'environnement arctique pour évaluer d'abord les conséquences climatiques de la fonte de la glace, et ensuite les effets induits par l'anthropisation de cet environnement.

L'environnement océanique est un excellent support permettant une propagation à grande échelle des sons sous-marins. Le bruit océanique possède donc des informations à la fois sur les événements locaux ou lointains, conférant au PAM des arguments essentiels pour constituer un pilier de la surveillance multi-échelle de l'environnement arctique. Il permet en effet la caractérisation de la biodiversité acoustique (du fait des signatures acoustiques spécifiques à chaque espèce, notamment les mammifères marins), l'observation des processus géophysiques signant (craquement, fracture, cisaillement de la banquise, etc.) et l'évaluation des pressions anthropiques.

Des efforts industriels ont permis de mettre sur le marché des enregistreurs acoustiques autonomes performants, de coût limité, permettant l'acquisition longue durée de données à haute résolution temporelle [Sousa-Lima13]. L'observation par acoustique passive dans l'Arctique et le subarctique canadiens au sein du RCE ArcticNet fait partie d'un large projet, ***surveillance long terme des eaux canadiennes***. Ce projet a pour but de surveiller les paramètres physiques, géochimiques et biologiques des eaux canadiennes. Des observatoires acoustiques fixes, constitués d'enregistreurs autonomes, ont ainsi été déployés dans l'Arctique, notamment à l'Est de la mer de Beaufort dans le Golfe d'Amundsen, les Baies de Baffin et d'Hudson de 2004 à présent (Fig. 1.6). Ces observations ont un double objectif : d'une part détecter et identifier les mammifères marins

qui peuplent ces environnements, leur utilisation de l'habitat par le biais de leurs vocalises spécifiques, et d'autre part surveiller l'évolution sonore de ces habitats. Les données acoustiques issues de la mer de Beaufort et de la Baie d'Hudson ont servi de base à mes travaux.

1.3 Positionnement de la thèse

1.3.1 Objectifs

Des travaux précurseurs ont montré l'intérêt de l'acoustique passive pour l'observation des conditions météorologiques du milieu marin [Nystuen86, Ma05a, Ma05c, Jeffrey10], de ses espèces [Marques09, Di Iorio12, Mathias13] et le suivi des activités anthropiques [Andrew11, Gervaise12b]. Le développement particulier des aspects algorithmiques et la détermination des proxy [Gervaise13], offre des perspectives intéressantes pour le monitorage de l'environnement marin.

Le RCE arcticNet dispose d'un jeu de données de monitorage dans l'Arctique, une région de première importance écologique et géopolitique. Cette région que l'on sait affectée par le changement climatique actuel est sensible à l'anthropisation (trafic maritime, recherche de matières premières, etc). Dans ce contexte, quels enseignements peut-on tirer des données? Quelles informations pertinentes peut-on extraire par l'acoustique passive? En quoi ces informations pourront-elles servir efficacement à la surveillance des régions polaires? Mes travaux s'inscrivent dans ce cadre et visent à contribuer à répondre à ces questions. On s'intéresse particulièrement aux sons générés par la glace en se fixant deux objectifs :

- Le premier objectif de mon travail consiste à déterminer les pilotes environnementaux pertinents dans des séries temporelles de bruit ambiant en fonction de l'état de l'environnement (surface libre ou couverte de glace). Le bruit ambiant peut être défini comme tout bruit indésirable qui interfère avec le fonctionnement normal d'un système acoustique actif ou passif [Ross87, Plaisant91]. Nous adoptons dans ce document la définition donnée par le NRC (National Research Concil) comme émanant de myriades de sources indistinguables [NRC03], alors que le bruit océanique désigne la mesure du paysage sonore sous-marin.
- Le second objectif vise à exploiter les transitoires acoustiques, en particulier ceux liés aux processus de déformation mécanique de la glace, pour améliorer l'observation et la compréhension de leurs mécanismes de génération.

Une telle approche nécessite la combinaison de données acoustiques, météorologiques (vents, précipitations, pression, température) et océaniques (couvert de glace, vitesse de dérive de la banquise, vitesses des courants) couplée à des méthodes robustes de traitement de la mesure acoustique.

1.3.2 Matériels et méthodologie

Pour étudier le bruit océanique et ses pilotes environnementaux, nous avons utilisé des séries annuelles de mesures acoustiques et de vitesse de courant, et les observations satellitaires de la surface de l'océan.

1.3.2.1 Données acoustiques et vitesse des courants marins

Les mesures acoustiques et de vitesses *in-situ* des courants marins utilisées dans cette étude sont issues des stations océanographiques résumées dans le tableau 1.1. Ces données, issues du RCE ArcticNet, ont été mises à disposition par le Pr. Yvan Simard, membre des réseaux de recherche Québec-Océan et RCE ArcticNet, et titulaire de la Chaire de Pêches et Océans Canada en acoustique marine appliquée à l'écosystème à l'Institut des Sciences de la Mer-Université du Québec à Rimouski (ISMER-UQAR).

Les données acoustiques et de courant ont été enregistrées dans le Golfe d'Amundsen, à l'Est de la mer de Beaufort (Fig. 1.6 CA08, 71°0.42' N, 126° 4.48' W), du 9 septembre 2005 au 2 Octobre 2006 (384 jours), et dans la Baie d'Hudson (Fig. 1.6 AN03, 24.47' N, 77° 55.79' W) pour deux années, du 1^{er} octobre 2005 au 13 septembre 2006 (347 jours), puis du 16 juillet 2010 au 13 septembre 2011 (424 jours). Les données ont été acquises au moyen d'enregistreurs autonomes AURAL (Autonomous Underwater Recorder and Listening), placés à environ 50 m dans la colonne d'eau pour des profondeurs de ∼397 m et ∼130 m dans le Golfe d'Amundsen et la Baie d'Hudson respectivement. Les données ont été enregistrées à raison de 7 ou 10 minutes par heure avec une fréquence d'échantillonnage de 8192 Hz et une résolution de 16 bits. Les eaux de ces régions libres de glace pendant l'été, gèlent en surface pendant l'hiver, isolant ainsi l'océan des forçages météorologiques.

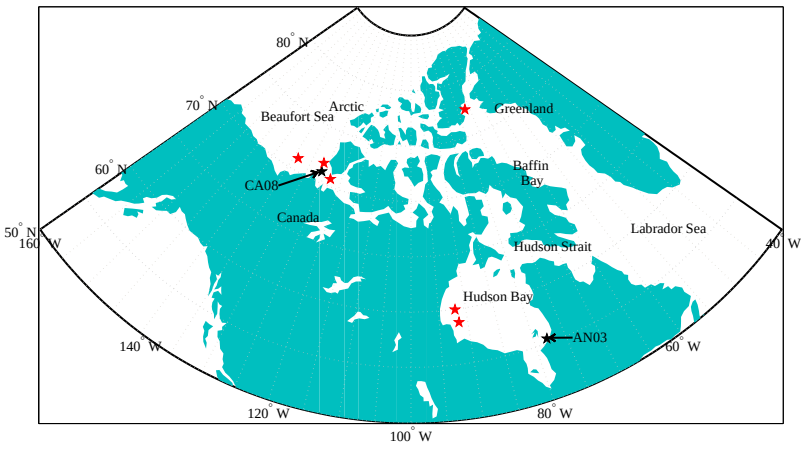

Figure 1.6: Position des observatoires acoustiques dans l'Arctique canadien. Les étoiles noires dans la mer de Beaufort (CA08) et dans la Baie d'Hudson (AN03) sont les mouillages desquels sont issues les données acoustiques utilisées dans mes travaux. Les détails de ces enregistrements sont donnés dans le tableau 1.1.

Les vitesses de courant *in-situ* dans la partie supérieure de la colonne d'eau ont été obtenues avec des ADCP (Acoustic Doppler Current Profiler), placés quelques dizaines de mètres en dessous des enregistreurs acoustiques. Ces derniers ont été programmés pour mesurer la vitesse du courant toutes les 20 minutes.

Table 1.1: Recapitulatifs des données acoustiques utilisées

Station	Longitude	Latitude	Prof. (m)	Aurals (m)	Début (UTC)	Fin (UTC)	Fe (Hz)	T/cyle (min/h)
CA08	126°4.48 W	71°0.42 N	397	50.9	09/09/2005	02/10/2006	8192	7
AN03	77°55.7939 W	55°24.47 N	130	54.1	01/10/2005	13/09/2006	8192	7
	77°55.7046 W	55°24.4388 N	130	46	14/09/2006	09/08/2007	8192	7
	77°55.8283 W	55°24.4858 N	136	48	10/08/2007	03/10/2008	8192	10
	77°55.8283 W	55°24.4858 N	136	48	16/07/2010	13/09/2011	8192	10

1.3.2.2 Les données environnementales

Les données météorologiques horaires (vitesse et direction du vent, température de l'air, pression atmosphérique) et journalières (précipitations) sont issues des stations météorologiques d'Environnement Canada situées à Cape Parry (70 °00.17' N, 124 °00.72' W), disponible sur internet (www.climate.weatheroffice.gc.ca).

Les données de couverture journalière de la glace, d'une résolution spatiale de 6.25 km×6.25 km, sont celles issues du capteur AMSR–E (Advanced Microwave Scanning Radiometer for EOS) porté par le satellite d'observation AQUA [Kaleschke01, Spreen08] rendues disponibles sur le site web (https://icdc.zmaw.de/) du ICDC (Integrated Climate Data Center). L'épaisseur de la banquise avec une résolution spatiale de 25 km×25 km, provient du satellite ICESat (Ice, Cloud, and land Elevation Satellite) [Rotschky11], et est obtenue sur le même site web. Les vitesses de dérive journalière de la glace de résolution spatiale 25 km×25 km, à l'échelle de l'Arctique, sont celles calculées en combinant les données satellitaires et de bouées [Fowler03, Maslanik11] et disponibles sur le site web du NSIDC (National Snow and Ice Data Center).

1.3.3 Synoptique du traitement des données

La mesure d'un paysage sonore est constituée d'un bruit ambiant et de transitoires occasionnels de forte puissance (Fig. 1.4). La mesure acoustique peut également être contaminée par du bruit non-acoustique lié aux artéfacts du système de mesure (vibration du mouillage, écoulement autour de l'hydrophone, etc.). Notre protocole de traitement des mesures recueillies associe donc plusieurs étapes décomposées en actions conformément à la Fig. 1.7, pour traduire les données brutes en descripteurs acoustiques (bruit ambiant et transitoire) afin de remonter aux pilotes environnementaux puis à certaines paramètres océaniques et géoacoustiques de l'environnement. Ce dernier aspect est exclu du présent travail et ne sera pas décrit plus en détail.

Action 1: réjection du bruit de strumming

La première action consiste à nettoyer la mesure du bruit non-acoustique si nécessaire. Ce bruit affecte généralement les extrêmes basses fréquences (<10 Hz) [Lewis87, Buck80]. Pour les mouillages océanographiques fixes utilisés dans notre travail, les artéfacts de la mesure se résument à la vibration du mouillage, sous l'influence des courants marins, mécaniquement transmise à l'hydrophone. Ces vibrations se traduisent alors par une série d'impulsions basse fréquence de largeur de bande variable, pouvant atteindre quelques centaines de Hz. Nous supposons donc que lorsque des vibrations existent, la puissance sonore des impulsions induites varie peu au

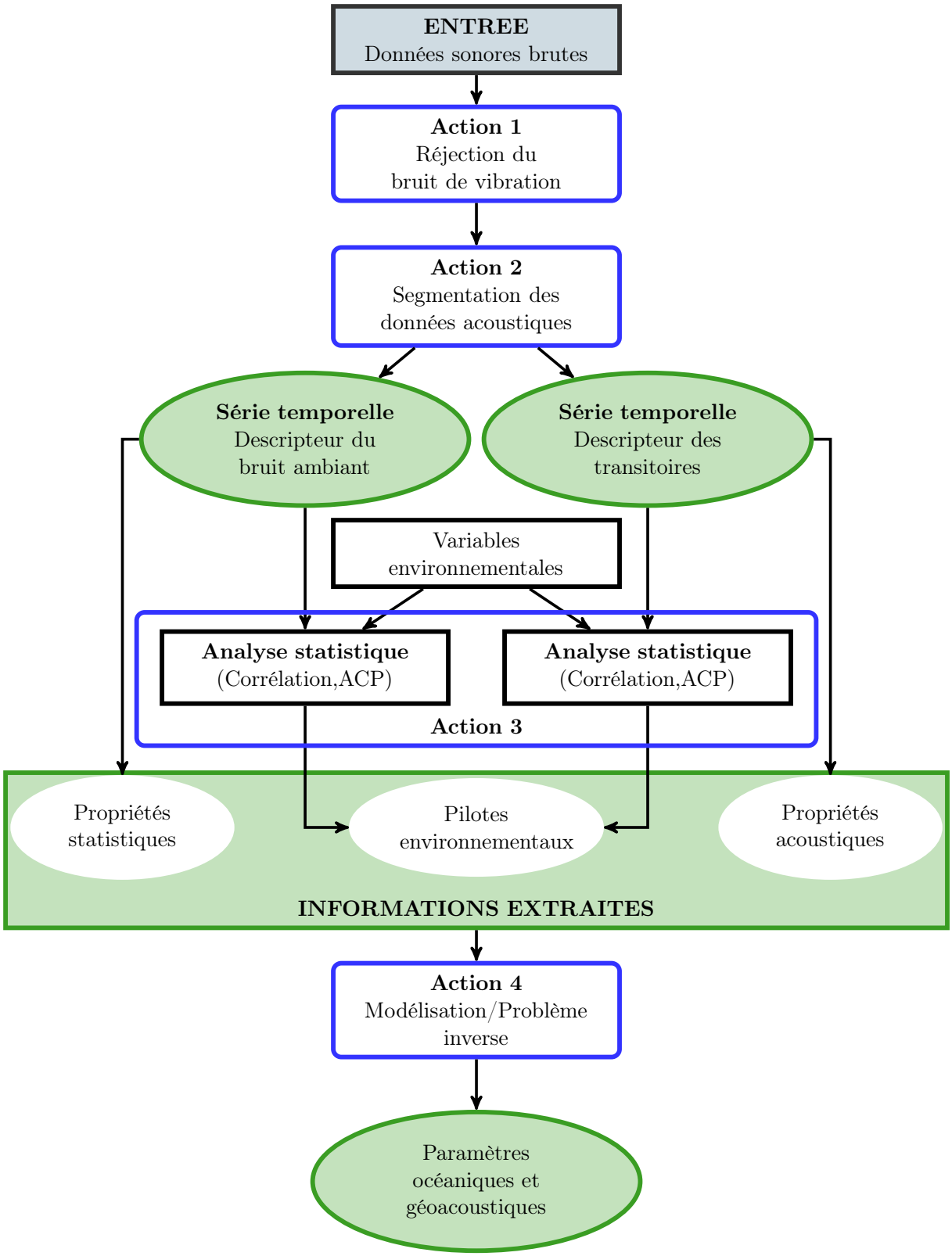

Figure 1.7: Synoptique d'extraction des descripteurs et d'interprétation des données acoustiques.

cours d'un cycle d'enregistrement. Nous avons alors développé un algorithme de prétraitement des données basé sur une analyse du rythme des impulsions et sur la mesure de la cohérence fréquentielle du spectrogramme. Comme les vibrations sont des impulsions basse fréquence, on procède en trois étapes:

- On vérifie le caractère impulsionnel du niveau large bande L_1 dans la bande infrasonique (typiquement 0–20 Hz), par une analyse de Fourrier. En absence de vibration, le niveau L_1 présente un spectre plat, alors qu'une mesure bruitée produit une série de Fourier à une fréquence donnée. La fréquence des vibrations correspond donc à la fréquence fondamentale du spectre de L_1.
- Si le niveau L_1 presente des raies spectrales, on calcule alors la corrélation entre le niveau L_1 et les niveaux large bande pris dans des bandes fréquentielles supérieures avec un recouvrement de 50%. Le dégré de signification du test de corrélation permet donc de déterminer la fréquence maximale (F_{Limit}) de la vibration dans le spectrogramme.
- Une fois ce paramètre déterminé, on procède au seuillage du spectrogramme délimité par la fréquence F_{Limit}, en supposant que les coefficients spectraux associés aux vibrations sont plus forts que ceux issus du bruit océanique. Un seuil peut alors être établi à partir de la fonction de densité cumulative (CDF pour cumulative density function) empirique de cette portion du spectrogramme. On rejette alors les coefficients du spectrogramme supérieurs au niveau correspondant au point d'annulation de la dérivée seconde de la CDF.

La méthode ainsi décrite est d'abord validée sur des données simulées. La vibration est alors modélisée par une série d'impulsions gaussiennes centrée à 20 Hz avec une largeur de bande de 40 Hz (Fig. 1.8 a), à laquelle on ajoute un bruit blanc gaussien. La fréquence de répétition de la vibration est de 2 Hz, et le rapport signal à bruit de 30 dB. Le spectrogramme de ce signal (Fig. 1.8 b), présentent les bandes fréquentielles contaminées. Le test sur la probabilité critique de l'inter-corrélation entre le niveau large bande calculé dans la bande de fréquences 0-50 Hz et ceux des fréquences supérieures, avec une largeur de 50 Hz et un recouvrement de 50% permet de fixer la limite de contamination (F_{Limit}, Fig. 1.8 c). L'analyse de Fourier du niveau large bande [0-50 Hz] donne la fréquence de réptition de l'impulsion (Fig. 1.8 d). La CDF de la portion du spectrogramme delimité par F_{Limit} donne le seuil (Fig. 1.8 e), tandis que la Fig. 1.8 f, présente le spectrogramme nettoyé des impulsions. La méthode s'est avérée efficace pour éliminer les bandes de fréquences affectées sur les données réelles.

Action 2 : séparation du bruit ambiant et des transitoires

Le bruit océanique est la somme de deux composantes indépendantes (Fig. 1.4) [Kinda13, Gervaise13]: le bruit ambiant et les transitoires occasionnels de forte puissance sonore. Nous avons alors développé un algorithme dédié pour extraire de façon systématique le bruit ambiant, supposé stationnaire pendant la durée du cycle d'enregistrement [Gervaise13, Kinda13]. Le spectrogramme d'un tel bruit suit une loi de khi-2 à 2 degrés de liberté [Kay98, Koopmans74]. En supposant que les valeurs faibles du spectrogramme sont celles issues du bruit ambiant, le spectre de celui-ci peut alors être estimé à partir des faibles percentiles du spectrogramme pris dans chaque ligne fréquentielle. On construit donc une série temporelle des spectres du bruit ambiant à raison d'un spectre par heure.

Pendant la période de couverture de la glace, les données acoustiques ont été visuellement examinées pour identifier les transitoires relatifs à des phénomènes physiques liés à la dynamique

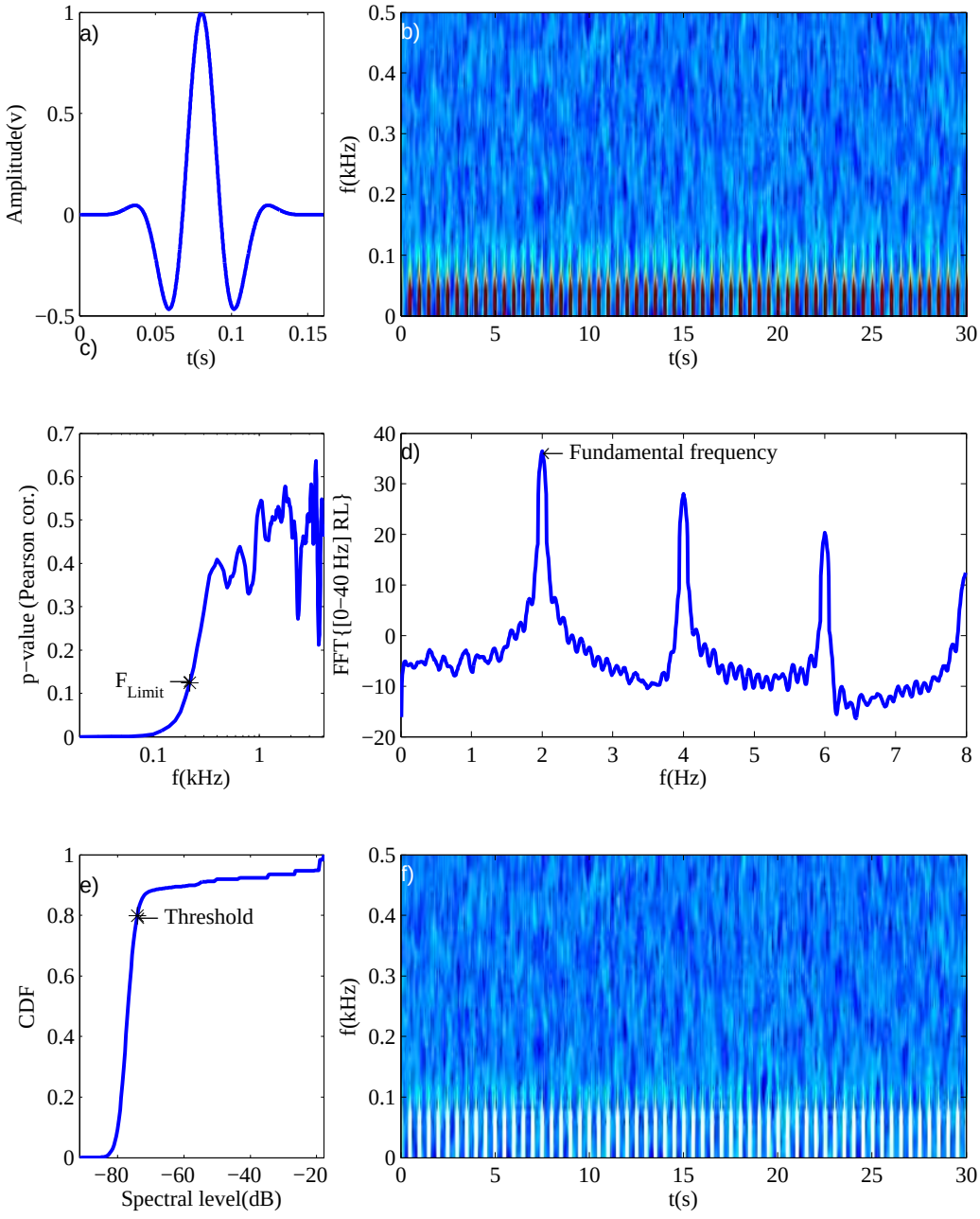

Figure 1.8: Elimination du bruit de vibration par seuillage du spectrogramme sur données simulées. (a) impulsion primaire ; (b) spectrogramme montant les bandes temps-fréquence contaminées ; (c) test de corrélation pour déterminer la largeur de la bande des impulsions ; (d) série de Fourier du niveau large bande (4–20 Hz) ; (e) fonction de densité cumulative empirique et seuil ; (f) spectrogramme nettoyé des impulsions (pixels blancs).

de la glace. On construit alors des séries temporelles de ces transitoires, en tenant compte de leur charactéristiques dans le plan temps-fréquence.

A l'issue de ces deux premières actions, on dispose de séries temporelles qui sont des descripteurs acoustiques liés au bruit ambiant et aux transitoires. Ces séries temporelles servent d'une part à construire les répartitions statistiques (stationnarité, niveaux, spectres, etc.) et d'autre part d'entrée pour la troisième action qui consiste à une recherche des pilotes environnementaux.

Action 3 : recherche des pilotes environnementaux

A partir des séries temporelles produites dans la seconde action, on recherche les pilotes aussi bien du bruit ambiant que des transitoires. Comme on l'a vu sur la Fig. 1.5, chaque source sonore (d'origine physique, anthropique ou biologique) possède une signature spectrale particulière (niveau et bande de fréquences). Dans les régions dépourvues d'activités industrielles significatives, la production sonore est essentiellement une réponse de l'environnement à la somme des forçages météorologiques et océaniques [Reeder11] d'une part, et des animaux marins. On prend donc en compte dans cette analyse les données environnementales disponibles (vents, pressions, courant, glace de mer, etc.). On utilise alors des méthodes statistiques (corrélation, analyse en composantes principales) pour identifier les pilotes environnementaux majeurs de chaque composante du paysage sonore.

1.3.4 Résumé des résultats

Cette section présente les contributions originales des travaux réalisés au cours de cette thèse à la connaissance du bruit océanique et de ses pilotes dans l'Arctique canadien.

1.3.4.1 Cycle annuel du bruit ambiant

Sur la base de la couverture locale de la glace prise dans un rayon de 100 km autour du point de mouillage, l'environnement d'étude se découpe en quatre périodes distinctes, suivant les quatre saisons de l'année dans les régions tempérées. La première période est la période d'eau-libre (été), de juillet à octobre (Fig. 1.9), lorsque la couverture de la glace est inférieure à 10%. La deuxième période, la plus courte correspond à l'automne et au passage d'environnement surface libre en couvert de glace, d'octobre à novembre pour l'année 2005 dans le Golfe d'Amundsen. La troisième période (couvert de glace, hiver), la plus longue des quatre saisons, couvre les mois de novembre à mi-juin et correspond à la période pour laquelle la couverture de glace atteint au moins 90% du disque de 100 km de rayon. La dernière période correspond à la période de fonte au printemps, où la banquise se disloque en morceaux, allant de mi-juin à juillet. Nous nous intéressons particulièrement aux périodes d'eau libre et de couverture de la glace.

A partir d'une série annuelle d'enregistrements sonores, nous avons montré que lorsque la surface de l'océan est libre de glace, le niveau du bruit ambiant est supérieur d'au moins 10 dB au niveau observé quand l'environnement est couvert de glace (Fig. 1.10). Cette différence qui semble être moins accentuée aux hautes fréquences est probablement liée à la limite de notre système de mesure dont le plancher de mesure est de $\sim$53 dB.

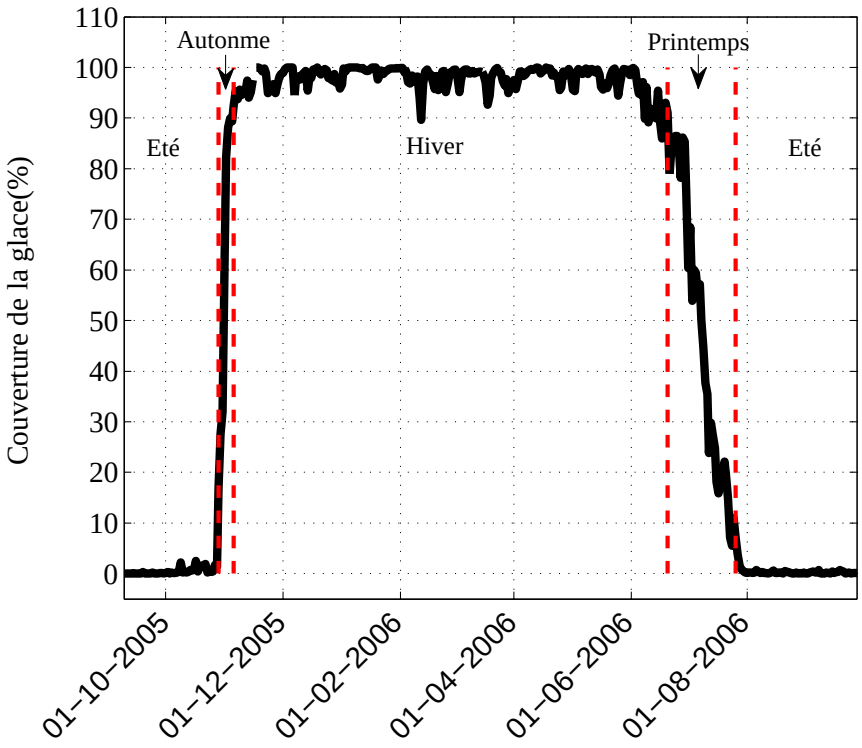

Figure 1.9: Couverture de la glace dans un rayon de 100 km autour du point de mouillage dans le Golfe d'Amundsen.

On peut remarquer également que la forme des spectres (niveaux absolus et dépendances en fréquences) permet de mettre en évidence la signature des deux périodes caractéristiques. Cette information doit pouvoir être exploitée pour mieux comprendre et mieux caractériser les processus (craquement, vêlage, effets des conditions météorologiques). Les courbes montrent ainsi que sans le couvert de glace, le milieu sonore est piloté par les forçages météorologiques, principalement le vent avec des lois conformes au modèle de Wenz [Wenz62] (Fig. 1.10). Pendant la période de couverture de la glace, ce modèle ne s'applique pas; les pilotes environnementaux du bruit ambiant sont différents de ceux qui le gouvernent en environnement ouvert.

Pendant la période de couverture de la glace, les spectres du bruit ambiant (hors vibrations et transitoires) atteignent la limite de notre système de mesure au-delà de 500 Hz et notre étude se limite donc à la bande fréquentielle 10-500 Hz. Nous avons montré que le niveau large bande (10–500 Hz) variait de 84.6 dB à 102.5 dB re 1 μPa dans le Golfe d'Amundsen et que les pilotes environnementaux de sa variabilité sont la triade [vent, dérive de glace, courant] (Fig. 1.11) conformément aux résultats publiés précédemment [Kinda13]. Une corrélation à l'échelle de l'Arctique entre vitesse de dérive de la glace et le niveau de bruit ambiant situe un maximum de corrélation à environ 300 km du point de mesure (Fig. 1.11 b, r = 0.57), localisée au niveau de la glace pluriannuelle (Fig. 1.11 c). Contrairement aux études précédentes [Milne64, Milne66, Milne67], nous n'avons pas observé de corrélation significative avec la température de l'air ou

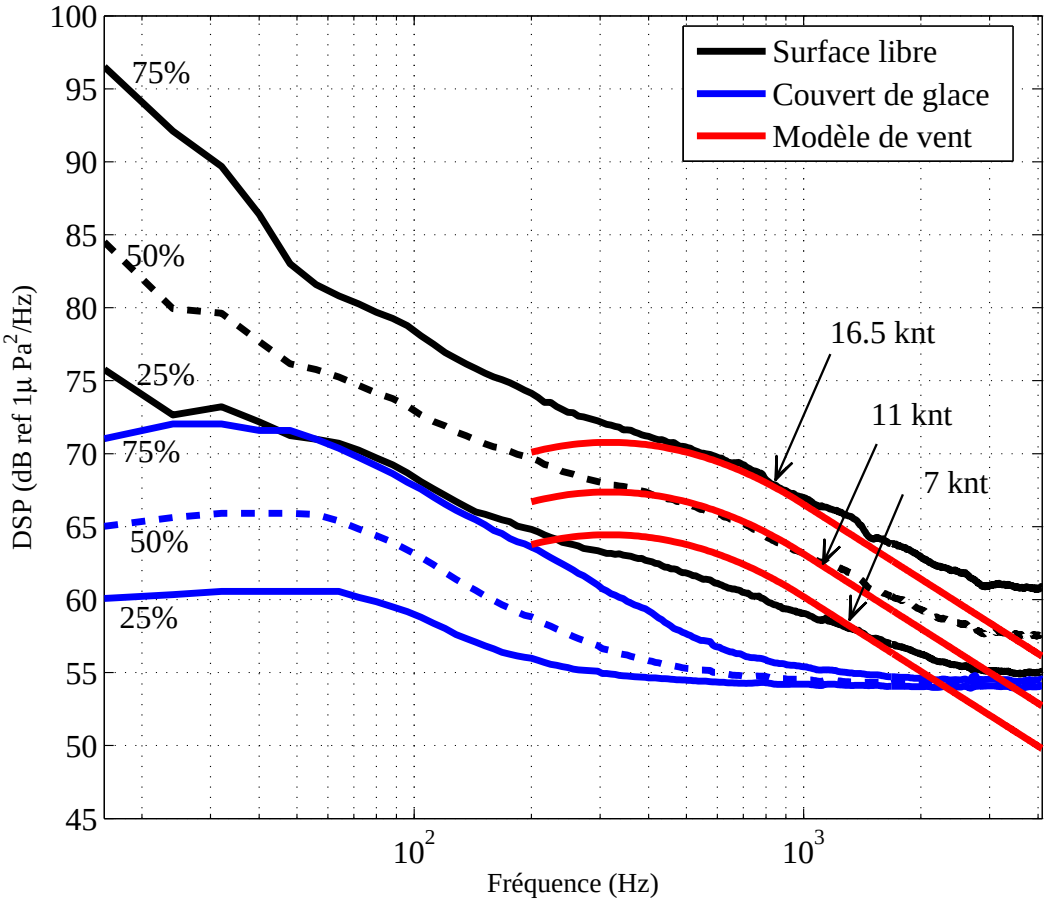

Figure 1.10: Comparaison des spectres de bruit ambiant mesuré et du modèle théorique de Wenz. Le spectre médian en été (sans couverture de glace) est supérieur d'au moins 10 dB au spectre médian observé sous la glace. Les 2^{me} et 3^{me} quartiles en environnement ouvert correspondent au modèle de Wenz, pour des vitesses de vent mesurées à environ 80 km du mouillage océanographique.

de ses variations. Les pilotes environnementaux du bruit ambiant dans cette zone sont donc les mêmes que ceux qui pilotent la circulation océanique de l'Arctique. Le bruit ambiant répondait aussi à des périodes de 7 jours, soit la période moyenne de passage des dépressions locales dans l'Arctique.

1.3.4.2 Les transitoires acoustiques

En étudiant les transitoires acoustiques pendant la période de couverture de glace, nous avons montré que l'on pouvait distinguer trois grandes familles de transitoires acoustiques liées à la dynamique spatio-temporelle de la banquise. Ces trois familles s'identifient par leur contenu temps-fréquences. Ainsi on a :

- Les transitoires large bande (Fig. 1.12 a) : ils couvrent généralement la bande de fréquence

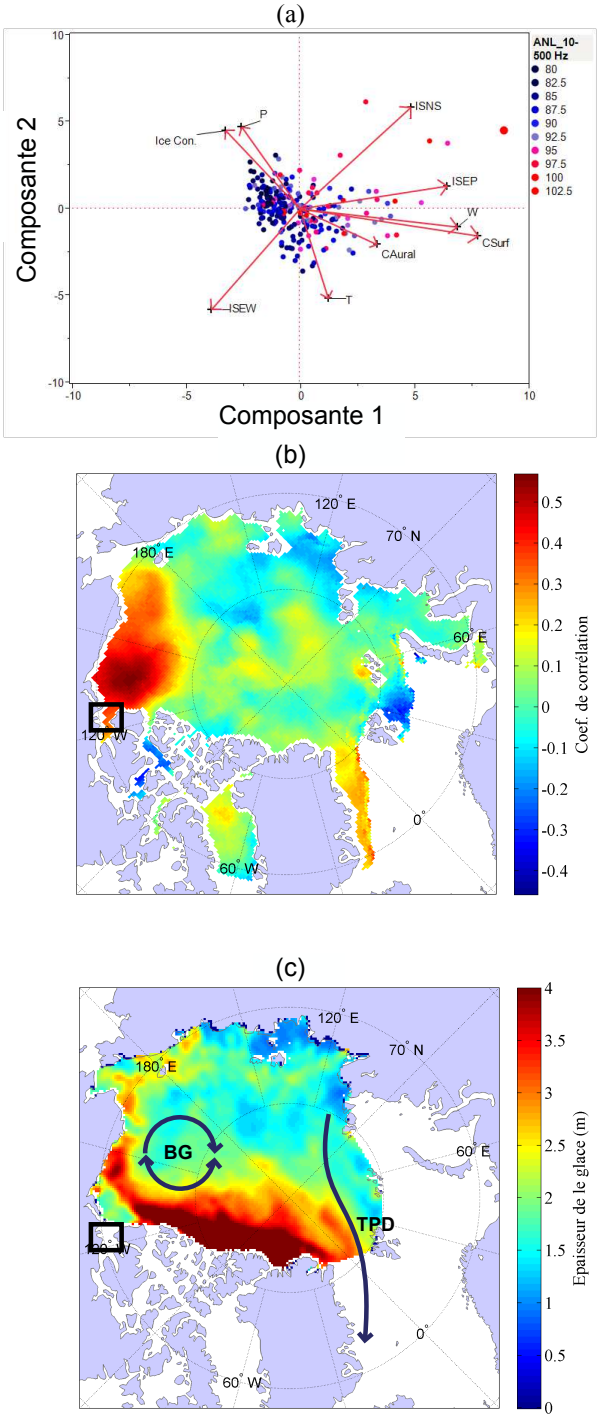

Figure 1.11: Pilotes du bruit ambiant sous couvert de la glace dans la mer de Beaufort. (a) : Analyse en composantes principales des variables environnementales et superposition des réalisations du bruit ambiant (points rouges: bruit de niveau fort, point bleus: bruit de niveau faible) dans le plan des prémières composantes; (b) : Coefficient de corrélation de Pearson entre le bruit ambiant et la vitesse de dérive de la glace a l'échelle de l'Arctique; (c) : Epaisseur de la glace et circulation dans l'Arctique (BG (Beaufort Gyre) = Gyre de Beaufort ; TPD (Transpolar Drift)= Dérive Transpolaire). Le rectangle indique la région de la mesure.

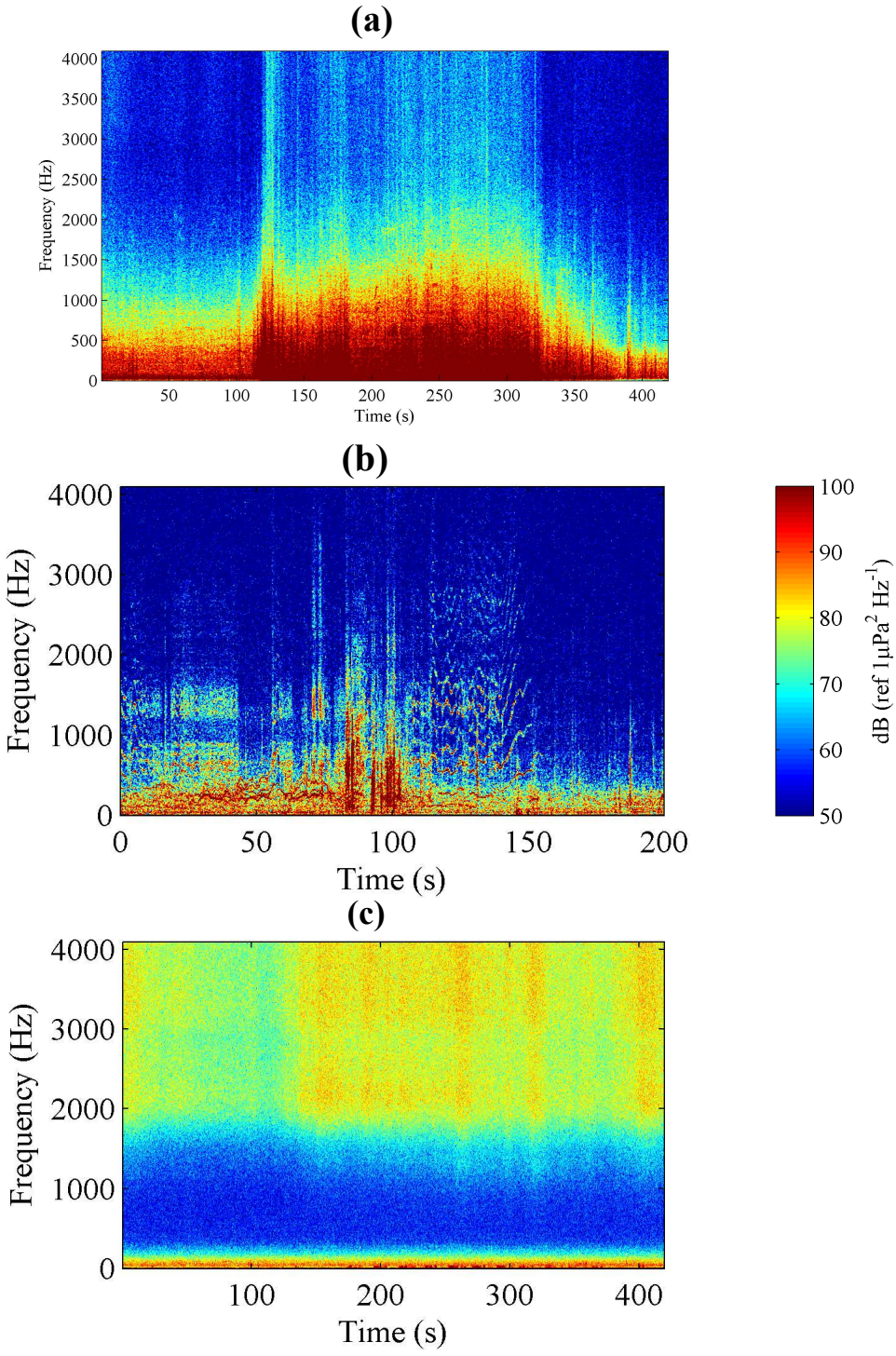

Figure 1.12: Dictionnaire des transitoires acoustiques sous la banquise. (a): transitoire large bande (catégorie 1) ; (b) : signaux modulés en fréquences (catégorie 1). (c) : signaux hautes fréquences (catégorie 3).

utile des enregistreurs utilisés. Ces transitoires possèdent une durée très variable, mais restent majoritairement de courte durée. Sur 742 signaux de cette nature, 50% ont une durée $\leq$23 s et seulement 5% ont une durée >418 s. Les niveaux reçus (RL) de ces transitoires étaient très élevés, avec une moyenne de 104$\pm$6.60 dB, et des maxima pouvant atteindre 135 dB.

- Les signaux modulés en fréquence (Fig. 1.12 b) : ils présentent généralement plusieurs harmoniques pouvant couvrir toute la bande fréquentielle disponible. Sur un total de 947 signaux de cette catégorie sélectionnés, la durée moyenne est de 189.64$\pm$149.24 s et seulement 5% ont une durée $\leq$18.1 s. Certains de ces signaux ont une durée qui excèdent la durée des enregistrements, soit 420 s. Les niveaux reçus de ces signaux étaient généralement plus faibles que ceux décrits précédemment, soit un niveau moyen de 95$\pm$6.48 dB, un minimum de 75.50 dB et un maximum de 130 dB.

- Le bruit haute fréquence (Fig. 1.12 c) : ils couvrent généralement la durée de l'enregistrement. La fréquence basse limite de cette catégorie de signaux est variable. Ces transitoires sont des signaux de faible énergie en comparaison des deux premières catégories sus décrites. Le niveau moyen reçu pour cette catégorie est de 92.93$\pm$3.7 dB et varie de 86.67 dB à 112.40 dB, pour 342 signaux de cette nature.

Les séries temporelles de la dynamique de glace (couverture et déformation, respectivement Fig. 1.13 a et b), montrent que les fortes déformations correspondent à des ouvertures de la banquise. En observant les séries temporelles de nos trois catégories de transitoires (Fig. 1.13 c,d et e), on remarque que ceux-ci ont des occurrences similaires aux périodes de forte intensité de la dynamique de la banquise. En nous appuyant sur une période particulière (rectangle gris sur la Fig. 1.13), nous avons pu lier les processus de déformation de la glace à la production des transitoires acoustiques observés. Des analyses statistiques nous ont permis de montrer que les transitoires observés sont généralement liés au cycle de vie des ouvertures d'espaces d'eau libre de glace dans la banquise. Le cisaillement et le vent ont été identifiés comme les principaux pilotes environnementaux d'apparition des transitoires observés.

1.3.5 Conclusions

Trois séries temporelles, d'une année au moins chacune ont été analysées pour décrire la géophonie des régions arctiques, notamment dans la mer de Beaufort, et dans la Baie d'Hudson. Les données de la mer de Beaufort ont été enregistrées en 2005-2006, soit avant l'ouverture de la route maritime du passage du Nord-Ouest suite à la chute spectaculaire de la couverture de glace en 2007. Ces données peuvent donc être considérés comme représentatives du paysage sonore primitif de l'Arctique canadien. L'analyse d'une session d'enregistrement acoustique couvrant une année entière dans ces régions est une première. Il en découle les deux principaux résultats suivants :

- Pendant la période d'eau libre, le bruit ambiant est principalement le bruit hydrodynamique de la surface, et répond au modèle classique de Wenz. Pendant l'hiver, en présence de couverture de la glace, le bruit ambiant dans la mer de Beaufort ne répondait pas aux fluctuations locales de la température, mais aux forçages environnementaux qui gouvernent la circulation océanique de l'Arctique. Ces résultats s'expliquent en partie par l'accélération de la dérive de la banquise ces 30 dernières années, qui entraine un changement de la structure multifactorielle du bruit.

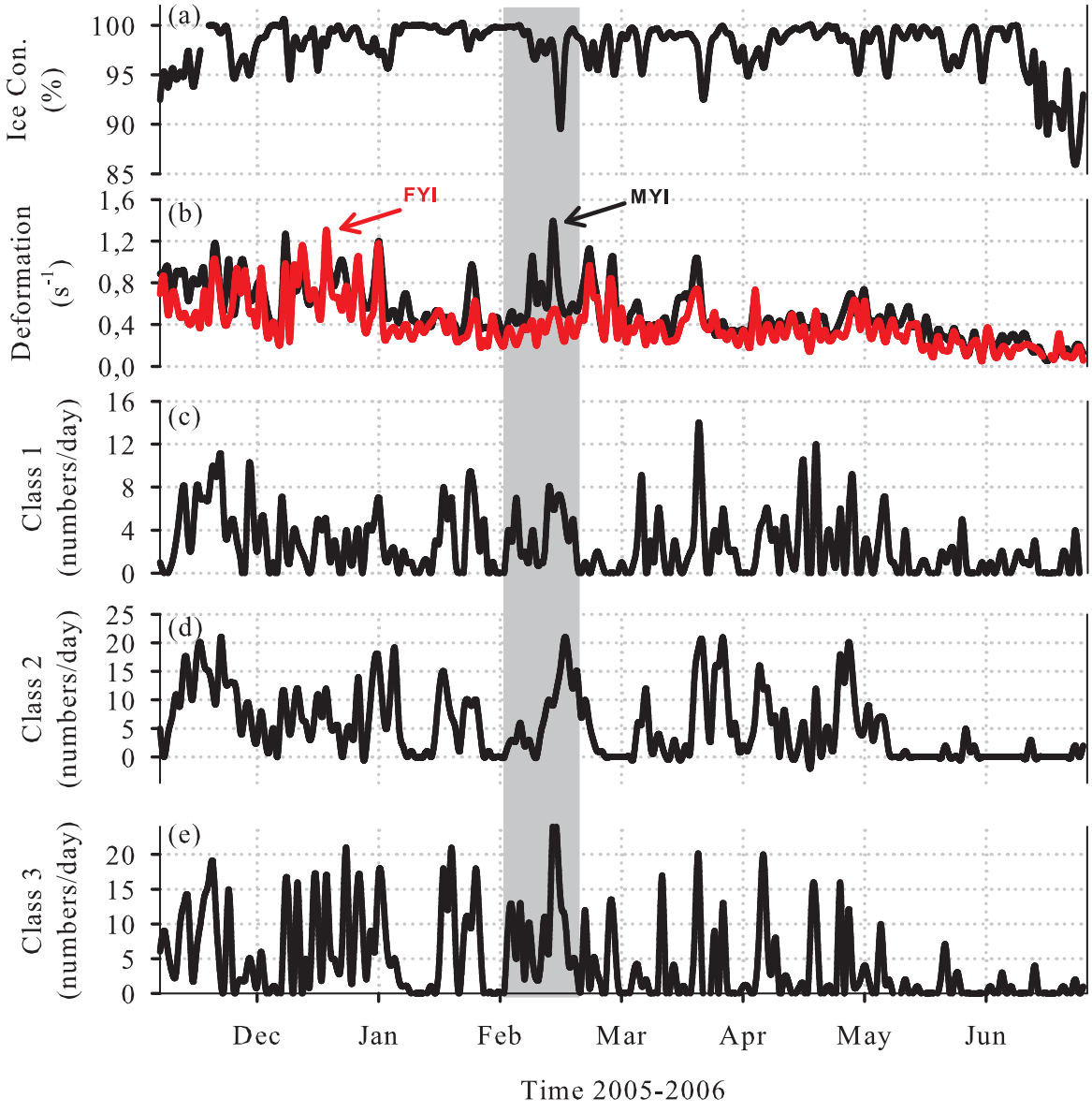

Figure 1.13: Séries temporelles des transitoires acoustiques et des variables liées au couvert de la glace dans le Golfe d'Amundsen. (a) : couverture de la glace dans un rayon de 100 km autour du point de mouillage dans le Golfe d'Amundsen ; (b) déformation de la banquise (courbe noire :glace pluriannuelle, courbe rouge :glace de première année) ; nombre d'événements observés par jours (c) : large bande, (b) : modulation de fréquence et (d) : signaux hautes fréquences.

La fonte estivale de glace expose les régions arctiques aux forçages météorologiques, avec pour conséquence une augmentation substantielle du niveau sonore de 10-20 dB.

- Divers transitoires sont liés aux déformations mécaniques du couvert de glace, qui se comporte comme une plaque à deux dimensions. Les déformations entrainent généralement des fractures aux endroits où la couverture de la glace présente des anomalies et où l'intensité de la déformation est la plus élevée. Ces processus de la déformation de la banquise à grande échelle, ainsi que les fractures produisent des sons caractéristiques facilement identifiables sur les enregistrements acoustiques.

Nous avons donc montré que le paysage acoustique de l'Arctique possède un potentiel pour la surveillance multi-échelle de la dynamique spatio-temporelle de la banquise. Le PAM présente ainsi l'avantage d'offrir plusieurs indicateurs de l'environnement sonore à partir d'une seule mesure à très haute résolution temporelle, contrairement aux méthodes classiques d'observation par satellite. La dérive, les déformations et les ouvertures de la banquise sont observées après coup par les satellites, ce qui ne permet pas un suivi de l'ensemble du processus physique. De plus, l'amincissement de la banquise et par conséquent l'augmentation de sa vitesse de dérive, va sans doute réduire l'échelle temporelle de ses déformations (fracture, ouverture, fermeture, etc.). Le PAM constitue de ce fait un moyen efficace complémentaire pour le suivi des mouvements de la glace.

1.3.6 Perspectives

Les résultats présentés ici couvrent l'année 2005-2006 pour la mer de Beaufort, et les années 2005–2006 et 2010–2011 pour la Baie d'Hudson. L'Arctique a connu deux minima record de couverture de la glace en 2007 et 2012. Une perspective immédiate s'inscrit donc dans l'étude de la dynamique de la structure du bruit océanique dans le même temps.

Les transitoires acoustiques, liés à la dynamique de la glace, peuvent servir pour localiser les points où la couverture de la glace présente des anomalies de structures, car ils constituent les points d'accumulation des déformations mécaniques de la banquise. De plus les fractures conduisant à des espaces libres de glaces interviennent à ces endroits. En mono–capteur comme c'est le cas ici, cela passe par un effort de modélisation et d'inversion. En outre, les modulations semblent être liées au mécanisme de déplacement de deux blocs de glace contigus dont une méthode de traitement appropriée permettrait d'en estimer la vitesse de déplacement.

L'océan Arctique et les mers subarctiques vont sans doute connaître une installation d'activités industrielles et de navigation commerciale saisonnière ou pérenne. Le passage du Nord-Ouest pourrait être la voie de navigation privilégiée, qui semble être aussi celle empruntée par les mammifères marins pour rejoindre l'Atlantique. La flotte maritime dans ce cas, sera sans doute similaire à celle observée dans des zones de trafic maritime intense, comme le rail de Ouessant qui voit passer 60000 navires/an. A cela, il convient d'ajouter l'activité de pêche et de tourisme dans ces zones. L'impact du bruit ambiant dans ces zones, jusqu'alors dépourvues de trafic significatif, peut être anticipé par un modèle de projection d'un trafic maritime multiforme. Les données de trafic maritime de la mer d'Iroise sont représentatives de la diversité du trafic pour une première approche. Il faut cependant considérer un modèle de propagation adapté, en tenant compte des paramètres géophysiques de l'environnement.

1.4 Production scientifique

Les travaux effectués au cours de cette thèse ont fait l'objet de publications dans des revues et des présentations orales dans des conférences nationales et internationales.

Publications

- **G. Bazile Kinda**, Yvan Simard, Cédric Gervaise, Jérome I. Mars, and Louis Fortier (2013), Under-ice ambient noise in Eastern Beaufort Sea, Canadian Arctic, and its relation to environmental forcing, J. Acoust. Soc. Am. Volume 134, Issue 1, pp. 77-87.
- Cedric Gervaise, **Bazile G. Kinda**, Julien Bonnel, Yann Stéphan and Simon Vallez (2012), Passive geoacoustic inversion with a single hydrophone using broadband ship noise, J. Acoust. Soc. Am. Volume 131, Issue 3, pp. 1999-2010.
- Cédric Gervaise, Yvan Simard, Nathalie Roy, **Bazile Kinda**, Nadia Ménard (2012), Shipping noise in whale habitat : Characteristics, sources, budget, and impact on belugas in Saguenay–St. Lawrence Marine Park hub, J. Acoust. Soc. Am. Volume 132, Issue 1, pp. 76-89.
- Cyril Chailloux, **Bazile Kinda**, Cedric Gervaise, Julien Bonnel, Yann Stéphan, Jerome I. Mars, J.P. Hermand (2011), Modelling of ambient noise created by a shipping lane to prepare passive inversion, application to Ushant case, In Proceedings of the 4^{th} Underwater Acoustics Measurements Conference (UAM 2011), Greece.
- **Kinda B.**, Gervaise C., Chauvaud L., Jaud V., Busson S., et Robson T. (2010), Sonoproxy : un capteur non intrusif du comportement de la coquille Saint Jacques, Annales hydrographiques 7, 776, 8.1-8.8
- Gervaise C., Di Iorio L., **Kinda B.**, Stéphan Y., et Josso N. (2010), Monitorage acoustique passif des campagnes d'océanographie acoustique en présence de mammifères marins : exemple de la campagne ERATO-09 Annales hydrographiques 7, 776, 6.1-6.11.

Conférences internationales

- **G. Bazile Kinda**, Yvan Simard, Cédric Gervaise, Jérome I. Mars, and Louis Fortier, Environmentally forced under-ice background ambient noise in Eastern Beaufort Sea, Canadian Arctic, 1^{st} Underwater Acoustics, Corfu, Greece, 23-28 June 2013.
- **G. Bazile Kinda**, Yvan Simard, Cédric Gervaise, Jérome I. Mars, and Louis Fortier, Under-ice transient noise in Eastern Beaufort Sea : relation with sea ice deformation,1^{st} Underwater Acoustics, Corfu, Greece, 23-28 June 2013.
- **G. Bazile Kinda**, Yvan Simard, Cédric Gervaise, Jérome I. Mars, and Louis Fortier, Under-ice noise in Eastern Beaufort Sea : ice drift forcing, fracturing and formation of leads, ArcticNet's eighth Annual Scientific Meeting (ASM2012), Vancouver, BC : Canada (2012).

- Yvan Simard, **Bazile Kinda**, Nathalie Roy, Cedric Gervaise, Jerome Mars and Louis Fortier, Global warming effects on Arctic and Subarctic underwater soundscapes and marine mammal frequentation from an acoustic observatory, ArcticNet's eighth Annual Scientific Meeting (ASM2012), Vancouver, BC : Canada (2012)
- Yvan Simard, **Bazile Kinda**, Cédric Gervaise and Louis Fortier, Annual time-series of marine mammal frequentation of Eastern Beaufort Sea from PAM methodology, IPY 2012, Montréal, Canada.
- Yvan Simard, **Bazile Kinda**, Cédric Gervaise and Louis Fortier, Removal of the Arctic ice cap by global warming : effect on underwater ambient noise and marine mammal soundscapes and communication range, IPY 2012, Montréal, Canada.

Conférences nationales

- **G. Bazile Kinda**, Yvan Simard, Cédric Gervaise, Jérome I. Mars, and Louis Fortier, Extraction et caractérisation du bruit ambiant dans l'Arctique canadien, SERENADE, Grénoble, France (2012).
- Folegot T., Gervaise C., Stephan Y., Clorennec D., and **Kinda B.**, Is received level average sufficient to describe ambient noise in heavy traffic areas ?, Acoustics 2012 Nantes - Acoustics 2012, France (2012)
- **Bazile KINDA**, Yvan Simard, Cédric Gervaise et Louis Fortier, Ambiance sonore de l'Arctique : extraction et caractérisation du cycle annuel en Mer de Beaufort, Québec Océan, Québec (2011).
- Folegot T., Gervaise C., Stephan Y., Clorennec D., and **Kinda B.**, Now casting Anthropogenic Ocean Noise in High Pressure Areas In Proceedings of the Acoustics 2012 Nantes Conference - Acoustics 2012, France (2012).

Living at the top involves a good understanding of things.

Rwandan proverb

Chapter 2

Introduction

Contents

The first chapter was dedicated to the synthesis of the thesis in French. In the following, we develop the main part of our work.

The Earth is an ocean planet with 71% of its surface covered by water, which could extend up to 85% if all water is included (oceans, lakes, rivers, wet vegetations, snow, land-ice, sea-ice) [Siedler01]. In the winter, the sea ice covers an area of up to 7% of the earth's surface [Thomas10]. Oceans play a fundamental role in the global climate balance and constitute the main reserve of the global food web. The ongoing greenhouse climate change could disrupt this balance. Polar Regions are those identified to be the most sensitive to the current changes and Arctic regions have caught the attention of the scientific community during the last 30 years. This chapter presents the Arctic Ocean in the global warming context. First, we present an overview of the Arctic Regions responses to the global warming. Second, we introduce the present study as a contribution to a better understanding of the global warming impact on the Arctic Ocean environment for the aspect concerning the ocean noise field.

2.1 The Arctic Ocean

2.1.1 Bathymetry and topography of the Arctic Ocean

The Arctic Ocean is the smallest of the word's five ocean regions, with approximative total area of 9.4×10^6 km^2 [Jones01] and covers $\sim$3% of the Earth's total surface area. It encompasses four basins in the Central Arctic (Canadian Basin, Makarov Basin, Amundsen Basin, and Nansen Basin) surrounded by seven seas (Beaufort, Chukchi, Siberian, Laptev, Kara, Barents, Greenland-Norway seas) [Jakobsson02, Dickson08]. The Arctic Ocean is also the shallowest ocean region with an mean depth of 1800 m, where shelf seas with a depth below 100 m, take up about one-third of the ocean area [Thomas10]. The Arctic is connected to the Pacific Ocean through the Bering Strait and the Bering Sea. For the Atlantic Ocean, two gateways connect it to the the Arctic Ocean. There are the Greenland-Norwegian seas through Fram Strait and the Barents Sea in the East (Fig. 2.1) [Jones01, Zhang03] and the Baffin Bay in the Southeast through a network of shallow channels in the Canadian Arctic Archipelago. The shallow channels network consists of $\sim$16 major passages that vary from 10 to 120 km in width and from a few meters to more than 700 m in depth [Archambault10, Spielhagen12]. The Fram Strait, $\sim$500 km wide, is the only deep–water passage with a depth of $>$2500 m while the Barents Sea is a shallow seaway (50–500 m) [Spielhagen12].

The Arctic Ocean presents the particularity of being covered with ice of variable thickness and age most of the year [Marsan04, Maslanik11, Marsan12, Stroeve12b]. In mid-winter (February/March) at its maximum extent, sea ice covers the entire Arctic Ocean extending from the North Pole to about 44°N in the Sea of Japan [Thomas10]. The minimum sea ice cover extent is observed in September [Thomas10, Stroeve12b, Wadhams12]. The seasonal sea ice cover in the Arctic then varies from $\sim15.5\times10^6$ km^2 in the northern winter decreasing to $\sim6\times10^6$ km^2 in the summer [Thomas10]. We then distinguish the multi-year ice (MYI) that covers permanently the central arctic and the first-year ice (FYI) which is the new formed ice covering the surrounding seas.

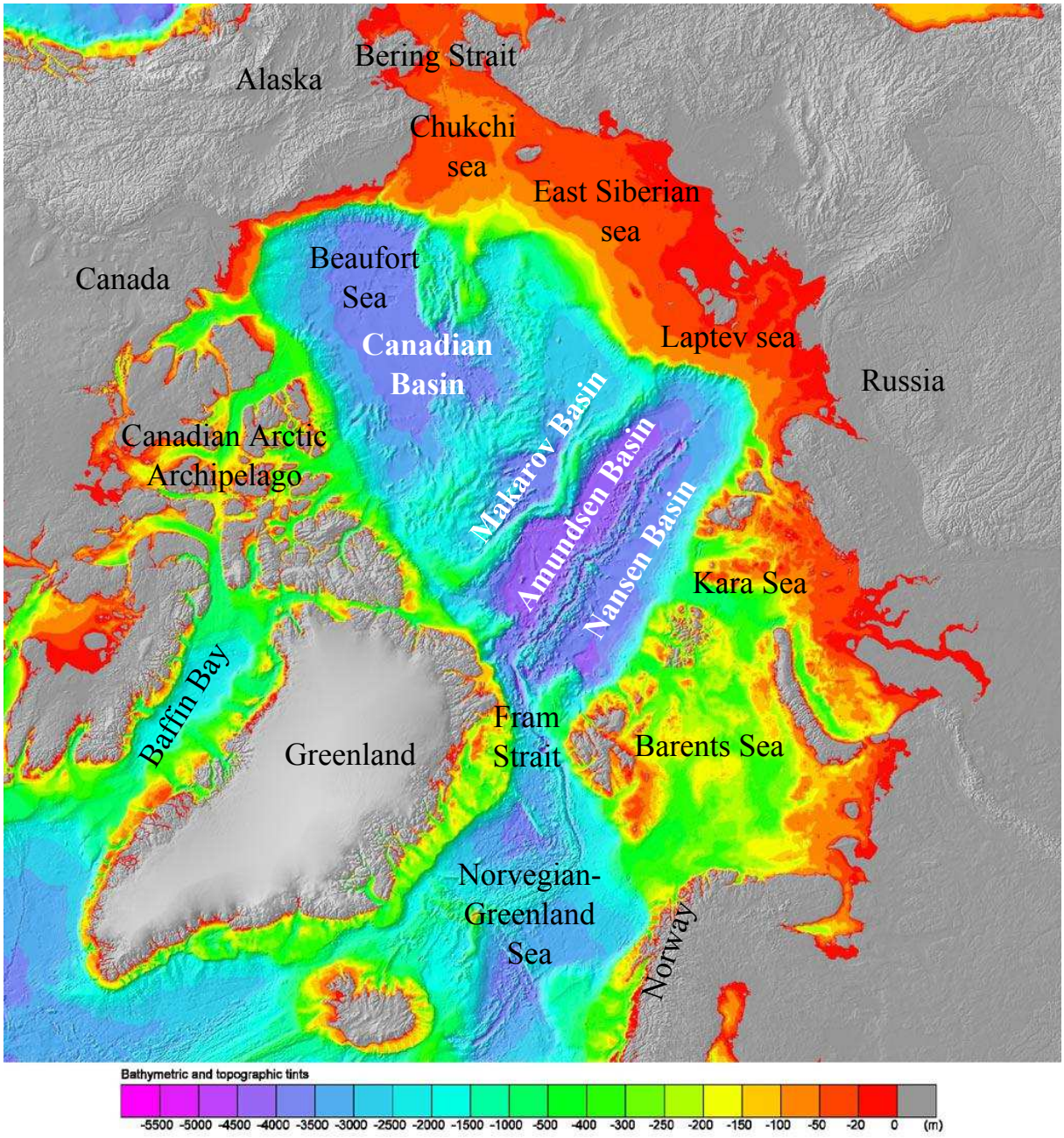

Figure 2.1: Arctic Ocean and subarctic seas showing the bathymetry. A large proportion of the Arctic is composed of shelf and slope environments. The background map is from http://www.ngdc.noaa.gov/mgg/bathymetry/arctic

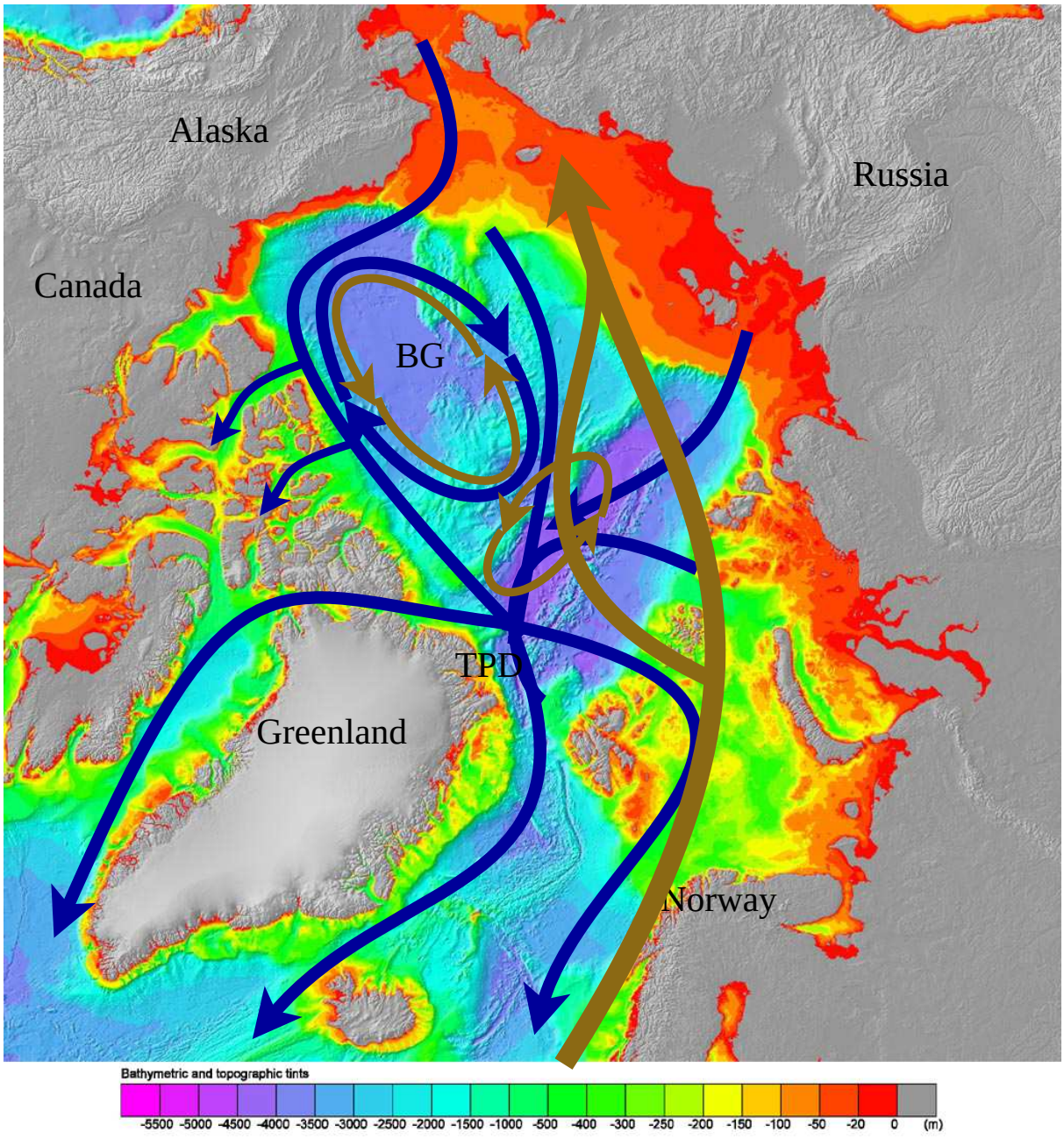

Figure 2.2: Circulation patterns in the north Atlantic and the Arctic Ocean. Brown arrows are the inflow north Atlantic and the Arctic surface circulation. Blue arrows are the inflow from Pacific and the outflow of the Arctic water to the North Atlantic. The background map is from http://www.ngdc.noaa.gov/mgg/bathymetry/arctic

2.1.2 Arctic Ocean circulation

The Arctic Ocean (Fig. 2.1) is an enclosed ocean. The upper layer circulation in each ocean basin is driven by the large-scale distribution of wind stress [Siedler01]. The Arctic circulation is structured within two main circulation patterns: the Beaufort Gyre (BG) and the transpolar drift (TPD) (Fig. 2.2).

The BG, a clockwise circulation centered at ∼(80 °N, 155 °W) [Barry93] constitutes the main circulation pattern in the Canadian Basin [Stein88, Asplin09, Lukovich09]. It contains approximately 45,000 km^3 of fresh water in the upper layer, " *a volume 10-15 times larger than the total annual river runoff to the Arctic Ocean, and larger than the amount of fresh water stored in the sea ice*" as mentioned by Proshutinsky *et. al.* [Proshutinsky02, Proshutinsky05]. The fresh water in the BG is separated from a more saline upper layer found in the Eurasian Basin (Nansen and Amundsen basins) by a primary front defining the baroclinic structure of the TPD [Dickson08].

During the winter, except the landfast ice, the Arctic Sea ice cover is in perpetual motion under five main forcings: wind, currents, Coriolis force, internal stresses, and sea ice surface tilt [Thorndike82, Barry93, Rotschky11]. The TPD, the second circulation pattern in the Arctic, tends to pile up the multi year ice (MYI) against the Canadian Arctic Archipelago (CAA) and the Greenland coasts, resulting in the thickest ice in this region of the Arctic Ocean [Barry93]. The Arctic ice is exported to the Atlantic through the Fram Strait (the main discharge gate), in the East coast of Greenland [Kwok09a, Smedsrud11, Tsukernik10]. In the CAA, the sea ice is emptying through the Straits of Amundsen Gulf, McClure and Queen Elizabeth Islands [Kwok06, Spielhagen12].

2.1.3 Arctic Ocean in the global system

The deep water circulation, called the global conveyor belt or thermohaline circulation [Siedler01], involves more complex processes over the global ocean. The deep and bottom waters produced by the polar oceans form part of this global thermohaline circulation [Thomas10]. The ice-ocean exchanges of heat and salt/freshwater appear to be crucial for this deep water formation [Goosse99]. Indeed, cold dense waters resulting from the combined effects of intense heat losses from the ocean surface to the atmosphere and salt rejection from the formation of sea ice, convect to form the deep and bottom waters of the global ocean [Grassl01] (Fig. 2.2). According to Hartmut [Grassl01] "*these water masses then spread to fill the deep ocean and volume conservation requires surface waters to flow poleward into these regions to replace this spreading deep water.*"

The Arctic Ocean than plays an important role in the Global Ocean thermohaline circulation, especially through its exchanges with the North Atlantic. Dieckmann and Hellmer [Dieckmann10] summarizes these exchanges as follows: "*In the Central Arctic Ocean, convection is restricted to the upper 50–100 m due to the strong stratification of the water column, the deeper layers being renewed by advection of water masses of Atlantic origin entering through the Fram Strait and across the Barents Sea*". The strength of the overturning circulation is related to this convective activity in the deep-water formation regions, most notably the Labrador Sea [Dickson08] which the variability is sustained by an interplay between the storage and release of freshwater from the central Arctic.

2.1.4 Arctic Ocean in the global warming context

The earth's near-surface temperature has increased by a linear trend of 0.74°C on average over the 100-years between 1906 and 2005 [IPCC07]. The rate of warming since 1976 was the most important during the last 1000 years [IPCC01]. The IPCC 2007s report also mentioned that 11 of the 12 years between 1995 and 2006 are among the 12 warmest years observed since 1850. The Arctic regions temperature has increased twice than almost any other region of the globe [IPCC07, Stroeve12a].

In the 1950s, the Arctic Ocean was sea ice covered all through the year [Langehaug13]. Sea ice controls, but is also controlled by the fluxes of heat, moisture and momentum across the ocean–atmosphere interface [Thomas10]. Indeed, the ice cover reflects 50–80% of the sun's energy, contributing to maintain the high latitudes cold [Stroeve12a]. Because it is relatively thin, sea ice is vulnerable to small perturbations within the ocean and/or the atmosphere and changes of sea ice coverage are commonly taken as an indicator for climate change monitoring [Haas10a]. Since 1979, the Arctic summer sea ice extent, often defined as the area with ice concentration $\geq$15% in a grid cell [Wang12], has declined at a rate of >11% per decade [Kattsov10]. The Arctic also experienced in the last decades, a drastic decline of its ice thickness. In the central Arctic, the sea ice has lost 40% of its winter thickness within the last 30 years, from 3.6 m in the 1980s to 1.8 m in 2008 [Kwok09b].

The climates models projection suggest that the Arctic could be sea ice free during summer season in the current century, between 2040 and 2100 [Stroeve12b, Wadhams12]. Because of the complex interactions between ice, ocean, atmosphere and Earth climate, the sea ice is a major scientific concern of this century. The consequences of a complete melting of the arctic ice are still unknown. However, some scientific evidences of the global warming at all levels in the boreal regions are already occurring, sometimes more rapid than model predictions [Walther02, Parmesan06, Soja07, Serreze07b].

2.1.4.1 Landscapes and marine ecosystems

The most visible impact of climate change is the continuous decrease in the ice cover and the reduction of snow in the Polar Regions. These changes in the recent years are accompanied by major changes in all aspects of the arctic regions, whose consequences are still poorly understood. Soja *et* al. [Soja07] noted that some scientific evidence of the transformation of landscapes due to changes in climate is mounting throughout the circum boreal zone in Alaska, Canada and Russia. The major impact and the most widespread in arctic land is the change of permafrost occurrence and distribution [Hinzman05]. Permafrost is perennially frozen ground which underlies 20–25% of the exposed land surface of the earth in regions with cold climates [Serreze00]. In the Arctic regions, the temperatures at the top layer of the permafrost have increased by up to 3°C since the 1980s [IPCC07].

Permafrost controls the local hydrography processes, as it prevents surface water from infiltrating to deeper groundwater zones, causing surface soils to be very wet [Hinzman05]. Permafrost also plays an important role in the sequestration of the carbon and the methane production [Jorgenson01]. Permafrost response to global warming depends on complex biophysical factors (*e.g.* thawing, soil, vegetation, fire), making its predictions difficult [Jorgenson10]. However, the disappearance of permafrost would result in soil drying accompanied by ecosystems reorganization, high fire frequency, and impact on latent and sensible heat fluxes [Hinzman05,

Walther02, Soja07, Henry12]. Important shifts in vegetation at the regional scale were already found in the Arctic regions, indicating an increase in plant growth [Serreze00, Henry12]. The alteration of such ecosystem moisture could result in the modification of population abundance, persistence, and distribution of the arctic terrestrial animals [Henry12, Hinzman05].

Inland water (rivers, streams, deltas, estuaries, lakes, ponds and wetlands) found across the circumpolar Arctic are major components of the Arctic landscapes ecosystems. In Arctic lakes particularly, the abundance and the diversity of biota, productivity and food web structure depend on the environmental conditions and the physical characteristics of individual lakes [Prowse06]. Future temperature increases are likely to disturb the arctic lakes physical and biological structures, such as seasonal thermal stratification, increases of total primary production [Prowse06, Wrona06], increases of propensity to deep water oxygen depletion and arrival of invasive generalist species which may alter the resident ecosystem and the lakes food web [Vincent12].

Marine ecosystems are centrally important to the biology of the planet and ongoing climate change is fundamentally altering ocean ecosystems [Hoegh-Guldberg10]. The reduction in albedo and increase in open water area would have significant effects on energy balances, atmospheric and oceanic circulation in the high latitudes [Johannessen04]. Some changes have already been observed in the 2000's in the Atlantic water at 200–900 m depth by the means of oceanographic cruises [Serreze00]. The freshening of the Arctic Ocean is expected to reduce North Atlantic Deep Water formation and then to alter the Atlantic thermohaline circulation [Peterson02, Parry07]. In the Arctic, the ongoing increase of water temperature impact the food web dynamics, from its basis (marine microbes) to the upper trophic level [Archambault10] and northward shifts in marine fish distributions have been already observed in the Bering Sea [Archambault10].

Arctic marine mammals, both the arctic historical inhabitant species (*e.g.* beluga, narwhal, polar bear, bearded seal) and subarctic species (*e.g.* potted and harp seals), are also faced with the effects of climate change and the sea ice cover reduction, accompanied by major transformations of their habitat [Laidre08]: total habitat area reduction, its fragmentation, its deterioration and the unidirectional changes on the timing of seasonal distribution and abundance of ice. Arcording to Moore [Moore08] "*the Arctic is changing so fast that despite their adaptive capacity, the survival and well-being of arctic marine mammals is a challenge.*"

2.1.4.2 Societal issues

Environmental changes in the Arctic have a direct impact on indigenous communities in the Polar Regions, who have to face it by adapting their lifestyle. In fact, shifts in the abundance and distribution of marine and terrestrial species and the Arctic thawing will necessitate further changes in traditional hunting and fishing practice [Ford04, Hinzman05, Ford06]. Climate changes will impact severely human infrastructures (high frequency of storms, permafrost thawing) in polar regions such as housing, traveling, industrial transportation routes through lakes, and pipelines [Berkes02, Ford04, Hinzman05].

The major unknown of the climate change is related to human health. Parkinson [Parkinson05, Parkinson09] postulated that "*climate change could cause changes in the incidence of infectious diseases in Arctic regions. Higher ambient temperatures in the Arctic may result in an increase in some temperature sensitive foodborne diseases such as gastroenteritis, paralytic shellfish poisoning and botulism. An increase in mean temperature may also influence the incidence of infectious*

diseases of animals that are spread to humans." The permafrost thawing and glaciers retraction are favor for migration of vectors insects such as mosquitoes [Epstein05].Parkinson *et. al.* [Parkinson09] mentioned that "*Public health capacity should be enhanced to promptly respond to infectious disease food and water-borne outbreaks.*"

2.1.4.3 Economic issues

One can also see in the Arctic sea ice melting some economic opportunities, as unexplored large areas of this region can abound large deposit of fossil energies (gases and oil) and other mineral resources. Some explorations have already been done in the Canadian Arctic Archipelago where natural gas reserves and small oil reserves were discovered between 1961 and 1986 [Masterson13]. The Arctic regions petroleum potential are well summarized by Nassichukby *et* al. [Nassichuk83] as follow: "*The Arctic Slope of Alaska has hydrocarbon reserves evaluated in the order of* 1.6×10^9 m^3 *of oil and* 750×10^9 m^3 *of natural gas. Recoverable reserves for the Beaufort Sea-Mackenzie Delta region of the Arctic Coastal Plain are tentatively considered to be* 0.15×10^9 m^3*. The potential natural gas reserves for the Beaufort Sea-Mackenzie Delta region are in the range of* 0.25×10^{12} m^3*. The Sverdrup Basin has yet to have significant reserves of oil indicated but the potential reserves of natural gas range from a minimum of* 0.45×10^{12} m^3 *up to what will probably prove to be more than* 565×10^9 m^3 *with effective delineation drilling. The Franklinian Geosyncline contains both oil and gas but no significant reserves have been developed. The undiscovered resource potentials of the Arctic Slope and contiguous Arctic Coastal Plain of Alaska have been estimated to have median values of* 3.0×10^9 m^3 *of oil and* 1.39×10^{12} m^3 *of natural gas.*" To these reserves, one must take into account the oil reserves in the Russian Arctic predominately in the Barents, Laptev, Siberian, Chukchi, Kara, provinces [Kontorovich10].

Some of the largest unexplored geological basins for hydrocarbon development are located in offshore seasonally ice-covered shelf-areas of the Arctic [Heide-Jørgensen13]. The natural gas and oil reserves in the north of the Arctic Circle have been estimated to be respectively 30% and 15% of the world's undiscovered fossil energies on the basis of probabilistic geology-based methodology. Undiscovered natural gas is three times more abundant than oil in the Arctic and is largely concentrated in Russia [Gautier09]. These reserves were also shown to be offshore under less than 500 m of water, but deep-water ($>$ 2000 m) reserves discoveries is also plausible and two thirds of Canada Basin lies in the oil or gas windows [Grantz12]. Other mineral resources had been identified in the Arctic Regions [Safonov10, Dobretsov10]: nickel, platinum, uranium, chromium, copper, diamond, manganese, gold, antimony, tin, tungsten, and rare metals.

Another economic aspect, and not the least, is the Northwest Passage, a shipping pathway that connects the Atlantic and Pacific oceans through multiple small waterways in the Canadian High Arctic Archipelago [Heide-Jørgensen12]. In September 2007, when the Arctic Sea ice area was extremely low, this shipping pathway was opened up [Field12, Stroeve12a]. The north hemisphere countries see this passage as an opportunity for their international commerce development. In fact China is for example 4000 nautical miles closer to the European Union and the East coast of North America sailing through the Arctic Ocean [Hong12].

2.2 Marine soundscape and passive acoustic monitoring (PAM)

2.2.1 Marine soundscape

A soundscape is defined as a collection of sounds from multiple sources including biophony, geophony and anthrophony that creates acoustical patterns in space and time [Pijanowski11b]. Marine soundscape can then be schematically represented as in Fig. 2.3:

- Biophony is the collections of sounds produced by all organisms at a location over a specific time. In the marine environment, it refers to the sounds produced by vertebrates (marine mammals, fishes, sea birds) and invertebrates such as bivalves, crustaceans, echinoderms, etc.
- Geophony refers to the sounds originating from geophysical processes. In the mid-latitude oceans, this component is largely dominated by wind, waves, sea state and localy rain. In ice-covered waters, the ice-air interactions and the ice motion are the main physical source of ocean noise. In addition to these specific sound sources, we have sounds originating from earthquakes and volcano.
- Antropophony is generated by human activities and includes impulsive sources (*e.g.* military sonar, oil and gas exploration) and chronic (shipping noise, oil, gaz and mineral production, construction, marine renewable energies). In ice-covered waters, where industrial activities are not significant, the man-made noise contribution to marine soundscape is reduced to snow mobiles and ice-breakers.

Depending on the nature of the sources and their distances to the receiver, measurement of ocean soundscapes results in two distinct components ([Gervaise13], Fig. 2.4): the background noise and intermittent transient noises. Background noise (Fig. 2.4, set_1) is the one that prevails in the absence of identifiable sources (Fig. 2.4, set_2). Background noise then consists of the propagation of distant sources or/and the ocean surface noise.

Wenz [Wenz62] summarizes this ocean noise in three distinct noise regions in the frequency domain (Fig. 2.5). The infrasonic zone (f$\leq$10 Hz), is dominated by the noise generated by the ocean surface waves, the turbulent pressure fluctuation and the seismic background, the two latest could extend up to $\sim$100 Hz. The marine traffic noise (site dependent) covers the frequency ranging from $\sim$10 Hz to 1 kHz. The frequency band 0.2–50 kHz is dominated by the wind-generated noise, with a broad maximum within 0.3–1 kHz. Heavy rain could produce high noise that mask the effect of wind. The intermittent transients consist of the earthquakes, biologics, sea ice, local shipping and other industrial activities generating sounds.

The soundscape is therefore a characteristic of the habitat, especially for marine animals which well-being depends on the sounds they emit and/or perceive. In fact, marine animals use sound for communication and sensing their environment [Fay99, Au08]. Therefore, the efficiency of their acoustic functions (communication, echolocation, predator avoidance) can be altered by the predominance of other sound sources in the area [Simpson05, Tyack08, Clark09, Moore12, Gervaise12b].

Anthropophony have become general concern in mid-latitudes oceans [Tasker10, Boyd11]. The shipping noise has been identified to be the major contributor to the ocean noise budget since the oceans industrialization. It could have been doubled every decade from the 1960's to present in some oceanic regions [Andrew02, Hildebrand04, McDonald06, Hildebrand09, Andrew11].

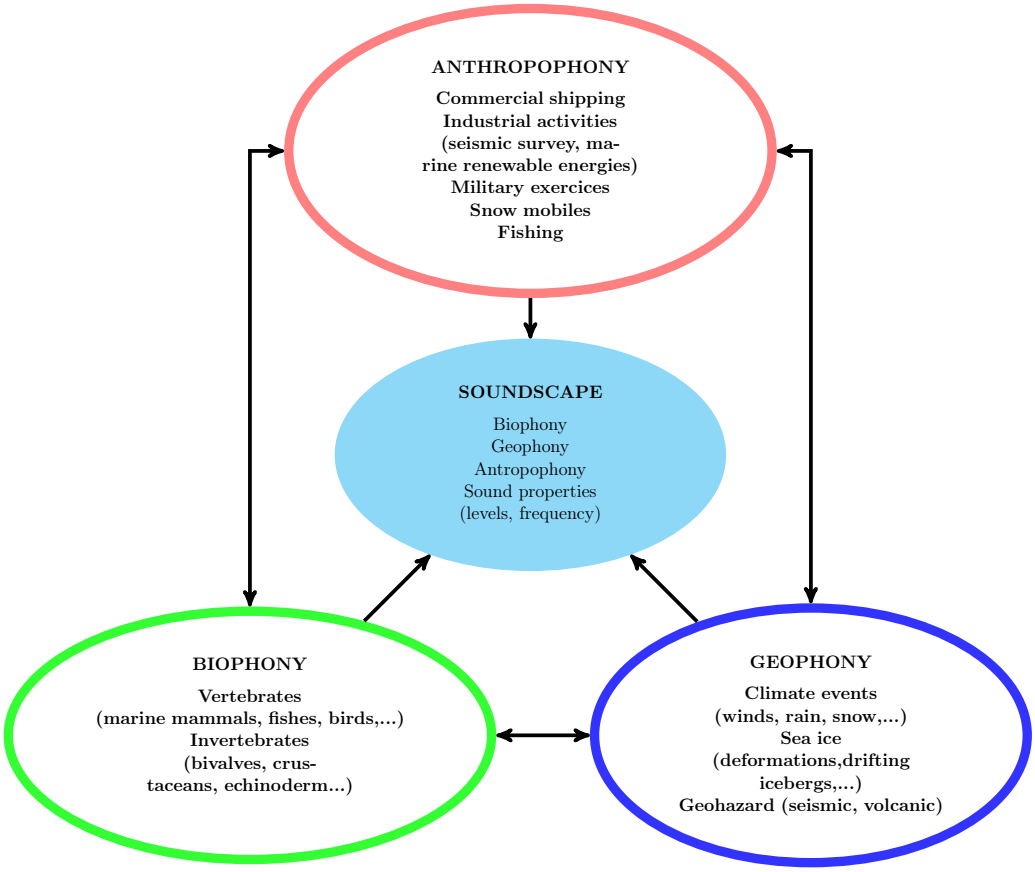

Figure 2.3: Marine soundscapes (source : Chaire CHORUS L. Di Iorio & C. Gervaise).

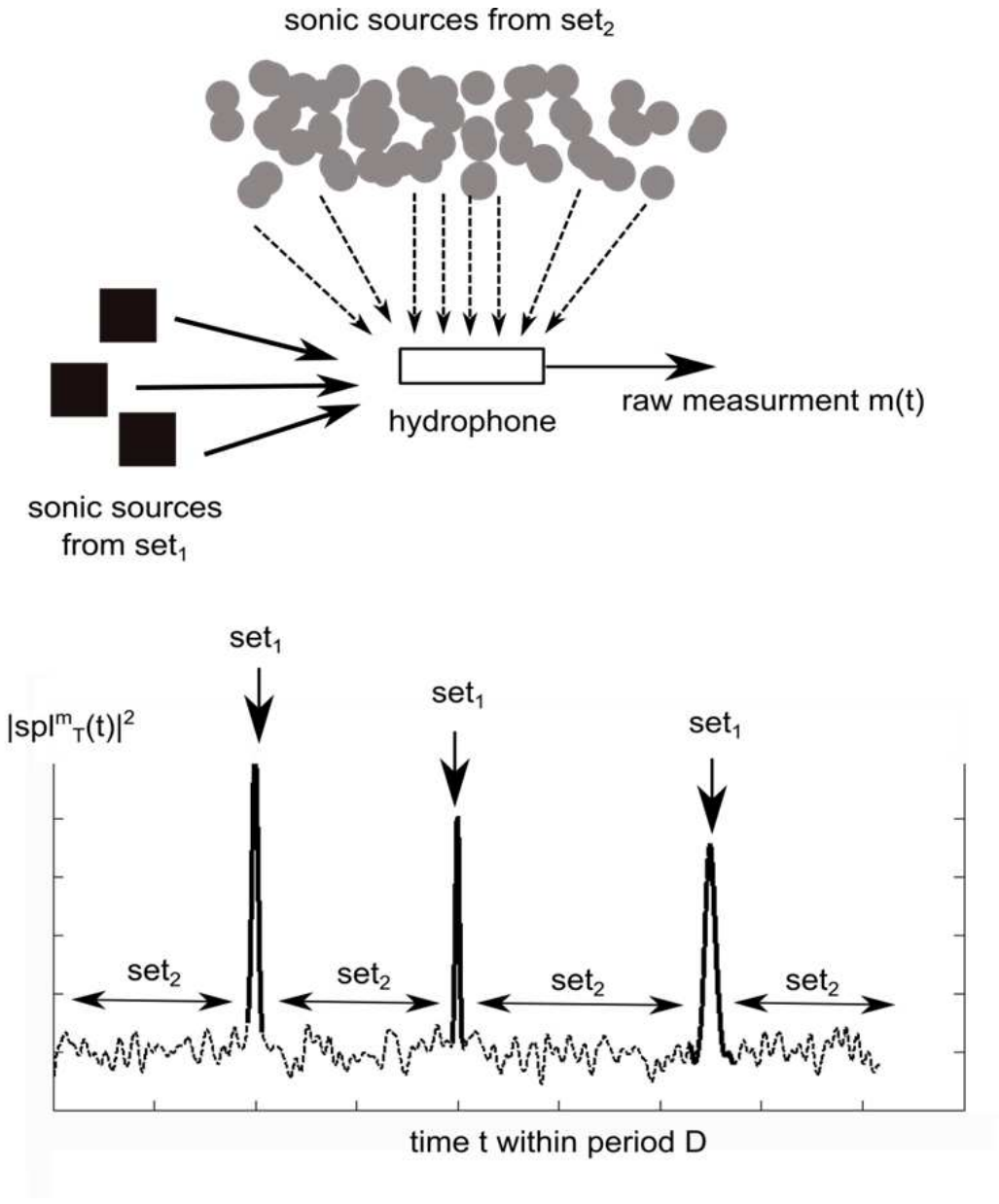

Figure 2.4: Ocean noise (marine soundscape measurement) consisting of occasional loud transient (set_2) overlaying the background noise (set_1) [Gervaise13]

The impact of the human sound sources, both impulsive (e.g. military sonar, oil and gas exploration) and chronic (shipping noise) on marine inhabitants (from fishes to marines mammals) begins to be well documented. In fact, depending on the sound sources characteristics (levels, time-frequency characteristics) the impact of noise on marine animals varies from simple discomfort [Southall08], to stress [Smith04, Rolland12], signal masking or communication range reduction [Clark09, Gervaise12b] and partial or total loss of hearing [Popper03, NRC03, Southall08, Codarin09, Halvorsen13].

To face marine pollution, regulations of ocean noise began to emerge. For example, Strategy Framework Directive for the Marine Environment requires European states to ensure a *"good noise condition"* in European waters by 2020. Good noise condition is then defined as a condition that does not adversely affect marine species. The evaluation of this *"good noise condition"* will be based on the ambient noise level in the shipping noise frequency band, and on quantities of impulsive signals in the area [Dekeling13].

As well as containing the specific acoustic signature of each individual sound source, a soundscape reflects the ecological quality of a given environment. Due to the good sound propagation in the water, ocean noise also captures some informations relative to the environment physical properties. Soundscape therefore provides an opportunity for ocean acoustic remote sensing.

2.2.2 Passive acoustic monitoring methodology

Ocean noise consists of intermittent acoustic transients overlaying background noise (Fig. 2.4). Passive Acoustic Monitoring (PAM) is one of the methodologies used in ocean monitoring. PAM consists in the characterization of the ocean soundscape to retrieve the ecological quality of an ocean region (marine animal, ambient noise). For example, the acoustics method have become widespread for marine life observation [Mellinger07, Marques09, Di Iorio12, Mathias13] and the monitoring of human activities [Andrew11, Gervaise12b]. PAM methods are also involved in the characterization of the physical processes in the ocean. As an example, Ma and Nystuen have proposed a series of methods to characterize the rainfall using their specific spectrum. Their method included rainfall detection and measurement [Nystuen86, Nystuen00, Ma05a] and the drop size statistical distribution [Nystuen96]. Finally, the ocean physical properties can be retrieved by passive way [Gervaise07, Gervaise12a].

The recent development of effective technical means [Sousa-Lima13] of sea noise recording allows long-term ocean monitoring. Although the soundscape measurement is informative of the environmental physical properties and the noise sources, strong skills in signal processing are required to achieve this objective. The PAM processing can then be decomposed into four actions, following Fig. 2.6.

- **Action 1**: Ocean noise can sometimes be merged with "non acoustic noise", resulting from the recorder and the mooring configuration. The first action is to clean the recordings from these contaminations. This is explained in detail in the sec. 4.1.2.
- **Action 2**: After cleaning the raw data, the ambient noise component is estimated. Ambient noise is assumed to be stationary for relatively short period ($\sim$10 min) and can be estimated from the ocean noise in the time-frequency domain (see sec. 4.1 for more details). The transients, which are generally loud, can then be detected by defining a threshold based on a predefined acceptable probability of false alarm and the ambient noise level. The

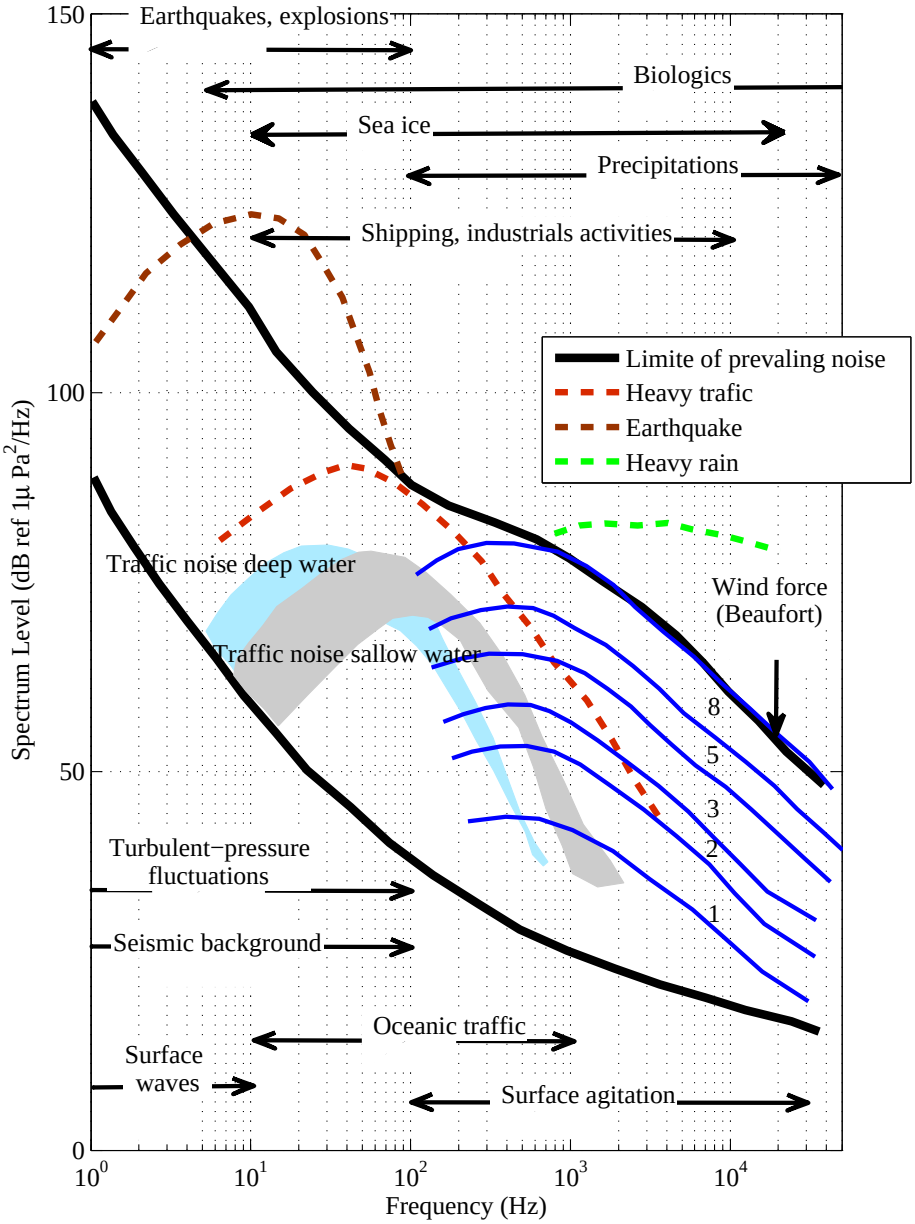

Figure 2.5: Wenz Ambient noise spectra [Wenz62], showing the different contributions to the ambient noise in the ocean. The infrasonic zone is dominated by surface wave, the low frequency by the shipping noise and the low to high frequency by surface agitation. Some occasional sound can dominate locally the ambient noise spectra.

transient detection will not be discussed further in this thesis. Action 2 produces the time series of each ocean noise component, from wich some characteristics could be extracted. They also serve as entry for the next step of the analysis.

- **Action 3**: In this action, statistical analysis, including correlations and principal component analysis are undertaken to highlight the environmental drivers of the soundscape. To do so, acoustic descriptor are examined in regard with environmental data (see sec. 4.3).
- **Action 4**: The last action in PAM processing is the retriaval of the oceanic and geoacoustic parameters (water temperature, water and bottom sound speed, etc). This step involves modeling effort and inverse problems solving. This action will be discussed further in the annex.

Passive acoustic is consequently suitable for the ocean monitoring, particularly for harsh environments, among which Polar Regions. In the following, we present PAM in the Canadian Arctic Context.

2.3 Canadian Arctic monitoring

2.3.1 PAM in the Canadian Arctic context

The evidence that the Arctic is undergoing rapid changes emerged in the 1990's [Serreze07a] characterized by the sea ice decline [Stroeve07, Stroeve12b] and the Arctic Ocean seems to inexorably become ice free in September [Mahlstein12]. The Passive acoustics monitoring (PAM) observatories are part of the large project in the ArcticNet program **Long-Term Observatories in Canadian Arctic Waters**, which aims to monitoring the physical, biological and geochemical properties of the Canadian Arctic waters. Archambault *et* al [Archambault10] noted that 52 of the 125 extant marine mammal species worldwide occur in Canadian Oceans including representatives from all major taxa, except sirenians and river dolphins.

In the past, the spatial and temporal distributions of these marine mammals were based on their direct observation in Canadian waters. The particular harsh weather conditions during the winter in the Arctic make these data very fragmented. Continuous marine marine mammal monitoring is now a major need in such regions. Some marine mammals, whales for example, may benefit from the changes that occur with climate disruption, resulting in foraging opportunities (abundance of prey and foraging period extension) [Laidre08, Commission09, Thomas10]. The sea ice cover reduction also supports exchange of marine organisms between the Atlantic and the Pacific oceans through the network of oceans channels in the Canadian Arctic Archipelago [Heide-Jørgensen12]. Underwater acoustic recorders (Fig. 2.7, Table 2.1) are then used to passively monitor marine mammals by the means of their specific vocalizations. It is useful and efficient to understand the effects of climate change on their habitat use and annual migrations.

The acoustic recordings used in the present study consist of 13-mouth (384 days) data in the Amundsen Gulf month from September 09, 2005 to October 2, 2006, Western Arctic (71°0.42' N, 126° 4.48' W), and two sets of 12-mouth time series in the Southeastern Hudson Bay (24.47' N, 77° 55.79' W) from October 1, 2005 to September 13, 2006 (347 days) and from July 16, 2010 to September 13, 2011 (424 days). Some AURALs (Autonomous Under Water Recording and Listening, Multi-Electronique Inc., Rimouski, Qc, Canada), were attached to oceanographic moorings, and were set up to sample the 16-bit digitized signal at 8192 Hz, for

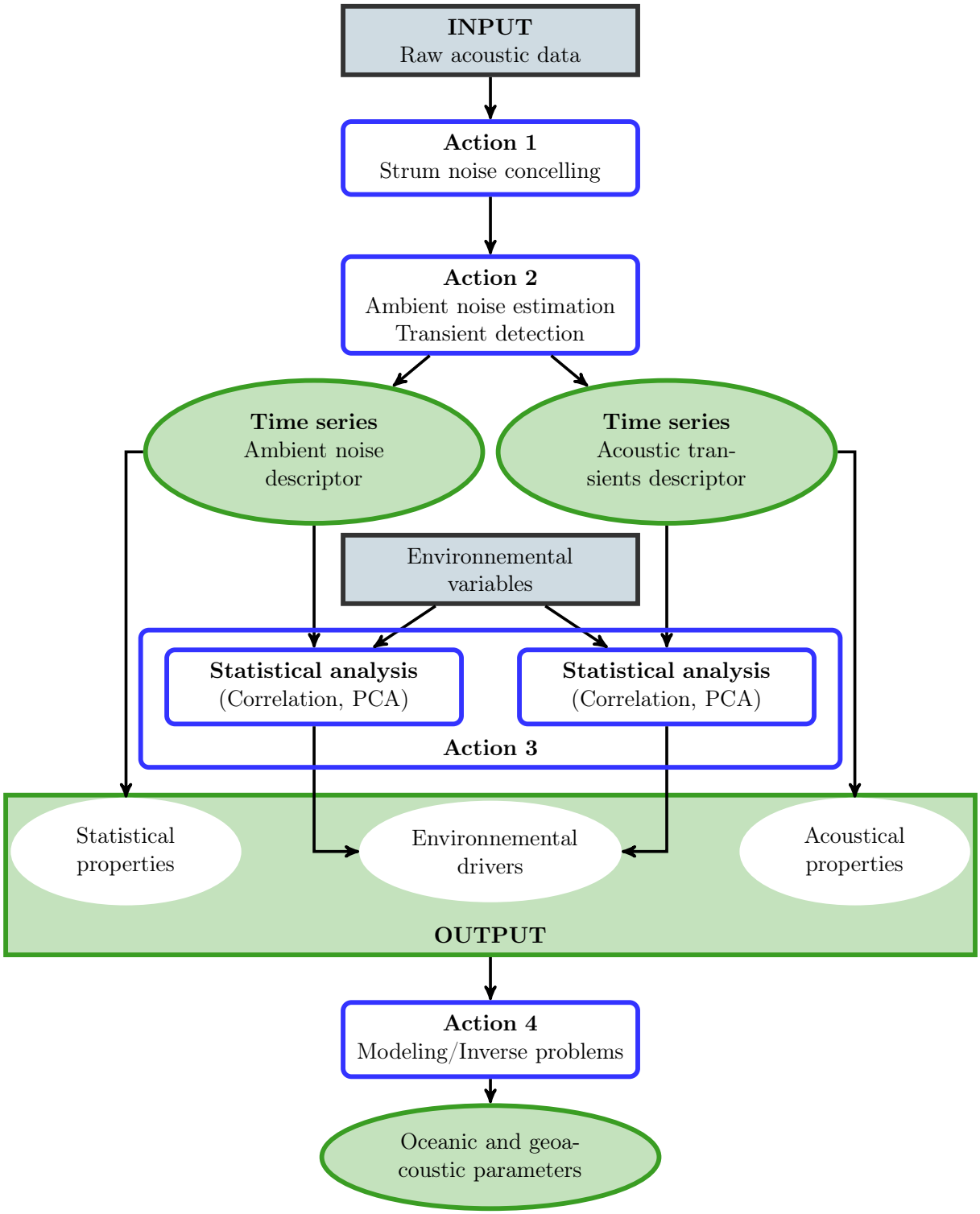

Figure 2.6: Conceptual diagram of passive acoustic monitoring processing.

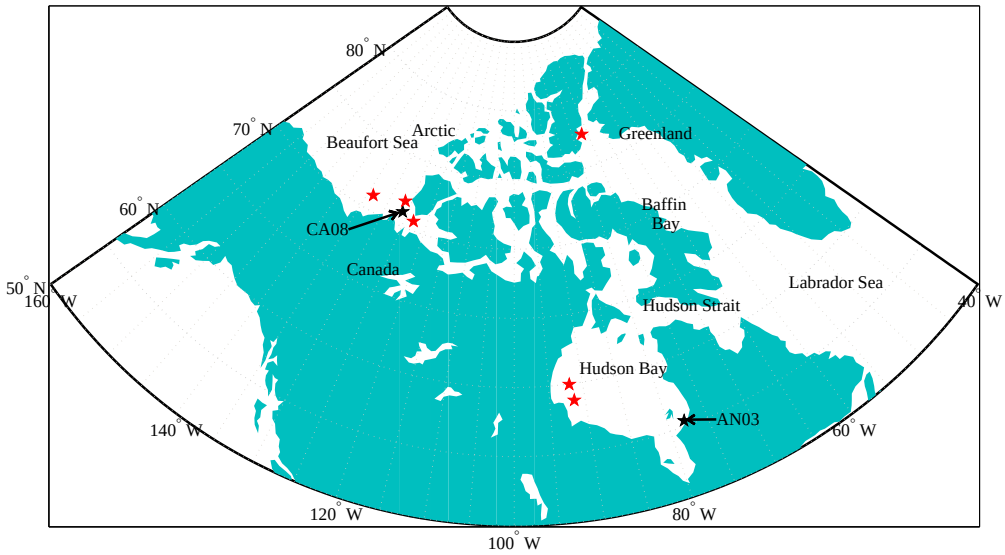

Figure 2.7: Passive acoustic moorings in the canadian Arctic and sub-arctic seas from 2005–2011. The black stars denote the data described in table. 2.1

7 or 10 min every hour, with a gain of 16 or 17 dB. An anti-aliasing elliptic filter of 8^{th} order is used in the AURAL recorder, which ensures a bandwidth from 0 to the half of the sampling rate. The receiving sensitivity of the HTI 96 MIN (High Tech Inc, Gulfport, MS)[1] hydrophone used with the AURAL was obtained from experimental calibration by measurements made at the Defense Research and Development of Canada - Atlantic calibration facility (Darmouth, NS). The receiving sensitivity is flat at -164 $\pm$ 1 dB re 1V μPa^{-1} over the measuring bandwidth. The hydrophone and the amplification setting used (17 dB) produce a self-noise of $\sim$ 0.06 % of the dynamic range, which corresponds to white noise floor of $\sim$ 53 dB re 1 μPa^2 Hz^{-1} from 0 Hz to 4096 Hz . The instrument also recorded its depth and the water temperature at the beginning of every duty cycle. In Western Arctic, recordings were done at a depth of $\sim$ 50 m from the surface, and bottom depth was 397 m. In Southeastern Hudson Bay, it was $\sim$50 or 40 m in a shallow water context (bottom depth 130-135 m).

The acoustic data were provided by Pr Yvan Simard, Chair of Fisheries and Oceans Canada in marine acoustics applied to the ecosystem at the Institute of Marine Sciences - University of Quebec at Rimouski (ISMER-UQAR).

2.4 Objectives of the thesis

2.4.1 Objectives

Arctic soundscapes are likely to undergo two rapid changes, accompanied by a possibly sudden and substantial increase of the ocean noise level. On the one hand, the Arctic sea ice melting will expose the ocean surface to the weather forcings. On the other hand, the development of the

[1] http://www.hightechincusa.com

Table 2.1: Summary of acoustic data used in this study (Wd: water depth; Ad: Autonomous recorder depth; BS: Beaufort Sea; HD: Hudson Bay.)

Station	Longitude	Latitude	Wd (m)	Ad (m)	begin (UTC)	End (UTC)	Fs (Hz)	T/cyle (min/h)
CA08 (BS)	126°4.48 W	71°0.42 N	397	50.9	09/09/2005	02/10/2006	8192	7
AN03 (HB)	77°55.7939 W	55°24.47 N	130	54.1	01/10/2005	13/09/2006	8192	7
	77°55.7046 W	55°24.4388 N	130	46	14/09/2006	09/08/2007	8192	7
	77°55.8283 W	55°24.4858 N	136	48	10/08/2007	03/10/2008	8192	10
	77°55.8283 W	55°24.4858 N	136	48	16/07/2010	13/09/2011	8192	10

Arctic and subarctic resources seems to be indispensable in the future [Dobretsov10]. This development includes the construction of ports, gas and oil exploration, their extraction, and their transportation by ships. The latter activity will intensify marine traffic through the Arctic Ocean and Subarctic seas, including the Northwest passage opened up in 2007 [Field12, Stroeve12a]. The effects of industrial activities on some arctic marine species are already the object of concerns. As example, Heide *et* al. [Heide-Jørgensen13] observed several narwhals entrapped by ice consequently to seismic exploration. The climatic impact of global warming will thereby accompanied by an ecological impact.

Within the ArcticNet program, long term ocean noise time series were recorded in the Canadian Arctic and Subarctic seas. These data are important for understanding the polar region soundscapes in the global warming context. Some obvious questions then arise: what metrics can be extracted from long term passive acoustic recordings? Are these metrics informative and relevant for monitoring the polar regions?

Our purpose is to contribute to the understanding of the Arctic pristine soundscape and then to contribute to answer these questions. We are particularly interested in the geophony component of Arctic soundscapes through the two following objectives:

- The identification of the relevant environmental drivers of some ambient noise time-series. This includes the characterization of the annual cycle of this ocean noise component depending whether the mooring area is free or ice-covered. By ambient noise, we mean the background noise exclusive of identifiable transients.
- The identification and the exploitation of the acoustic transients encountered in ice-covered area. We focus on the transient related to the mechanical behavior of the ice cover. We aim to improving the observation and understanding of this transient generation mechanisms, and evaluating the potentiality of PAM to be a complementary method for Arctic Ocean monitoring, specially its ice cover dynamics.

To meet these objectives, some signal processing and statistical methods were developed jointly at ENSTA Bretagne, GIPSA Lab (French) and at the Institute of Marine Sciences (Canada). The acoustic recordings of table 2.1 were used, in combination with meteorological, oceanic and sea ice data.

2.4.2 Outlines of the thesis

The manuscript is organized as follow:

The next chapter proposes an overview of the Arctic Ocean noise research, including the characterization of the sound sources, the spatial coherence and the environmental forcings.

The third chapter deals with the ambient noise, exclusive of acoustic transients. Our noise estimation algorithm is presented, and the ambient noise is seasonally analyzed. When the environment was ice-free, the ambient noise was essentially driven by wind speeds, and was about 10 to 12 dB above the levels observed under the ice cover in the Amundsen Gulf and the Hudson Bay. When the measurement area was ice-covered, we combined Arctic Ocean sea ice dynamic (ice drift, currents), the meteorological data (wind, air temperature and pressure) and the acoustic recordings to highlight the environment drivers for the chronic background noise. We will show that the ambient noise level in the Amundsen Gulf responded to the large-scale circulation of Beaufort Gyre and to the local passage of depression.

The forth chapter is devoted to the analysis of the acoustic transients relative to physical processes observed in the Amundsen Gulf. This analysis includes the determination of their time-frequency contents and their connection with the physical behavior of the moving ice body in the Arctic. We will show that some of these transients can be attributed to the ice fracturing, others to the ice shear deformations and to the wind effects on the refreezing ocean surface when leads opened.

The last chapter concludes this thesis by summarizing the essential results and presents the future research perspectives to full understand the Arctic Ocean noise production mechanism.

Chapter 3

Arctic Ocean noise: background

Contents

The presence of an ice cover is responsible for particular underwater ocean noise characteristics in comparison to the open water conditions. The underwater ocean noise then depends on the characteristics of this ice coverage such as spatial extent, thickness, its mechanical behavior, and its seasonal aspect. In September, when the ice coverage extent reaches its minimum, three distinct oceanic environments are present in the Arctic Ocean: the pack ice in the Central Arctic, the marginal ice zone (MIZ) and the open water environments. The MIZ is a transition area between the pack ice and the open water environment consisting of a mixture of water and ice with variable distribution. We will focus on a brief review of the under-ice physical noise transients, their relationships with the environmental variables and the particular case of the MIZ.

3.1 Under ice Ocean noise sources

The ice sheet is the most important noise source in ice-covered waters. The ice cover, an interface between the atmosphere and the ocean, undergoes mechanical deformations under both internal and external forcings. Arctic Ocean noise is then seasonal, depending on the sea ice characteristics (continuous, broken, moving or shore-fast), the air temperature and the speed of the wind [Urick84, Lewis88].

Noise from mechanical behavior, thermal cracking and wind generated-noise is presented below.

3.1.1 The thermal cracking

Since the work of Milne and Ganton [Milne64], winter and spring Arctic Ocean noise is known to be the sum of a background component and an impulsive noise, endowing Arctic Ocean noise as a nonstationnary process in time regard to both amplitude distribution and pressure spectrum [Ganton65]. Under continuous ice sheet, (winter period in the Arctic Ocean and subarctic seas), the primary under-ice sources of impulsive noise is the response of the ice cover to the atmosphere cooling, known as thermal cracking. Acoustic transients from such events are very short bursts consisting of a decaying sinusoid, lasting few milliseconds, and which spectrum has a broad maximum in the 0.1–1 kHz decade [Ganton65, Urick84]. Thermal cracking acoustic events are also high-energy impulsive, having a peak pressure of about 40 dB or more above the background level [Milne64]. Cummings *et al.*, showed that in very shallow water, thermal cracks average spectrum level was 79 dB with 0.1–0.3 s duration including reverberation. The cracks energy also extended up to 10 kHz, with peak in 400-900 Hz [Cummings89]. The thermal cracking themselves occur at the top few centimeters of the ice sheet where the maximum thermal stress is found [Ganton65] decaying exponentially with depth [Xie91] and running for distances of the order of meters or tens of meters [Xie91, Zakarauskas91].

Using synthetic aperture radar (SAR) images, air photography, *in situ* measurement of meteorological data (wind, air temperature) and an array acoustic recordings near the boundary of two quite distinct ice fields (first-year ice of $\sim$1.75 m and multi-year ice), Xie and Framer [Xie91] spatially localized the ice cracking events origins and showed that most of the cracking occurred into the multi-year ice. Indeed thermal cracking requires low temperature and atmosphere cooling, and low salinity [Zakarauskas91], which are found in the MYI. Xie and Farmer also showed that the direct paths of cracking signal has a frequency range of 100–300 Hz while

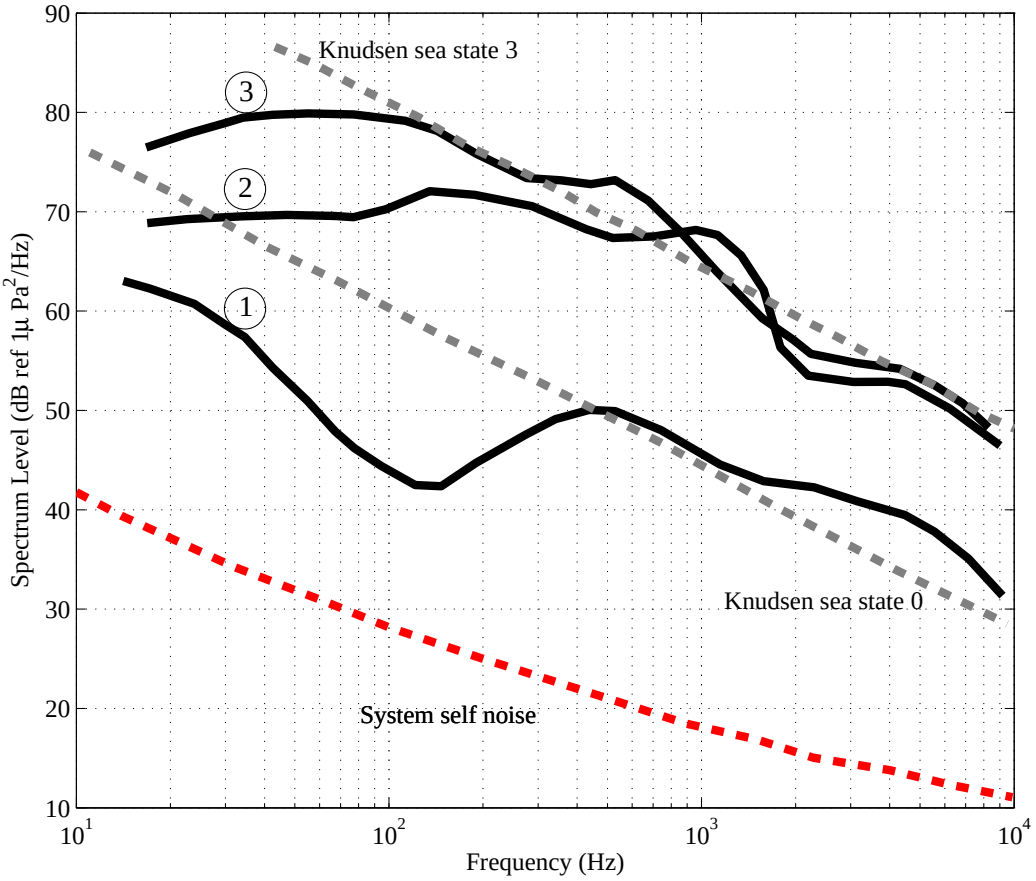

Figure 3.1: Spectra of ocean noise recorded by Milne and Ganton in February 1963 under ice pack (source: [Milne64]). 1-2: noisy period (cracking with ice cooling) and 3: quiet period without thermal cracking.

the seafloor reflected signal is centered at approximately 400–600 Hz and concluded that the ambient sound, beneath ice sheet is the sum of the direct path and seafloor reflected signal.

The spatial distribution of the thermal cracking is isotropic in the central Arctic [Greening94] and anisotropic at the margin of two distinct ice fields [Xie95]. With increasing depth below the ice, the noise spikes become more numerous and overlap in time leading the amplitudes to acquire a quasi-Gaussian distribution, in accordance with the Central Limit Theorem [Urick84, Zakarauskas91]. In the absence of ice cracking transients, the under-ice ocean noise can be very low and the noise spectrum level is about 20–25 dB below Knudsen Sea State Zero (Figs. 3.1 &3.3) [Macpherson62, Payne64, Urick84]. When a continuous ice sheet cools rapidly, the noise level in the Arctic becomes some 20 dB greater than Knudsen Sea State Zero, so as to reach the levels of Sea State 3 or 4 in open water (Fig. 3.1) [Urick84]. As cracks are the response of the ice cover to the thermal stress, their occurrence increases during the nighttime hours as the ice continues cooling. The thermal cracking noise has therefore a diurnal variations (Fig. 3.2) [Milne67]

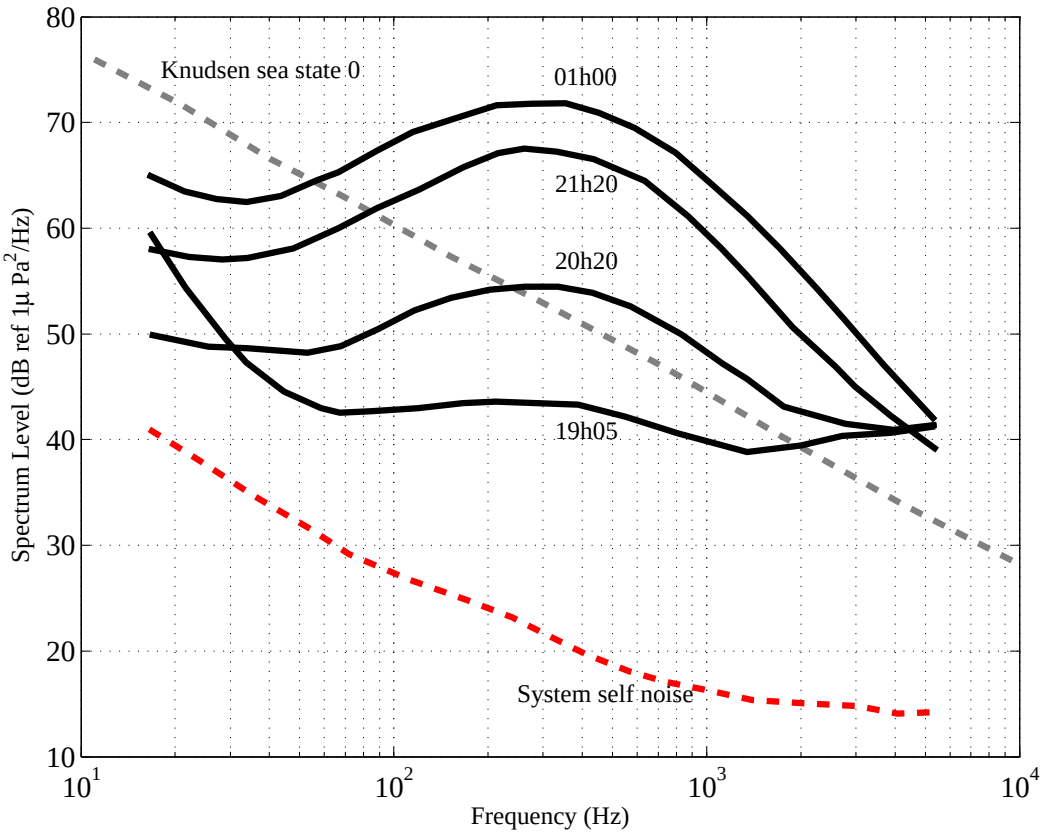

Figure 3.2: Ocean noise spectrum level during atmosphere cooling for 6 hours, from 19h00 to 1h00 (source: [Milne67]).

3.1.2 Wind-generated noise

The wind effect on Arctic underwater noise depend on the ice coverage and its characteristics. The ice broken area environment will be presented in the section 3.3. When the Ocean is continuously ice covered, the direct effects of wind on under-ice noise is reduced to its interactions with snow covering the ice surface, resulting in the background noise observed by Milne and Ganton [Milne64]. Two mechanisms are involved in wind noise production, namely its own turbulence and the displacement of the small snow and ice crystals [Milne66, Kibblewhite76].

The under-ice wind-generated noise is almost Gaussian within the frequency band 1–10 kHz (Fig. 3.3) [Ganton65, Milne67, Urick84]. The sound intensity is dependent on the roughness and the scale size of the snow particles. It was shown to be proportional to the wind speed to the 5.3 power [Ganton65] corresponding to an increase of 16 dB for doubling wind speed within the octave band 3.2–6.4 kHz. Cummings *et al.* [Cummings89] showed by measurement in the Chukchi Sea, that snow pelting over the newly frozen ice produces broadband noise (>20 kHz) which peaked at 1500 Hz, and decreased with a slope of 2.5 dB/octave. Dugan *et al.* [Dugan97] noted that the wind dependence of ambient noise near 5 m. s^{-1} was very nonlinear. They visually determine that this corresponds to the threshold speed that is required to lift the ice crystals from the surface while Ganton and Milne identified the onset of the wind speed to be 1.34–2.23 m. s^{-1}

[Ganton65].

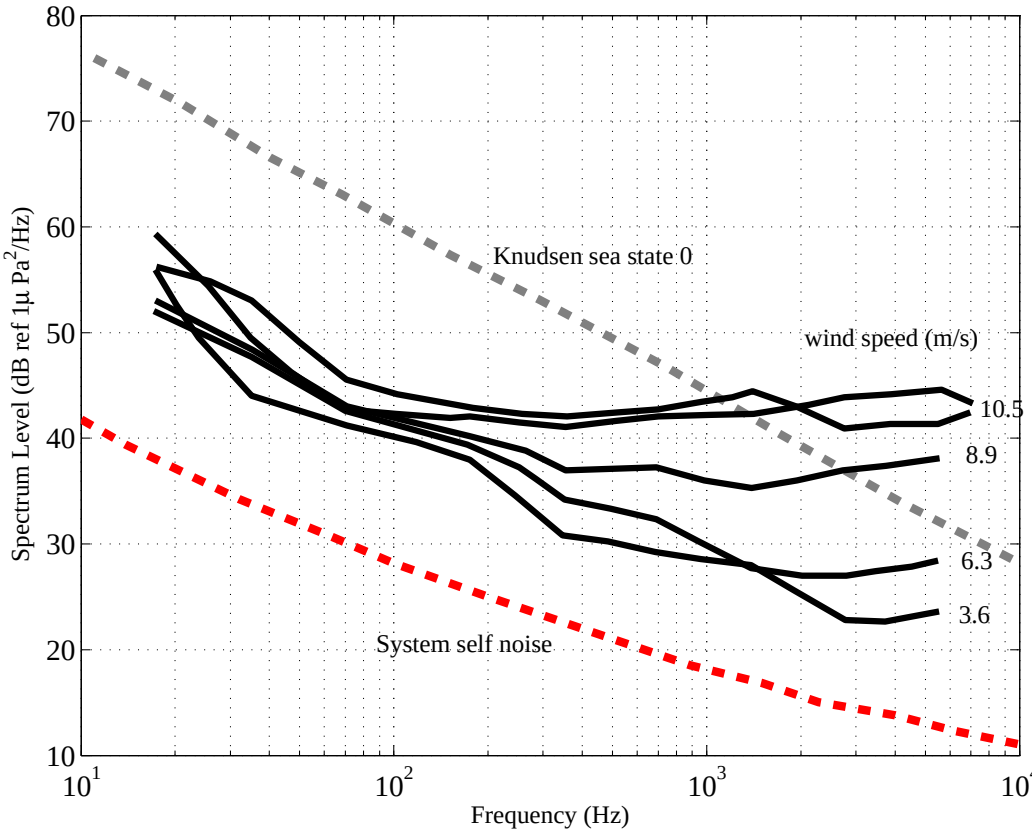

Figure 3.3: Spectra of wind noise under shore-fast ice for several wind speeds (source: [Milne67]).

3.1.3 Noise from the mechanical behavior of the ice cover

As the ice cover is in perpetual motion, it deforms under the stresses caused by the combination of wind, currents, Coriolis Force, and the surface tilt. The stresses described as shear and divergence, are generally accommodated in fracturing of the ice cover at regions where the ice is weak or the stress is important, sometimes followed by leads opening consisting of open water areas enclosed in the ice cover.

The ice break-up is accompanied by strong acoustics transients [Zakarauskas91]. Xie and Farmer [Xie92] described the entire process of landfast ice breaking. Their ocean noise was recorded beneath a 1-m thick first-year ice, in the Amundsen Gulf in the spring of 1987. The authors identified three sequential transient sounds composing the noise field produced by the ice break up. These transients were related to three phases of the ice breaking process. The first phase consists of the emission of individual sound pulses, as the ice started breaking on its weaker regions. If the stress induced by the wind and/or the current continues, the ice kept breaking and produced series of impulsive sounds radiating in the water, corresponding to the second phase of the breaking.

The last sound transient was the longest, lasting ∼25 s, and consisted of a pure tone centered at 778 Hz with a minor fluctuation. Under the wind and currents influences, the newly formed ice floes, slide longitudinally, rubbing against each other and the authors identified this floe interaction as the concluding stage of the break-up. The pure tone signal was due to the rubbing which can be described in terms of boundary value problem. The frequency of this tone then depends on the ice thickness and the shear wave speed.

Various acoustics transients are encountered in the leads areas, as they may close rapidly by refreezing or by a shift in the direction of ice-stressing mechanisms. Cummings *et al.* [Cummings89] identified, ice squeaks in very shallow water (∼32 m), caused by the ice plate movement induced by incoming swell from the lead. Ice squeaks were short events (0.5–3.2 s), and were low frequency (<2 kHz) and peaked within the 1–1.5 kHz frequency band. The impulsive collision of the ice chunks driven by the swell also creates sort acoustic transients 0.04–1.4 s, which energy peaked in the 0.01–0.5 kHz frequency band extending to 14 kHz. Buck and Wilson [Buck86] measured ambient noise at 100 m near active ice ridge over 3 days in 1979 and showed that ice-ridging produces low frequency noise of high amplitude. This kind of noise exhibits a broad maximum within the 10–400 Hz frequency band. The ridges themselves consist of parallel motion of ice floes and the pressure formed after a lead ice is pushed on the top of the floe.

3.2 Environmental correlate, space and time scale

Ocean noise in ice covered areas depends on the stresses induced by air temperature, pressure, wind, currents. Thermal cracking were identified to mostly occur in the central Arctic during cooling period and therefore, presented diurnal variation, as does the air temperature [Greene64, Ganton65, Kibblewhite76]. Makris and Dyer [Makris86] used the stresses induced by wind, currents, drift and temperature to highlight the environmental correlation with the under ice noise in the Central Arctic. The acoustics data consisted of 23.7 day recorded in April 1982 at 93 m depth, averaged over hourly intervals, in the octave band from 10–20 Hz. The authors found that the ambient noise was not correlated to the temperature stress and that the cross-correlation coefficient depends on the time series length. Indeed it was 0.84, 0.84, 0.70 and 0.76 for water, wind, Coriolis, and pressure stresses respectively for 9.9 day. When the length of the time series was extended to ∼24 days, the wind and the Coriolis stresses cross-correlation coefficient fell down to 0.71 and 0.74 respectively. It was hypothesized that some constants in wind stress calculation could be responsible of this decrease.

Lewis and Denner provided the most complete description of seasonal variability of the ocean noise in the Central Arctic and its relation to the environmental variables [Lewis88]. The acoustic recordings they examined was recorded in 1975–1976 within the AIDJEX (Arctic Ice Dynamics Joint Experiment) project, using 40 satellites-tracked buoys. The acoustic data consisted of 45-s averages sampled every 3 h in a 1/3 octave band centered at 10, 32, and 1000 Hz. The authors first calculated statistical relationships for three different periods (summer, fall, and winter) corresponding to the seasonal variations of the characteristics of sea ice in the Arctic Basin. The 32-Hz noise level showed good and seasonal correlations with the ice translation movement magnitude and its squared. In summer, these correlations were 0.82 and 0.80 for respectively ice translation movement magnitude and its squared while 0.66 and 0.56 were respectively observed in winter. The authors concluded that the summer low-frequency noise was generated by the ice rushing through the water, by the translation motion of individual ice floes in fall and was not associated with ice motion during the winter.

The summer high frequency noise was best correlated with the square of the translation movement magnitude and seems to be regional in winter. No significant correlation existed during fall. The authors [Lewis87] also measured the spatial and temporal coherence of the ocean noise for the same frequency band (10 Hz, 32 Hz and 1 kHz). Based on an e–folding criterion, i.e. when the zero-lag cross correlation between the ocean noise from two buoys or the autocorrelation at each recorder is less than e^{-1}, the spatial and time scales are summarized in Table 3.1.

Lewis and Denner postulated that there are distinct regions in the Arctic in which the temporal variations of the noise are similar. Indeed, the Eastern Beaufort Sea was then found to be distinct region in summer while the Western Beaufort Sea was found to be distinct ocean noise region in fall and winter. The 32 Hz and 1 kHz noise were found to be the noise induced by the ice motion. As the length scale tended to increase from summer to winter, Lewis and Denner suggested that ice coverage characteristics (thickness, concentration) and air temperature may play a role in ambient noise space scale. During the fall, the time scale of the lower frequency data (10 Hz and 32 Hz) indicated greater intensity noise toward the coastal regions of the Beaufort Sea. This suggested that the noisy zone is the active zone between the pack ice and the landfast ice; and that the high frequency noise (1000 Hz) seems to be the result of lateral shearing stresses between the central arctic ice driven by the Beaufort Gyre and the landfast ice. The low variability of spring temporal scale within the entire Arctic basin led to the conclusion that the entire region has close to a single signature of noise that is generated by ice motion. However, the winter noise temporal scale did not reveal a specific signature. They also found correlations with wind speed, changes in air temperature, and atmospheric pressure. Under-ice noise characteristics appear therefore to depend on multi-scale atmospheric effects acting on ice internal stress and structural integrity, and to ice drift and shearing.

Table 3.1: A summary of the results of the length scale analysis and the time scale analysis (source: [Lewis87]).

	Length scale (km)			Time scale (h)		
	10 Hz	32 Hz	1000 Hz	10 Hz	32 Hz	1000 Hz
Summer	300	440	300	7–20	12–30	15–30
Fall	325	660	170	14–27	16–26	5–19
Winter	825	775	240	25–80	24–80	3–15
Spring	440	1000	300	23–30	27–32	5–11

Although the study of under-ice ambient noise has a long history, acoustic recordings were short terms. The recent development of autonomous recorders allowed recording of acoustic data which cover the entire annual cycle.

Roth *et al.* [Roth12] recently described the seasonal dynamics of the ambient noise spectrum in the Arctic Ocean and concluded that differences in surface conditions result in distinct regimes of ambient noise. Their study was based on a year-long continuous recordings in 2006–2007 and a 50% duty cycle from 2007 to 2009. They found that, in the frequency band 10–250 Hz, the ambient noise spectra reaches their maximum in September and October, corresponding to little ice coverage in the study area. May was found to be the month of lowest noise. When the transient events were included in their analysis, the ocean noise level in winter was 5–20 dB lower than open-water conditions. The summer and fall noise was wind-dependent as revealed

by correlation computation.

3.3 Ambient noise in the Marginal Ice Zone (MIZ)

The marginal ice zone, that region where the Arctic ice–canopy becomes discontinuous, breaks up into larger and smaller foes and eventually merges into the open ocean [Uscinski99] is the most dynamic area in the Arctic Ocean. Specific sound sources are encountered in the MIZ in addition to those described in the precedent section. During the spring warming, large pieces of ice break off the edge of the ridged ice and fall into the sea, producing sharp impulses, which peak at 350 Hz [Cummings89]. This transient sounds, including reverberation, last 7.5 s.

Wave slaps were also identified to be the major noise source in the frequency band 0.2–1 kHz, and individual slaps were up to 40 dB over the prevailing ambient noise and decreased at a slope of 25 dB/octave [Cummings89].

The MIZ is a noisy zone and ambient noise levels at the ice-water boundary are significantly higher than either open water or under-ice. Diachok and Winokur provided a complete description of the ambient noise level in the MIZ (Fig. 3.4). Their work was based on a series of noise measurements made using 8 air-deployed sonobuoys during the period 1971-1972, approximately spaced 28 km in a line normal to the ice edge in the East Greenland Sea. The ambient noise level, exclusive of the spikes noise, from 100 Hz to 1 kHz was found to be higher at the ice-edge than both under pack ice and open water environments. This noise levels depend on the ice floes distribution in the MIZ, according to whether it is compact or not. The measured noise levels near a compact edge were then about 12 dB higher than open water levels and about 20 dB higher than levels far in the ice field (Fig. 3.4 a).

Near a diffuse ice edge, the noise levels were ∼4 dB higher than open water, and ∼10 dB than levels far in the ice edge (Fig. 3.4 b). When moving away from the MIZ, the decrease in the noise level was not symmetrical and more abrupt slope was generally observed under ice field.

Regardless of the ice edge compactness, ambient noise in the MIZ was dominated by the low-frequency (100 Hz, 315 Hz). The ice-water boundary acts as a spatially well-defined source of ambient noise, probably excited by waves and swells which interact with individual ice floes. Urick [Urick71] previously identified flat noise in the 0.1–10 kHz frequency band generated by icebergs when melting. The mechanism of generation of such noise was the expansion of entrapped air bubbles as they burst out of the ice or the implosion of air cavities during the melting process. The observed noise therefore depends on the size, the depth, the air content, the bubble pressure and the rate of melting of the icebergs. This component may contribute to the noise level observed by Diachok and Winokur.

By examining the noise level in the 25–50 Hz frequency band, Makris and Dyer [Makris91] found that the gravity wave amplitude explains about 86.5% of the ambient noise variance (r = 0.93). These authors postulated that gravity wave interaction with ice may then generate low-frequency noise including floes colliding, and the ice concentration is a key parameter for noise level, as high ice concentration increases the density of potential surface sound sources.

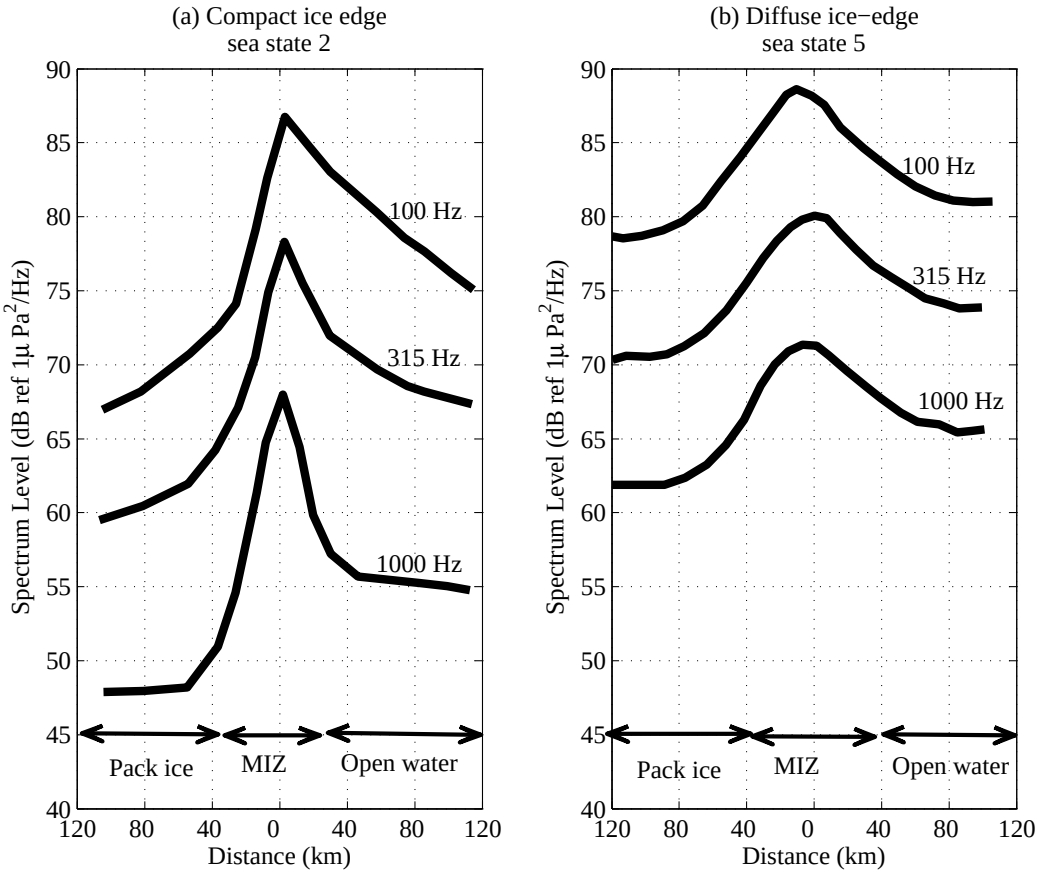

Figure 3.4: Ocean noise spectrum level at the ice-water boundary (source: [Diachok74]).

Chapter 4

Arctic pristine underwater soundscape

Contents

The footprint of the ocean industrialization, where maritime traffic is the most important component on ambient noise levels, is significant in mid-latitudes especially at low frequencies [Andrew02, Boyd11, Rolland12]. The Arctic Ocean and sub-Arctic Seas have the advantage of being devoid of significant maritime traffic and other industrial activities. However, these regions could experiment during this century the impact of the global warming, accompanied by its industrialization including the development of the maritime traffic. In this chapter, we aim to establish the initial state of the background noise level, as defined by [NRC03], in the marginal ice zone (MIZ) of the Canadian Arctic and the Hudson Bay. For the first time, the relations between ambient noise level and the environmental forcing will be addressed by PAM, depending whether the environment is ice–covered or not.

The chapter is organized as follow. The next section (sec. 4.1) presents our work on background noise estimation from the spectrogram of the ocean noise recordings, including a particular study to remove the strum noise. In sec. 4.2 we study the summer ambient noise spectra in the MIZ of the Beaufort Sea and Hudson Bay. We show for this time period that the noise spectra responded to the wind speed in the Amundsen Gulf and that the removal of the ice cover increases the ambient noise level by at least ∼10 dB. Sec. 4.3 is dedicated to the winter period for the Amundsen Gulf measurements by examining its potential links with meteorological forcing (wind, air pressure, air temperature) and oceanic forcing (current, sea ice drift). We establish that the winter ambient noise did not respond to the local environmental forcing but is mainly controlled by the same meteorological and oceanographic forcing processes that drive the ice drift and large-scale circulation in this part of the Arctic Ocean. This section is in part a reprint of the material published in the Journal of Acoustical Society of America [Kinda13]. This chapter ends with some conclusions and remarks.

4.1 Background noise estimation

4.1.1 Robust noise estimation

Robust background noise estimation is commonly encountered in signal processing as the signals of interest are generally merged with noise of various origins. Several algorithms have been then developed to isolate the useful signal from noisy measurement. For impulse signal and stationary background noise, the latest can be estimated from the measurement in the time domain by the means of all zeros filtering [Kandia06], which the z-response is given by Eq. (4.1), where a is a real number and $a << 1$.

$$H(z) = \frac{a}{1 - (1 - a) z^{-1}} \tag{4.1}$$

In the time-frequency domain, the background noise variance can be estimated under some statistical considerations. The classical statistics (median, mean) are biased estimators of the local background noise variance because they are sensitive to extreme values [Aja-Fernández09]. The median absolute deviation (MAD) is seen to be an useful alternative for the noise variance assessment, following Eq. (4.2), [Huber09, Aja-Fernández09] where $m = \{m_i, ..., m_n\}$ is a sample of the measurement, and Φ^{-1}, is the inverse of the cumulative distribution function.

$$\sigma = \frac{MAD}{\Phi^{-1}\left(\frac{3}{4}\right)}, \tag{4.2a}$$

$$MAD = median\left(|m_i - median\left(m\right)|\right) \tag{4.2b}$$

Other method based spectrogram quantile were also proposed to estimate the background noise power spectrum density [Martin01a, Evans02]. These authors assumed the lowest levels of the spectrogram to be related to the noise power in an observed time-window, in the case of noisy signal, especially in speech enhancement domain. In this section, we adopt a similar approach for estimating the background noise spectra from ocean noise recordings.

The ambient noise level, defined by [NRC03] to refer to the background noise emanating from a myriad of unidentified sources, is estimated on the basis of the assumption that the recorded ocean noise is the sum of two independent components following Eq. (4.3) as:

$$m(t) = b(t) + \mu s(t), \tag{4.3a}$$

$$\mu = \{0, 1\}, \tag{4.3b}$$

$$p(\mu == 0) \approx 1 \tag{4.3c}$$

where *b(t)* is the ambient noise, assumed Gaussian and stationary for short term observations [Urick84], *s(t)* is the additional contribution of distinguishable occasional sources exceeding the ambient noise level and the coefficient μ is a binary variable representing the presence (μ=1) or the absence (μ=0) of transients signals; the latest case having a high probability, close to 1.

The spectral density (power or energy) for a given signal $s(t)$, γ_s at frequency f is the Fourier transform (FT) of its autocorrelation function Γ_s, at the time lag τ, as:

$$\gamma_s(f) = FT\{\Gamma_s(\tau)\}. \tag{4.4}$$

Since the ambient noise and the transient signal are assumed independent, the autocorrelation function of the recorded ocean noise $m(t)$ is the sum of the autocorrelation functions of the ambient noise and the transient signals:

$$\Gamma_m(f) = \Gamma_b(\tau) + \mu^2\Gamma_s(\tau). \tag{4.5}$$

We get from Eqs. (4.4) and (4.5):

$$\gamma_m(f) = FT\left\{\Gamma_b(\tau) + \mu^2\Gamma_s(\tau)\right\}, \tag{4.6a}$$

$$= \gamma_b(f) + \mu^2\gamma_s(f). \tag{4.6b}$$

where $\gamma_m(f)$, the Power Spectral Density (PSD) of the acoustic recordings is a linear combination of two independent PSDs.

When faced with real data with finite number of measurement points, the PSD is estimated by the periodogram [Stoica97, Kay98], following Eq. (4.7)

$$\tilde{\gamma}_m(f) = \frac{1}{Nf_e} |M(f)|^2 , \tag{4.7a}$$

$$= \frac{1}{Nf_e} \left[\Re(M(f))^2 + \Im(M(f))^2 \right] , \tag{4.7b}$$

$$M(f) = [FFT] \{m(t)\} . \tag{4.7c}$$

where f_e is the sampling rate of the signal, N the window length used for the fast Fourier transform (FFT) computation, and $M(f)$ the fast Fourier transform of the measurement $m(t)$. $\Re$ and $\Im$ denote the real and the imaginary part of the FFT. In case of absence of transient noise (case μ=0), the measured PSD $\tilde{\gamma}_m$(f) is reduced to the ambient noise periodogram, which can be expressed as the sum of two squared Gaussian random components with identical marginal variances:

$$\tilde{\gamma}_m(f) = \frac{1}{Nf_e} |M(f)|^2 , \tag{4.8a}$$

$$= \frac{1}{Nf_e} \left[\Re(B(f))^2 + \Im(B(f))^2 \right] , \tag{4.8b}$$

$$B(f) = [FFT] \{b(t)\} . \tag{4.8c}$$

The periodogram $\tilde{\gamma}_m$(f) then follows a centralized Chi-2 distribution [Kay98, Koopmans74] with 2 degrees of freedom of mean and variance equal to the true PSD,(γ_m(f)). This hypothesis is based on the circularity [Huillery08b, Huillery08a] of the spectral coefficients verified in the case of white Gaussian noise.

We wish to extend this assumption to the spectrogram from the ocean noise recordings. A circularity test is then performed to verify the circularity of the spectrogram when no transient is observed. This test is described by [Ollila11] in the case of complex distribution. In fact for such distribution, the circularity quotient is given by Eq. (4.9), where ρ is the circularity quotient, τ is the pseudo–variance and σ^2 the variance of a random complex distribution Z as:

$$\rho = \frac{\tau}{\sigma^2}, \tag{4.9a}$$

$$\tau = E \left[(Z - E(Z))^2 \right] , \tag{4.9b}$$

$$\sigma^2 = E \left[|Z - E(Z)|^2 \right] , \tag{4.9c}$$

$$Z = X + jY, \tag{4.9d}$$

The hypothesis for a sample z of length n taken in the distribution Z to be circular is rejected when Eq. (4.10) is satisfied for a probability of false alarm α.

$$\frac{n |\widehat{\rho}|^2}{\widehat{\delta}_0} > \chi^2_{2,1-\alpha}, \tag{4.10}$$

where $\chi^2_{2,1-\alpha}$ is the $(1-\alpha)^{th}$ quantile of the chi-squared distribution with 2 degrees of freedom, $\widehat{\rho}$ is the maximum likelihood estimator of the circularity quotient given by Eq. (4.11) and $\widehat{\delta}_0$ is

derived from the estimated circularity quotient and the complex kurtosis following Eq. (4.12). The term $\bar{z} = 1/n \sum_{n}^{i=1} z_i$ in Eq. (4.11) & (4.12) refers to the mean of the distribution.

$$\widehat{\rho} = \frac{\frac{1}{n}\sum_{i=1}^{n}(z_i - \bar{z})^2}{\frac{1}{n}\sum_{i=1}^{n}|z_i - \bar{z}|^2}, \tag{4.11}$$

$$\widehat{\delta}_0 = \frac{\widehat{\kappa}}{2 + |\widehat{\rho}|^2}, \tag{4.12a}$$

$$\widehat{\kappa} = \frac{\frac{1}{n}\sum_{i=1}^{n}|z_i - \bar{z})|^4}{\left[\frac{1}{n}\sum_{i=1}^{n}|z_i - \bar{z}|^2\right]^2}. \tag{4.12b}$$

Each frequency bin of the FFT computed for a duty cycle of the ocean noise recordings, when transient signal were absent, is shown to be circular for $\alpha \leq 0.05$, except for the frequencies close to 0 and $f_e/2$ [Millioz11]. It is shown at the same time that the background noise is stationary because circularity is sufficient condition for strict stationary [Socheleau12], hence the assumption for $b(t)$ is justified. The spectrogram of the ambient noise component of the recordings can then be assumed to satisfy the hypothesis of being a chi-squared distribution.

We attempt to estimate the ambient noise PSD γ_m(f), from the spectrogram of a segment of the signal that produces a set of $\tilde{\gamma}_m$(t(i),f),$i \in [1, L]$. For simplicity, let the quantity $Q = \{\tilde{\gamma}_m(t_1, f)...\tilde{\gamma}_m(t_n, f)\}$ be representative of the ambient noise distribution, and γ_m(f) its variance that we aim to estimate. The PDF of such a distribution, calculated for a given value L of Q, is given by:

$$f_Q(L) = \frac{1}{\gamma_m(f)} e^{-\frac{L}{\gamma_m(f)}} U(L) \tag{4.13}$$

where U is the step function. The corresponding CDF is:

$$F_Q(L) = 1 - e^{-\frac{L}{\gamma_m(f)}} U(L) \tag{4.14}$$

The probability p associated to the p^{th} percentile (q_p) of the assessed set Q values of the distribution, is then defined by:

$$p = 1 - e^{-\frac{q_p}{\gamma_m(f)}} U(L) \tag{4.15}$$

which can be transformed in:

$$\gamma_m(f) = -\frac{q_p}{ln(1-p)} \tag{4.16}$$

The proposed method is applied to the measured acoustic recordings $m(t)$, which can contain transient signals merged with ambient noise. As transient signal have a high level relative to ambient noise, by choosing a low percentile value for (q_p) we can limit the considered set of Q values to represent only the ambient noise portion for the estimation of the variance $\gamma_m(f)$. It was found that this solution is robust for percentiles from 4 to 20.

In summary, the ambient noise PSD is estimated as follows:

- Step 1: choice of the percentile value ($0.04 \leq p \leq 0.20$);
- Step 2: choice of the signal segment;
- Step 3: spectrogram computation;
- Step 4: ascending sort of each frequency line of the spectrogram;
- Step 5: estimation of the spactral value at frequency bin f corresponding to the chosen percentile;
- Step 6: estimation of the PSD of ambient noise at frequency bin f;
- Step 7: Repeat for all frequency lines of the spectrogram.

4.1.2 Non–acoustic noise cancellation

Ocean noise can be merged with some non-acoustic noise of various origins, particularly at very low frequency, making recording of clean ocean noise in these frequency bands difficult. Strasberg [Strasberg79] identified three sources of non-acoustic noise in the infrasonic band ($\leq$10 Hz) associated with the flow of water around the hydrophone as follow: "*These sources are the pressure fluctuations generated on the hydrophone surface by turbulent water streaming past, pressure fluctuations generated by initially non–turbulent water streaming past and the "electrical" noise generated by the hydrophone because of its sensitivity to temperature inhomogeneities in the turbulent water.*" The author established an empirical formula (Eq. (4.17)) to quantify the noise spectra in the infrasonic band, where L_p is relative to $1\mu Pa$ in a 1–Hz band, U_0 is the currents speed in knots and f the frequency in Hz.

$$L_p\,(f) = 119 + 37\ logU_0 - 27\ log\,(f)\,. \tag{4.17}$$

Lewis *et* al. [Lewis87] and Buck [Buck80] later identified cables strum as contributor to the non-acoustic noise in the same bandwidth. Indeed, they postulate that "*vortex shedding causes cables to flutter and the resulting vibrations are mechanically conducted to the hydrophone element.*" Buck [Buck80] proposed a method to eliminate such contaminated noise by the means of two uncoupled hydrophones spaced at distance less than the wavelength considered in the infrasonic band. The ambient noise estimated from such method is given by Eq. (4.18), where N_a is the ambient noise level, N_1 and N_2, the noise level at the two independent hydrophones and ρ_{12} the cross-correlation between the two sensors. The correction term $10\ log\rho_{12}$ is very important in the presence of non-acoustic noise, because the two hydrophones are in the same ambient noise environment.

$$10\ logN_a = 5\ logN_1 + 5\ logN_2 + 10\ log\rho_{12}. \tag{4.18}$$

Non-acoustic noises were encountered in the data sets recorded in the Beaufort Sea and the Hudson Bay and were not confined to the infrasonic band (f$\leq$10 Hz, Figs. 4.3 a & 4.4 a). *In-situ* current measurements on the same moorings showed that the spectrum level in the infrasonic band does not verify Strasberg's formula for some identified recordings contaminated by non-acoustic noise. The interference from non-acoustic noise in our database was then from part of mooring line vibration, driven by the currents. Furthermore, the acoustic recordings were made

using a single hydrophone, from bottom mounted mooring and Buck's method cannot be simply implemented. However for such fixed mooring, the non-acoustic noises generally consist of low frequency pulses with variable bandwidth. The measurement can then be modeled following Eq. (4.19).

$$m(t) = s(t) + \mu \times b_{tr}(t), \tag{4.19a}$$

$$b_{tr}(t) = \sum \delta(t - nT), \tag{4.19b}$$

where $s(t)$ is the acoustic signal of interest, b_{tr} is the self non-acoustic (strum) noise resulting from the mooring behavior under the influence of currents. The term μ is a binary variable symbolizing the presence or absence of the strum noise.

When strum noise exists, it is assumed to be a periodic series (period T) of low–frequency pulse with duration d and bandwidth Δf. This assumption is based on the fact that the mooring line acts as an inverted pendulum, and therefore has an oscillating movement. When the contamination rate $\tau_{b_{tr}} = d \times N/T_m$ is less than 25% (Fig. 4.1), the non-acoustic noise did not require particular treatment as it falls within the general framework of the estimation described in section 4.1.1. However, beyond this threshold, the noise is overestimated and it is necessary to eliminate the time–frequency bins affected by the non-acoustic pulse.

As the strum noise is assumed to be periodic and to be low-frequency narrow-band signal, the affected time–frequency bins can be tracked. A method is then developed to detect the strum period based on these properties and to remove the affected time-frequency bins by the means of some statistical considerations. The hypothesis H_0, (i.e., strum noise is present) is rejected when Eq. (4.20) is not verified.

$$p_{value} < 0.05 \tag{4.20a}$$

$$L_1 \sim \sum \delta(t - nT) \tag{4.20b}$$

where p_{value} is the critical probability of the cross-correlation described by Eq. (4.21)

$$\Gamma_{1,i} = E\left[\left(L_1 - \bar{L_1}\right)\left(L_i - \bar{L_i}\right)\right] \tag{4.21}$$

L_1 is the spectral level taken in an infrasonic band, and L_i the spectral level taken in a higher frequency band computed from the spectrogram of a duty cycle recording.

The term Eq. (4.20a) measures the spectral levels coherence in the infrasonic band, and in higher adjoining frequency bands, whereas Eq. (4.20b) is used to determine the periodic nature of the infrasonic band spectral level, by the computation of its Fourier transform. In fact, the pulses in the time series are reflected in the frequency domain with the same period depending on the window size and the overlap used for the spectrogram computation. This results in a periodic signal in time which Fourier transform shows a Fourier series with peaks located at $f = n/T$, where T is the period of the pulses. The fundamental frequency (n=1) then allows the estimation of the period T and the contamination rate. Under H_0 and under the assumption of low-frequency narrow band non-acoustic noise, the limit of contamination bin F_{limit} is reached when Eq. (4.20a) is no longer verified. Once theses parameters are determined, one proceeds as follow:

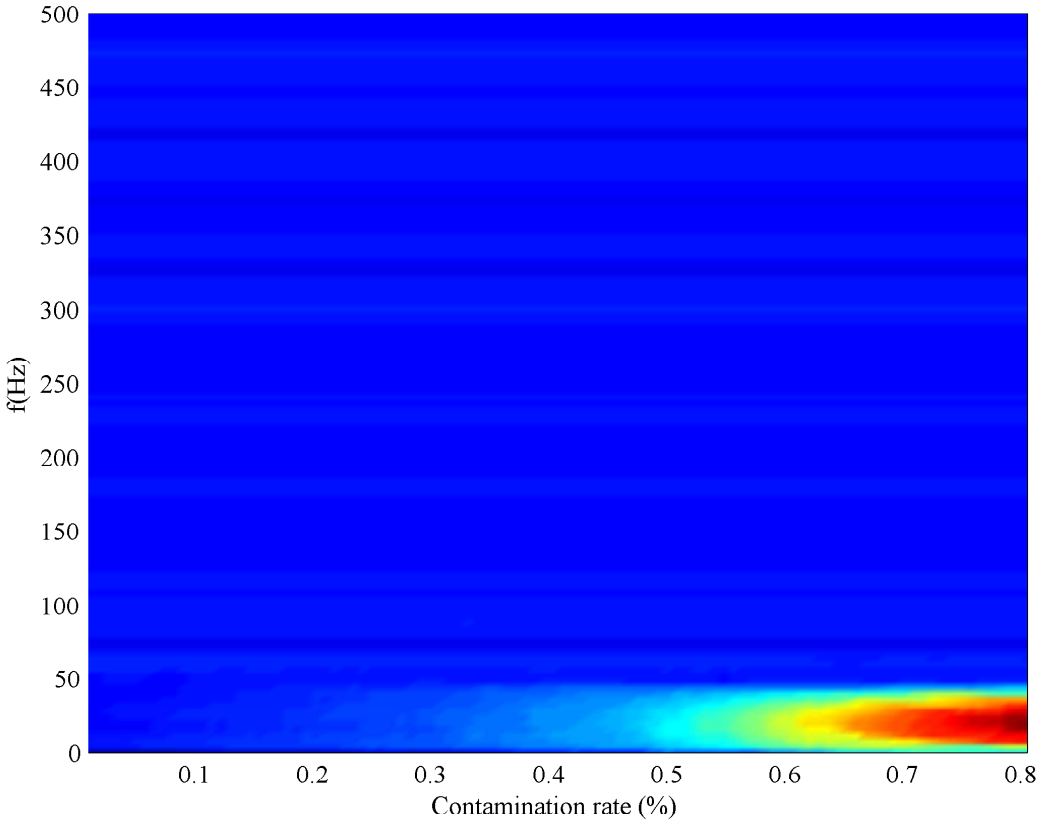

Figure 4.1: Estimation of the noise spectrum in the case of a Gaussian white noise and low-frequency pulses, using the noise estimator described in Sec 4.1.1. The spectrum is overestimated in the pulses bandwidth when the coverage ratio (i.e. the cumulative pulse duration / total duration of the signal) is greater than 25%

1. Considering the fundamental frequency, it is easy to check whether the spectrogram need a particular treatment by computing the contamination rate. In real data, the pulse duration is not available; however the window size used for the spectrogram computation is a good approximation.

2. If the spectrogram requires a treatment to eliminate the affected frequency bins, only its portion bounded by F_{limit} is considered. It is assumed that the spectral levels in this portion relative to the ocean noise follow a Gaussian distribution and so are the spectral levels relative to non-acoustic noises, the latest having high levels. A threshold can then be determined from the empirical Cumulative Density Function (CDF) of the sum of the two distributions. The threshold is set at the minimum of the second derivative of the empirical CDF, which corresponds to the outliers.

This method was validated by simulation according to Fig. 4.2. The primary strum noise was then modeled by a Gaussian pulse (Fig. 4.2 a) with a center frequency of 20 Hz, a bandwidth of 40 Hz and a duration of 0.15 s. The simulated ocean noise merged with strum noise consists of the sum of this signal repeated every 0.5 seconds (2 Hz frequency) for a total duration of 180 seconds and a Gaussian white noise. The Signal to Noise Ratio was set at 30 dB. Fig. 4.2 b represents a portion of the spectrogram of this signal computed with a Hamming window of length 1024 points with 50% overlap. The correlation test (Fig. 4.2 c, Eq. (4.20a)) was computed using spectral levels in 50 Hz bands with 50% overlap. The limit of strum noise contamination was obtained for $F_{Limit} = 200\ Hz$. The Fourier transformed of the first frequency band (Fig. 4.2 d), shows the fundamental frequency (2 Hz) of the strum noise and the two first harmonics of the Fourier series. The empirical CDF of the spectrogram delimited by F_{Limit} and the threshold is shown in Fig. 4.2 e. The cleaned spectrogram, where the time-frequency bins affected by the pulses are discarded is showed in Fig. 4.2 f.

The algorithm was then applied to the acoustic data recorded in the Amundsen Gulf, where contamination occurred during 6.70% of the annual time-series, 13.10% during the open-water period, and 2.20% during the ice-covered period. As shown in Figs. 4.3 & 4.4, this method is robust to detect and remove the non-acoustic noise in the time-frequency domain for both moderate and severe vibrations of the mooring line.

After showing the ambient noise estimation and the strum noise cleaning processing, we will focus on the analysis of the ambient noise in the Arctic.

4.2 Increase of Arctic ocean noise from winter sea ice melting alone

By melting the Arctic ice cap, global warming will increase the natural ambient noise level over a large bandwidth by a factor of ten or more. Using recordings from the annual ice margin in Canadian Arctic and the Hudson Bay, we estimated the annual time-series of ambient noise and showed that their spectral levels are lowered by ∼10 dB by the presence of the ice cover. The observed seasonal changes of this pristine natural soundscape in this part of the Arctic Ocean allowed assessing the expected effect of the gradual lengthening of the open-water season in response to global warming.

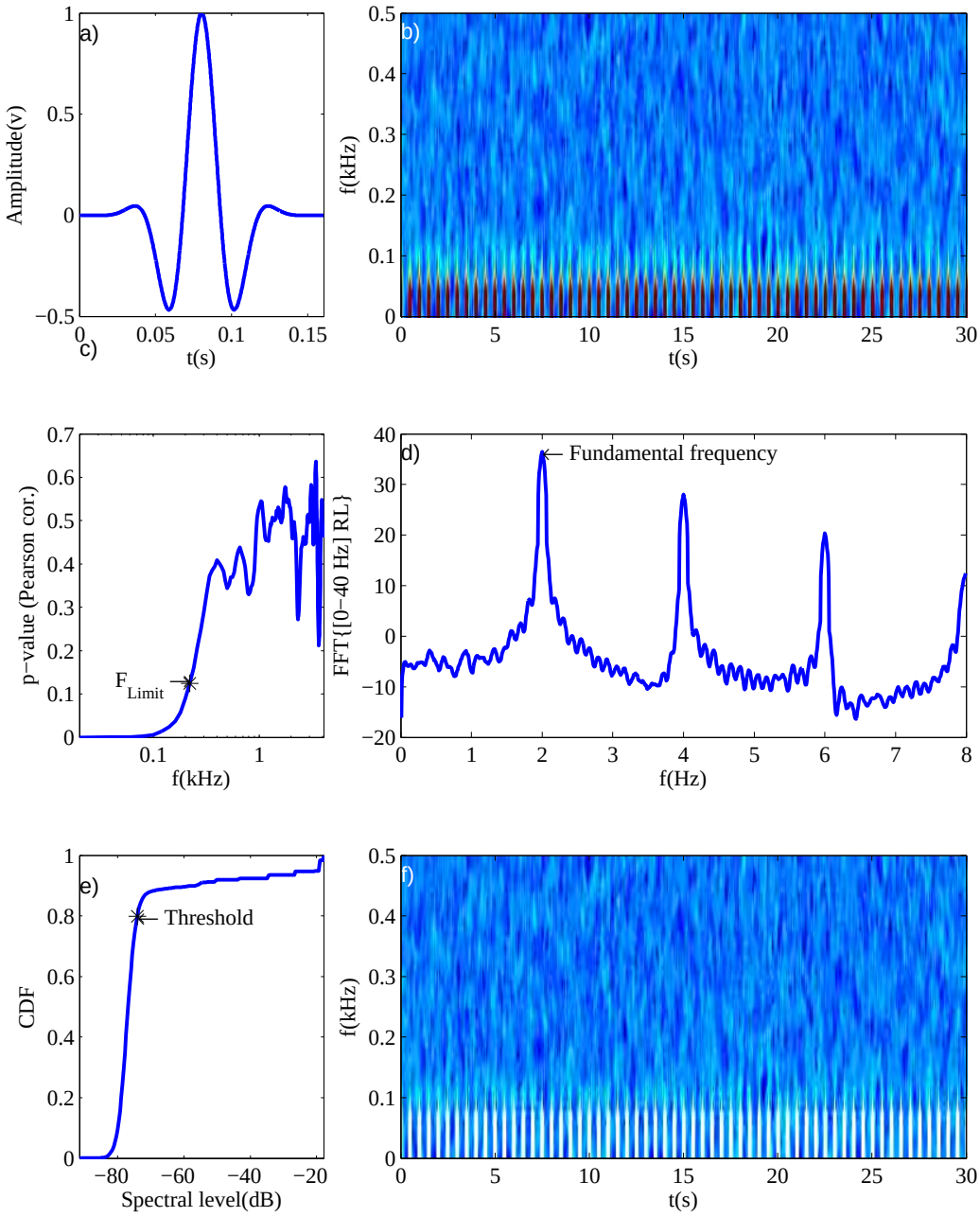

Figure 4.2: Strum noise cleaning in simulated data. a) primary impulse; b) spectrogram showing the contaminated time-frequency bins; c) p_{value} test on cross-correlation between low-frequency band spectral level and adjoining higher frequency bands; d) Fourier transform of the spectral level in the low-frequency band (4–50 Hz) showing the fundamental frequency and the two harmonics; e) Empirical CDF of the spectrogram for frequency $\leq F_{Limit}$; f) Cleaned spectrogram, the white pixels are the times-frequency bins discarded.

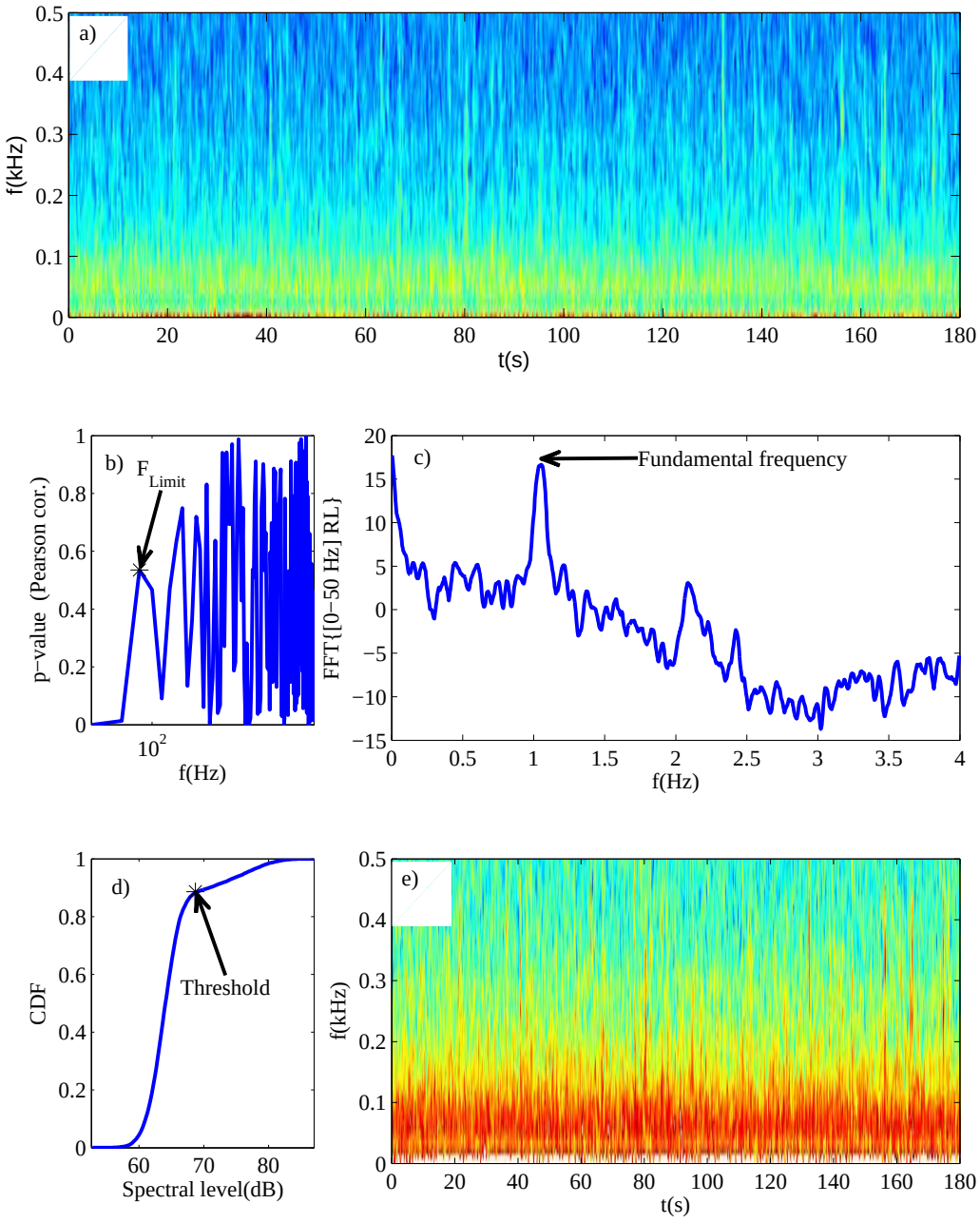

Figure 4.3: Moderate strum noise canceling in real data (Amundsen Gulf). a) spectrogram showing the contaminated time-frequency bins; b) p_{value} test on cross-correlation between low-frequency band spectral level and adjoining higher frequency bands ; c) Fourier transform of the spectral level in the low-frequency band (4–50 Hz) showing the fundamental frequency; d) Empirical CDF of the spectrogram for frequency $\leq F_{Limit}$; e) Cleaned spectrogram (the white pixels are the time-frequency bins discarded).

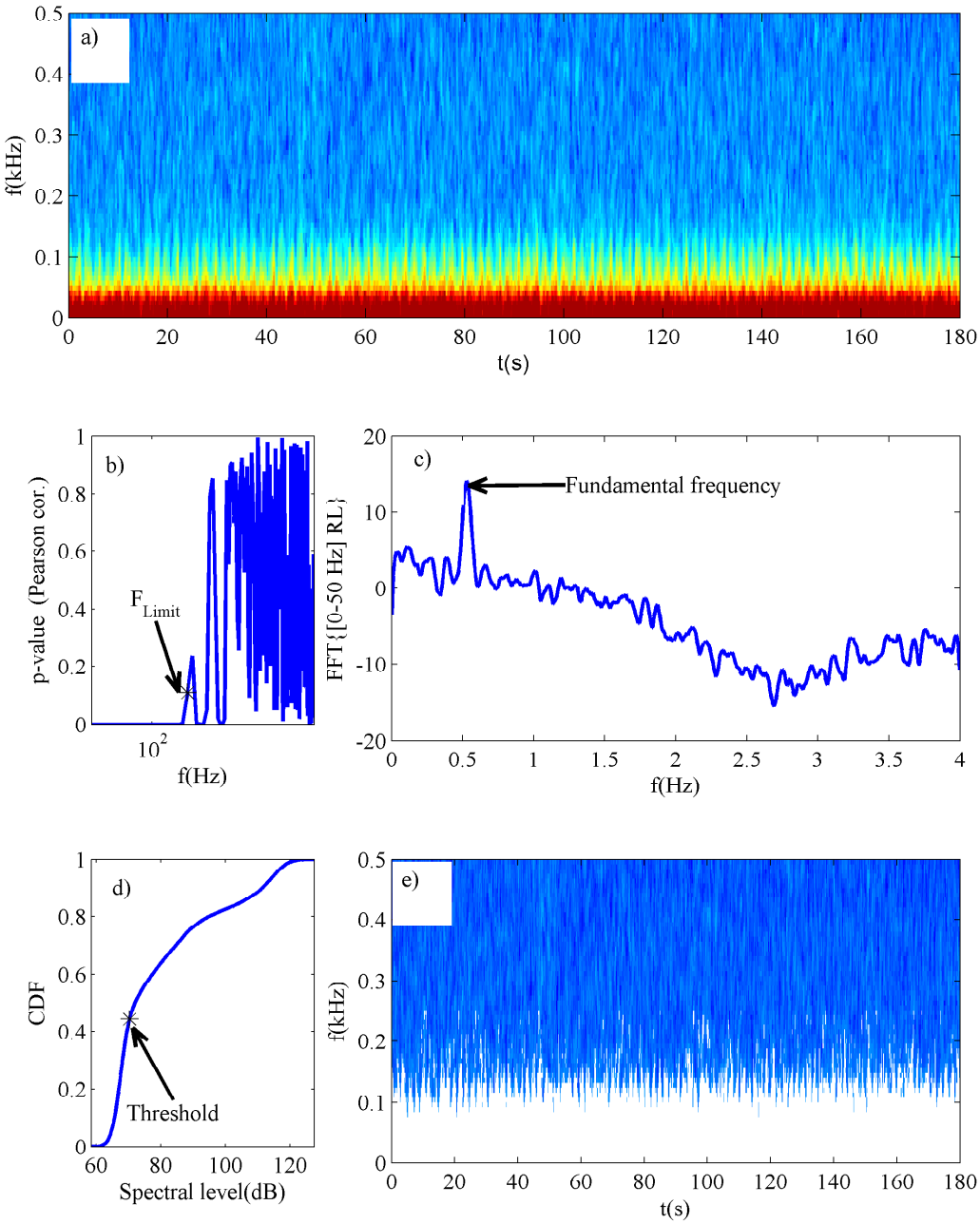

Figure 4.4: Drastic strum noise canceling in real data (Amundsen Gulf). a) spectrogram showing the contaminated time-frequency bins; b) p_{value} test on cross-correlation between low-frequency band spectral level and adjoining higher frequency bands ; c) Fourier series of the spectral level in the low-frequency band (4–50 Hz) showing the fundamental frequency; d) Empirical CDF of the spectrogram for frequency $\leq F_{Limit}$; e) Cleaned spectrogram, the white pixels are the times-frequency bins discarded.

4.2.1 Context

Polar regions are devoid of significant man-made noise sources. In the Arctic Ocean, the natural ambient noise can range from very low in the central Arctic to very high in the MIZ (MIZ) [Uscinski99] characterized by complex dynamic processes [Diachok74], as the ice-canopy break-up into floes in spring, which melt into open water in summer. In the Eastern Beaufort Sea, the MIZ is closing in during October [Barber12, Galley12]. Under continuous ice sheet, winter period in the Arctic Ocean and sub-Arctic seas, the primary sound sources are from thermal cracking [Milne64, Milne66, Zakarauskas91], fracturing and shearing [Xie92], ridgings [Buck86], ice squeaks, ice stuck and bump, and lead opening [Cummings89]. The MIZ is a noisy zone and ambient noise levels at the ice-water boundary are significantly higher than either open water or under pack ice [Diachok74, Urick84, Feller94].

In this section, a part of a paper proposed for publication to the Journal of the Acoustical Society of America, a focus is made on the open-water period by examining the relationship between the ambient noise level and the meteorological forcing to highlight the difference of the under-ice and open water ambient noise spectra. We will show that the ambient noise during the open-water period was mainly responding to wind forcing and that the ambient noise is lowered by at least 10 dB by the presence of an ice cover in winter. The results presented in this section are based on the analysis of acoustic recordings in the Amundsen Gulf (13 months) and two series of >12-months recordings in the Hudson Bay.

4.2.2 Experiment and data analysis

The acoustic data are those described in sec. 2.3.1. The ice concentration, daily time series, are those derived from satellite Advanced Microwave Scanning Radiometer for EOS (AMSR-E) 89-GHz channel [Kaleschke01, Spreen08] and were obtained with a 6.25 km x 6.25 km resolution from the ICDC (Integrated Climate Data Center). Western arctic wind speed were obtained from Cape Parry Environment Canada weather station (70 °00.17 'N, 124 °00.72 'W), located ∼80 km from the acoustic recording location (see map of Fig. 4.5).

The raw acoustic recordings were first converted to instantaneous sound pressure level using the AURAL A/D conversion parameters, gain, and the hydrophone receiving sensitivity calibration curve. Hourly ambient noise spectra, with an 8-Hz resolution, were then estimated from the ambient noise estimator (sec. 4.1). As in other studies (*e.g.*, [Lewis87]), low frequencies were sometimes contaminated by periodic strum from the mooring. In our year-round data set, such contamination occurred during 6.70% of the annual time-series, 13.10% during the open-water period, and 2.20% the ice-covered period. For fixed mooring on a vertical line, strum noise is often pulsed and contaminates acoustic recordings from low to high frequencies. A supervised signal processing tool (Sec. 4.1.2) was developed based on these properties, to identify the contaminated time-frequency bins, which were often patterned with tractable beats of a few seconds. The contaminated time-frequency bins were tagged as missing values. Their missing spectral levels were estimated for each time step using a least-square exponential fit adjusted to the uncontaminated part of the estimated Power Spectrum Density (PSD). Tests with uncontaminated signals showed a high correlation of the fit with the actual spectral levels and no bias.

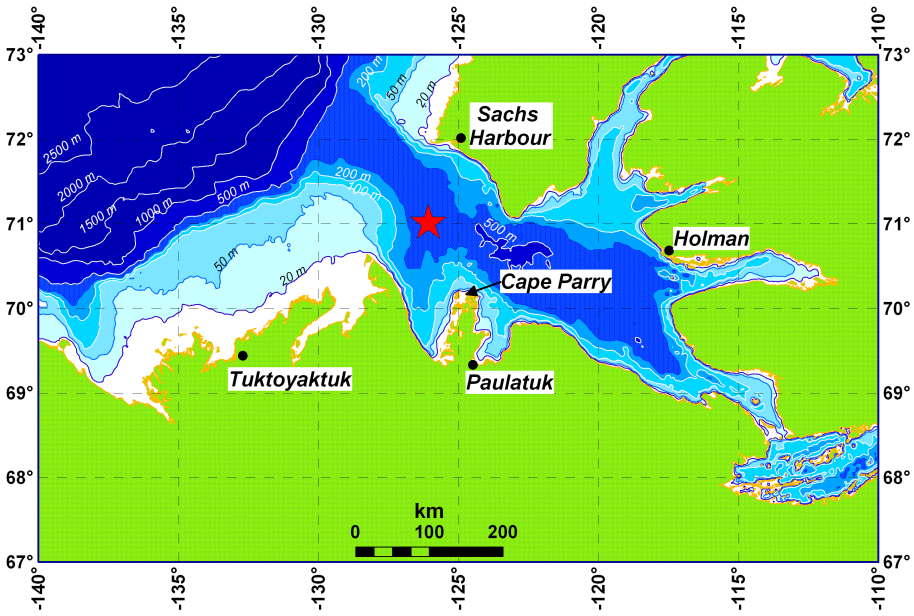

Figure 4.5: Map of the study area showing the bathymetry and the locations of the recording station in the Amundsen Gulf (red star), and of the coastal weather stations of Cape Parry and Sachs Harbour.

4.2.3 Results

The first result, the broadband noise level in the [10 -500] Hz frequency band, indicated that the ambient noise level (ANL) in the Amundsen Gulf mouth (Fig. 4.6, dotted line) decreases as local ice concentration increases (Fig. 4.6, solid line). The daily median of this noise level, over the annual cycle was strongly negatively correlated with the presence of the ice cover (Pearson r = -0.66, $p < 0.001$). The low ambient noise season began ∼1 month after freezing in fall and persisted until complete open-water resumed in spring. The lowest noise levels were observed in the mid to late winter, from February to July, and the highest noise levels were observed for the ice free environment, from August to October.

The ice cover is often defined on the basis of a 15%–threshold of the presence of ice in a grid box, whereby grid cells with less than 15% ice concentration are considered open-water [Rayner03, Wang12]. In our analysis, open-water and ice covered period were then defined, based on the local ice concentration in a 100 km radius around the mooring positions. The ice free environment is ≤10% ice–covered (150 days) and the under-ice period with ≥90% ice covered (230 days in the Amundsen Gulf during winter 2005/2006) (Fig. 4.6); the intermediate values pertain to the transition periods from open-water to ice-covered or *vice versa*.

The ambient noise spectra of the 230-days ice-covered period showed a large dispersion at low frequencies. The percentiles of the ambient noise spectra (Fig. 4.7, 1^{st}–99^{th} percentile) are within a ∼36 dB envelop at 10 Hz and is reduced to ∼9 dB at 4.1 kHz. However the latter range is biased because the low percentiles, up to the median, reached the instrument self-noise spectrum artefact at frequencies above ∼800 Hz.

The percentiles of the open-water period (Fig. 4.8) showed also high dispersion at low-frequencies and were contained in an envelope of ∼56 dB at 10 Hz and ∼14 dB at 4.1 kHz. The

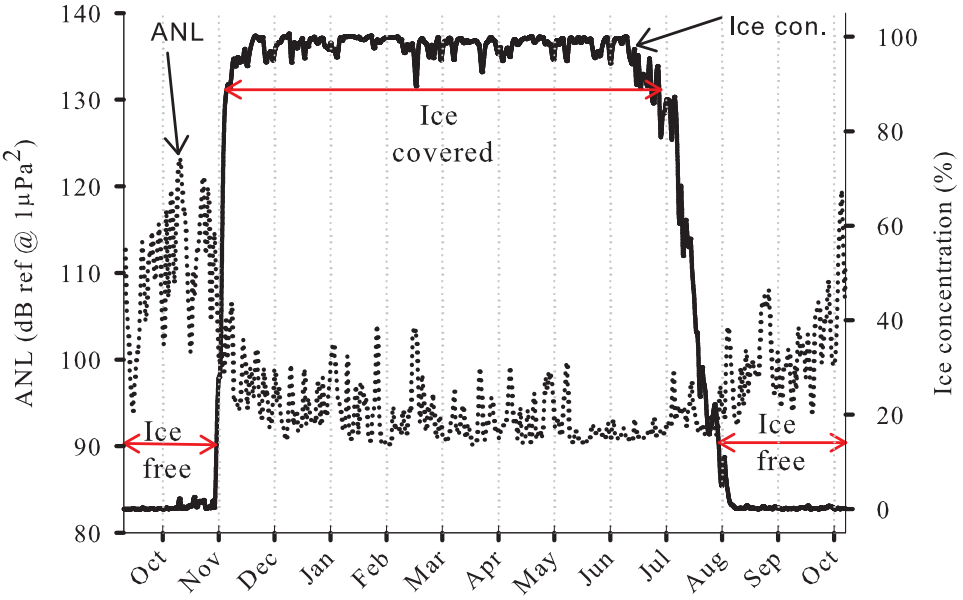

Figure 4.6: Annual cycle of daily ice concentration and hourly ambient noise level (ANL) in the [10–500 Hz] frequency band in the Amundsen Gulf mouth.

low percentiles (up to $\sim 25^{th}$ percentile) reached the instrument self-noise spectrum (Fig. 4.8), at frequency above 2000 Hz. The higher percentiles presented virtually the same slope. Half of the values were contained within an envelope of $\sim \pm 20$ dB at 10 Hz narrowing to ± 6 dB at 3 kHz around the median.

In the Amundsen Gulf, wind speed explained more than 50% of this open-water ambient noise spectral variance above 100 Hz (zero–lag $r^2 > 0.5$), the correlation peaking at 550 Hz. The median spectrum of open-water ambient noise level decreased with frequency from 80 dB (re $1\mu Pa^2\ Hz^{-1}$) at 10 Hz with a steady slope of 10-12 dB per decade down to $\sim$3 kHz (Fig. 4.8 & 4.9). The median spectrum for the winter period (Fig. 4.9) were 65 dB (re $1\mu Pa^2\ Hz^{-1}$) at 10 Hz, lowering by $\sim$15 dB the open-water median.

The open-water/under-ice difference was examined through quantiles ratio, for quantiles $\geq$50%, as the under-ice noise levels reached the instrument self-noise spectrum for $<$ 50% quantiles. The under-ice noise were shown to be shifted by 10–16 dB at 50 Hz, and by $\sim$10 dB at $\sim$150 Hz for all percentiles, from 50–99% (Fig. 4.10). A systematic broadband maximum were observed in the [200–1000] Hz frequency band, where the under-ice noise spectra were lowered by $\sim$10–13 dB. This open-water/under-ice difference, were $\sim$5–10 dB at 2 kHz.

Similar results were obtained for two years in shallow water in the Hudson Bay, in 2005/2006 and 2010/2011 (Fig. 4.11). The two series, also processed to eliminate the strum noise, exhibited a similar broadband maximum ratio in the same frequency band, and the under-ice ambient noise spectra were shifted from $\sim$8–15 dB in the [200–1000] Hz frequency band. The Hudson Bay noise spectra showed also a near constant ratio for all quantiles $\geq$50%, $\sim$1 dB and $\sim$5 dB at $\sim$50 Hz, for respectively 2005/2006 and 2010/2011. A difference of 4–10 dB were observed at 2 kHz.

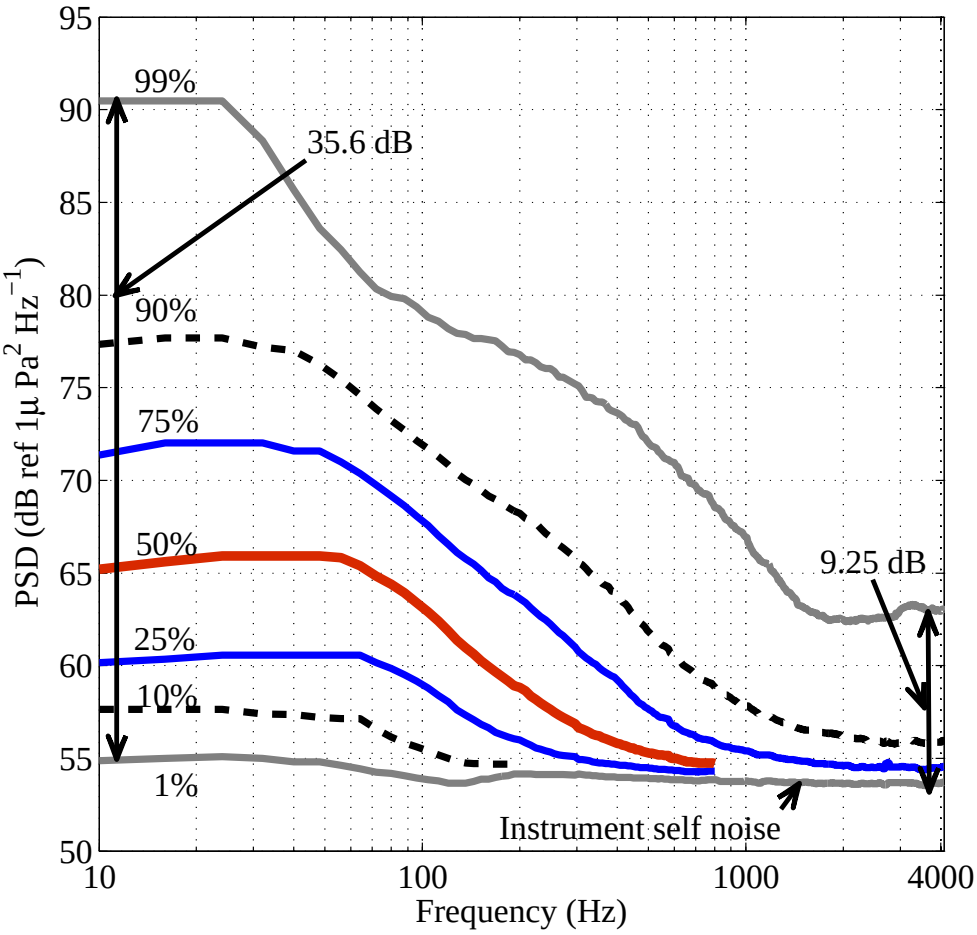

Figure 4.7: Winter period ambient noise spectra percentiles from November 6, 2005 to June 23, 2006 in the Amundsen Gulf mouth.

4.2.4 Discussion

The ambient noise level in the MIZ of the Beaufort Sea decreased and reached its minimum in the late winter, when the Arctic Sea reached its maximum extent and thickness, following the seasonal modulation as described by Lewis *et* al. [Lewis87]. The ocean noise levels in the Arctic Ocean depends upon the nature of the ice, whether continuous, broken, moving or shore-fast, the temperature of the air, and the speed of the wind [Urick84]. Indeed, in continuous shore–fast ice with little wind, the noise levels can be extremely low, (lower than typical ice–free water at sea state 0 [Macpherson62, Payne64, Urick84]). This explains the fact our measurements were truncated in low noise conditions, because our instrument was set up to record normally strong signals.

At the ice-water boundary in the MIZ, the ambient noise generating mechanism was shown to be likely the interactions of wave and swell with individual ice floes [Diachok74, Uscinski99] and to the open ocean surface gravity waves [Makris91]. Urick [Urick71] showed that the icebergs may produce in some conditions, white spectrum up to 10 kHz, by the expansion and the implosion

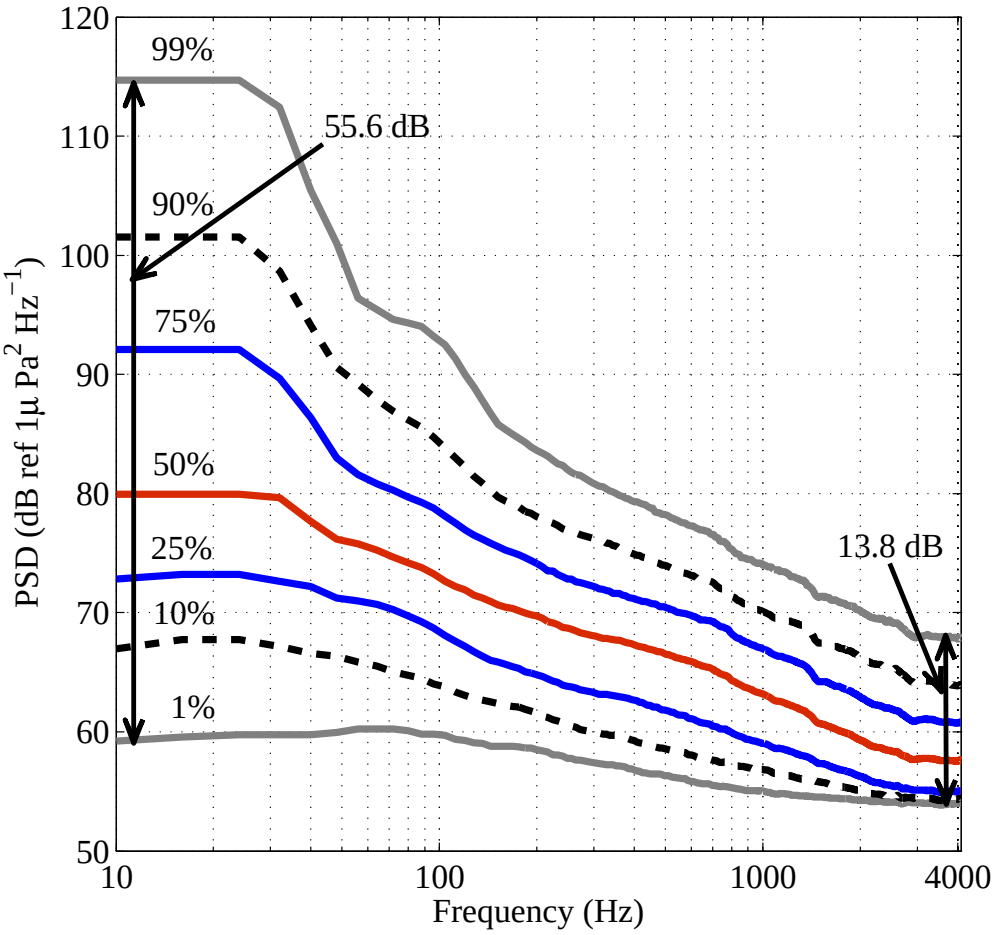

Figure 4.8: Summer period ambient noise spectra percentiles September 9 to October 28, 2005, and from July 26 to October 2, 2006 in the Amundsen Gulf mouth

of the air cavities they contain. The noise level produced in such process can dominated the wind-generated noise. The noise level at the ice-water boundary can reach ∼12 dB higher than the levels in open water and ∼20 dB higher than the levels inside the ice field [Diachok74]. The differences we currently observed are similar to Diachok and Winokur studies. The selected open-water period, based on an ice cover <10% within a 100 km radius around the moorings minimized the effect of ice-water boundary interactions.

The quantile ratios showed similar aspects in the two study areas, although the two oceans environments do not have the same topography. The Hudson bay is a shallow water environment (∼135 m) while the Amundsen Gulf mouth is ∼390 m water deep. The limit of 2 kHz in Figs. 4.10 & 4.11 were chosen for comparison purpose. Indeed, the data in the Hudson Bay were contaminated by electronic noise at higher frequencies. The quantile ratios presented a broad maximum in the frequency band of wind-generated noise (Fig. 4.9). This suggests a reduction in the wind effects during the ice-covered period.

In ice-free environments devoid of significant chronic anthropogenic sound sources, the mid

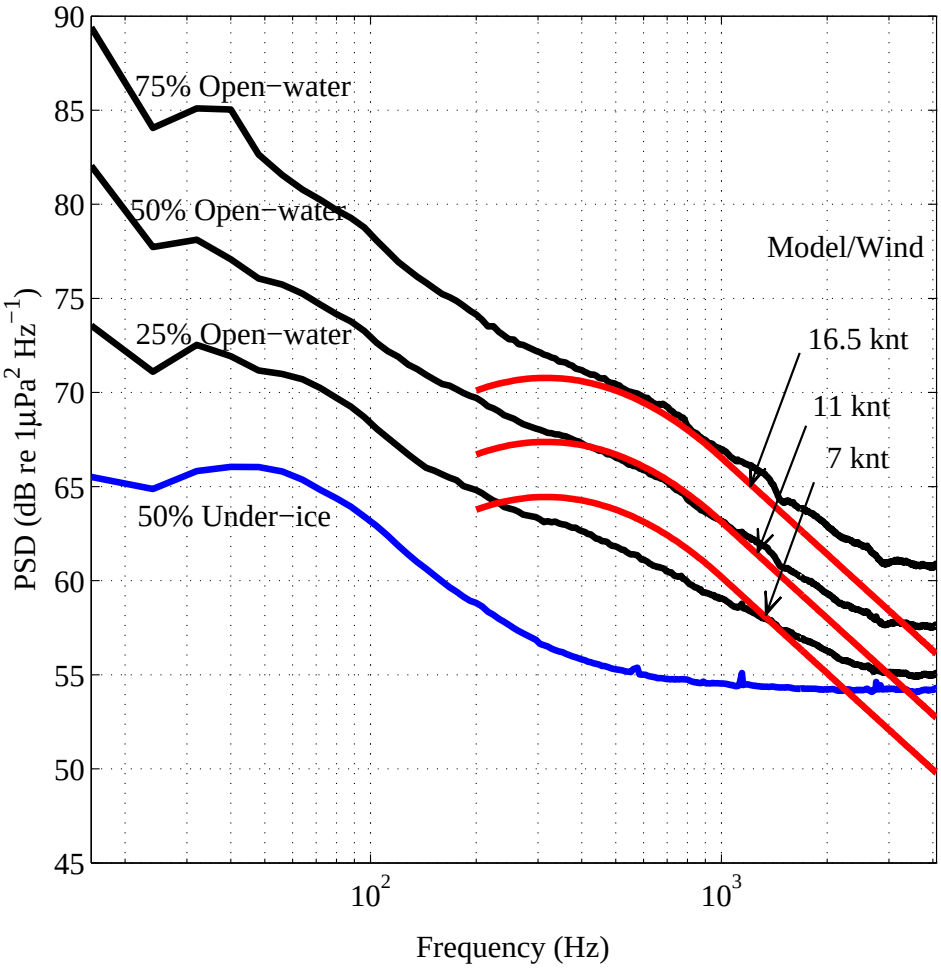

Figure 4.9: Open-water (±1 quartile) ambient noise spectra and under-ice median spectrum in the Beaufort Sea. Modeled wind-generated ambient noise in the 200-4000 Hz bandwidth are given for the 25^{th}, 50^{th} and 75^{th} percentiles of open-water period winds in the Amundsen Gulf mouth.

frequency ambient noise spectra, exclusive of biophony, are dominated by the wind interactions with the ocean surface [Wenz62, Cato02, Reeder11] . This noise spectra can occasionally be masked by heavy precipitations [Wenz62, Nystuen86, Ma05a, Ma05c]. In Western Arctic, wind speed explained more than 50% of open-water ambient noise spectral variance above 100 Hz (zero-lag r^2 >0.5), the correlation peaking at 550 Hz, as expected for wind dominated environments [Cato02, Wenz62]. The result of the classical Wenz noise model fed with the local winds match well the observed noise spectra in the 400 Hz – 2 kHz frequency band (Fig. 4.9). This corresponds to the strongest correlation bandwidth and to the broad maximum observed in the winter/summer ambient noise spectra differences (Figs. 4.10 & 4.11). The melting of the seasonal ice in the MIZ then exposes the ocean surface to the meteorological forcings which results in an increase in the ambient noise levels by $\geq$ 10 dB.

Our ambient noise spectrum during the open-water period showed also significant zero-lag

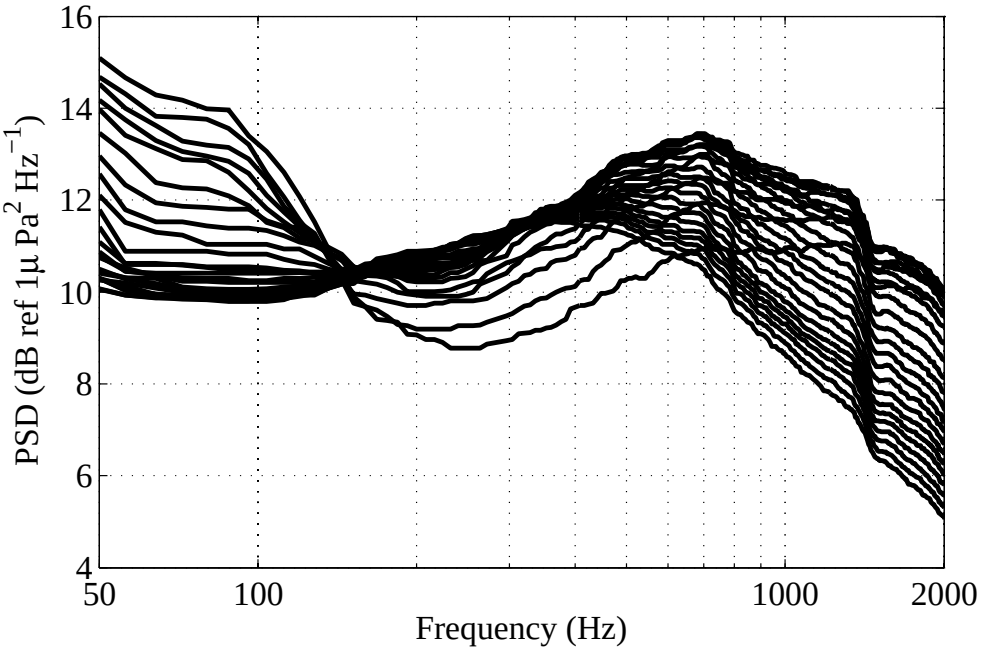

Figure 4.10: Ratio open-water/under-ice ambient noise spectra for percentiles ≥50% in the Amundsen Gulf mouth 2005–2006.

correlation with wind speeds in low frequency (<200 Hz). These results are consistent with those published by [Reeder11, Cato02, Piggott64, Crouch72]. However the under-ice ambient noise in the same frequency band showed significant correlation of same order, suggesting the persistence of wind effects at such low-frequency.

The Arctic ocean is getting more and more free of ice in summer [Galley08, Deser08] with possible complete melting for summer period in the next decades [Stroeve07, Bader11, Stroeve12b] accompanied by some alteration in the Arctic underwater soundscapes. This silent under-ice environment, characteristic of the Arctic Ocean and the polar seas, will then be progressively replaced by a more noisy one dominated by wind and precipitations prevailing in open water environments [Ma05c, Reeder11].

Sounds are vital for marine animals which well-being depends on the sounds they emit and/or perceive [Fay99, Au08]. The soundscape is therefore a characteristic of the habitat and some of the arctic animals are adapted to winter quiet ocean conditions [Moore12]. These arctic species have to face first the increasing of their natural soundscape level from natural sources before the anthropogenic noise from shipping eventually invades Arctic ecosystems.

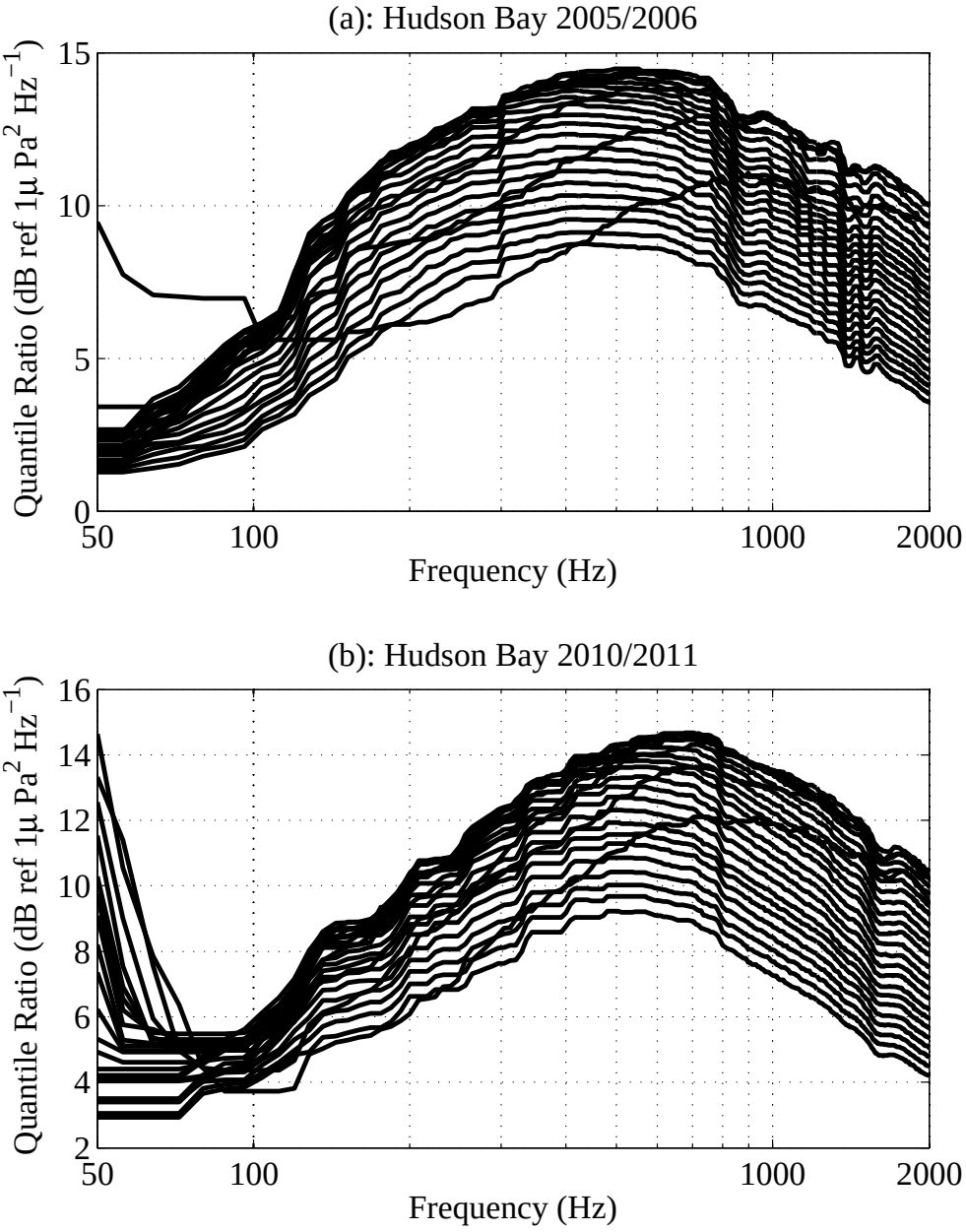

Figure 4.11: Ratio open-water/under-ice ambient noise spectra for percentiles ≥50% in the Southeastern Hudson Bay for 2005–2006 (a) and 2010-2011 (b).

4.3 Under-ice background noise and its relation with environmental forcing

An 8-month time-series of the underwater noise in western Canadian Arctic was recorded at the mouth of Amundsen Gulf, in the MIZ of the Eastern Beaufort Sea, from November 2005

to Mid-June 2006 when the area was >90% ice covered. The time-series of the ambient noise component was computed using our ambient noise estimator, filtering out transient acoustic events from 7-min hourly recordings of total ocean noise over a [0 - 4.1] kHz frequency band. We will show that the under-ice ambient noise did not respond to thermal changes but exhibited consistent correlations with large-scale regional ice drift, wind speed, and measured currents in upper water column. The correlation of ambient noise with ice drift peaked for locations at ranges of ∼300 km off Amundsen Gulf mouth. These locations are within the multi-year ice (MYI) plume that the large Beaufort Gyre circulation causes to extend westerly along the coast in eastern Beaufort Sea. These results reveal that ambient noise in Eastern Beaufort Sea in winter is mainly controlled by the same meteorological and oceanographic forcing processes that drive the ice drift and large-scale circulation in this part of the Arctic Ocean.

4.3.1 Context

The Arctic Ocean is entirely covered with ice of variable thickness and age during winter [Marsan04, Maslanik11, Marsan12, Stroeve12b]. The seasonal extent of this polar ice cap, as well as the ice thickness, is changing rapidly in response to global warming [Polyak10, Stroeve12b, Wadhams12] as we showed in Sec. 2.1.4. The Canadian waters, up to ∼ 74 °N latitudes are generally free of ice in late summer, when the arctic sea ice extent reaches its minimum in September (Fig. 4.12a, for September 2005). The MIZ, between the perennial ice and the coast, is closing in during October (Fig. 4.12c, for October/November 2005) [Barber12, Galley12]. The maximum ice extent and thickness [Stroeve08, Stroeve12b] are reached in late winter, in March/April, (Fig. 4.12b,d), before the melt-down, which is complete in July. Except for land-fast ice, the Arctic sea ice is in a perpetual motion during winter, in response to five main forcings: wind, currents, Coriolis force, internal stresses, and sea ice surface tilt [Thorndike82, Barry93, Rotschky11].

In the Arctic, this motion is structured into two main circulation patterns: the Beaufort Gyre (BG) and the transpolar drift (TPD) (Fig. 4.12 e). The BG, centered at about (80 °N, 155 °W) [Barry93] (Fig. 4.12 e), is an anti-cyclonic (clockwise) circulation. It is the main circulation pattern of the Arctic sea ice drift in the Canadian Basin [Stein88, Asplin09, Lukovich09]. This large-scale circulation pattern tends to push the ice against the Canadian Archipelago and pile up multi-year ice in this region [Barry93] (Fig. 4.12 c, d). In the East, the TPD forces the eventual evacuation of the ice to the Atlantic through Fram Strait [Tsukernik10, Smedsrud11] (Fig 4.12 e). In the west, in eastern Beaufort Sea, the multi-year ice (MYI) is extended westward by the BG into a plume at the marginal ice boundary and is not fast to the coast in the Amundsen Gulf, where essentially only first-year ice (FYI) is found (Fig. 4.12 c, e) [Kwok06, Barber12, Galley12].

In this part of the current chapter (from [Kinda13]), he examine the under-ice noise from an 8-month time-series of [0 - 4.1 kHz] recordings. The data set was recorded by an autonomous underwater recorder in the MIZ of the western Canadian Arctic. We analyze the relations with the possible regional forcing processes, notably ice drift, wind speed, current speed, air temperature, and air pressure. To prevent the estimated noise level of being dominated by nearby transient events such as, ice knocking, fracturing, cracking, shearing, and ridging, the ambient noise level (ANL) metric is used. Ambient noise has been defined by [NRC03] as the noise originating from a myriad of indistinguishable sources, and this component was extracted from the measured total ocean noise using our algorithm described in Sec. 4.1.

The next three sections present the additional data sets used in the study, the numerical analysis, the results, followed by a discussion.

4.3.2 Material and methods

4.3.2.1 The data set

In addition to the acoustic data described in sec. 2.3.1, the meteorological variables and the ice concentration described in the previous section, ice thickness and drift speed are used. Ice thickness maps derived from ICESat data [Rotschky11] were obtained from ICDC with a 25 x 25 km resolution for October-November 2005 and February-March 2006. Daily ice drift vectors time series, calculated using gridded satellite-derived ice motion and Arctic Buoy Program data [Fowler03, Maslanik11], were obtained with a 25 x 25 km resolution from the NISDC (National Ice and Snow Data Center)[1].

4.3.2.2 Data analysis

The low levels of under-ice ambient noise at frequencies > 500 Hz sometimes reached the detection floor ($\sim$ 53 dB re 1 μPa^2 Hz^{-1}) of our 16-bit dynamic range instrument. The analysis of the relations between the ambient noise level (ANL) and the environmental variables were therefore limited to the [10 - 500 Hz] low-frequency band. They included correlations and principal component analysis (PCA, [Legendre98]) using both hourly and daily data. The PCA were performed on correlation matrices so that all considered variables have the same weight in the analyses. The daily correlation with the current speed used the low-pass filtered current, removing $<$ 25-h components to eliminate the tidal fluctuations which the maximum daily period in the area is $\sim$24 h 50 min. The daily mean ice drift at the station was the average of the drift vectors grid within a 100-km radius from the station, which covers about the full width of mouth of the Amundsen Gulf at this location. In order to locate the regional sourcing area of the ambient noise, the correlations were computed for all nodes of the ice drift vectors grid over the entire Arctic Ocean and were computed for different percentiles of the daily CDF of the hourly estimated [10 - 500 Hz] ANL.

4.3.3 Results

The spectrogram showing the annual variation of the total ocean noise spectral levels (Fig. 4.13 a) indicates the predominance of low-frequency noise with a bandwidth of a few hundred Hertz and generally low noise levels above 1 kHz, except during the open water period (from September 9 to October 28, 2005, and from July 26 to October 2, 2006), the ice formation period (October 29 - November 5, 2005) and the ice cover break up (June 24 - July 25, 2006). The ambient noise contributes to a large part of the ocean noise (Fig. 4.13 b) as shows the general spectrogram pattern, but the ratio ocean noise/ANL expressed in dB (Fig. 4.13 c) shows evidences of common events of transient noise exceeding 0 dB and lasting a few hours, especially at the beginning and the end of the ice covered period. Most of the time, the high-frequency part of the under-ice ANL reached the measurement floor (Fig. 4.13 a,b), truncating the CDF of PSDs

[1] http://nsidc.org/

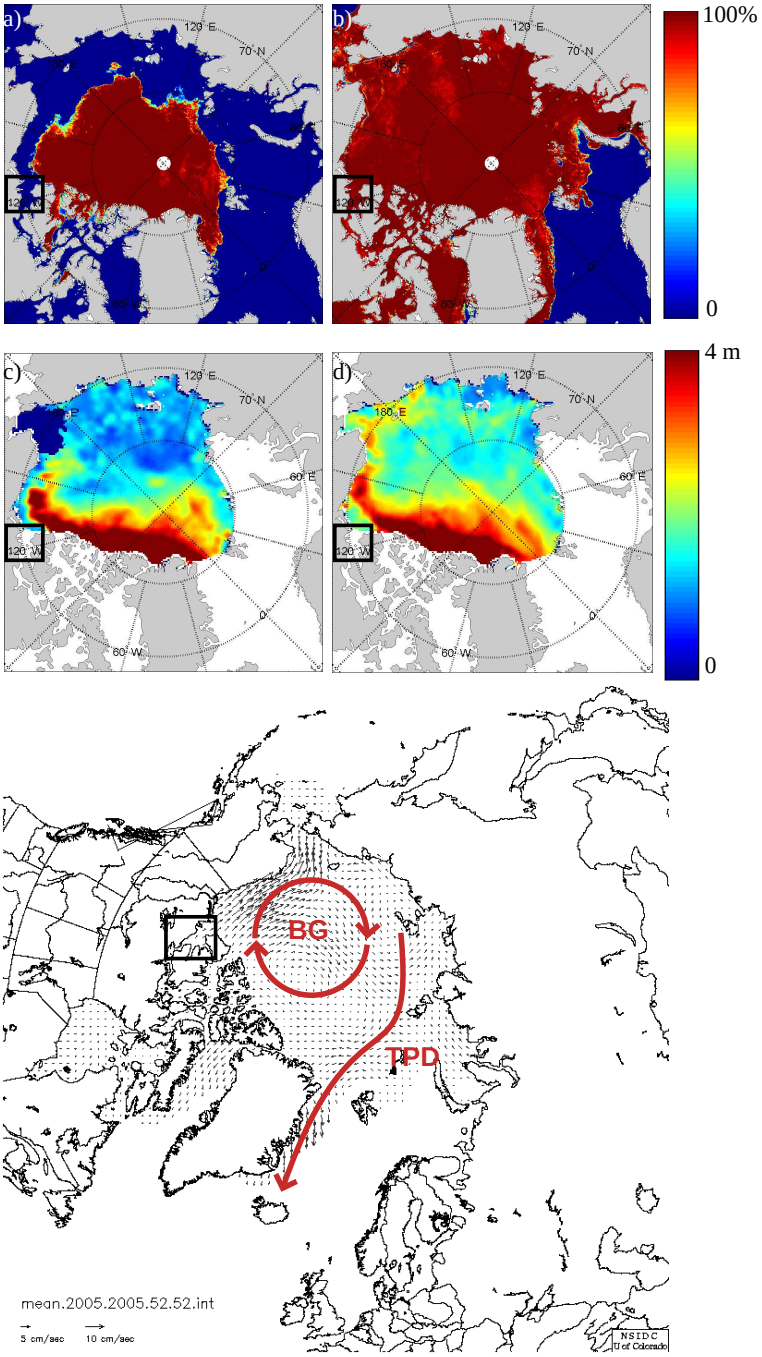

Figure 4.12: Arctic ice cap characteristics; the rectangle indicates the study area in the Eastern Beaufort Sea (CA08 in Fig. 2.7): (a) Sea ice concentration during minimum extent in September 2005, and (b) maximum in March 2006 from NSIDC;(c) ice thickness in October/November 2005 from NSIDC (National Snow and Ice Data Center) ice thickness data showing the accumulation of multi-year ice along the Canadian archipelago, and (d) its extension in West direction, up to the Alaskan coast, during the winter (February/March 2006); (e) Arctic Ocean dominant current structure, showing the Beaufort Gyre (BG) and the transpolar drift (TPD), and an example of ice drift vectors filed from NSIDC ice drift data on December, 2005 (week 52).

below the 50^{th} percentile above 500 Hz and the 75^{th} percentile above 3 kHz (Fig. 4.13 d). The daily median ANL over the annual cycle was strongly negatively correlated with the presence of an ice cover, as given by the ice concentration in a radius of 100 km around the station (Pearson r = -0.66, $p < 0.001$). This strong under-ice/open-water difference was presented in the previous section (sec. 4.2).

Based on a 90% ice coverage criterion, the 230-day under-ice period at the station started on November 6, 2005 and ended on the June 23, 2006 (Fig. 4.14 a). The local ice concentration often differed from 100% and showed notable 1-3 day duration of clear water and leads, reducing the ice concentration down to 89% (ex. February 13, 2006). The air temperature oscillated around a mean of -20.5 ºC , from -36.4 ºC to -6.5 ºC, until the end of April, before a steady rise reaching > 0 °C temperatures after May 11, 2006, which corresponded to the start of the ice cover break up (Fig. 4.14 b). The daily pressure level showed regular changes, with higher amplitude before the steady rise of temperature in spring (Fig. 4.14 c). The PSD of this pressure time-series showed peaks at periods of 7 and 15 days, corresponding to the local passage of depressions (Fig. 4.15 a, Table 4.1). Median daily wind speed also exhibited regular fluctuations with maximum speed reaching 18.6 m s-1 (37 kt) (Fig. 4.14 d). The PSD of the time-series indicated that recurrences were mainly at periods of 4 and 7 days with possible larger scale events (Fig. 4.15 b, table 4.1). The strong winds were mainly directed along the mean coastline (90 ° or 270 °, Fig. 4.16 a).

Table 4.1: Periods corresponding to significant peaks in the spectra of the hourly time-series of under-ice [10–500 Hz] ANL and environmental variables, with their interpretation.

variable	**Time period (days)**				
	0.26	0.52	∼4	∼7	∼15
ANL [10-500 Hz]				x	
Air pressure				x	x
Wind			x	x	
Raw currents at 11 m	x	x	x		x
Interpretation	Tidal M_2	Tidal M_4	Storm	Storm	Tidal M_{SF}

The mean ice drift speed in the Amundsen Gulf mouth was 2.1±1.8 cm s^{-1}, with peaks reaching 15.3 cm s^{-1} (Fig. 4.14 e, solid line). Important drift amplitudes were observed before the beginning of the steady temperature rise in April. In contrast to the previous atmospheric environmental variables, these fluctuations did not show strong periodicity, from the autocorrelation and/or spectral analyses (not shown). As for the wind, the PDF of the ice drift direction has two modes, one at ∼100-110° and a second one in the opposite direction, at 280-290° corresponding to the strongest ice drift speed (Fig. 4.16 b). These 2 modes correspond to in and out directions of the Amundsen Gulf. The immediate under-ice raw currents (in 7-15 m bin) averaged 11.0 ±11.7 cm s^{-1} and presented occasional occurrences of stronger pulses exceeding 30 cm s^{-1} (Fig. 4.14 f, solid line). As expected, current fluctuations were strongly related to the tidal forcing at typical periods of ∼6 h (quarter-diurnal lunar M4), 12 h (semi-diurnal lunar M2) and 14 days (one-half of a synodical month MSF) (Fig. 4.15 c, Table 4.1). The currents at the depth of the AURAL recorder (∼50 m) were 1.9 times lower on average, with a mean of 5.82±2.63 cm s^{-1} (Fig. 4.14 f, dash line), and were also tidally modulated.

The under-ice [10-500 Hz] ANL daily median oscillated by ∼8 dB, between 84.6 to 102.5 dB

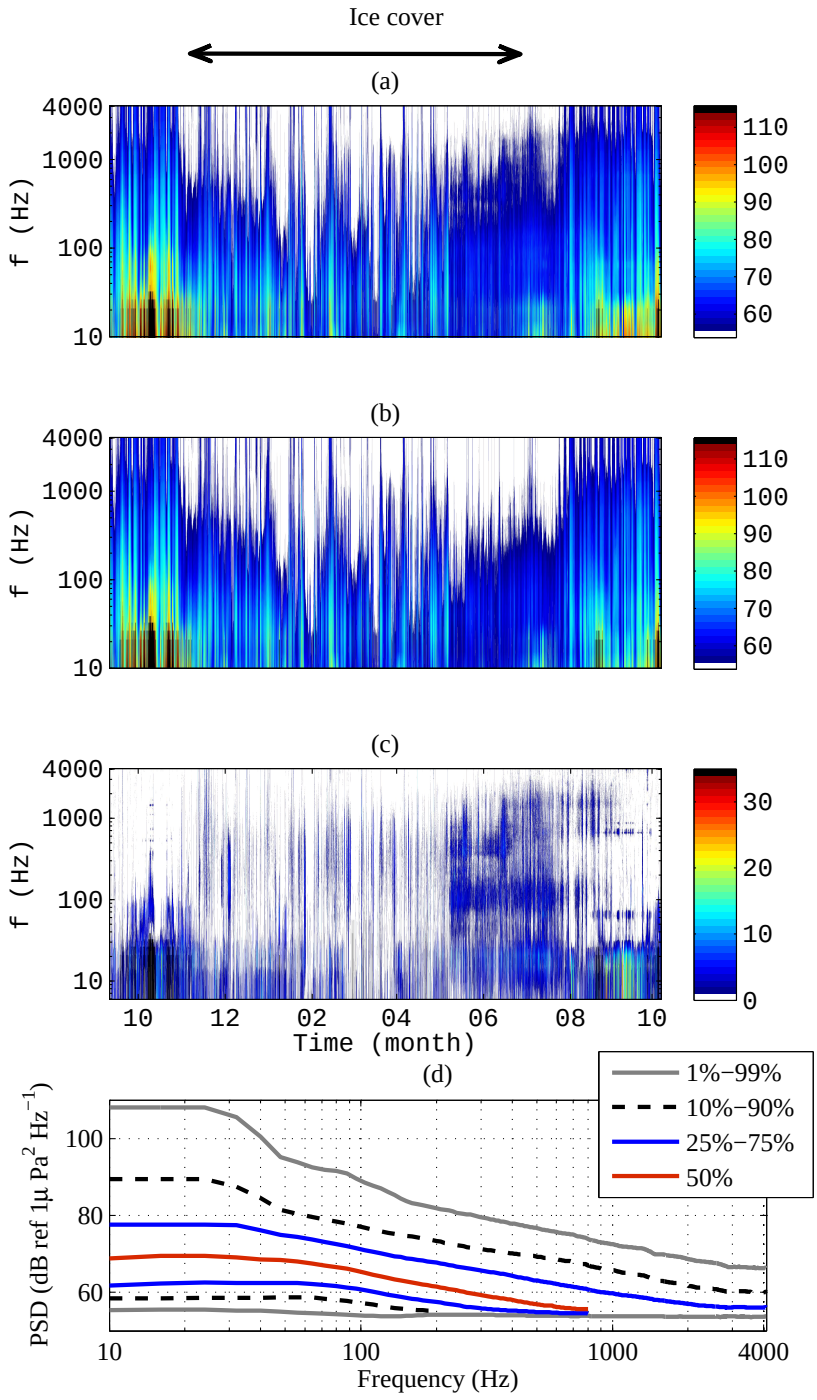

Figure 4.13: Annual spectrograms of the recordings in the Amundsen Gulf showing, (a) the total ocean noise hourly spectral levels; (b) ANL hourly spectral levels; (c) their ratio; and (d) the ANL percentiles. White pixels correspond to bins with levels below the instrument self noise in (a) and (b) and to a ratio of 1 (0 dB) in (c).

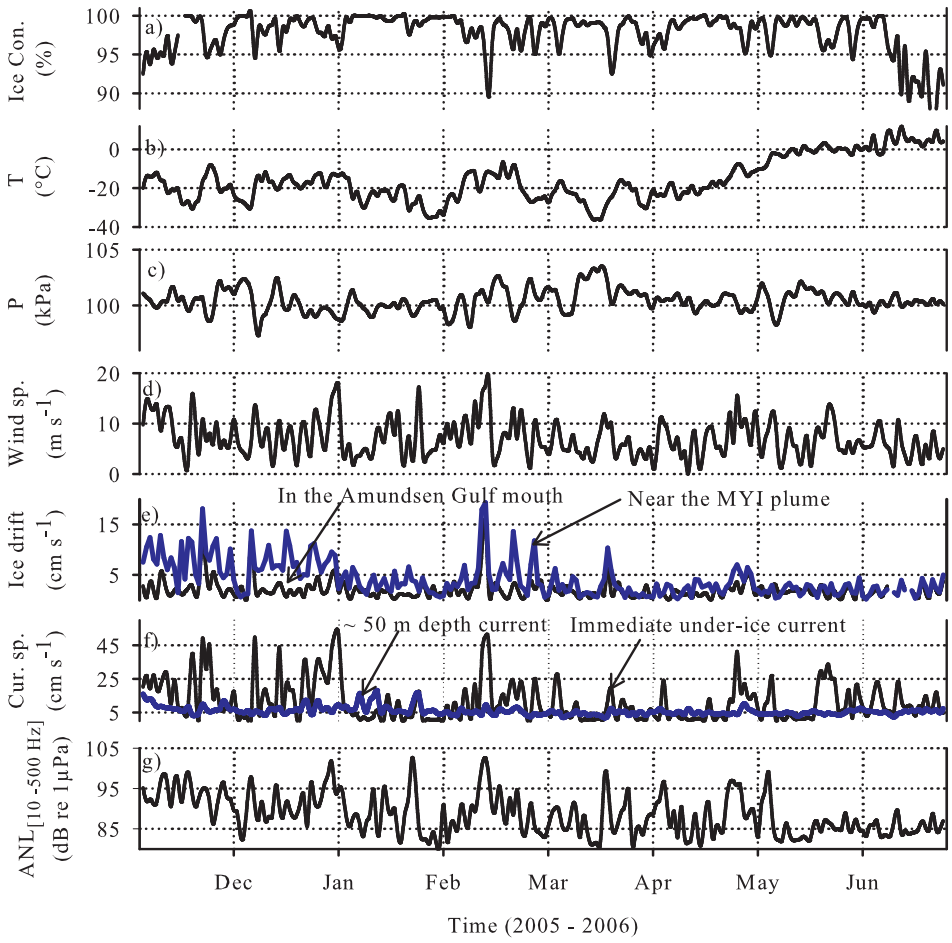

Figure 4.14: A
NL at the mouth of Amundsen Gulf in winter 2005-2006]Time-series (daily median) of the environmental variables and under-ice [10-500 Hz] ANL at the mouth of Amundsen Gulf in winter 2005-2006. (a) local ice concentration (100-km around the mooring position); (b) air temperature; (c) air pressure; (d) wind speed; (e) ice drift speed in the Amundsen Gulf (solid line) and near the multi-year ice plume (dash line); (f) *in-situ* current speed (solid line: immediate under-ice current; dash line: 50 m depth current) ; and (g) [10 - 500 Hz] ambient noise level.

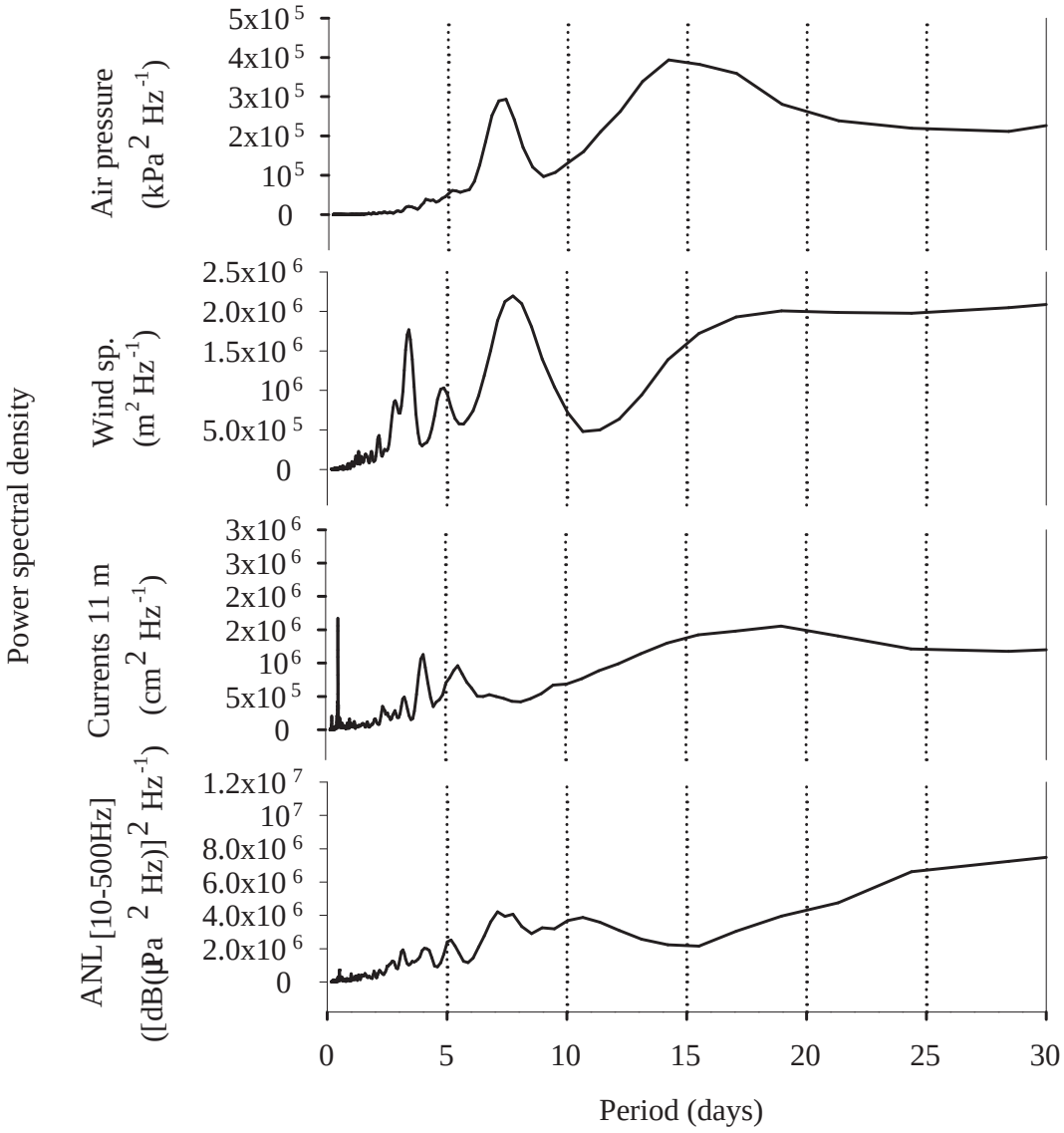

Figure 4.15: PSDs of the hourly time-series of ANL and environmental variables: (a) air pressure; (b) wind speed; (c) currents at 11 m ; and (d) [10-500 Hz] ANL presented in Fig. 4.14.

re $1\mu Pa^2$, before the meltdown in May-June, when the amplitude of the fluctuations decreased to $\sim$2 dB (Fig. 4.14 g). Its PSD peaks indicate recurrences at 7-day periods (Fig. 4.15 d, Table 1). High ANL sometimes co-occurred with noticeable events in ice cover, drift, wind, and immediate under-ice currents (e.g., Fig. 4.14 a,d,e,g, February 13, 2006).

As the ANL is assumed to depend on environmental forcing, a PCA analysis was performed to see how the environmental conditions, represented by the combination of atmospheric, ice and underwater variables, were structured within the data set, and if the ANL was responding to this structure. This was evidenced by color mapping the ANL in the space of the principal components of the environmental variables (Fig. 4.17). The first two principal components explained 51% (30.4% for the 1st component and 20.30% for the 2^{nd} component) of the total

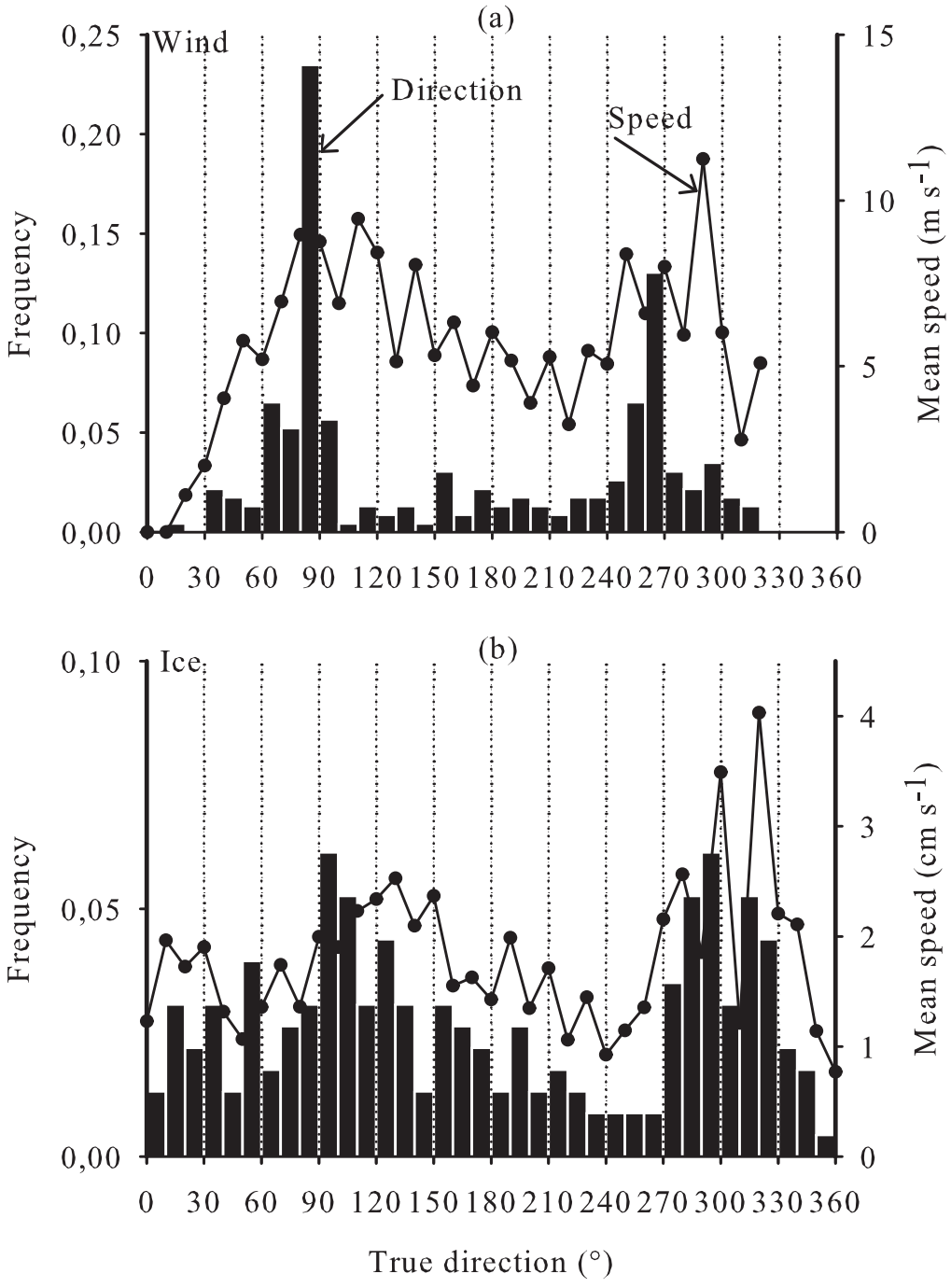

Figure 4.16: Frequency of true directions (bars) and mean speed in that directions (lines) of (a) median daily wind and (b) ice drift within 100-km radius from the station corresponding to the period November 06,2005 to June, 23, 2006 shown in Fig. 4.14.

environmental variance. The overlaid plot of factor loadings in the two-component plan indicates that the noise-separating first principal component is increasing when wind, ice, and current speeds increase. The second component opposes the air temperature and ice drift in eastern

direction and aligns with air pressure, ice concentration, and ice drift in northern direction. The first principal component separates the low-ANL observations, mainly found in the left half space, from the high-ANL observations. High-ANLs are observed during low ice concentration, low air pressure, high winds, currents, and ice drift, in particular when this drift is directed towards the northwest, i.e., out of the Amundsen Gulf while low-ANLs respond to high ice concentration, low air pressure, wind, currents, and ice drift directed in of the Amundsen Gulf.

Pearson correlations between [10-500 Hz] ANL and environmental variable pairs (Table 4.2) indicate that the ANL was strongly positively correlated with this [wind/ice drift/surface currents] triad (Pearson r: 0.37, 0.57, and 0.45 respectively). The ANL tended to increase with the northward and westward drift. Ice drift magnitude was positively correlated with wind speed and with immediate under-ice currents, the latter two variables being strongly correlated (Pearson r = 0.72). The ice concentration during winter was negatively correlated with air temperature, which contributed little to explain ANL variance, and with immediate under-ice currents. Correlating the ANL with hourly changes in air temperature or pressure (not shown) did not improve the correlation coefficients. The correlation of the ANL with daily changes in ice drift was also computed (not shown) and was not significant.

Table 4.2: Pearson correlations between under-ice [10-500 Hz] ANL and daily median and environmental variables. Underlined: $p < 0.05$; bold: $r^2 > 0.10$.

		Currents		**Ice**					**Air**		
Variables		50 m.	11 m.	drift east.	drift north	drift 100 km	drift 300 km	conc.	wind speed	press.	temp.
ANL	[10–500 Hz]	**0.28**	**0.45**	**-0.18**	**0.29**	**<u>0.38</u>**	**<u>0.57</u>**	**-0.09**	**<u>0.37</u>**	**<u>-0.07</u>**	-0.15
Air	temp.	-0.07	**0.21**	**0.04**	**-0.14**	**0.04**	-0.08	**<u>-0.44</u>**	**<u>0.04</u>**	-0.17	
	press.	-0.24	**-0.26**	**-0.20**	**0.10**	**-0.03**	-0.14	**<u>0.07</u>**	**<u>-0.23</u>**		
	wind.	0.20	**0.72**	**-0.17**	**0.22**	**0.27**	0.40	**<u>-0.20</u>**			
Ice	conc.	-0.11	**-0.34**	**0.00**	**0.03**	**-0.18**	-0.14				
	drift 100 km	0.26	**0.53**	**-0.23**	**0.38**	**0.63**					
	drift 300 km	0.09	**0.41**	**-0.43**	**0.59**						
	drift north	0.04	**0.30**	**-0.63**							
	drift east	0.08	**0.23**								
Current	11 m	0.25									

Correlations of the under-ice [10-500 Hz] ANL with ice drift time-series at every node of the entire grid over the Arctic Ocean basin locate the maximum in a ∼500-1000 km wide area of eastern Beaufort Sea (Fig. 4.18). The core of maximum correlation is located north-west of Amundsen Gulf, ∼300 km from the recording station, in the direction of the Gulf axis. The magnitude of the correlation at the core decreased slightly with the higher percentiles of the daily CDF of the hourly estimated [10-500 Hz] ANL. A good spatial continuity existed within ice drift field over a radius of ∼250 km from the location of the correlation core, as the correlation map indicates (Fig. 4.19).

4.3.4 Discussion

The present acoustic data set was collected from the near-surface (∼50 m) portion of the water column, where acoustic signals converge due to the upward refracting sound speed profile.

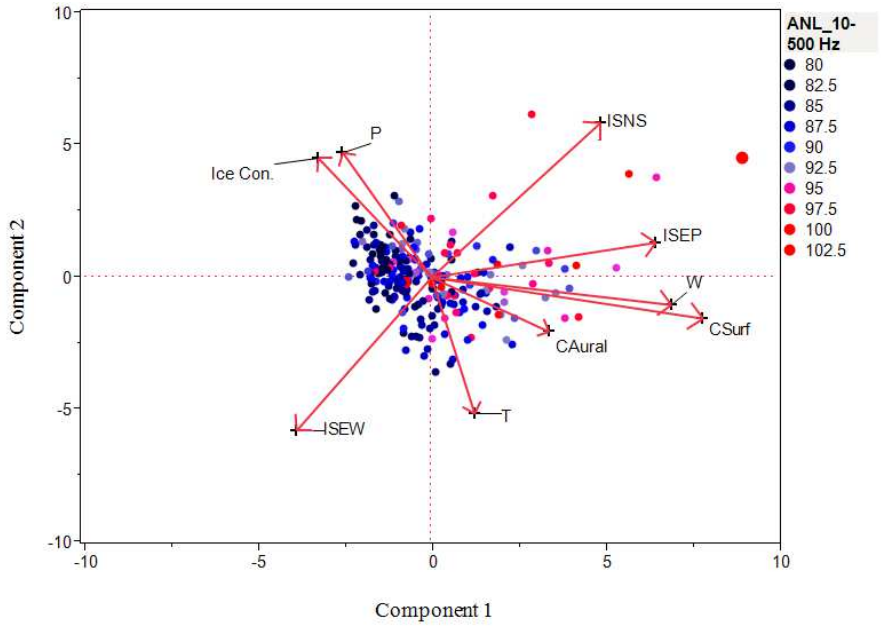

Figure 4.17: Scatter plot of the PCA factor scores in the plan of the first two principal components, along with the factors loadings for each environmental variable. Dots indicate the daily median [10-500 Hz] ANL with red dots corresponding to high ANL and blue ones to low ANL. Ice Con: ice concentration; P: air pressure; ISNS: ice speed north-south component, with northward positive; ISEW: ice speed east-west component, with eastward positive; ISEP: ice speed; W: wind speed; CSurf: current speed at 11 m; CAural: current speed at 51 m; T: air temperature.

The measurements were made near the mouth of the 550-km long Amundsen Gulf. To our knowledge, it is the first long-term time-series covering an entire annual cycle in this part of the Arctic Ocean.

Ocean noise levels are the sum of the slowly changing ambient background and stronger transient sources, which dominate the root mean square sound pressure level in areas where their occurrence is high. Such strong acoustic events are common under ice, due to ice fracturing and movements (*e.g.*, [Pritchard90, Xie91, Xie92]). Under-ice ocean noise levels are therefore strongly imprinted by local events, and are then representative of limited local areas of the 3D volume of the regional ocean basin. For noise level assessments and comparisons at larger scales, the contribution of strong transient sources should preferably be removed. In the present study, we propose a systematic method to objectively estimate the ambient noise component from total ocean noise, as defined by [NRC03].

At low frequencies ($<\sim$100 Hz), contamination of the recorded acoustic signal by vibrations of the hydrophone and strum from the deployment line is frequent (cf. [Lewis87]) and often pulsed for fixed deployments because of the natural variability in instantaneous current forcing. This makes the collection of clean low-frequency acoustic data difficult from fixed moorings. We encountered this difficulty, especially during the open water season, and much less frequently during the ice covered period. We made a special effort to detect and filter out such low-frequency contaminated data (sec. 4.1.2), and estimate the noise level in the missing time-frequency bins by PSD extrapolation. The low correlation of the ANL with the current speed at the depth of the instrument, compared to the high correlation with the immediate under-ice current speed,

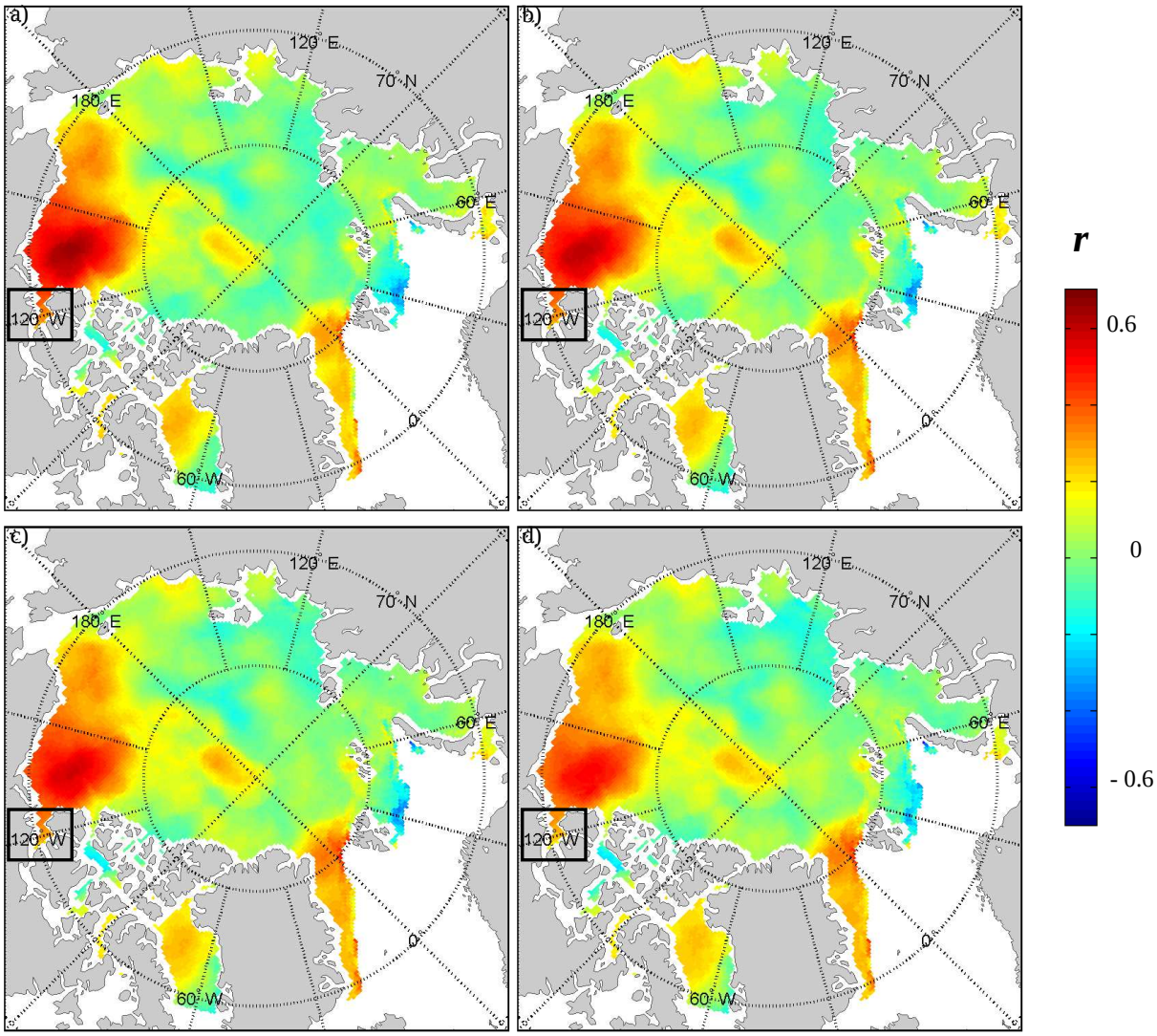

Figure 4.18: A
NL and Arctic ice drift magnitude]Maps of correlations (Pearson r) between the daily [10-500 Hz] ANL and Arctic ice drift magnitude for (a) the 10^{th} percentile; (b) the 25^{th} percentile; (c) the 50^{th} percentile and (d) the 75^{th} percentile of the daily CDF of hourly ANL estimates.

supports the efficiency of our handling of such interference from pseudo noise induction due to flow and strum. We are therefore confident that the data presented here are not significantly affected by strumming interference.

The measured under-ice noise levels sometimes reached the instrument floor during the ice-covered period, even below 500 Hz. This affected the lowest percentiles of the [10-500 Hz] ANL CDF, but not the median level retained for the analysis (Fig. 4.13 d). The lowest measured [10-500 Hz] ANLs are therefore clipped, but not severely because the dominant contribution of the unaffected lowest frequency (<100 Hz) noise to the [10-500 Hz] ANLs (Fig. 4.13 d).

As the ice cover formed in November, the underwater noise level in the Amundsen Gulf decreased to a minimum under consolidated ice during the winter period. Such effects of the

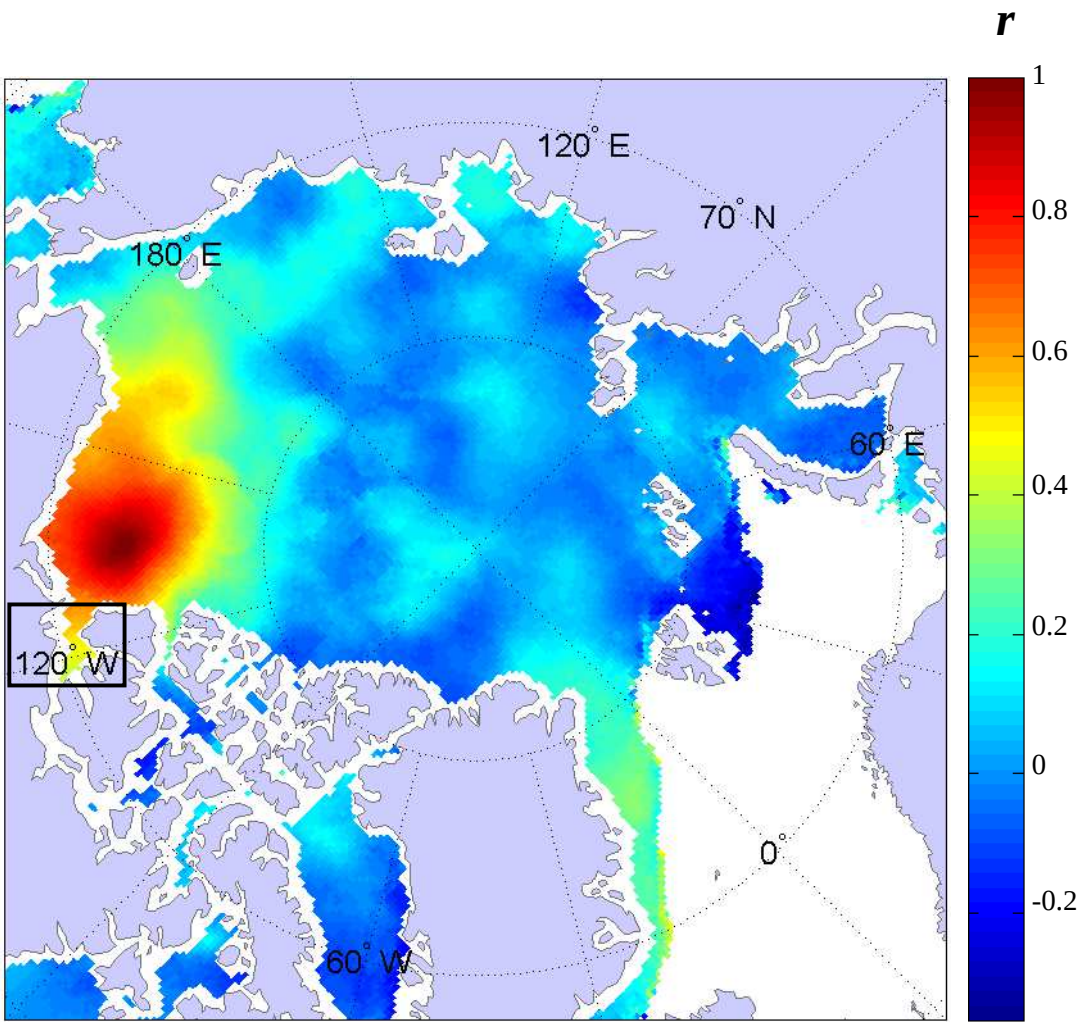

Figure 4.19: Map of correlations (Pearson r) between the ice drift at the location of maximum correlation in Fig. 4.18, and the other nodes of the ice drift grid showing the large-scale continuity in regional ice drift.

ice cover on underwater noise level were observed in other seasonally ice-covered Arctic and sub-Arctic basins [Roth12]. Ocean noise seasonal modulation was also observed under perennial ice during summer, fall and winter in response to the seasonal heat cycle affecting ice motion and fracturing [Lewis87]. This strong seasonal modulation was observed in both the ocean and ambient noise components. This is due to the strong dominance of the ANL contribution relative to the hourly averaged contribution of transient events, which exceeded 1.4 dB only 10% of the time over the [0.01-4.1 kHz] band for the entire 13-month time-series (Fig. 4.13 a-c). The use of ocean noise instead of ambient noise degrades the strength of the correlations and the clarity of the results presented here, although the general conclusions remain the same.

The estimated under-ice ANL was centered around 65 dB re $1\mu Pa^2$ Hz^{-1} at 100 Hz and half of the values were comprised within a 10 dB envelope around this median. This differs by only 1 to 3 dB from under-ice ocean noise observations of March and May 2009 in Chukchi Sea slope region, despite the different depth (235 m) of the recordings and the different period

([Roth12]'s Fig. 4.13 b,c). The spectral slopes between 100 and 1000 Hz for the same two sets of observations are also very similar at ∼-10 dB per decade. The total envelope of our ANL observations at 100 Hz is 36 dB (1^{st} to 99^{th} percentiles) while [Roth12] report 34 dB (March 2009). At lower frequencies however, our 1^{st} percentile of 55 dB re 1μPa^2 Hz^{-1} at 10 Hz is 17 dB lower than that reported by Ruth et al. (2012). The 10-Hz medians also differ by the same amount (respectively 67 vs 82-88 dB re 1μPa^2 Hz^{-1}). Our measurements in this low-frequency (<100 Hz) band however agree with the range of under-ice values published for the Arctic by Ganton and Milne (1965) and by [Lewis87] for 32 Hz, but they do not for 10 Hz.

The correlations and PCA analyses revealed that the [10-500 Hz] ANL in the Amundsen mouth does not significantly respond to the air temperature and pressure, nor to their temporal gradients. This indicates that the main forcing for ANL was not local short-term thermal ice cracking and fracturing due to meteorologically forced internal ice stress, contrary to the expectations for total ocean noise levels based on studies of Greene [Greene64], Makris [Makris86] and Milne [Milne66]. This is likely due to the fact that our ANL estimates exclude transient events in contrast to the total ocean noise of the other studies, and possibly to our longer time period (230 days) compared to the short time-series of the other studies (from 1 to 24 days). In addition, since the early 1960's works, global warming has forced drastic changes in the Arctic ice sheet, resulting in a decrease in the multi-year ice thickness and an increase in the ice drift speed [Rampal09, Weiss09b, Rampal11]. These changes are likely to impact the ambient noise production mechanisms and consequently its multidimensional structure. The strongest correlations of ANL with environmental variables were due to the inter-correlated triad [wind/ice drift/surface currents]. As sea ice motion is responding to geostrophic winds, the ice pack generally moves at ∼0.77 to ∼2% of surface wind speed [Thorndike82, Kimura04]. As surface currents are driven by the ice motion [Thorndike82, Nakayama12], such a correlation triad is consistent with our knowledge of the functioning of this physical process. The correlation with the ANL therefore indicates the dominant contribution of ice drift to the regional ANL.

The correlation maps showed that the relation of ANL with ice drift was not local but distant from our recording station by ∼300 km. The correlation core was located within the plume of multi-year ice, moving westerly off the mouth of the Amundsen Gulf (Fig. 4.12 c,d). The correlations of ANL with local ice drift were positive with northwestward drift, therefore along the direction of the multiyear ice plume displacement, which indicates the regional momentum. Strong noise appears to be associated with the westerly pulsed advances of this plume along the Beaufort Gyre, which entrains westward and northward the local ice covering the mouth of the Amundsen Gulf. The movement of this plume, which averaged 4.1±3.5 cm s^{-1} and peaked at 19.3 cm s^{-1} (Fig. 4.14 e, dash line), is responding to the frequent 180° shifts in dominant winds, aligned along the coastline. The ice field at the mouth of the Amundsen Gulf appears to also respond to this wind forcing, moving in and out of the Gulf, likely guided by the topographic direction of the Gulf mouth.

The possibility that the source of the measured ANL is located in the above area of the maximum correlation core within the multi-year ice plume is plausible. The median under-ice ANL at the recording station was 65.6 dB re 1μPa^2 Hz^{-1} at 100 Hz. The transmission loss (TL) from a distant source in the MIZ of Beaufort Sea can be approximated by 20 log10 (D) + 10 log10((R-D)/D), where D is water depth and R is the source-to-receiver range, from Milne and Ganton (1964)'s experiments within a similarly exposed fjord, McClure Strait - Melville Sound, located north of the Amundsen Gulf. With D = 2.5 km and R = 300 km, we get a total loss of ∼88.7 dB. Then a 300-km distant SL that would be responsible for the measured ANL at 100 Hz

would be (SL = ANL + TL) 154 dB re 1μPa^2 Hz^{-1}. Such high noise levels were measured during ice fracturing and ridging events at the observation station. They can surely occur during the movements of the multi-year ice plume where the correlation peaked. The large correlation area of ~500-km diameter represents a surface of 196 350 km^2, from which such high noise events can be recruited to produce the observed ANL in the upper water column sound channel of the Arctic at the mouth of Amundsen Gulf.

In conclusion, it appears that under-ice ANL in eastern Beaufort Sea at the mouth of Amundsen Gulf is most likely controlled by large-scale ice drift, connected to the Beaufort Gyre, and responding to an average of 7-day wind-forced pulses from the local passage of depressions, which generate a continuous myriad of sources that are summed into a blended background hum at large ranges. Due to its topography, the ambient noise in the Amundsen Gulf appears to be from 300-km distant sources, recruited over a ~200 000-km^2 large area, as schematically represented in Fig. 4.20.

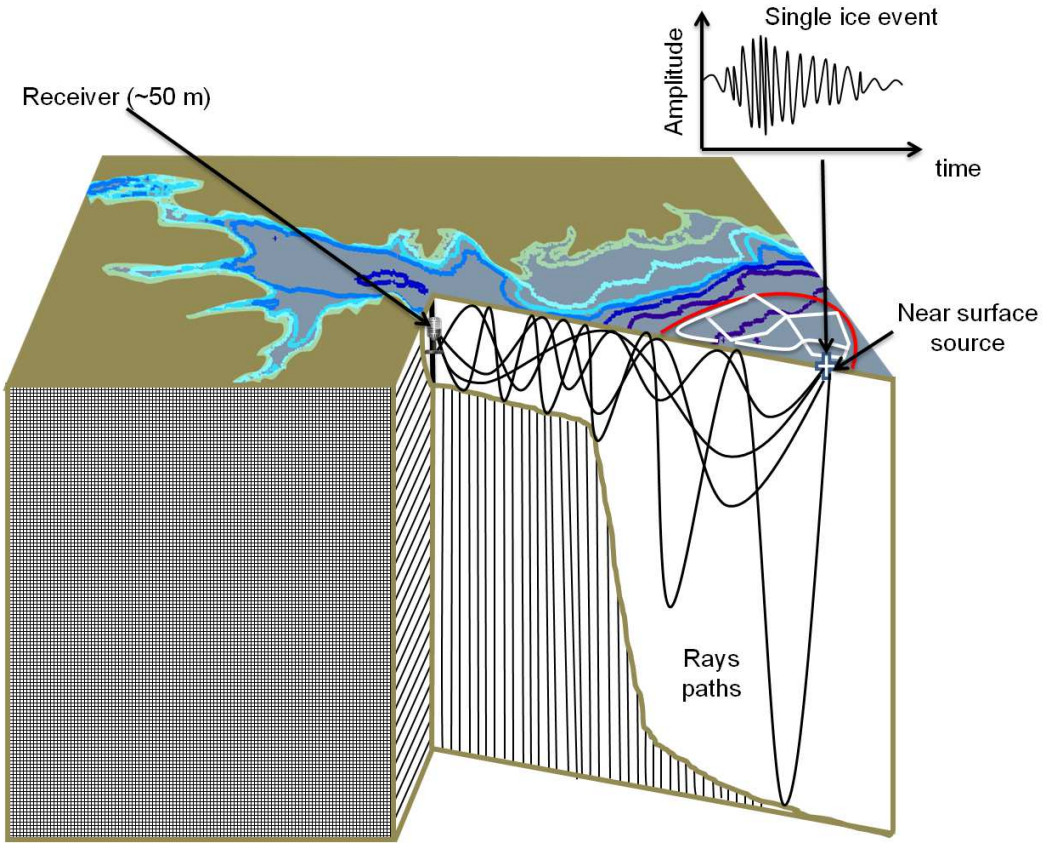

Figure 4.20: Schematic representation of ocean noise propagation from the multi-year ice plume drifting westerly from offshore Beaufort Sea to the 50-m deep recording location on the shelf in Amundsen Gulf.

4.4 Conclusion

The ambient noise levels in the Arctic Ocean is seasonal [Roth12, Lewis88] and respond to the environmental forcings. For the open-water period, wind-generated noise is observed in the

Eastern Beaufort Sea and in th Hudson Bay. The wind speed explained >50% of the background noise variance in the mid frequencies, and match Wenz wind-generated noise model [Wenz62] for the 2^{nd} and 3^{rd} quartiles of the the ANL and the measured wind speed. The mismatch for the 1^{st} quartile may due to wind speed recorded at the ∼80 km weather station from the mooring location, as low winds may be assumed to be more local. At the low frequencies, the seismic explorations and other industrial activities may contribute to the ANL, as such sound sources can propagate at long distance [Rice13] and add to the background noise.

The sea ice monitoring from satellite observations since 1979 showed that the Arctic summer sea ice extent, often defined as the area with ice concentration ≥15% of a grid cell [Wang12], has declined at a rate of >11% per decade [Kattsov10] and the projections suggest that the Arctic could be sea ice free during summer between 2040 and 2100 [Stroeve12b, Wadhams12]. Arctic could then experience long periods during which the noise level increases by at least ∼10 dB, the difference currently observed between under-ice and open-water ANL. The Arctic will, with probably very noisy episodes due to the accentuation of cyclones and precipitations.

Under ice pack, the background noise level, excluding nearby identifiable sources, is controlled by the large-scale Beaufort Gyre circulation, which likely generated myriad of sources. Arctic sea ice is getting more and more thin and young, as the ice thickness experienced a decay in the central Arctic of 48% in winter, from 3.64 m in 1980 to 1.89 m in 2008, and of 53% in summer [Kwok09b] resulting in an increase in the ice drift speed [Rampal09, Weiss09b, Rampal11]. As the sea ice thickness declines accelerate during the last decade (NSIDC), the ice drift is expected to accelerate and so will probably be the under-ice ambient noise level.

Arctic Ocean and sub-Arctic Seas are free a significant man-made noise source and the ambient the soundscape of such polar regions are pristine. Fig. 4.21 summarizes the comparison with others areas noise for various traffic intensities. In a relatively devoid of man-made noise source environment, Reeder (Reeder et al. 2011) showed a linear dependence of noise psd with the logarithm of the wind speed, with a slope of 26.6 dB at 1 kHz, assumed a time lag of 30 min between the noise and wind speed. In the Amundsen Gulf, such lag was not yet observed for the summer ambient noise, probably because of our wind data collected at ∼80 km from the moorings. Reeder's minimum noise spectrum (Fig. 4.21, green dashed) has virtually the same slope as the Wenz [Wenz62] minimum level and their 9-kt wind one (Fig. 4.21, green solid line) is under the minimum we observed in summer (Fig. 4.21 black solid line). This is due to the limit of our recorders, adapted for loud low frequencies recordings.

Gervaise *et al.* [Gervaise12b] estimated wind-generated noise (Fig. 4.21 purple) to be the 9.4^{th} percentile of the ocean noise from 42 d measurements made at the Saguenay mouth, with is consistent with the median observed in the Amundsen Gulf mouth (Fig. 4.21 black solid line) in the 10–2 kHz frequency band.

It is generally known that in heavy shipping areas, the ambient noise in the mid frequency band is essentially generated by ships. A particularly heavy traffic exposed area noise, (Fig. 4.21 Ushant median), showed that, the median ambient noise is 14.5 dB higher than the median noise observed in the Beaufort Sea at 50 Hz, narrowed to 8.5 dB in the [0.15– 1] kHz frequency band, and to ∼3 dB at 4 kHz.

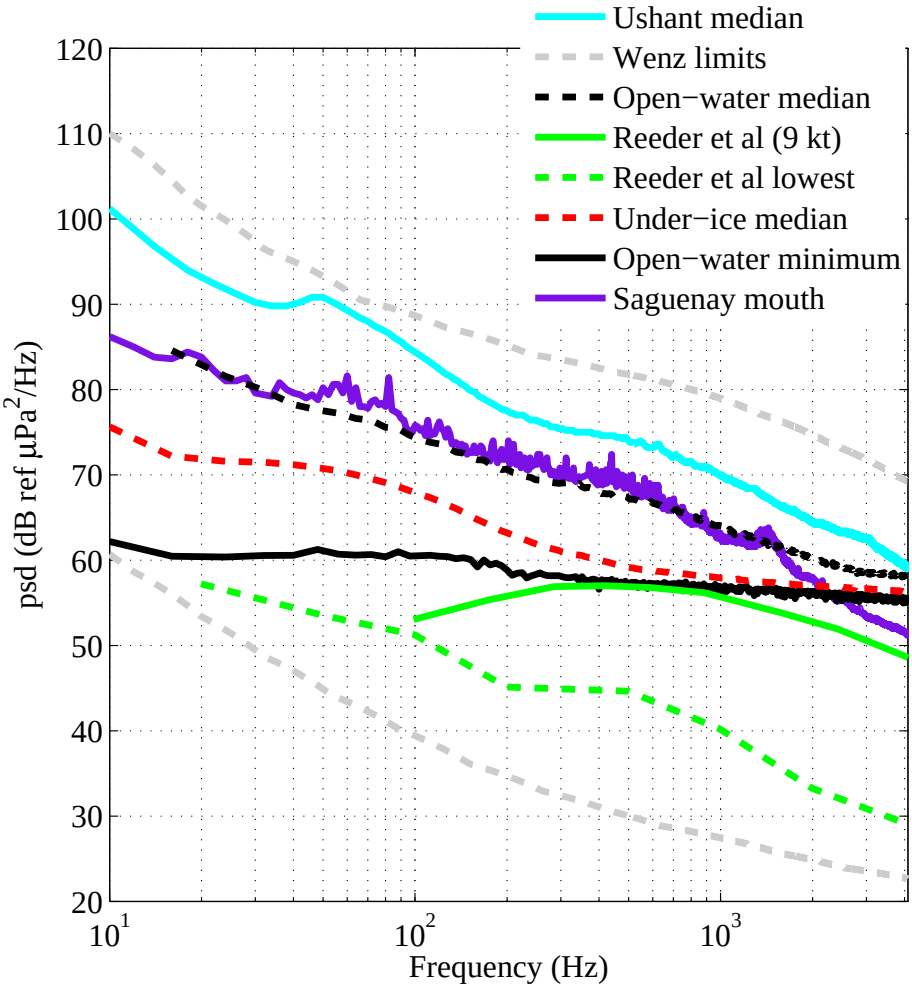

Figure 4.21: Comparison of the the Arctic Ocean pristine ambient noise with other soundscapes of the world where the contributions of anthropogenic chronic sources are prominent.

Chapter 5

Acoustic transient events under Arctic ice cap

Contents

Ocean noise is composed of ambient noise and identifiable transient events, where ambient noise refers to the background noise emanating from a myriad of unidentified sources [NRC03]. In the Arctic and under ice covered conditions, the physical sources of ocean noise, and hence the identifiable transient events, are from the mechanical deformation of the ice cape. In the precedent chapter a year-long time series of the ambient noise component was systematically extracted using a dedicated algorithm from acoustic recordings in the Amundsen Gulf, in the MIZ of the Canadian Arctic, Eastern Beaufort Sea. The analysis of the ambient noise multivariate structure was undertaken using the meteorological forcing, the arctic ice drift and the *in-situ* current speed, depending whether the study area is ice covered or not. We showed that the under-ice ambient noise, in the Amundsen Gulf was driven by the large-scale ice drift entrained by the Beaufort Gyre and responded to 7-day wind-forced pulses from the local passing of depressions. The present section is intended to complement this previous work, as it examines the under-ice acoustic transients relying on physical processes, using the acoustic data set and the environmental variables (winds, ice concentration, ice drift, *in-situ* currents) described in chapter 3.

By combining the satellite observations of Arctic sea ice concentration and velocity field, and year-long acoustic recordings in the marginal ice zone in the Canadian Arctic, we address the acoustic transient events relation with the large-scale ice deformations. This chapter is organized as follow. The next section describes the global warming effect of the Arctic ice cape and its mechanical behavior. Sec. 5.2 examines the under-ice acoustic transients in the MIZ by analyzing their time-frequency content and their relations to the environmental forcings. This section, in part, is a reprint of the material proposed for publication in the Journal of acoustical society of America. The last section gives some conclusions and remarks.

5.1 Arctic ice cap

5.1.1 The arctic sea ice decline

In winter, the sea ice covers an area of up to 7% of the earth's surface [Thomas10] and plays a fundamental role in the Earth climate system [Weiss04] as ice processes contribute to the driving of the global distribution of water mass characteristics [Thomas10]. In the 1950s, the Arctic Ocean was sea ice covered all through the year [Langehaug13] and changes of sea ice coverage are commonly taken as an indicator for climate change [Haas10b]. The sea ice monitoring from satellite observations since 1979 showed that the Arctic summer sea ice extent, often defined as the area with ice concentration $\geq$15% of a grid cell [Wang12], has declined at a rate of >11% per decade [Kattsov10], while winter ice coverage of the Arctic Ocean decreases at a much slower pace of only 2.8% per decade [Haas10b]. After the unexpected drop of the Arctic sea ice extent in summer 2007 alarming the sea ice scientific community, the Arctic Ocean experienced a new record minimum in August 2012, earlier than usual, by 18% of the lowest extent observed in 2007 (from 4.17x10^6 km^2 to 3.41x10^6 km^2) [Zhang13] as shows Fig. 5.1.

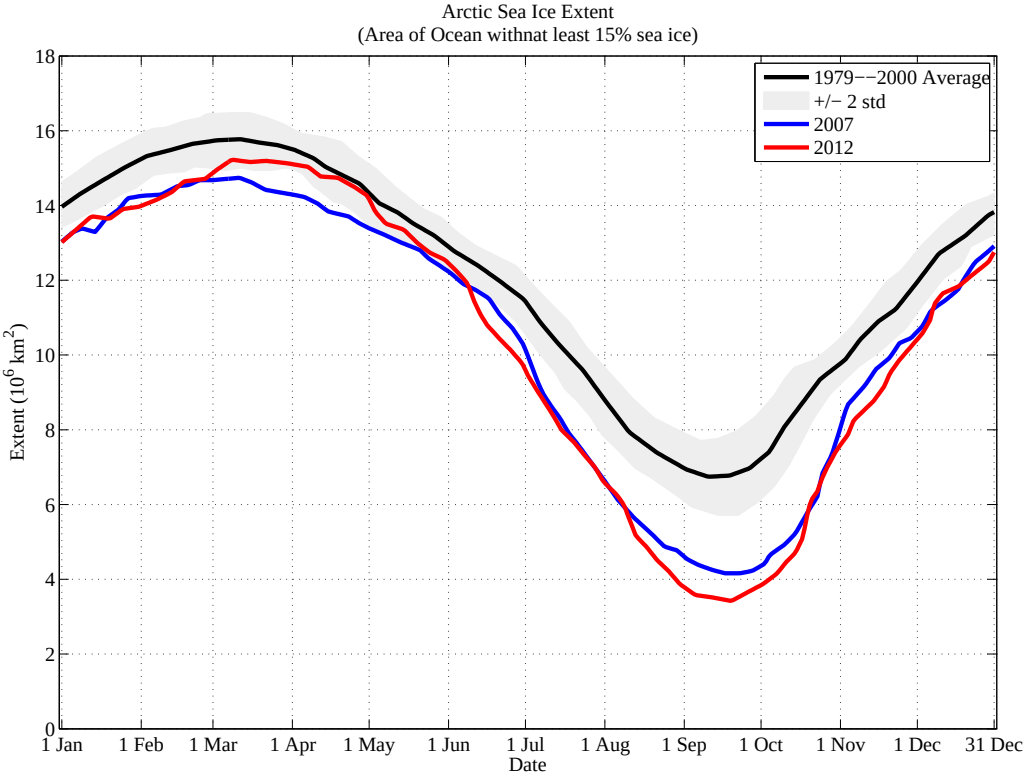

Figure 5.1: Annual Arctic Ocean ice extent from the from the national snow and ice data center (NSIDC) website (http://nsidc.org/arcticseaicenews/ (last viewed: 25/09/2013))

Arctic sea ice is getting also more and more thin and young. The ice thickness experienced a decay in the central Arctic of ∼48% in winter, from 3.64 m in 1980 to 1.89 m in 2008 on average, and of ∼53% in summer, as observed by submarine within 1958 – 2000 and ICESat (Ice, Cloud, and Land Elevation Satellite) from 2003 to 2007 [Kwok09b]. At the end of summer 2010, <15% of the ice remaining in the Arctic was >2 years old, compared to 50–60% during the 1980s [Kattsov10]. It can be seen from Fig. 5.2 that the MYI (Multi Year Ice) along the West coasts of the Canadian Archipelago and Greenland has undergone a drastic decay from 22004–2008 to present by ∼2 m. Despite the dispersion between global climate models, projections suggest that the Arctic could be sea ice free during summer between 2040 and 2100 [Stroeve12b, Wadhams12].

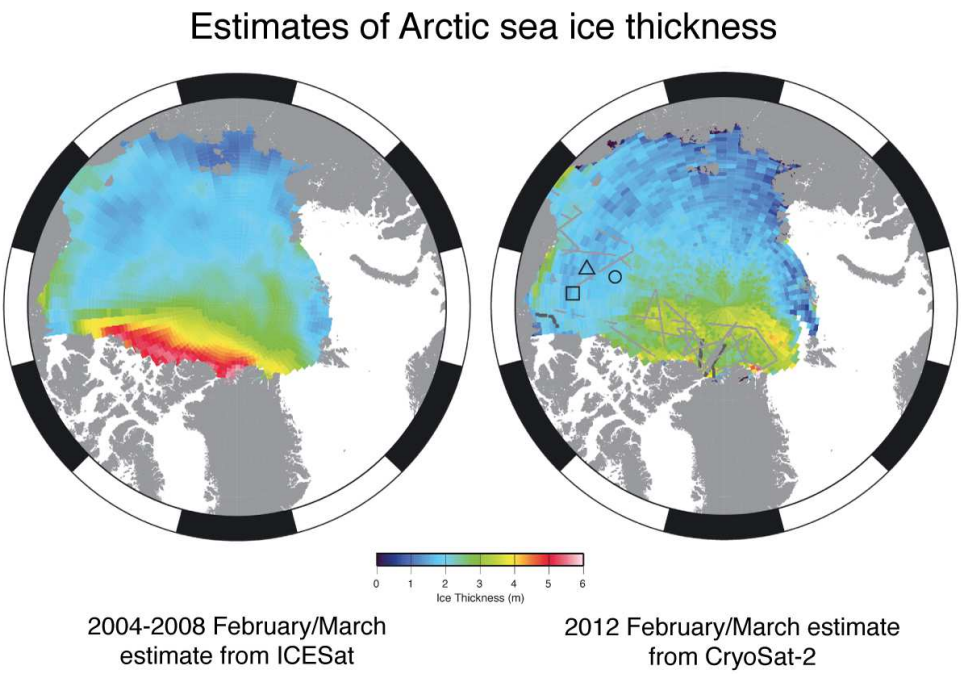

Figure 5.2: Estimates of February/March average sea ice thickness in the Arctic Ocean for 2004 to 2008 from NASA's ICESat (left) and February/March 2012 from CryoSat–2 (right). Colors indicate ice thickness in meters, with blue indicating 1-meter thick sea ice and red indicating 5-meter thick sea ice. The black and gray lines in the CryoSat–2 image are tracks of airborne data collected for validation. The triangle, circle, and square are locations of upward-looking sonar (ULS) moorings, also used for validation of the CryoSat–2 estimates (from NSIDC website :http://nsidc.org/arcticseaicenews/ (last viewed: 25/09/2013)).

5.1.2 Mechanical behavior of the Arctic ice cape

The ice cover is a dynamic sheet moving and deforming under the action of several heterogeneous forcings [Hibler III79, McPhee80, Thorndike82, Weiss04, Girard09] : winds, ocean currents, internal stresses, Coriolis Force, sea surface tilt. The average thickness of the Arctic ice cover is a few meters and the momentum balance when the sea ice tilt is neglected, in a 2D modeling framework, is described by Weiss et al. [Weiss04]:

$$m\frac{\partial\, u}{\partial\, t} = \tau_w + \tau_g - m f_c k \times u + \nabla.\sigma, \tag{5.1}$$

where, m is the mass per unit area, u the ice velocity, τ_w and τ_g respectively the water and wind stresses, f_c is the Coriolis Force, and σ the divergence of the internal ice stress tensor, described by Eq. (5.2),

$$\sigma = 2\eta_b \frac{d\epsilon}{dt} + \left[(\eta_s - \eta_b)\, T\left(\frac{d\epsilon}{dt}\right) - \frac{P}{2}\right] I, \tag{5.2}$$

where η_b and η_s are respectively the shear and bulk viscosities, $d\epsilon/dt$ is the strain-rate tensor, T() the trace of a tensor, P the ice strength, and I the two-dimensional unity tensor.

Sea ice deformation largely controls the ice thickness distribution and the mechanical behavior of the ice pack [Rampal08]. The deformation rate is important for understanding the

global sea ice mass balance in climatic models [Lindsay03, Girard09]. Indeed, deformations result in fracturing, leads opening and closing, shear, ridge ice [Kwok01, Lindsay03].

The deformation rate can be determined from the spatial gradients of the velocity field [Kwok01, Rampal08, Kwok12] as follow:

$$\zeta = \frac{\partial v}{\partial x} - \frac{\partial u}{\partial y}, \tag{5.3a}$$

$$\nabla d = \frac{\partial u}{\partial x} + \frac{\partial v}{\partial y}, \tag{5.3b}$$

$$s = \left[\left(\frac{\partial u}{\partial x} - \frac{\partial v}{\partial y} \right)^2 + \left(\frac{\partial u}{\partial y} + \frac{\partial v}{\partial x} \right)^2 \right]^{1/2}, \tag{5.3c}$$

$$\tau = \left[d^2 + s^2 \right]^{1/2}. \tag{5.3d}$$

where, u and v are the East-West and North-South component of the ice drift speed at the coordinates (x, y), ζ the vorticity, d the divergence, s the shear deformation rate and τ the total deformation rate of the ice velocity field.

This ice deformation is a complex space/time coupling strongly intermittent and heterogeneous, following Eq. (5.4) as described by [Rampal08, Weiss09a]:

$$\tau \sim t^{-\alpha(R)}, \tag{5.4a}$$

$$\tau \sim R^{-\beta(t)}, \tag{5.4b}$$

where the intermittence term $\alpha(R)$ decreases with increasing spatial scale, from $\alpha = 0.89$ for R$\approx$ 1 km to α= 0.30 for R$\approx$300 km in winter (respectively 0.87 and 0.25 for summer). The degree of heterogeneity $\beta(t)$, decreases with increasing time scale, from $\beta = 0.85$ for t$\approx$1 h to $\beta = 0.35$ for t$\approx$1 month in winter (respectively 0.85 and 0.42 for summer). In the Arctic, the mean shear values vary 1.0% d^{-1} for winter and 1.6% d^{-1} as measured by buoys [Thorndike86] to 0.87% d^{-1} for winter and 1.13% d^{-1} for summer as observed from satelittes measurements [Lindsay03].

The sea ice deformations are essentially accommodated by transient fracturing events of various scales and size [Weiss09a]. Some leads therefore appear at the zones where velocity gradient are spatially discontinuous, and where the rates of shear, divergence, convergence, and vorticity are concentrated [Schulson09]. Under-ice, it may result in various types of acoustic transient events (*e.g.* [Xie92, Xie95, Buck86]). The arctic ambient noise generation mechanism were therefore examined through a variety of ice field descriptors and dynamical forcing functions including ice concentration, expansion, expansion rate, divergence rate, principal shear strain rate [Makris86, Makris91].

5.2 Acoustic transient signal from sea ice deformation in Eastern Beaufort Sea

From long term ocean noise recording session in Eastern Beaufort Sea, in the marginal ice zone of the Canadian Arctic, from September 2005 to October 2006, strong acoustic transient

events from biological or physical sources were detected. When the study area was ice covered (> 90%), from November 2005 to mid-June 2006, the dominant physical sources were related to the sea ice deformations under heterogeneous forcings. Sea ice fracturing, cracking, shearing, and ridging generated various acoustic transients. A dictionary of these sounds was built and presented. The opening/closing of leads in the Arctic, identified by the sea ice concentration patterns from satellite observations, were used to evidence the different types of wideband noise tones and impulses due to the Arctic Sea ice dynamic. Some of these acoustic transient events, of variable durations, are repeated with a period corresponding to waves and can sometimes be confounded with marine mammal songs. The correlations of the transient occurrences with the environmental variables showed that the loud acoustic transients, which can propagate over long distances, were related to sea ice shear deformation.

5.2.1 Context

As we saw previously, the Arctic Ocean is entirely covered with ice of variable thickness and age during winter [Marsan04, Maslanik11, Marsan12, Stroeve12b]. The acoustic sound sources in the Arctic Ocean depend on its ice cover extent, and the Arctic under-ice ocean noise is the response of this ice cover to the environmental forcing [Farmer89] as we described in chapter 3. Since the pioneer work of Milne and Ganton [Milne64, Milne66], primary sources of Arctic ocean noise in winter and spring was known to be the discrete acoustic events caused by the combination of the thermal, wind and current stresses on the ice canopy. Arctic under-ice ocean noise is then a mixed spectrum, with stationary Gaussian intermixed high occasional high intensity transients noise [Veitch85], observed when the sources are close or loud enough [Zakarauskas91]. The spatial distribution of the thermal ice cracking, the response of the ice cover to the atmosphere cooling [Dwyer83], depends on the ice age; it mostly occurs in the multi-year ice, as shown by [Xie91], using synthetic aperture radar images and air photographs of the ice correlated with acoustic recordings. Thermal cracking sources were also shown to radiate acoustic energy in the water, recorded by hydrophone, and seismic wave into the ice cap, recorded by geophone [Xie95]. These authors also observed pure tones related to ice break-up in the MIZ that frequency depends on the ice thickness and the shear wave speed [Xie92]. Other processes related to the Arctic sea ice dynamic, such as the pressure and shear ridge are responsible for particular acoustic transient events in the Arctic Ocean, as observed by [Buck86] over 3-days period in April 1979. In addition to those listed above, [Cummings89] summarizes other types of transient events such as, ice squeaks, ice stuck and bump, lead opening in diverse conditions, snow pelting, wave slap, mostly observed in shallow water environment (∼8 m) in the MIZ.

The MIZ in the Canadian Arctic, Eastern Beaufort Sea, is an area with high seasonal dynamics. Cyclically, this MIZ goes from an open-water environment in July to September to an under-ice environment from November to June (see Fig. 14 a,b). The Arctic Ocean, even entirely ice covered, presents two main circulation patterns which control its ice coverage and thickness distribution (see Fig. 14 c,d,e).

The Arctic ice cover is not an uniform continuous sheet [Weiss04]. Open water areas are widely distributed throughout the entire Arctic Ocean and represents ∼10% of its surface in the winter [Simon82]. These ice-free surfaces are classified as leads and polynyas. Polynyas are mesoscale areas of open water or thin ice that are recurring at predictable locations in sea ice-covered regions [Stringer91] and have a rectangular or oval aspect ratio with length scales of order 100 km [Martin01b]. The polynyas formations and their maintenance is a complex

process involving winds, the nature of the ice, the heat vertical exchanges, and the currents [Hannah09]. In contrast to polynyas, leads are generally linear transient openings that may extend over hundreds of km, delimiting quasi-rigid floes, and resulting from sea ice deformations from highly episodic fracturing sequences [Weiss04]. Leads have generally a much smaller area than polynyas and are not restricted to a particular location [Martin01b].

These various deformations processes can result in high intensity acoustic transients events, as reported by [Xie92]. In this section, we use the combination of the sea ice concentration and velocity field from satellite observations to assess the acoustic transient events observed in the MIZ during the winter 2005/2006.

5.2.2 Numerical analysis

The raw 16-bit acoustic recordings on a [0-4.1 kHz] were first converted to instantaneous sound pressure level using the AURAL A/D conversion parameters, gain, and the hydrophone receiving sensitivity calibration curves. For the under-ice period, from November, 6, 2005 to June, 23, 2006, spectrograms of 7-min hourly recordings were computed using the Fast Fourier Transform (FFT) algorithm and a Hamming window of 2048 points, with 50% overlap, and visually examined to classify the acoustic transients based on their time-frequency characteristics. Three classes were considered: wideband (class 1), frequency modulated (class 2) and high frequency transients (class 3). The time-series of daily occurrence of each transient class was then computed. The low frequencies were sometimes contaminated by periodic strum from the mooring and for fixed mooring on a vertical line, strum noise is often pulsed and consisted in recognizable low-frequency impulses of variable bandwidth [Kinda13] that were discarded from the analysis.

For each transient class, a subsample of 40% of the transients, uniformly distributed through the time-series, were extracted for statistical characterization of duration and frequency patterns of the transient class. The received levels of the selected transients were then computed following Eq. (5.5), where the time integration term T refers to the transient duration. For class 2 and class 3 transients (modulated and high frequency), the acoustic data were filtered using bandpass or highpass filters with cutoff frequencies adapted for each transient prior to the received level computations. The spectral characteristics of class 1 and class 3 transients were estimated using the time average of their spectrogram computed using the parameter described above. The peak frequency of the wideband transient (class 1) corresponds to the maximum of the averaged spectrogram.

$$P_{rms} = \sqrt{\frac{1}{T}\int_T s^2(t)dt}, \tag{5.5a}$$

$$SPL = \frac{P_{rms}^2}{P_{ref}^2}, \tag{5.5b}$$

where P_{rms} is the root mean square pressure, T is the integration time, $s(t)$ the acoustic recording, SPL is the sound pressure level and and $P_{ref} = 1\mu Pa$ the reference pressure level in water.

The daily total sound pressure level (SPL) was derived from the hourly SLP following Eq. (5.6):

$$SPL_d = \sum_{24} SPL_h, \tag{5.6a}$$

$$SPL_h = \frac{60 \times SPL}{T}, \tag{5.6b}$$

where SPL_d and SPL_h are respectively daily and hourly SPL, and T referred to the duration of the hourly recordings.

The links between the transient occurrences and the environmental variables were examinated through correlation and principal component analysis (PCA), [Legendre98] using daily data. The PCA were performed on correlation matrices so that all considered variables have the same weight in the analyses. The sea ice deformation was computed from the ice drift used in [Kinda13] following Eq. (5.3) as described by [Kwok01, Rampal08, Kwok12]. For each node of the Arctic ice drift field, the divergence, shear, and total deformation rate were then computed. The relatively low resolution of ice drift field (25 km x 25 km) did not allow a proper computation of local ice deformation around the mooring in the Amundsen Gulf mouth. An average of this deformation, were taken at MYI plume and in the FYI of the MIZ.

5.3 Results

5.3.1 Class 1: wideband transient

Two examples of these acoustic events are presented in Fig. 5.3. The two transients covered the entire 7-min hourly recordings with very high-energy received levels for ∼90% and ∼50% respectively. The maximum energy was within the [20-500 Hz] band (Fig. 5.3 a,b,c,d) The frequency peaks on the average power spectral density (psd) were ∼250 Hz and ∼48 Hz.

The subsample of 742 transients of this type varied little in peak frequency, which was within the 10-250 Hz bandwidth 95% of the time (Table 5.1). Their duration however were more variable, averaging 76.9 s and ranging from ∼0.90 s to the whole 7-min hourly recording cycle (Table 5.1). Nevertheless 50% of the detected transients were short events, lasting 23 s or less, and only 5% exceeded 418 s. The broadband received levels averaged 104 dB re 1 μPa, were within a 20-dB envelope 90% of the time, and peaked at 135 dB re 1 μPa.

Table 5.1: Statistical characteristics of the wideband transients.

	Average±std	min	5%	25%	50%	75%	95%	max.
T(s)	76.9±115.15	0.91	3.81	9.07	23.27	85.46	418.84	420
RL(dB re 1μPa^2)	104±6.60	92.32	96.05	99.64	103.40	108.93	115.80	135.12
PF(Hz)	66.30±137.24	16	16	16	32	48	265	1344

5.3.2 Class 2: pure tone modulation transients

Several pure tone modulations of variable bandwidth and duration were found (Fig. 5.4). Some of these modulations had wavy oscillations and several harmonics, that sometimes covered

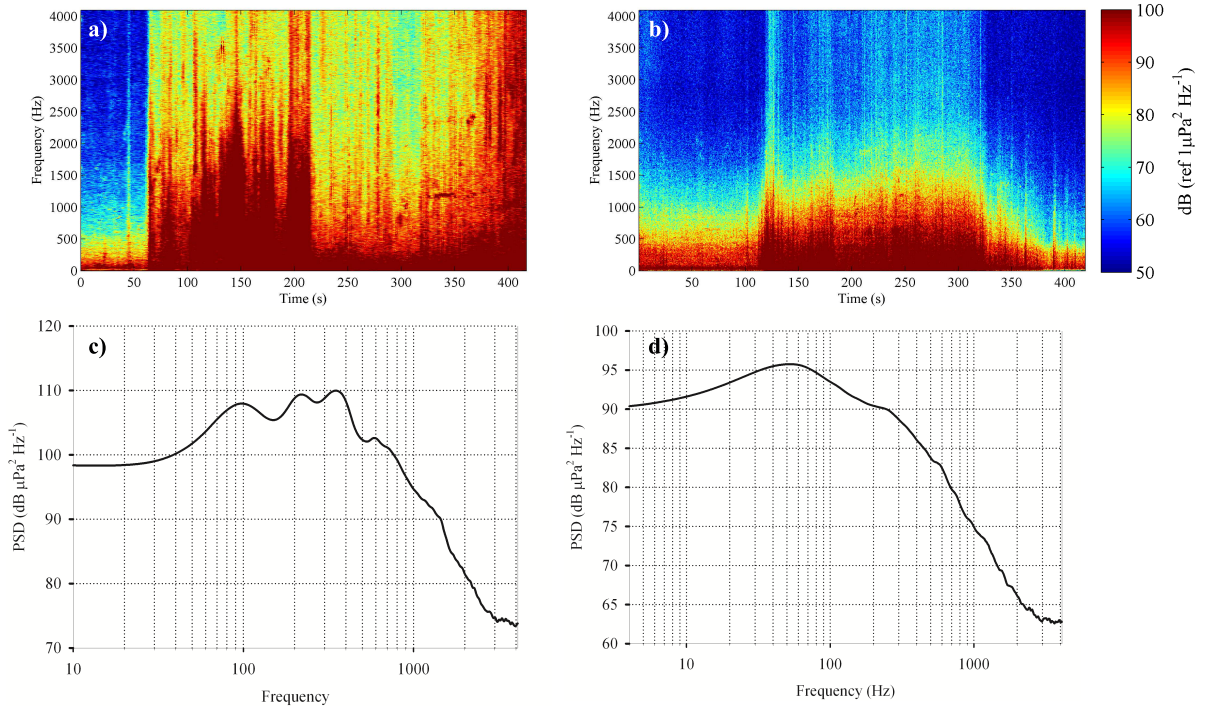

Figure 5.3: Spectrograms of wideband transient (a) observed on December 15, 2005, at 05:00 pm and (c) its psd, (b) observed on February 6, 2006 at 12:00 am and (d) its psd. The maximum energy is located in the frequency band 20–500 Hz.

the entire bandwidth of the recorder (Fig. 5.4 a,b). Their occurence were sometime pulsated (Fig. 5.4 b,c,e), and repeated at regular intervals (Fig. 5.4 f).

A subsample of 977 of such transient events were selected for statistical analysis (Table 5.2). Their duration was highly variable, averaging 189.6±149.2 s, and ranging from 1 s to ≥420 s, the duration of a recording duty cycle. Their frequency band was quite variable, 50% of the transients were within a [1-3 kHz] envelope and less than 5% were <500 Hz (Table 5.2). The received levels averaged 95 dB re 1 μPa, and were contained within a 21-dB envelope around this value 90% of the time (Table 5.2). The minimum received level was 75.5 dB re 1 μPa and the maximum 129.9 dB re 1 μPa.

Table 5.2: Statistical characteristics of the frequency modulated transients.

	Average±std	min	5%	25%	50%	75%	95%	max.
T(s)	189.64±149.24	0.97	18.1	55.32	120.06	359.44	419.6	420
RL(dB re 1μPa^2)	95±6.47	75.50	85.60	90.60	94.70	98.86	106.62	130.0
BW(Hz)	2032.30±1013.81	138.60	544	1095.20	1812.50	2910.50	4024	4086

5.3.3 Class 3: High frequency noise transient

This particular class of high-frequency noise transients includes quasi-continuous events (Fig. 5.5 a) or clearly pulsed pattern (Fig. 5.5 b), sometimes associated with the class 2 transients

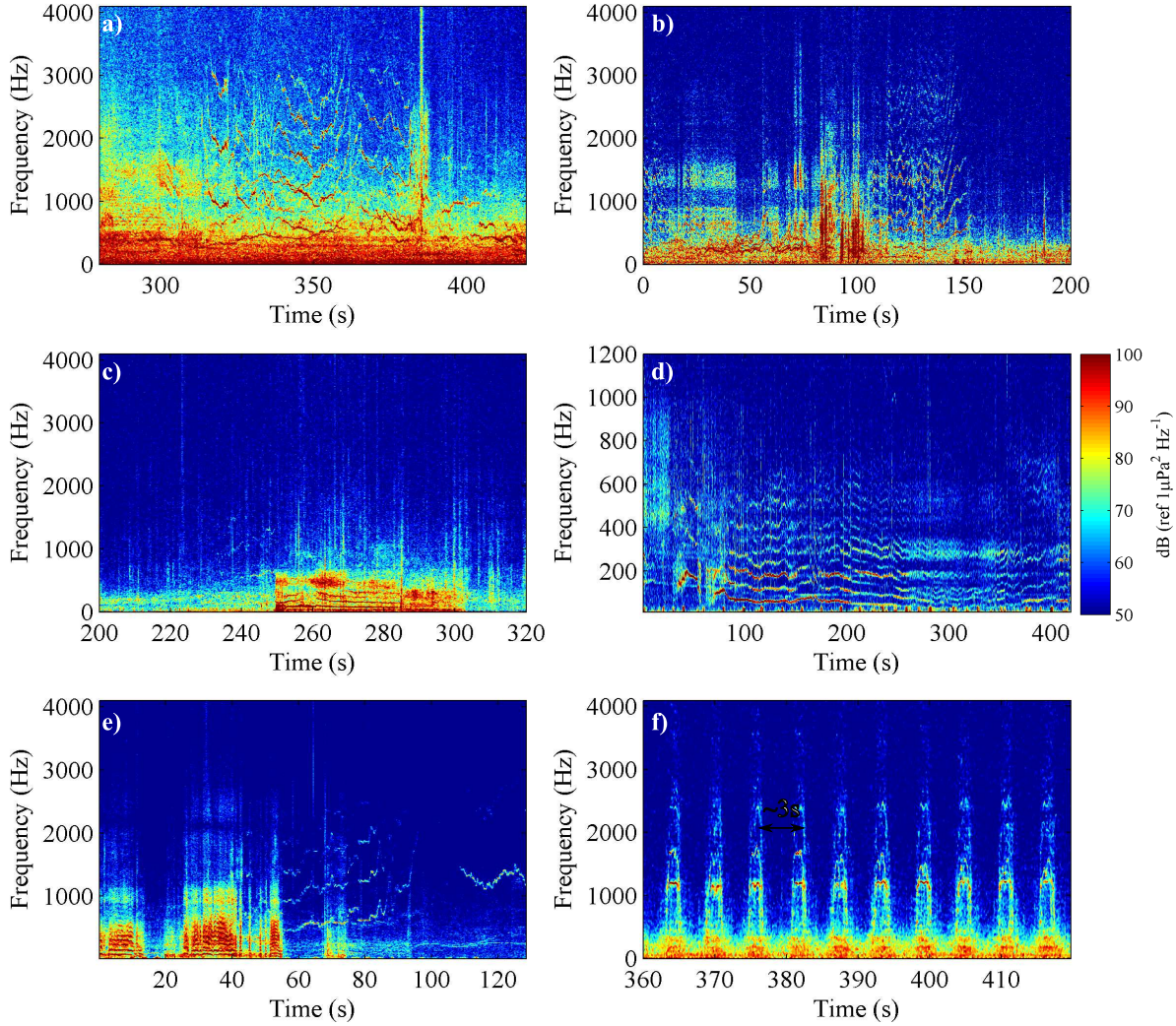

Figure 5.4: Various frequency modulations observed in the Amundsen gulf. (a), (b), (c), (d) and (e): spectrograms of recordings of February 12, 2006. (a),(b) and (d) exhibits harmonic covering the full bandwidth of the acoustic recorder while (c) and (e) reveals low frequencies modulations; (f): short pulsed modulations with ∼3 s time period observed on March 19, 2006.

(Fig. 5.5 b,d). The mean psd (Fig. 5.5 c) of the acoustic shown in Fig. 5.5 a decreases ∼20 dB per decade in the 10–400 Hz frequency band, reaches the measurement floor (∼53 dB) between 400 Hz and ∼1000 Hz, before increasing to reache a plateau at ∼2000 Hz (Fig. 5.5 c).

The minimum frequency of the 398 subsampled transients was ∼130 Hz and the highest was ∼3 kHz. These transient events generally covered the full 7-min duty cycle of the recordings (Fig. 5.5 a,b). Their broadband levels were narrowly distributed around a mean of 92 dB re 1 μPa, with 90% of the distributon contained in an envelope of 11 dB (Table. 5.3).

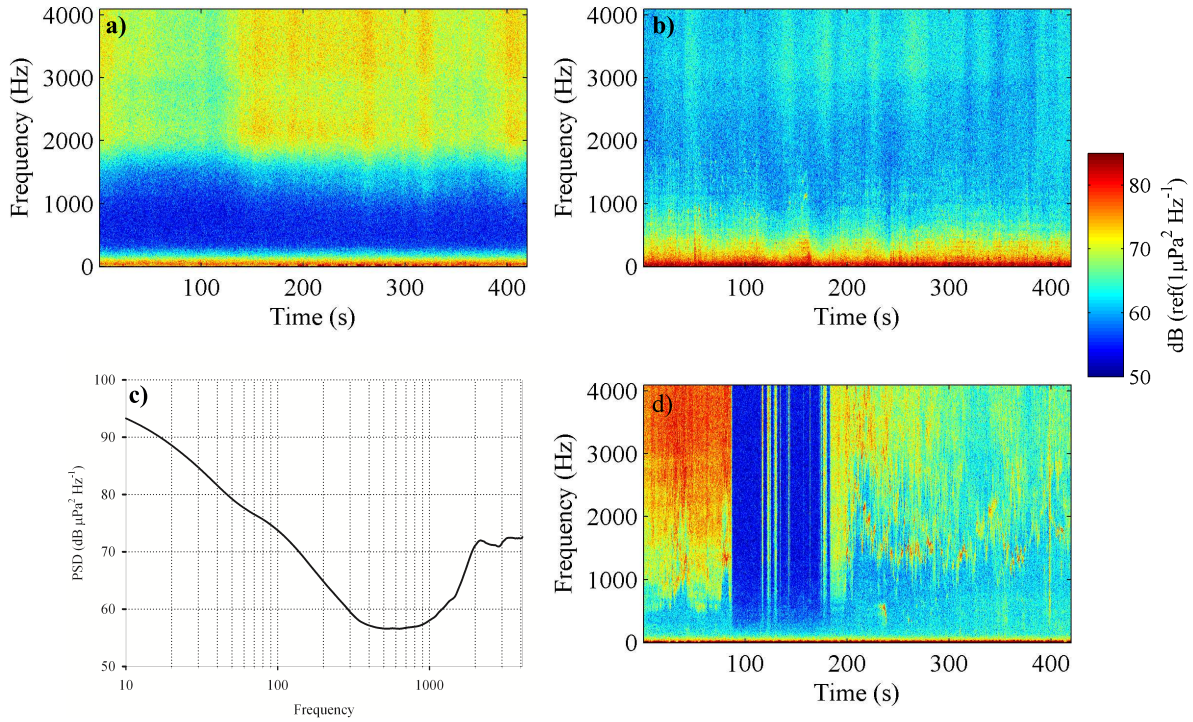

Figure 5.5: Hourly spectrogram of high frequency noise observed on February 12, 2006; (a), showing almost continuous high frequency sound; (b) pulsed sound and short low frequency modulations; (c) psd of the noise observed in (a); and (d) almost continuous high frequency noise and modulations.

Table 5.3: Statistical characteristics of the high frequency transients.

	Average±std	min	5%	25%	50%	75%	95%	max.
T(s)	420							
RL(dB re 1μPa^2)	92.93±3.70	86.67	88.40	90.08	91.95	95.66	99.50	112.40

5.3.4 Transient sounds and leads opening

The total daily ocean noise levels (ONL) winter time-series exhibited high levels that co-occurred with notable reductions of the local ice cover (Fig. 5.6 a) and strong ice deformation rates (Fig. 5.6 b). The ONL was also highly correlated with the ice deformation rate (Fig. 5.6 c, pearson r=0.57). An event of co-occurring high ONL, deformation rate and decrease of ice concentration was observed for several days in February 2006 (From 03–14 February, rectangle in Fig. 5.6 a,b).

The shear deformation rate for this selected period was computed at every node of the ice velocity field in the Amundsen Gulf and the entire Beaufort Sea. The resulting maps show the large-scale spatio-temporal variations in ice shear deformation (Fig. 5.7). An increase of this shear rate appeared along the Alaskan coast, south-west of the Beaufort Sea on February 5, 2006 (Fig. 5.7 c). This shear deformation intensified on February 6, 2006 (Fig. 5.7 d) and spreaded over the entire basin of the Beaufort Sea (Fig. 5.7 e). Then the deformation receded but remained high along the MYI plume, and extended to the west coast of Banks Island (Fig. 5.7 f,g,h, Feb.

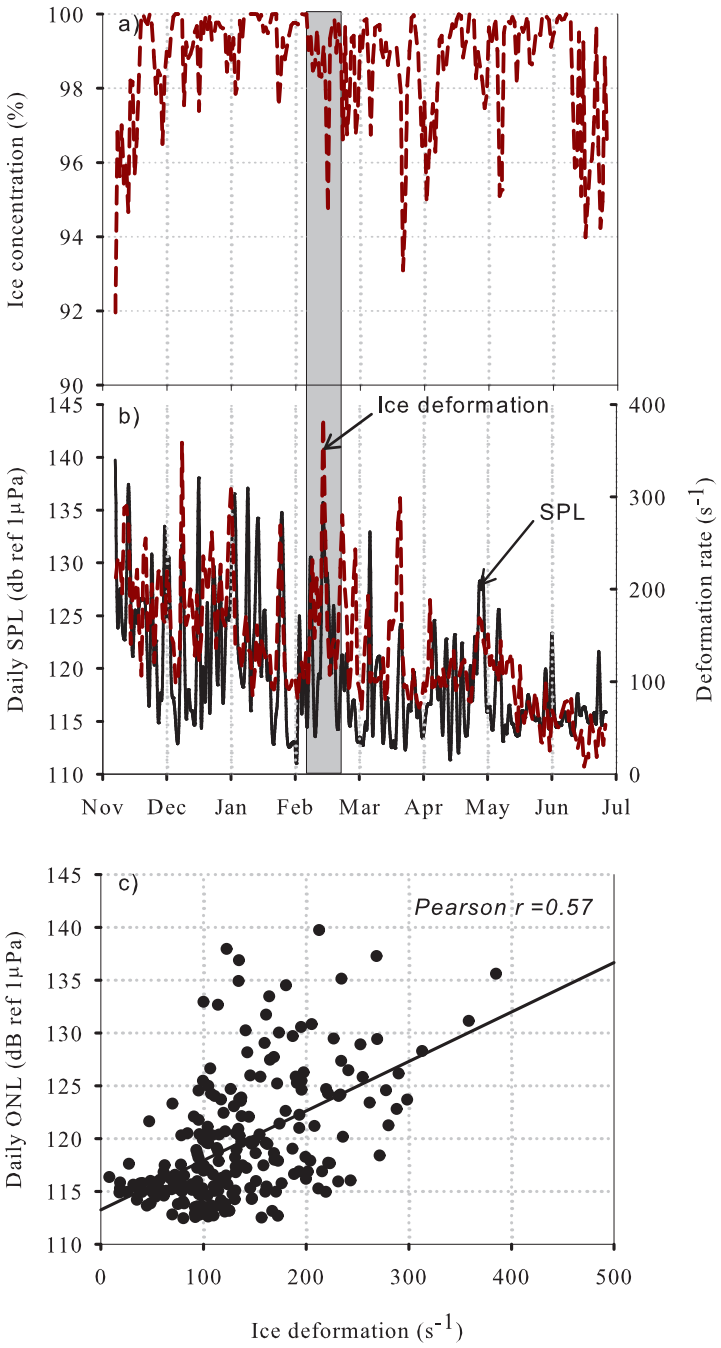

Figure 5.6: (a): Time series of the local ice concentration in a radius of 100 km around the mooring position in the Amundsen Gulf mouth; (b): the received ocean noise levels (black line) and the mean MYI ice deformation (red line). The rectangle indicates an example of high ocean noise levels co-occurring with lead opening as observed on February 03–14, 2006 in the ice concentration.

8–10, 2006). At the same time, another major large-scale ice shear strain is initiated north of Bering Strait (Fig. 5.7 h, Feb. 10, 2006), before spreading and intensifying into the central

Beaufort Sea on February 11–12, 2006 (Fig. 5.7 i,j). Finally, the deformation decreased and faded out and became more diffuse after February 13, 2006 (Fig. 5.7 k,l).

The examination of the Arctic ice cover in Eastern Beaufort Sea for the same period reveals the opening of 3 large leads, ∼300-500 km long by a few tenths km wide, at the shoreward margin of the MYI plume off the Mackenzie shelf (L1) and west coast of Banks Island (L2), and south coast of Amundsen Gulf (L3) (Fig. 5.8 d,e,f). The opening coincided with the peak of the large-scale ice deformation off Alaskan coast (Fig. 5.7 d) which later extended in Eastern Beaufort Sea (Fig. 5.7 e,f). This large stream of open waters within the ice cover was clearly visible during 3 days before closing on February 9 and 10, 2006 (Fig. 5.8 g,h), becoming undistinguishable for L2 with this ice cover image resolution (6.25 x 6.25 km pixels). This episode was followed by a re-opening of the three leads on February 12, 2006 (Fig. 5.8 i,j), which reached their maximum size on February 13 and 14, where a large part of the ice cover in the Amundsen Gulf is detached from the coast (Fig. 5.8 k,l). The change from closing to a re-opening again occurred during a second peak of large-scale ice shear deformation located offshore in Beaufort Sea, closer to the mouth of the Amunsden Gulf (Fig. 5.7 i,j).

Arctic sea ice deformation is a complex process involving winds, ocean currents, Coriolis Force, sea surface tilt, and thermal strain induced by rapid variations of air temperature [Weiss04]. The external forcings results in two processes in the sea ice behavior [Schulson91, Schulson04]: the development of internal stress, and its relaxation through viscous flow. The sea ice deformation is temporally structured by strongly episodic sequences of deformation and fracturing and is accommodated in space by leads opening [Weiss04]. This is in close agreement with the large-scale spatio-temporal patterns of ice deformation rate and mean ice concentration we observed (Fig. 5.7, Fig. 5.8, Figs. 5.10 a,e).

Several episodic acoustic transients were observed with time location corresponding to the description of the shearing deformation maps (Fig. 5.7) and leads opening described in Fig. 5.8. In fact some of the spectrograms shown in section 5.3 (Fig. 5.3 b, Fig. 5.4 a–e, Fig. 5.5) were part of recordings from this time period.

Our wideband transients (class 1) were similar to the ice breaking sound pulses described by Xie And Farmer [Xie92]. They observed that lead opening (the fracturing of the layer of ice in its full thickness over distances of several kilometers) in landfast ice in the Amundsen Gulf produces loud acoustic transient events. The under-ice ocean noise was therefore a combination of impulses until the fracturing process ends.

In fact, our wideband transients (Fig. 5.3) were from a series of loud events of such nature, of various durations, repeated over several days (Fig. 5.9). Because of our discontinuous recording, with a 12% duty cycle, we did not capture the whole process but only sample. Similarly, snapshots satellite images of ice concentration are refreshed a daily frequency only, which does not allow to see the dynamics of the large lead opening that occurred between images of February 5 and 6, 2006 (Fig. 5.8). In addition to this visible lead, there were probably some secondary leads and cracks that could not be detected with the coarse resolution of the ice concentration. The wideband sound spectra presented here for class 1 transients (Fig. 5.3) had similar peak frequency to those identified by [Cummings89] as resulting from ice stash and bump for shorter transient noise events (0.04–1.4 s) than ours (0.9–≥420 s) which they observed during ice break-up. We conclude that our class 1 acoustic transients could be considered as originating from intensive ice fracturing, accompanying the leads opening and their networks of secondary cracks. Hereafter, this transient's class will be termed as ice fracturing sound.

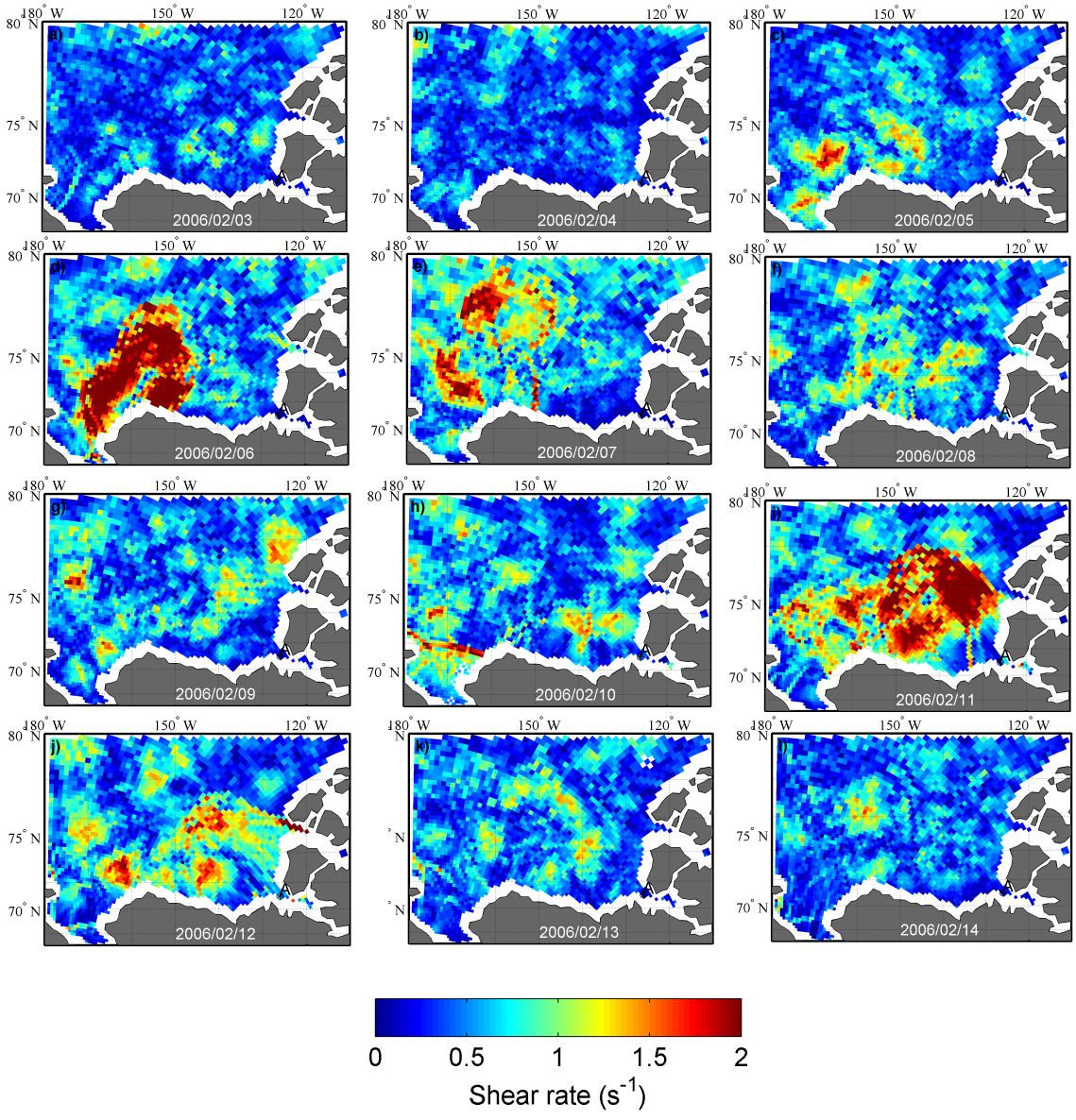

Figure 5.7: Arctic Ocean sea ice deformation computed for each node of the Arctic ice velocity field from February 3, 2006 to February 14, 2006

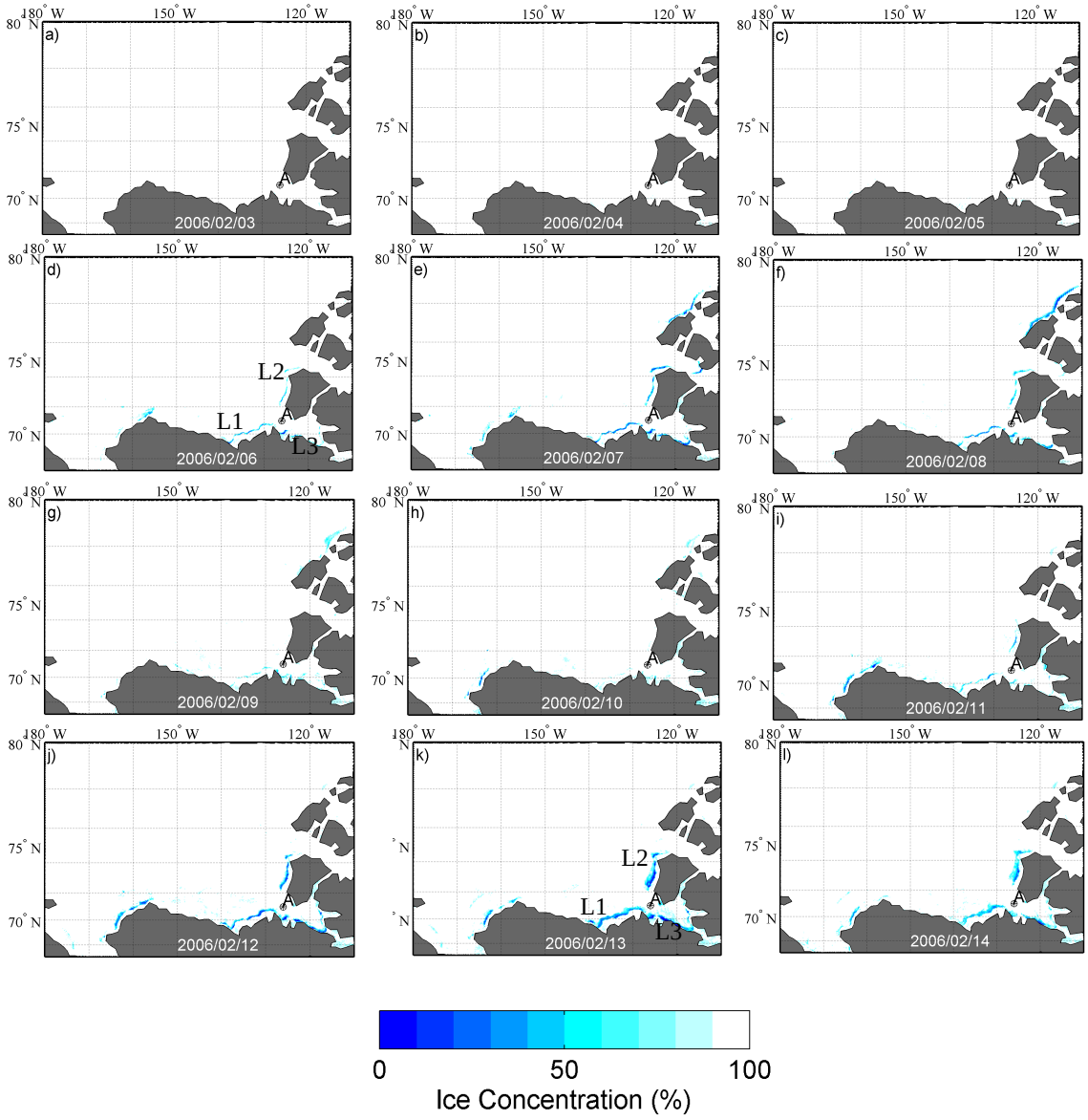

Figure 5.8: Ice Concentration in the Beaufort sea and the Amundsen Gulf from February 3, 2006 to February 14, 2006, showing leads openings and closings.

Part of the frequency modulated transients shown on (Fig. 5.4) was observed on February 12, 2006 which corresponded to the re-opening of the previously developed large leads (Fig. 5.8). Xie and Farmer [Xie92], associated these pure tones (778 Hz) occurring during the ice break-up in land fast ice to the dry friction between the new formed ice floes sliding longitudinally and rubbing against each other. Ye [Ye95] postulated later that the interacting surfaces roughness encountered in the noise field and that the pure tone may be related to the resonance of the SH waves within the ice floe. However, our tonal transients are not confined to a single frequency and were sometimes mixed with impulses sounds. Indeed, our tones generally consisted in a low-frequency fundamental (<200 Hz) and several harmonics which may extend beyond 4.1 kHz. The good correlation (Pearson r = 0.66) observed between class 1 wideband transients and class 2 tonal transients suggests some links in their production mechanism. The relatively high correlation of class 2 transients' time-series with the ice shear deformation rate, and the long duration of these transients support a slow generating process, in this case the ice shear. Some of class 2 tonal transients were short and repeated with periods similar to that of ocean waves. This suggests some interactions of ice floes rubbing with the swell generated in the large leads. Periodic fluctuations in frequency are also generally accompanying the tones and might be also related to the effect of waves on the ice shear speed.

The class 3 high frequency noise is similar to the well-known rain and wind generated noise in open water environments (*e.g.* [Ma05c, Ma05b]). It is tempting to attribute this high frequency noise to the snow pelting on the ice cover. However, the class 3 transient spectrograms of Fig. 5.5, for example, were recorded on February 12, 2006 and the meteorological data recorded at Tuktoyaktuk and Cape Parry weather stations showed that the regions did not experiment a significant snowfall for this period. February 12 corresponded to the re-opening of the large lead along the Canadian coast, in Southeastern Beaufort Sea and Amundsen Gulf (Figs. 5.8 i,j). The leads remained open for several days and the ice concentration in the Amundsen Gulf around the mooring position (Fig. 5.8 k), showed that large areas were not completely covered by ice (∼80%). Under supercooling conditions, crystal ice (frazil ice) is formed at the surface of open water, grow, and stick to one another forming aggregates [Brown94]. Moreover Arctic Sea ice concentration consist of 5-20% of frazil ice [Thomas10]. The observed class 3 high frequency noise seems to result from this sea surface state, under strong winds forcing (Fig. 5.9).

5.3.5 Environmental correlates of under-ice transients

The primary sound source in the Arctic has been identified to originate from the response of the ice cover to the stress. Thermal cracking, the response of ice cover to the atmosphere cooling, is a major contributor to the ice noise [Farmer89]. These transients are very short (0.1 s – 0.3 s, [Cummings89]), local and radiate small energy per crack within the ∼300–900 HZ bandwidth [Cummings89, Zakarauskas93]. Such short events were observed, but they were not considered in our analysis.

The local ice concentration, the air temperature, the air pressure and the wind speed are those described in chapter 3, sec.4.3 (Fig. 15 a,b,c,d). The local ice coverage showed noticeable lead openings and clear water of 1-3 days (Fig. 5.10 a), which reduced ice concentration down to 89% (ex. February 13,2006). The air temperature oscillated around a mean of -20.5 ^{o}C, from -36.4 ^{o}C to -6.5 ^{o}C, until the end of April, before a steady rise reaching >0 °C temperatures after May 11, 2006. The temperature rise in April corresponded to the start of the ice cover break up.

The total deformation rate (Fig. 5.10 b, solid line) of the MYI plume, West of the Beau-

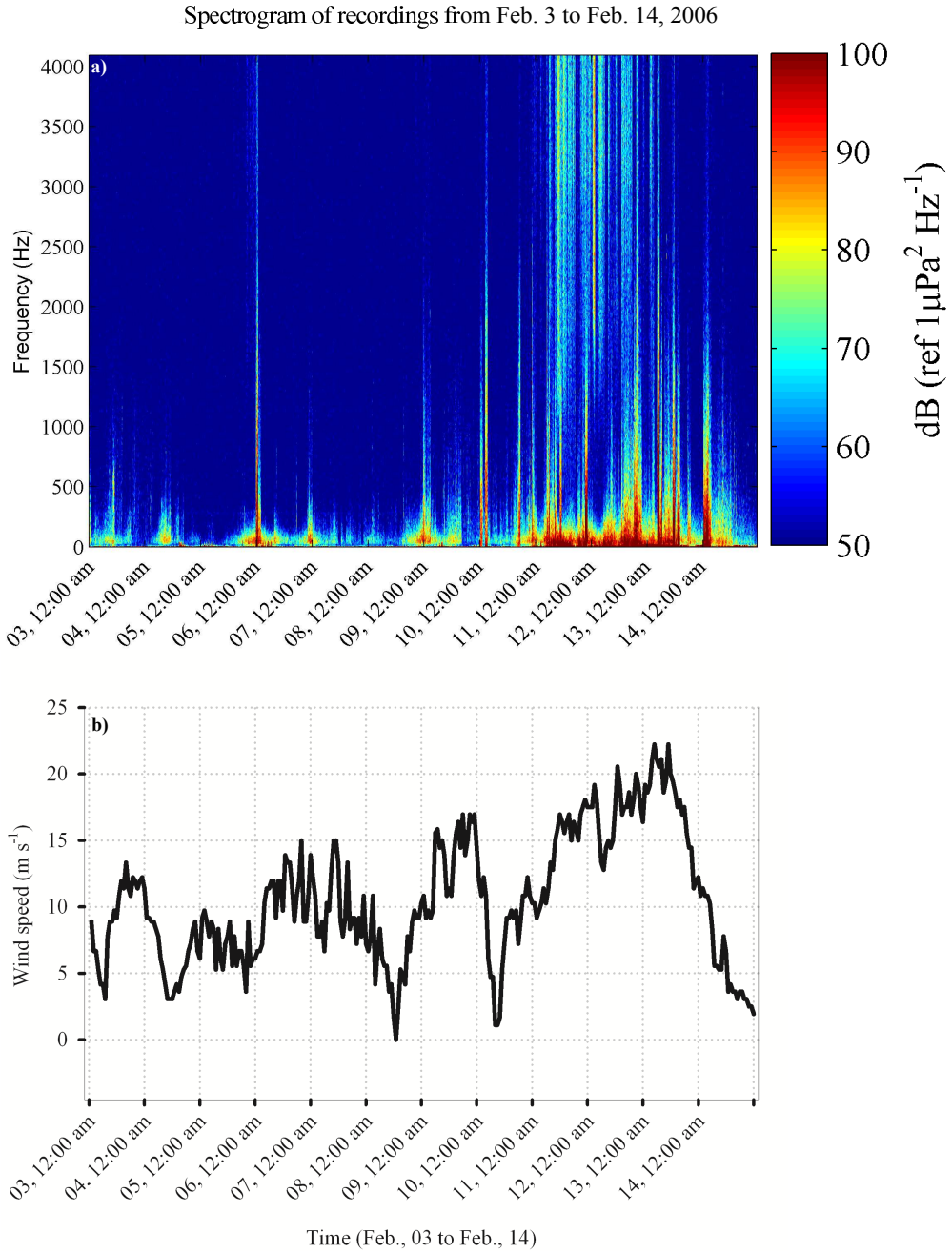

Figure 5.9: Episodic acoustic fracturing events observed for several consecutive hours in the Amundsen Gulf mouth, from February 03, 2006 to February 14, 2006. Leads were observed on ice concentration map for the same time period.

fort Sea, averaged 0.523±0.253 s^{-1}, with strong pulses which can reach 1.39 s^{-1}. In the FYI (Fig. 5.10 b, dotted line) taken upstream of the MYI plume, the deformation rate averaged 0.405±0.227 s^{-1} and peaked at 1.304 s^{-1}. The two deformation time-series had similar fluctuations (Pearson r = 0.79, Table 5.4), with higher amplitude before the steady rise of temperature in spring, after which they vanished. The occurence of classes 1 to 3 transients(Fig. 5.10 c,d,f), expressed as the number of 7-min hourly recording cycle the events were observed per day, showed similar general trends and co-occurrence in fluctuations. All transient classes occurences vanished after the steady rise of air temperature.

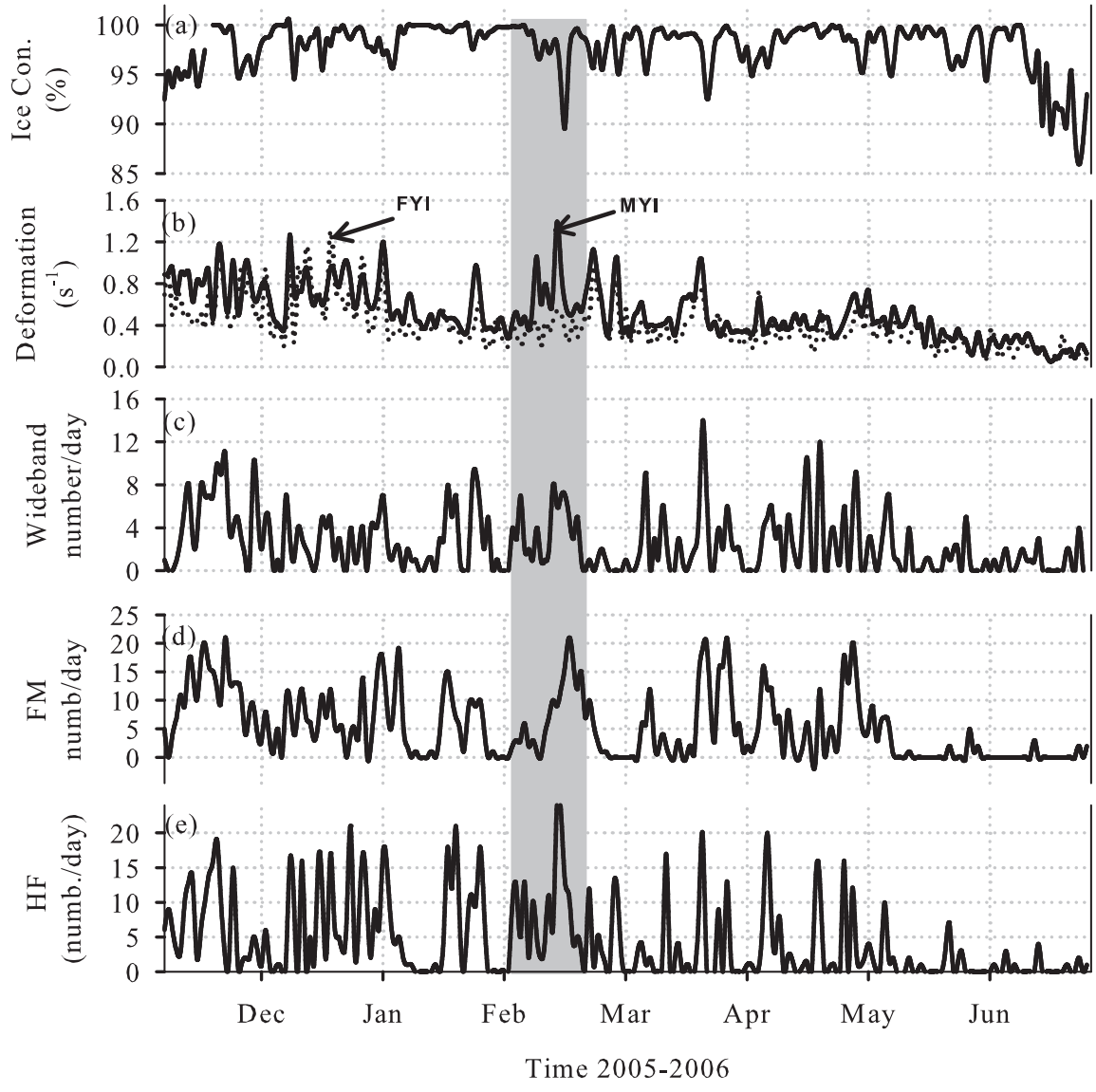

Figure 5.10: Time series of the occurrences of transient events and environmental variables in the Amundsen Gulf for the winter 2005–2006. (a) Local ice concentration (100-km radius around the recording station).(b) ice deformation in the FYI (dotted line) and in the MYI plume off the Gulf (solid line). (c) Fracturing occurrences. (d) Shearing occurrences. (e) frazil noise occurrences.

In chapter 3, we concluded that the ambient noise level in the Amundsen Gulf might be the sum of acoustic transients recruited over a large area (∼200 000 km^2) in the Beaufort Sea. In this case, the transient events can be assumed to be responding to the ice cover stress, under the forcings described in sec. 5.1.2. The same analyzes (Pearson correlation, PCA) were then reappointed to see whether the occurrences of the acoustic transients responded to the same environmental forcing as those governing the ambient noise level in the Amundsen Gulf. Instead of ice drift speed magnitude, we used the deformation rates computed from the ice velocity field. A PCA was performed with the environmental variables as descriptors and the resulting scores in the space of the first two principal components were color-coded with the daily occurrence for the three transient noise classes. From scatter plot of the scores in the first two principal components plan, we note that the first component, explaining ∼30% of the environmental variance, sorts the transients by their daily occurrence rate for each class (Fig. 5.11 a,b,c). The high occurrences are mainly found in the right half space, which correspond to high wind speed, high shear rate in both MYI and FYI areas as indicated by the overlaid factor loadings (Fig. 5.11, arrows). The transients were absent during low wind and ice deformation rates (Fig. 5.11 a,b,c).

The Pearson correlations between environmental variable pair, including the occurrences of the transient events, air pressure, and wind speed is shown in Table 5.4. Significant negative correlations were found between the air temperature and all the other variables, including acoustic events, except the ice divergence rate. However temperature best correlated with the divergence rate and the local ice concentration. Only the ice divergence rate at the MYI plume did not show significant correlation with the wind speed. The occurrence of class 3 transients had the highest and positive correlation with wind speed (Pearson r = 0.44). Significant negative correlations were observed between the divergence rate and the air pressure in both MYI and FYI areas. All acoustic transient occurence rates were strongly correlated with the deformations rates (mainly shear rate) regardless ice age (MYI or FYI). Moreover, the highest correlations of this transient triad were observed with the MYI deformation rates (Pearson r=0.54, 0.46, 0.36 in the MYI *vs* 0.41, 0.39, 0.32 in the FYI).

The transient sounds in the Amundsen Gulf were not responding to the thermal stress of the ice cover. The PCA analysis and the correlation showed that the acoustic transient occurences were related to the ice mechanical deformation rate, mainly the shear of the MYI plume. In fact, the MYI plume is entrained by the Beaufort Gyre large-scale circulation and the induced ice deformation caused the ice cover to fracture where it presented faults. The ice concentration did not correlate with either the ice deformation processes, or the acoustic transients. This suggests that the acoustic transients are prior to leads opening observed from satellite. Our result is therefore consistent with Weiss *et al.* [Weiss04] postulation that the most significant sea ice fracturing features are associated with shear deformation. The high variability of the wideband transient (class 1) durations therefore reflects the multi scale structure of the ice cover fracturing.

As demonstrated by Xie and Farmer[Xie92] and later by Ye [Ye95], the frequency of the pure tones depends on the characteristics of the ice cover. Consequently, they depend on the period of the year, which contribute to explain the large dispersion in the observed bandwidth of class 2 transients (Table. 5.2). Moreover, the class 2 transient occurrences vanished when the ice cover break-up, when the number of ice floes likely increased. The class 2 tonal transients may therefore rely on the winter solid ice pack. Some of these transients were in the same frequency band than bowhead whales (*e.g.* [Tervo11], Fig. 3, [Stafford08], Figs. 3, 5 and Table II) but differed from them by their durations and absence of repeated well defined song templates. Thus, these exclusively winter transients cannot be attributed to marine mammals songs, as

winter leads had short life cycle in the study area.

Leads closing also involve two processes: the free surface freezing and the movement of the ice floes on either side of the lead. In the surface freezing process, ice crystals (frazile ice) are formed first and then aggregate into pancake ice. Wind blows predominantly in the main axis of the leads, and the class 3 high frequency transients were showed high correlation with the wind speed. We suggest that class 3 acoustic transients were produced by wind effects on the frazil ice. The pulsed nature of these transient that was sometime observed (*e.g* Fig. 5.5 b) may then be caused by the swell generated in the leads.

Table 5.4: Pearson correlations between the variables pair including meteorological variables (T = temperature, wind = wind speed; press = air pressure), ice concentration (IC) and deformation rates (d = divergence, s = shear; τ = total deformation), and acoustic transient events (C_1 = class 1; C_2 = class 2; C_3 = class 3) observed in the Amundsen Gulf mouth. The ice concentration is computed in a 100 km radius around the mooring.

			Transients			**Ice**						
						FYI			**MYI**			
Variables			C_3	C_2	C_1	τ	s	d	τ	s	d	IC
		T	-0.24	-0.22	-0.26	**-0.30**	**-0.30**	0.17	**-0.38**	**-0.39**	0.14	**-0.43**
Air		wind	**0.44**	0.29	0.25	0.26	0.27	0.18	**0.40**	**0.40**	0.02	-0.25
		press.	-0.08	-0.01	-0.03	-0.12	-0.15	**-0.30**	-0.06	-0.06	-0.29	0.07
		IC	0.03	-0.01	0.00	0.08	0.08	-0.10	0.10	0.10	-0.03	
		d	-0.11	-0.11	0.00	-0.14	-0.13	0.28	-0.17	0.14		
	MYI	s	**0.54**	**0.46**	**0.36**	**0.78**	**0.78**	0.05	**0.98**			
Ice		τ	**0.53**	**0.43**	**0.36**	**0.79**	**0.78**	0.05				
		d	-0.02	0.06	-0.00	0.12	0.15					
	FYI	s	**0.41**	**0.39**	**0.32**	**0.98**						
		τ	**0.41**	**0.39**	**0.30**							
Transient		C_1.	**0.53**	**0.66**								
		C_2	**0.55**									

5.4 Conclusion

The recorded under-ice loud acoustic transients observed under-ice result from the sea ice dynamics responding to the environmental forcings. The class 1 wideband transients were shown to correlate with ice shear deformation but not to ice concentration. The resolution of the ice concentration images was however too coarse to account for the whole range of leads, which can vary from a few meters to several hundreds of km [Schulson09, Farmer89]. Leads, when closing by water surface refreezing and under wind effects, produces particular high frequency noise. Besides, the leads are observed after their opening [Schulson09] and do not reflect the ice fracturing mechanism. The sea ice deformation, computed using the velocity field, reflect the sea ice cover behavior. However, the temporal resolution of the ice velocity field (daily) not track the complete process of the sea ice internal stress and fracturing, as acoustic recordings can do(Fig. 5.9). *In-situ* ice drift speed, stresses and acoustic recordings are needed to confirm this hypothesis.

The variability of the fracturing sounds duration and their peak frequencies suggest a relationship between the acoustic energy radiated in the water volume and the leads size. In fact,

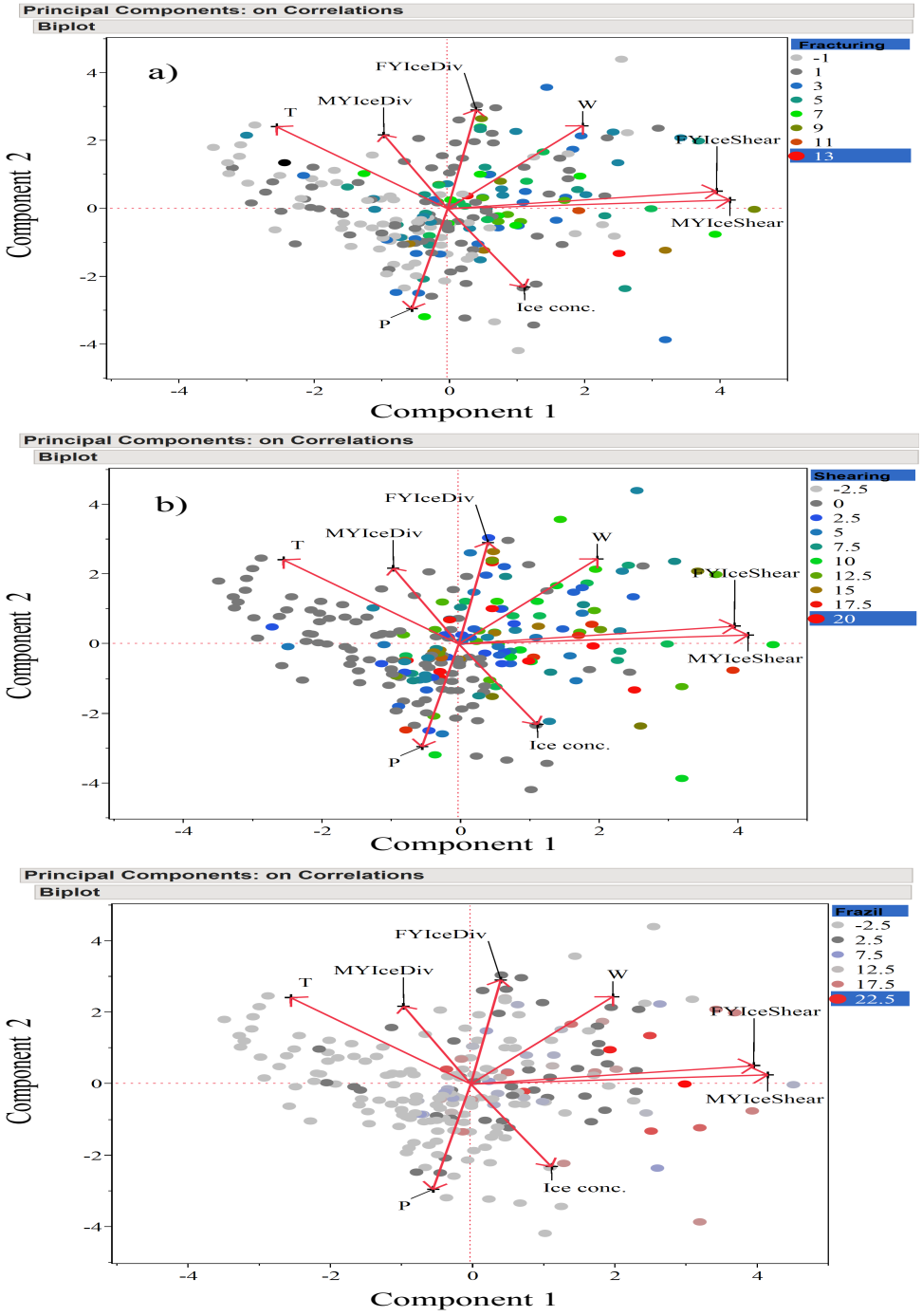

Figure 5.11: Scatter plot of the PCA factor scores in the spaces of the first two principal components, along with the factor loadings for each environmental variable. Color scale indicates the daily occurrences of the transients. (a) fracturing; (b) shearing; and (c) frazil noise. Ice Con., ice concentration; P, air pressure; T, air temperature; W, wind speed; FYIceDev, first year ice divergence; MYIceDev, multi-year ice divergence; FYIceShear, first year ice shear deformation; MYIceShear, multi-year ice shear deformation.

fracturing and lead opening of various size are consequent to the shear rate [Weiss04, Schulson09]. Although clearly identify to rely on the ice cape shear deformations, the modulated frequency sound mechanism seems to be more complex. The acoustic transients they produced showed high variability in the duration and the excited frequency band. Nevertheless, we can retain that the FM transients of short durations, often repeated, responded to the ocean waves. The long term durations FM, were sometimes observed over 24 hours of consecutive recordings and responded to continuous processes. Surprisingly, the ice shearing revealed by class 2 transients were frequent during winter until the beginning of the ice break-up in spring. During the spring in fact, the ice cover in the MIZ is turned to ice floes before melting. All these transients depended not only on the state of the sea ice (FYI or MYI), but also on the integrity of the ice cover. Future researches are needed to clearly establish a formal relation between acoustics and ice deformations.

Arctic sea ice is becoming rapidly thin and is characterized by an increase of the sea velocity and deformation rates [Weiss09b]. This will probably result in smaller time scale of leads opening and closing. The current satellite capabilities do not follow this changes and passive acoustic, with high temporal resolution, is therefore a complementary effective means for multi scale monitoring of the MIZ ice behavior, from local thermal cracking to long distance ice fracturing.

Sometimes I raise my head and look at my brother Ocean in friendship: he feigns infinity, but I know that he also runs around its limits, and this is , no doubt, all this tumult, all this crash.

Romain Gary

Chapter 6

Conclusions and perspectives

Contents

6.1 Conclusions

Arctic Ocean soundscapes are likely to undergo two rapid changes, accompanied by a possibly sudden and substantial increase of the ocean noise level. This study focused on the natural soundscape of Polar Regions (Arctic Regions) prior to their possible industrialization. This soundscape is driven by the Arctic sea ice exposed to the ocean surface and environmental forcings (weather, currents, air temperature etc.). In order to anticipate the future development of Arctic and sub-Arctic regions, it is necessary to evaluate sound budget in these areas. We have first given a brief revue of the impact of global warming on Arctic Regions. To study these effects, particularly the dynamics of the ice cover and its consequences on the ecosystems, we used long term monitoring. Even if the ice cover is classically monitored by satellites, with low spatial and time resolution, we proposed to use long term ocean noise measurements as a complementary method for sea ice monitoring.

6.1.1 Methods and tools provided

The first originality of this work is to provide a full description of sea ice soundscape in two components. The first component, called ambient noise, is related to acoustic sound created by numerous distant sources and generated by the ice. These ambient noises were recorded at one point and bring information from the chorus of the sources, mixed together. The second component, characterized by several series of transient signals is clearly emerging from the ambient noise. These transient signals are probably emitted by sources relatively close to the recording point.

To obtain this description into two components, an original algorithm dedicated firstly to the estimation of the ambient noise power spectral density and secondly to detect transient signals has been developed in this thesis [Kinda13, Gervaise13]. This algorithm based on specific spectrograms segmentation has been efficiently used and validated on real passive acoustic dataset to separate each component (ambient noise and transient signals). Previously to this operation, an appropriate pre-processing has been applied on real dataset to detect and eliminate cable strum noise induced by the vibration of the mooring line. Thanks to theses proposed algorithms, we define, for each of these components (ambient noise and transients), different acoustics descriptors. The use of these descriptors and their properties allows extracting time series from long measurement of raw data.

A second originality (from the description of Arctic acoustic soundscapes) was to explain the variability of acoustic descriptors by their link with environmental drivers and/or their relationship with the dynamics of Arctic sea ice. For this, we investigated linear dependencies between acoustic descriptors and a large set of environmental parameters. This has been, validate for the first time on several multi-variate dataset coming from: mooring line (current speed via ADCP), open data recorded by the Canadian governmental departments (winds, temperature, precipitation, tide) and National Snow and Ice Data Center (ice coverage, ice thickness, sea ice motion) from satellite observations.

6.1.2 Properties of the Canadian Arctic soundscapes

All these originalities must be credited by the fact that we have access to a very long time measurement series of acoustic dataset collected by Prof. Y. Simard (in the ArcticNet Program context). This network is unique as the data continuously cover several annual cycles. To our knowledge, these dataset, considered as the longest data analyzed for this purpose, are crucial to describe the sound production for sea ice monitoring. From this set and for the Canadian Arctic sea ice, we can describe more precisely the two ocean noise components.

6.1.2.1 The first component: Ambient noise in [10 Hz-500 Hz] frequency band

In order to describe the ambient noise level (ANL), we first rejected all transients by a developping a dedicated tool. Secondly we built the time series of the ambient broadband noise level in a specific frequency band [10 Hz-500 Hz]. We found, on the Amundsen Gulf site, that when the ice concentration increases, the ANL goes down, and when the sea ice-cap is missing, this level is mainly driven by wind forcing. Indeed, during this latter period, the ANL obeys the classical models (Wenz model) used on open waters. So the ANL reached a minimum in late winter correlated to a maximum extent and thickness of the ice cap.

By comparing the level of the soundscape with and without ice cover, we showed first that the ice-covered periods were much more quiet (<12 dB) and secondly that no direct wind dependencies are highlighted during these time of ice cap covering.

Looking for the environmental parameters driving the ambient noise level, we showed after an ACP reduction of environmental parameters, that two groups of properties involved in >50% of the variance of environmental data were highlighted. The first axis (triad: wind, ice drift, current) explained the high values observed for ambient noise. A search of the area maximizing the correlation between the ambient noise levels observed and the ice drift identified some areas where the multi-year ice is pulled up by the action of the Beaufort Gyre. This area is identified as a potential source of noise heard over ∼200 miles away. We can confirm that ambient noise in Eastern Beaufort Sea was mainly controlled by meteorological and oceanographic forcing processes (wind, current, ice drift, large scale circulation). We find also for the 10-500 Hz broadband frequencies, ANL did not respond to the air temperature and pressure fluctuations as reported in the earlier studies.

6.1.2.2 Second component: Transient signal generated by the sea ice

From a database covering an annual cycle, we applied our algorithm to detect transient signals and we used a manual classifier to identify each group of transient events. These were divided into three families depending on their statistical distributions and properties (levels, center frequency, bandwidth, duration).

We analyzed the time series and the three resulting families during a period where some major leads (open surface) appeared in the sea ice. We showed that transients signals recorded during this period have been associated to some ice classified events. The first class consists of broadband transients signal associated to the leads opening. The second one is related to a frequency-modulated signals linked to the high shear stress appearing in the ice cover. Finally a third class is made of broadband signal with high frequency related to the presence of frazil ice in

the open space within the ice cover. Looking for the environmental parameters make it possible the proof of these transient signals highlighted the ice deformation and ice concentration as two major parameters involved in the Arctic under-ice soundscape.

6.1.3 Limits of our work

Concerning the characterization of ambient noise, we performed analysis only in the [10 Hz-500 Hz] band, because, above this frequency, the power spectral density of natural ambient noise is less energetic than the electronic measurement noise (noise from the hydrophone & sittings, HTI hydrophone 96 min and 16-bit system AURAL). So, the soundscape description for higher frequencies is missing and informations of the environmental parameters driven these frequency is not possible. For transient signals, it is clear that manual classification is not appropriate for longer and several sites databases analysis. For a thorough analysis taking into account several mooring sites, automatic classification procedure would be required. Furthermore, our studies was limited to single-sensor approaches and do not allow the location of the events, which can be of great interest to associate transient noise and the area of the sea ice physical phenomena.

6.1.4 How passive acoustics can be complementary with other studies and other means of observation

Previous to this work, marine mammals vocalizations time series have been established from the same acoustic recordings data sets [Simard12a, Simard12b]. It is therefore interesting to note that the passive acoustic monitoring approach allows to describe i) marine biodiversity including attendance of marine mammals in a given area and ii) the dynamics of the sea ice cover and iii) look for potential correlations between sea ice and attendance mammals. Complementarity with other means of observation (satellite for example), passive acoustics records provide a good description of the events at a fixed point in the area around the point of measurement with a very high temporal resolution. However, the acoustic soundscape must be calibrated by "ground truth" measurement such as vibration recording by geophones in the ice cover. This calibration would link the dynamics of ice undoubtedly with its acoustic behavior. Once this calibration performed, passive acoustic is an excellent complementary mean to satellite observation (with limited temporal resolution) for multi-scale sea ice monitoring.

6.2 Perspectives

6.2.1 Sea ice acoustic observation

Several studies can be put forward regarding the ambient noise and the Arctic acoustic transients.

On the one hand, regarding the ambient noise, the current conclusions concerns mainly the low frequency band, particularly during the ice-cover period. It would be then interesting to replicate the measurements with low noise hydrophones, to take into account the higth frequency band in order to increase the range of environmental parameters driving Arctic soundscapes. Current results were also observed during the year 2005/2006 while the Arctic has undergone major changes in recent years. Comparison with recents measurements are necessary to understand how

Arctic soundscapes are affected by the recent decline in sea ice cover and thickness. The noise level recorded in the Amundsen Gulf were likely to be produced at the muti-year ice plume. It is desirable to replicate our analysis method on databases taken elsewhere in the Arctic Ocean, to confirm this hypothesis and to determine the influence of the measurement location topographic configuration.

On the other hand, regarding the transient events, the first research axis is an automatic classification of ralated acoustic sea ice events and there location from a network of hydrophones listening. Some studies (*e.g.* [Schulson09]) showed that the sea ice fractures occur at the fault locations of the ice cover structure. Therefore the localisation of the ice fracturing sound sources would be tantamount to the description of the spatial structure of the ice cover. A second research axis is related to modulated frequency events. Indeed, the deformation of the ice under different stresses is described in the 2D mechanical framework modelling. Thus, the induced stresses excite specific modes whose frequencies radiated into the water volume depend on the dimensions of the moving plates. These signals can be considered in this perspective, which would allow to find the physical properties of the plates (thickness, size, drift spped, etc.) via inverse problems.

6.2.2 Impact of human activities in the Arctic

There is no doubt that global warming will lead to a partial melting of the Arctic ice and will lengthen the ice free season. A direct consequence will be the gradual development of human activities in the Arctic Regions. The question of assessing the acoustic impact of human activities on these acoustic soundscape and marine biodiversity including mammals is now crucial. The work done in this thesis can serve as the basis for future analyzes.

From our study, it is clear that the exposure of the Arctic Ocean surface to meteorological forcings consequently to the ice cap melting will causes an increase of the ambient noise level of $\sim$10 dB without considering human activities. The latter aspect will include offshore industries and the openning of new pathways for commercial shipping. The impact of human activities on the Arctic soundscapes can be evaluated based on simulations. This work must address i) the establishment of sound sources templates issued by ship type and by other types of industrials activities and ii) the computation of acoustic simulation to evaluate the acoustic consequences of particular scenarios.

To establish the soundscapes templates from sources regarding shipping, we can propose the following protocol. Acoustic recordings from single hydrophone or array should be made along a pathway. In addition to the acoustic recordings, the ships positions, obtained from AIS (Automatic Identifications System) will allow the identification of the specific acoustic signature for different ship classes. We can then develop more efficient algorithm to evaluate the environmental impact of the considered pathway. Two projects of such nature are under development: in the St. Lawrence by Prof. Y. Simard and his team where $\sim$6000 vessels/year sail and in the Ushant shipping where $\sim$180 commercial vessels are sailing every day. The latest project is supported by Mr. Y. Stéphan, researcher at the SHOM. A part of this project is presented in annex.

Based on these study, sound recorded by hydrophones or antennas will be used as input into computer codes to study anthropohony as those developed by Erbe *et al.* [Erbe00, Erbe02, Erbe08]. It is interesting to note that these models must be powered by not necessarily well-

known geo-acoustic data. In this context, the use of passive geo-acoustic inversion can be used to exploit the sources of opportunity as ship [Vallez09, Gervaise12a] or marine mammals [Thode00] to produce an adequate and accurate description of the oceanic-geo-acoustics models used to feed the simulation tools. It will be also very interesting to test our proposed algorithm to evaluate soundscape for other sea ice cap regions (as Antarctic sea for instance) and for other part of ocean where human activities will be more and more present.

So numerous are the finished works, those remaining are more numerous to be done.

Burkinan proverb

Appendix A

Shipping noise

In the mid-latitude oceans, the low frequency (10 Hz–1 kHz) ambient noise is dominated by shipping noise. In this section, we summarize the work carried out regarding to this ocean noise component. This included the potential use of shipping noise for environmental parameters assessment and shipping noise modeling using marine traffic spatial distribution.

Noise radiated by ships

Ship radiated-noise involves three mechanisms [Urick83]: The machinery noise, the propeller noise and the hydrodynamic noise. The machinery noise results from the mechanical vibrations produced by diverse parts of the vessel. The main contributors to this noise component are the explosions in the engine cylinders, the rotations of the shaft and turbines blades, etc. At low speed, shipping noise spectrum is essentially machinery noise [Arveson00] and therefore consist in line-spectrum with fundamental frequencies within 4-20 Hz inherent to machinery. The propeller produces a set of line components within 6-10 Hz and a continuous spectrum [Gray80], while the hydrodynamic noise results from the flow of water on the hull.

Although the spectrum of noise radiated by ships is composed of lines spectrum overlaying continuous spectrum [Urick83], the noise radiated by vessels sailing at a speed close to their cruising speed is dominated by the propeller noise. Shipping noise spectrum can therefore be modeled as continuous spectrum. Historical shipping source spectrum model was proposed by Ross [Ross87], who postulated that the ship source can be derived from a mean spectrum taking into account the vessel characteristics as follow:

$$S(f) = S_0(f) + \tau(f, \alpha), \tag{A.1}$$

where α denote the vessel displacement parameters (speed, displacement tonnage). Noting that the spectrum decreases by ∼20 dB/decade, Ross proposed to derive the spectrum from the total noise level SL_0 in the frequency band 0.1–10 kHz following Eq. (A.2), where SL_0 is in unit of dB and f in unit of Hz.

$$S(f) = SL_0 + 20 - 20log(f), \quad (f \geq 100), \tag{A.2}$$

For frequency below 100 Hz, the spectrum was highly variable. In fact, this frequency band contains spectral lines characteristics of the propeller [Aleksandrov62, Trevorrow08].

However, the most widespread shipping noise model used is a continuous spectrum that considers the vessel length and speed, as these parameters are generally available following Eq. (A.3) [Hamson97, Wales02]:

$$S(f, V, L) = S_0(f) + c_V 10log(V/V_0) + c_L 10log(L/L_0) \tag{A.3}$$

where V_0 and L_0 are respectively the reference speed and the reference length, and $S_0(f)$ the reference spectrum, c_V and c_L are constants (taken as 6 and 2 respectively by [Hamson97, Wales02]).

Individual vessel noise recorded with a single hydrophone generally shows two components in the time-frequency domain (Fig. A.1): line component overlaying an interferences pattern centered at the CPA (Closest Point of Approach: the minimal distance between the ship trajectory and the hydrophone). The interference patterns result in the constructive and destructive

interactions between the direct and reflected paths of the moving source. It therefore depends on the source depth and the distance between the vessel and the receiver. For commercial ship, the source depth is generally taken between 7 and 14 m [McKenna12]. Line components and the interference patterns are both informative of the environmental properties and can be used to retrieve the geo-acoustic parameters of the environment.

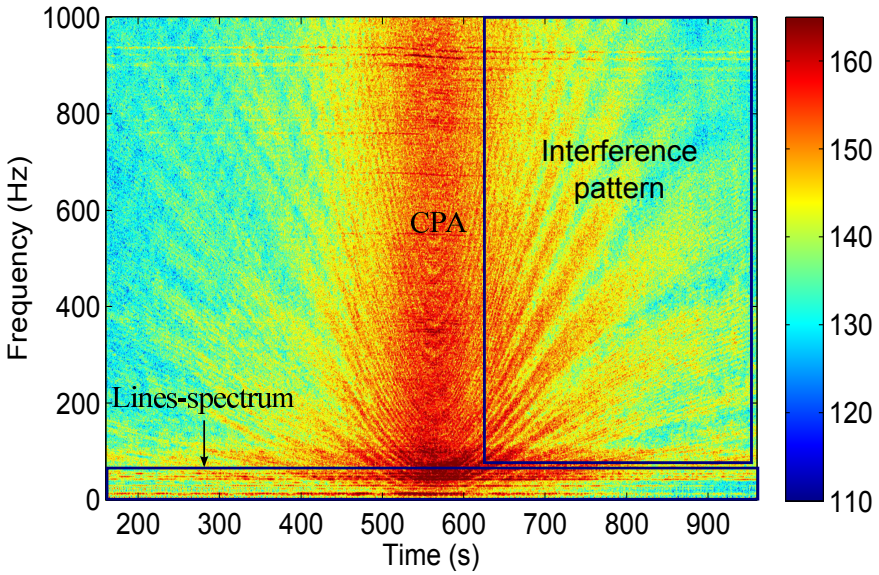

Figure A.1: Spectrogram of ocean noise from a moving vessel

Environment assessment using individual ship noise

Several methods have been developed to retrieve ocean physical properties from shipping noise and we summarize some of them as examples. Matched-field processing method was proposed by [Battle03] using towed HLA. Park *et al.* [Park05] proposed an inversion scheme in the time domain using matched impulse response filter applied to the noise recorded by a towed HLA and back-propagation of the resulting signal to estimate the water depth, the bottom geoacoustic parameters (sound velocity and density), source depth, and the array position (depth, range and bow).

We proposed [Gervaise12a] an inversion scheme using the interference pattern of the spectrogram (Fig. A.1), in a single receiver and very shallow water context. In fact, mid frequency (50–500 Hz), propagation in such environment is mainly driven by reflexions at the boundaries. The transfer function between the source and the receiver, using normal mode theory under range-independent environment assumption is given as:

$$H(f) \simeq \sqrt{2\pi} \sum_{m=1}^{N} g_m(z_s) g_m(z_r) \frac{e^{-jk_m(f)r}}{\sqrt{k_m(f)r}}, \tag{A.4}$$

where $g_m(z)$ represents the modal function of index m, $k_m(f)$ is the radial wavenumber of index m at frequency f, z_s and z_r are respectively the source and receiver depth, r is the radial

distance and N is the number of propagating modes. The radial wavenumbers $k_m(f)$, that are frequency (f) and mode index m dependent constitute an acoustic signature of the environment. For a moving vessel, the receive level in the time-frequency domain can be expressed following Eq. (A.5a), wich can be rearranged in Eq. (A.5b).

$$I(t,f) = |h(t,f)|^2 \gamma_e(f) \tag{A.5a}$$

$$= \frac{\gamma_e(f)}{r(t)} \left(\sum_n A_n^2 + 2 \sum_{n,m} A_n A_m cos[\Delta k_{m,n} r(t)] \right) \tag{A.5b}$$

where $\gamma_e(f)$ is the source spectrum, $\Delta k_{m,n} = k_m - k_n$ and $A_m = \frac{g_m(z_s) g_m(z_r)}{\sqrt{k_m}}$. These two quantities only depend on the environmental parameters and frequency, they are constant in terms of time and range. For known vessel trajectory, the receive level $I(t,f)$ can be translated into range-frequency $I(r,f)$ using distance-time equivalence. The propagation feature $\Delta k_{m,n} = k_m - k_n$ is then easily accessible by the Fourier transformed of the received level:

$$I(k,f) = FT_r[I(r,f)] \tag{A.6a}$$

$$= \sum_{n,m} A_n A_m \delta(k - \Delta k_r^{mn}(f)), \tag{A.6b}$$

The curves $\Delta k_{m,n} = k_m - k_n$ thus obtained are the relative dispersion curves of the environment and were used to retrieve the geoacoustic parameters via an optimization of the following cost function:

$$J(\theta) = \int_f \int_k I(k,f) M(k,f,\theta) dk df. \tag{A.7}$$

where $M(k,f,\theta)$ is a masking function corresponding to the relative dispersion curve for a set of parameters θ), taken in a width of $2\pi/(R_{max} - R_{min})$. R_{max} and R_{min} are respectively the minimum and the maximum range corresponding to the $I(r,f)$ portion selected for the inversion.

The multiparameter cost function optimization can be solved via an efficient global search based on genetic algorithms [Vallez08, Vallez09], but the result was not satisfactory. My contribution is the study of the performance of the inversion scheme, including its robustness to noise and the structure mismatch between the guessed environment and the true one. I proposed to regularize the problem using the Hamilton Formula [Hamilton80]. If attenuation is neglected bottom density and sound speed can be linked through:

$$C_b = \frac{C_w}{1.18 - 3.4\phi + 0.0013\phi^2} \tag{A.8a}$$

$$\rho_b = \frac{28.85 - \phi}{10.275} \tag{A.8b}$$

$$\phi = -log_2(\mu), \tag{A.8c}$$

where C_b and C_w are respectively sound speed in the water and in the bottom, ϕ is the grain size parameter, μ the sediment mean grain diameter in mm. This choice was motivated by

the weak dependence of the cost function on the attenuation and its strong correlation with the couple (ρ,C_b), as revealed by simulations. We also demonstrated from simulations that a layered waveguide can be modeled by a Pekeris with depth-average seabed sound speed the modal function vanished with depth in the bottom. The multiparameter optimization is then reduced to a single parameter grid search over C_b. This method has been successfully applied to real data, for 15 m recorded in 2005 (Fig. A.2). The results for two ship tracks were {(C_b=1790 m s^{-1}, ρ=1.84 g cm^3); (C_b=1750 m s^{-1}, ρ=1.80 g cm^3)}, consistent with a core sample taken near the hydrophone, consisting in homogeneous sandy sediment type 1800 m s^{-1}. For more details see Gervaise, Kinda *et al*. [Gervaise12a].

This work is a contribution to MODE II project (Discrete Observation Methods of the Environment), within the research contract No. 07 CP 0001 between ENSTA Bretagne and SHOM, funded by the Direction Générale pour l'Armement (DGA)

Shipping noise modeling

Shipping noise is a major contributor to ocean noise in the low frequency band. In deep water environment, shipping noise dominated the frequency band 20–200 Hz. In the absence of identifiable shipping noise, deep ocean noise modeling requires the summation of ship over large areas, up to 1000 miles radius [Dyer73]. Indeed, the deep sound channel (∼1000 m) is favorable for long distance propagation. In coastal areas, long distance propagation is no longer supported. However, some coastal areas may be subject to a significant maritime traffic. In such area, shipping noise could extend up to 1 kHz [Wenz62].

Shipping noise modeling requires spatio-temporal distribution of shipping and a priori information on the radiated spectrum of each individual ship. Wagstaff [Wagstaff73], proposed in the RANDI ambient noise model a set of source spectra (Fig. A.3), corresponding to five vessel classes, based on the vessels size (table A.1).

The present widespread use of AIS (Automatic Identification System) by vessel provides a fine spatial and temporal distribution of vessels in a given location. In fact, AIS data provides the vessels type, its position, its physicals characteristics (length, breadth, draught) and its speed. This made it possible efficient shipping noise modeling [Hatch08, Merchant12]. The next section presents an ongoing direct modeling of ambient noise using AIS data in an area of intense marine traffic.

Table A.1: Ship classes in RANDI ambient noise model.

Ship type	**Length(m)**	**Speed(m s^{-1})**
Supertanker	244–366	7.7–11.3
Large Tanker	153–214	7.7–9.3
Tanker	122–153	6.2–8.2
Merchant	84–122	5.1–7.7
Fishing	15–46	3.6–5.1

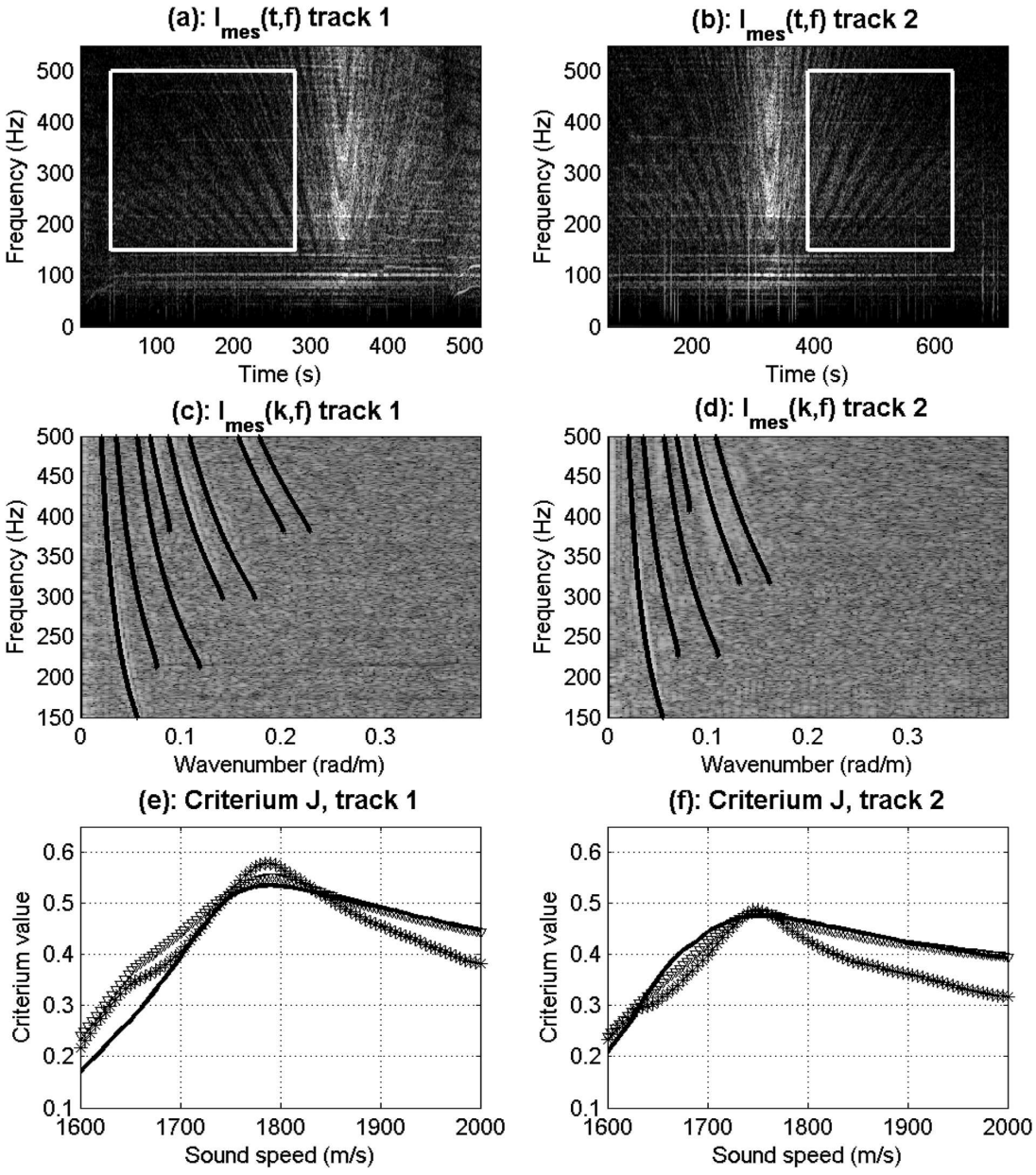

Figure A.2: Geoacoustic inversion using ship noise;(a) and (b) $I_{mes}(t, f)$ for tracks 1 and 2, white boxes identify the data used to compute $I_{mes}(k, f)$, the ship's range in these boxes is approximately 1500 m between 300 m and 1800 m, striations are clearly visible on $I_{mes}(t, f)$. (c) and (d) I_mes(k, f) for tracks 1 and 2, and corresponding inverted RDC curves (in black) a good match between local maxima of $I_m(k, f)$ and optimal theoretical RDC is visible. (e) Objective functions for track 1: real data SNR=12.5 dB (continuous line); simulated data with ship's range=1500 m and SNR=12.5 dB (crosses); simulated data with ship's range=750 m and SNR=12.5 dB (triangles). (f) Objective functions for track 2: real data SNR=9.8 dB (continuous line); simulated data with ship's range=1500 m and SNR=9.8 dB (crosses); simulated data with ship's range=750 m and SNR=9.8 dB (triangles).

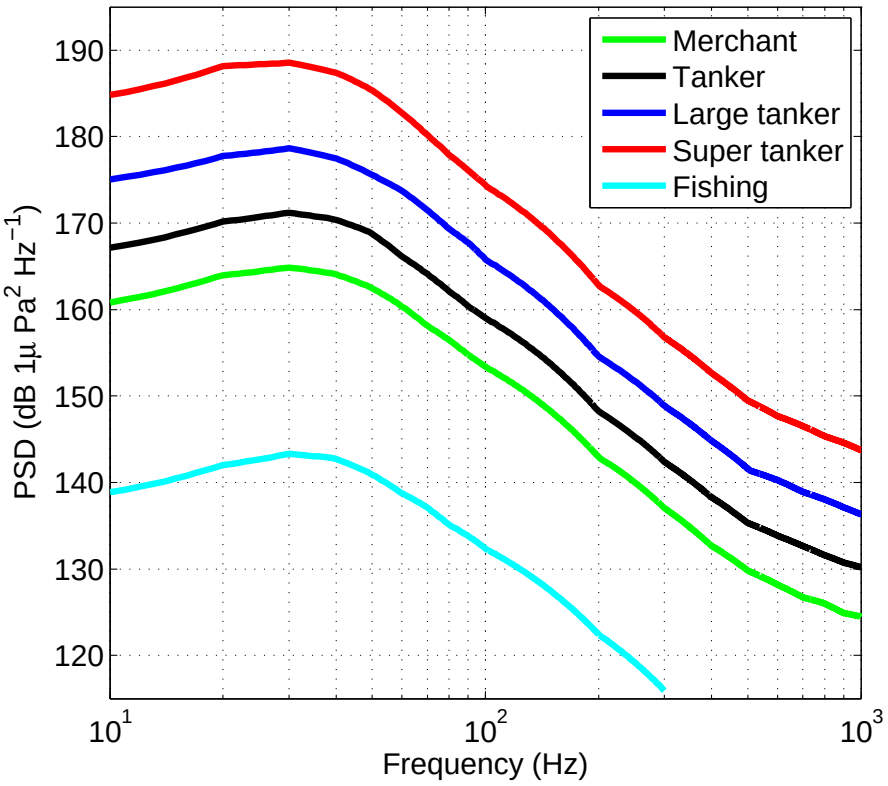

Figure A.3: Ship noise spectra from RANDI model, for value of length and speed for each ship type (Source : NRC2003)

Table A.2: Marine traffic in Ushant regions.

Category	**Total**	**Length**				**Speed**			
		Mean	25%	50%	75%	Mean	25%	50%	75%
Cargo	5519	151	90	134	190	12.3	10.4	12.8	15.9
Tanker	2448	156	106	144	183	9.6	11.6	13.1	14.3
Hazardous	1639	179	126	159	226	12.8	12.6	14.8	17.30
Other	498	98	36	80	113	7.4	5.0	9.6	13
Fishing	376	26	21	24	25	5.2	3.0	4.6	9.0
Passenger	179	141	62	162	181	12.3	12.1	15.0	18.5
Tug	172	40	30	35	50	3.2	5.7	7.6	9.9
Military	102	117	58	130	175	6.7	7.6	10.5	14.6
Dredging	101	86	72	86	99	7.0	7.3	10.1	11.8
Pleasure	62	57	34	52	69	6.9	9.17	12.9	15
Towing	45	47	30	35	58	7.1	5.6	7.1	8.9
Pilot	31	34	13	16	19	10.2	9.2	12.2	18.2
Search	28	40	15	44	70	2.6	6.5	10.7	13
High Speed	23	85	86	86	98	17.6	20.4	31.4	34.8
Spare	5	36	33	40	40	4.9	5.8	8.2	10.5

Ushant shipping lame case

The Ushant marine area is a multiform area of maritime traffic. In fact, this area hosts one of the most important waterways in the world. There are approximately ∼180 commercial vessels sailing through the Ushant shipping lame a day. Moreover, seasonal recreational shipping and fisheries are encountered in this zone.

We aim to model the shipping noise in this area using the temporal and spatial distribution of vessels. To do so, we used some AIS data from the *Centre D'Etudes Techniques Maritime et Fluviales (CETMEF)* within the CETMEF and SHOM agreement n° 144-2010 agreement. The raw AIS data consist of six months recordings in the English Channel and the Atlantic Ocean off Ushant, from February 2010 to August 2010.

Shipping distribution

The cumulative statistics of the shipping from the six months data analysis are summarized in Table A.2. As expected the commercial shipping (Cargo, Tanker, Hazardous) is the major component and represents 85.5% of vessels in the geographic zone delimited by 47°N–51°N and 0°W–0°W.

Regarding the spatial distribution in 15"×15" grid cells (number of vessels in the area), it can be seen that commercial vessels are mainly within the shipping lane (Fig. A.4), with some secondary roads that connect the coastal area. In contrast, fishing activity is concentrated along the coasts and is more diffuse in the ocean area (Fig. A.5). The density of the remaining vessels (passenger, tug, military, etc) follows almost the same spatial distribution as the commercial shipping (Fig. A.5).

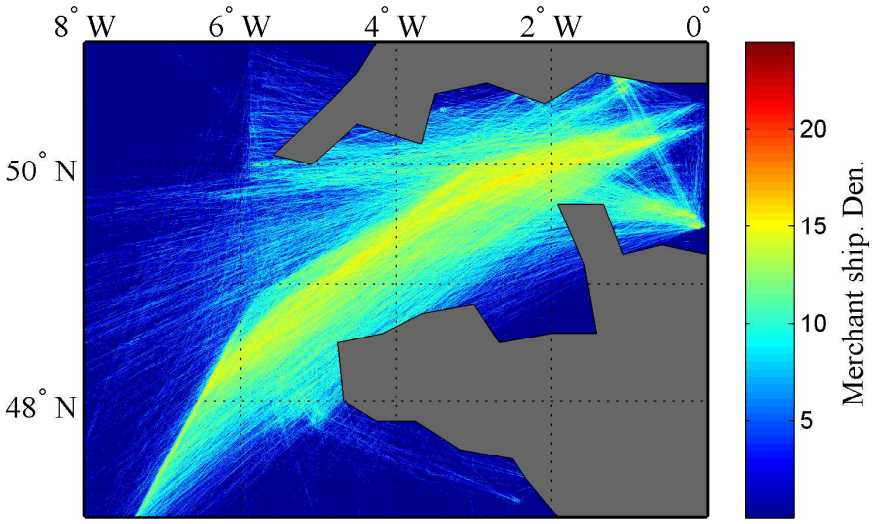

Figure A.4: Spatial distribution of commercial shipping in the Atlantic Ocean off Ushant

Shipping noise modeling

From the spatial density of the shipping type, the received level at any position in the area around Ushant can be computed. A first approach is the use the RANDI model spectra (Fig. A.3) and the shipping type obtained from the AIS data processing.

For a given position, the received level RL at a single hydrophone is given in a direct modeling framework as follow:

$$RL(f) = \sum_{i=1}^{N} SL_i \times H(f, r_i) \tag{A.9}$$

where N is the number of sources in the area, $SL_i(f)$ is the source level for each ship at considered frequency, and $H(f, r_i)$ the source-receiver transfer function. In shallow water and low frequency context, normal mode theory is used and the transfer function is given by Eq. (A.4).

Using the 15"×15" grid cells, the receive level in each grid cell area can be computed as :

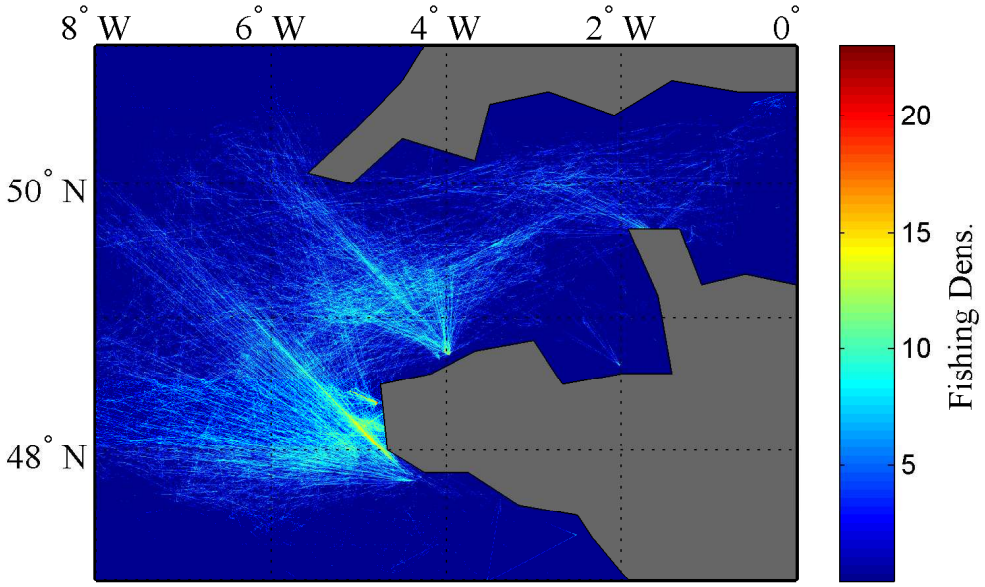

Figure A.5: Fisheries spatial distribution in the Atlantic Ocean off Ushant

$$RL_c(f) = SL_c(f) + \sum_{i=1}^{N} SL_i(f) \times H(f, r_i), \tag{A.10a}$$

$$SL_c(f) = \sum_{j=1}^{K} SL_j(f) \tag{A.10b}$$

$SL_c(f)$ is the contribution of the vessels in the considered cell, N the total number of vessels in the area at distance r_i from the center of the considered cell. As the vessels of each class shows variability in speed and length, RANDI spectra are regularized by taking into account the length and the speed of individual ship following Eq. (A.3). The ship was also determined from its length following Table. A.1 instead of its type in the AIS data.

The results of such processing is given in Fig. A.7. The environment consisted in range-independent environment. The sound speed in the water column was constant and the bottom

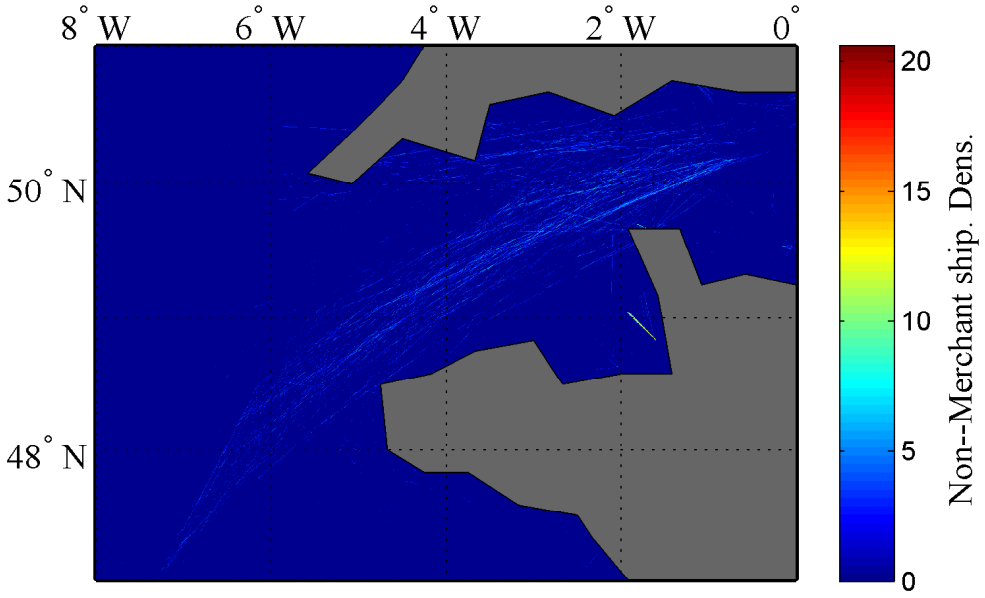

Figure A.6: Spatial distribution of other shipping in the Atlantic Ocean off Ushant

was considered as coarse sandy (∼1800 m.s^{-1}). The transfer function was computed using the modal code ORCA [Westwood96].

Perspectives

The immediate work is to compare the model with *in-situ* acoustic measurements. To do so, the model needs to be adjusted incorporating real geoacoustic parameters in the transfer function computation. The next step will consist to establish a probabilistic approach in space and time. In fact, commercial shipping is concentrated along some specific locations. Fisheries are more encountered in coastal areas. Looking at the daily spatial density of each shipping component, a probability density function can be determined in each cell.

Our model can serve as basis for shipping noise prediction in other areas, such as the Canadian Arctic. Individual ship noise inversion may then provide the geoacoustic parameters

for efficient modeling.

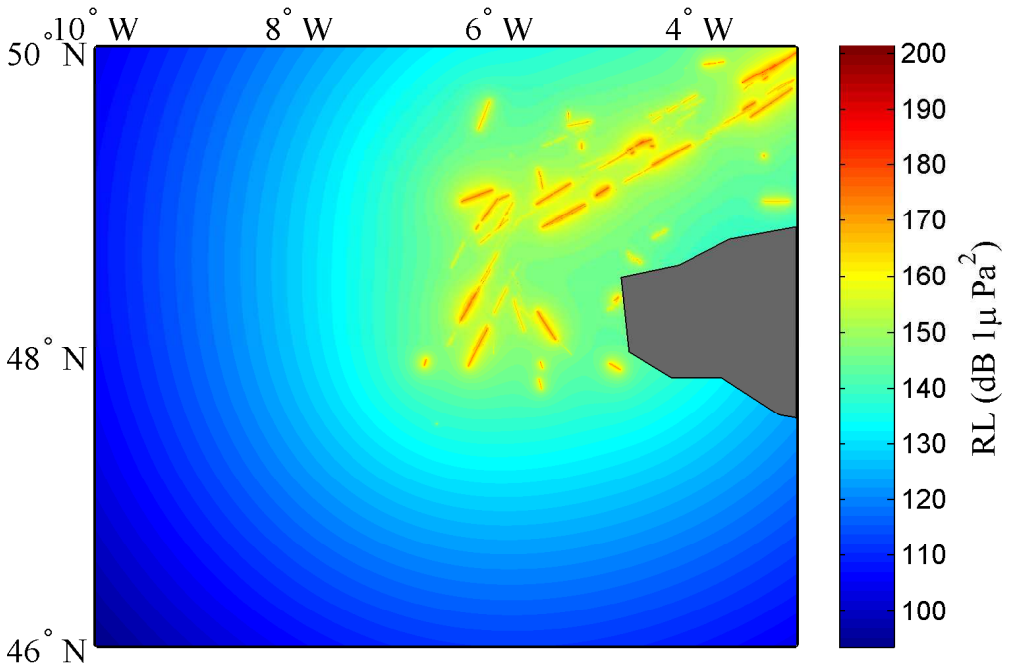

Figure A.7: Spatial distribution of cumulative hourly shipping noise in Ushant, from simulation using RANDI spectra and the ship position from AIS. The received level was computed in the 1/3 octave around 65 Hz

Bibliography

[Aja-Fernández09] S. Aja-Fernández, G. Vegas-Sánchez-Ferrero, M. Martín-Fernández, and C. Alberola-López. Automatic noise estimation in images using local statistics. additive and multiplicative cases. *Image and Vision Computing*, **27**(6):756–770, 2009.

[Aleksandrov62] I. A. Aleksandrov. Physical nature of the "rotation noise" of ship propellers in the presence of cavitation. *Soviet Physics - Acoustics*, **8, No. 1**:23 –28, 1962.

[Andrew02] R. K. Andrew, B. M. Howe, J. A. Mercer, and M. A. Dzieciuch. Ocean ambient sound: Comparing the 1960s with the 1990s for a receiver off the california coast. *Acoustics Research Letters Online*, **3**(2):65–70, 2002.

[Andrew11] R. K. Andrew, B. M. Howe, and J. A. MerMercer. Long-time trends in ship traffic noise for four sites off the north american west coast. *J. Acoust. Soc. Am.*, **129**:642, 2011.

[Archambault10] P. Archambault, P. V. R. SnelgSnelgrove, J. A. D. Fisher, D. J. Gagnon, J.-M.and Garbary, M. Harvey *et al.* From sea to sea: Canada's three oceans of biodiversity. *PLoS One*, **5**(8):e12182, 2010.

[Arveson00] P. T. Arveson and D. J. Vendittis. Radiated noise characteristics of a modern cargo ship. *J. Acoust. Soc. Am.*, **107**(1):118–129, 2000.

[Asplin09] M. Asplin, J. Lukovich, and D. Barber. Atmospheric forcing of the Beaufort Sea ice gyre: Surface pressure climatology and sea ice motion. *J. Geophys. Res.*, **114**:C00A06, 2009.

[Au08] W. W. Au and M. C. Hastings. *Principles of marine bioacoustics*. Springer, 2008.

[Bader11] J. Bader, M. D. S. Mesquita, K. I. Hodges, N. l. Keenlyside, S. Østerhus *et al.* A review on northern hemisphere sea-ice, storminess and the north atlantic oscillation: Observations and projected changes. *Atmospheric Research*, **101**(4):809–834, 2011.

[Barber12] D. Barber, M. Asplin, R. Raddatz, L. Candlish, S. Nickels *et al.* Change and variability in sea ice during the 2007 - 2008 Canadian International Polar Year program. *Climatic Change*, **115**(1):115–133, 2012.

[Barry93] R. G. Barry, M. C. Serreze, J. A. Maslanik, and R. H. Preller. The Arctic sea ice-climate system: Observations and modeling. *Rev. Geophys.*, **31**(4):397–422, 1993.

[Battle03] D. J. Battle, P. Gerstoft, W. A. Kuperman, W. S. Hodgkiss, and M. Siderius. Geoacoustic inversion of tow-ship noise via near-field-matched-field processing. *Oceanic Engineering, IEEE Journal of*, **28**(3):454–467, 2003.

[Berkes02] F. Berkes and D. Jolly. Adapting to climate change: social-ecological resilience in a canadian western arctic community. *Conservation ecology*, **5**(2):18, 2002.

[Boyd11] I. L. Boyd, G. Frisk, E. Urban, P. Tyack, J. Ausubel *et al.* An international quiet ocean experiment. *Oceanography*, **24 (2)**:174–181, 2011.

[Brown94] R. S. Brown, S. S. Stanislawski, and W. C. Mackay. Effects of frazil ice on fish. *In Workshop on environmental aspects of river ice. Environment Canada, National Hydrology Research Institute, Symposium*, vol. 12, 261–277. 1994.

[Buck80] B. M. Buck and C. R. Greene. A two-hydrophone method of eliminating the effects of nonacoustic noise interference in measurements of infrasonic ambient noise levels. *J. Acoust. Soc. Am.*, **68**:1306, 1980.

[Buck86] B. Buck and J. Wilson. Nearfield noise measurements from an Arctic pressure ridge. *J. Acoust. Soc. Am.*, **80**:256–264, 1986.

[Carey11] W. Carey and R. Evans. *Ocean Ambient Noise: Measurement and Theory*. 1st edn. Springer, 2011.

[Cato02] D. H. Cato and R. D. McCauley. Australian research in ambient sea noise. *Acoust Aust*, **30**:13–20, 2002.

[Clark01] P. U. Clark, S. J. Marshall, G. K. C. Clarke, S. W. Hostetler, J. M. Licciardi *et al.* Freshwater forcing of abrupt climate change during the last glaciation. *Science*, **293**(5528):283–287, 2001.

[Clark02] P. U. Clark, N. G. Pisias, T. F. Stocker, and A. J. Weaver. The role of the thermohaline circulation in abrupt climate change. *Nature*, **415**(6874):863–869, 2002.

[Clark09] C. W. Clark, W. T. Ellison, B. L. Southall, L. Hatch, S. Van *et al.* Acoustic masking in marine ecosystems as a function of anthropogenic sound sources. *Report to the International Whaling Commission. SC-61 E*, **10**, 2009.

[Codarin09] A. Codarin, L. E. Wysocki, F. Ladich, and M. Picciulin. Effects of ambient and boat noise on hearing and communication in three fish species living in a marine protected area (miramare, italy). *Marine pollution bulletin*, **58**(12):1880–1887, 2009.

[Commission09] M. M. Commission. *Marine Mammal Commission: Annual Report to the Congress: 2009*. Marine Mammal Commission, 2009.

[Crouch72] W. W. Crouch and P. J. Burt. The logarithmic dependence of surface-generated ambient-sea-noise spectrum level on wind speed. *J. Acoust. Soc. Am.*, **51**:1066–1072, 1972.

[Cummings89] W. C. Cummings, O. I. Diachok, and J. D. Shaffer. *Acoustic Transients of the Marginal Sea Ice Zone: A Provisional Catalog.* Tech. rep., DTIC Document, 1989.

[Dekeling13] R. Dekeling, M. Tasker, M. Ainslie, M. Andersson, M. André *et al. Monitoring Guidance for Underwater Noise in European Seas - 2nd Report of the Technical Subgroup on Underwater noise (TSG Noise).* Tech. rep., 2013.

[Deser08] C. Deser and H. Teng. Evolution of arctic sea ice concentration trends and the role of atmospheric circulation forcing, 1979–2007. *Geophys. Res. Lett.*., **35**(2), 2008.

[Di Iorio12] L. Di Iorio, C. Gervaise, V. Jaud, A. A. Robson, and L. Chauvaud. Hydrophone detects cracking sounds: Non-intrusive monitoring of bivalve movement. *Journal of Experimental Marine Biology and Ecology*, **432**:9–16, 2012.

[Diachok74] O. I. Diachok and R. S. Winokur. Spatial variability of underwater ambient noise at the Arctic ice water boundary. *J. Acoust. Soc. Am.*, **55**:750, 1974.

[Dickson08] B. Dickson, J. Meincke, and P. Rhines. *Arctic–subarctic ocean fluxes: defining the role of the northern seas in climate.* Springer, 2008.

[Dieckmann10] G. S. Dieckmann and H. H. Hellmer. The importance of sea ice: An overview. *In* D. N. Thomas and G. S. Dieckmann, (Eds.) *Sea Ice*, 2nd edn. Blackwell Publishing Ltd, 2010.

[Dobretsov10] N. L. Dobretsov and N. P. Pokhilenko. Mineral resources and development in the russian arctic. *Russian Geology and Geophysics*, **51**(1):98–111, 2010.

[Dugan97] J. Dugan, W. Morris, and Z. Williams. *Vibrational Motion of Arctic Pack Ice.* Tech. rep., DTIC Document, 1997.

[Dwyer83] R. F. Dwyer. A technique for improving detection and estimation of signals contaminated by under ice noise. *J. Acoust. Soc. Am.*, **74**:124–130, 1983.

[Dyer73] I. Dyer. Statistics of distant shipping noise. *J. Acoust. Soc. Am.*, **53**(2):564–570, 1973.

[Epstein05] P. R. Epstein. Climate change and human health. *New England Journal of Medicine*, **353**(14):1433–1436, 2005.

[Erbe00] C. Erbe and D. M. Farmer. A software model to estimate zones of impact on marine mammals around anthropogenic noise. *J. Acous. Soc. Am.*, **108**:1327–1331, 2000.

[Erbe02] C. Erbe. Underwater noise of whale-watching boats and potential effects on killer whales (orcinus orca), based on an acoustic impact model. *Marine Mammal Science*, **18**(2):394–418, 2002.

[Erbe08] C. Erbe. Critical ratios of beluga whales (delphinapterus leucas) and masked signal duration. *J. Acoust. Soc. Am.*, **124**:2443–2451, 2008.

[Evans02] N. W. D. Evans, J. S. Mason, and B. Fauve. Efficient real-time noise estimation without explicit speech, non-speech detection: an assessment on the aurora corpus. *In Digital Signal Processing, 2002. DSP 2002. 2002 14th International Conference on*, vol. 2, 985–988. IEEE, 2002.

[Farmer89] D. M. Farmer and Y. Xie. The sound generated by propagating cracks in sea ice. *J. Acoust. Soc. Am.*, **85**:1489–1500, 1989.

[Fay99] R. R. Fay and A. N. Popper. *Comparative Hearing: Fish an Amphibians*, vol. 11. Springer, 1999.

[Feller94] D. Feller. *Environmental Forcing of Ambient Noise in the Nansen and Amundsen Basins of the Arctic Ocean*. Tech. rep., DTIC Document, 1994.

[Field12] C. B. Field, V. Barros, T. F. Stocker, and Q. Dahe. *Managing the Risks of Extreme Events and Disasters to Advance Climate Change Adaptation: Special Report of the Intergovernmental Panel on Climate Change*. Cambridge University Press, 2012.

[Ford04] J. D. Ford and B. Smit. A framework for assessing the vulnerability of communities in the canadian arctic to risks associated with climate change. *Arctic*, 389–400, 2004.

[Ford06] J. D. Ford, B. Smit, and J. Wandel. Vulnerability to climate change in the arctic: a case study from arctic bay, canada. *Global Environmental Change*, **16**(2):145–160, 2006.

[Fowler03] C. Fowler. Polar Pathfinder Daily 25 km EASE-GRID Sea Ice Motion Vectors, National Snow and Ice Data Center. *Boulder, CO, USA, Digital media*, 2003.

[Galley08] R. J. Galley, E. Key, D. G. Barber, B. J. Hwang, and J. K. Ehn. Spatial and temporal variability of sea ice in the southern beaufort sea and amundsen gulf: 1980–2004. *J. Geophys. Res.: Oceans (1978–2012)*, **113**(C5), 2008.

[Galley12] R. Galley, B. Else, S. Howell, J. Lukovich, and D. Barber. Landfast sea ice conditions in the Canadian Arctic: 1983-2009. *Arctic*, **65**(2):133–144, 2012.

[Ganton65] J. H. Ganton and A. R. Milne. Temperature and Wind Dependent Ambient Noise under Midwinter Pack Ice. *J. Acoust. Soc. Am.*, **38**(3):406–411, 1965.

[Gautier09] D. L. Gautier, K. J. Bird, R. R. Charpentier, A. Grantz, D. W. Houseknecht *et al.* Assessment of undiscovered oil and gas in the arctic. *Science*, **324**(5931):1175–1179, 2009.

[Gervaise07] C. Gervaise, S. Vallez, C. Ioana, Y. Stéphan, and Y. Simard. Passive acoustic tomography: new concepts and applications using marine mammals: a review. *Journal of the Marine Biological Association of the United Kingdom*, **87**(01):5–10, 2007.

[Gervaise12a] C. Gervaise, G. B. Kinda, J. Bonnel, Y. Stephan, and S. Vallez. Passive geoacoustic inversion with a single hydrophone using broadband ship noise. *J. Acoust. Soc. Am.*, **131**:1999, 2012.

[Gervaise12b] C. Gervaise, Y. Simard, N. Roy, B. Kinda, and N. Ménard. Shipping noise in whale habitat: Characteristics, sources, budget, and impact on belugas in Saguenay Lawrence Marine Park hub. *J. Acoust. Soc. Am.*, **132**:76, 2012.

[Gervaise13] C. Gervaise and L. Di Iorio. Shallow water soundscape descriptors for environmental monitoring and noise impact studies. *J. Acoust. Soc. Am.*, **in press**, 2013.

[Girard09] L. Girard, J. Weiss, J. M. Molines, B. Barnier, and S. Bouillon. Evaluation of high-resolution sea ice models on the basis of statistical and scaling properties of arctic sea ice drift and deformation. *J. Geophys. Res.*, **114**(C8):C08015, 2009.

[Goosse99] H. Goosse and T. Fichefet. Importance of ice-ocean interactions for the global ocean circulation: A model study. *J. Geophys. Res.: Oceans (1978–2012)*, **104**(C10):23337–23355, 1999.

[Grantz12] A. Grantz and P. E. Hart. Petroleum prospectivity of the canada basin, arctic ocean. *Marine and Petroleum Geology*, **30**(1):126–143, 2012.

[Grassl01] H. Grassl. Climate and oceans. *In* J. G. Gerold Siedler, John Church, (Ed.) *Ocean Circulation and Climate: Observing and Modelling the Global Ocean*, vol. 77 of *International geophy*, chap. 1, 1–43. Academic Press, 2001.

[Gray80] L. M. Gray and D. S. Greeley. Source level model for propeller blade rate radiation for the world's merchant fleet. *J. Acoust. Soc. Am.*, **67**(2):516–522, 1980.

[Greene64] C. Greene and B. Buck. Arctic ocean ambient noise. *J. Acoust. Soc. Am.*, **36**(6):1218–1220, 1964.

[Greening94] M. Greening and P. Zakarauskas. Spatial and source level distributions of ice cracking in the Arctic Ocean. *J. Acoust. Soc. Am.*, **95**:783–790, 1994.

[Haas10a] C. Haas. Dynamics versus thermodynamics: The sea ice thickness distribution. *In* D. N. Thomas and G. S., (Eds.) *Sea Ice*, 2nd edn., chap. 4. Blackwell Publishing Ltd, 2010.

[Haas10b] C. Haas *et al.* Dynamics versus thermodynamics: The sea ice thickness distribution. *Sea Ice*, 82, 2010.

[Halvorsen13] D. G. Halvorsen, M. B.and Zeddies, D. Chicoine, and A. N. Popper. Effects of low-frequency naval sonar exposure on three species of fish. *J. Acoust. Soc. Am.*, **134**(2):EL205–EL210, 2013.

[Hamilton80] E. L. Hamilton. Geoacoustic modeling of the sea floor. *J. Acoust. Soc. Am.*, **68**:1313–1340, 1980.

[Hamson97] R. Hamson. The modelling of ambient noise due to shipping ans wind sources in complex environments. *Applied Acoustics*, **51**:251–287, 1997.

[Hannah09] C. Hannah, F. Dupont, and M. Dunphy. Polynyas and tidal currents in the Canadian Arctic Archipelago. *Arctic*, **62(1)**:83–95, 2009.

[Hatch08] L. Hatch, C. Clark, R. Merrick, S. Van Parijs, D. Ponirakis *et al.* Characterizing the relative contributions of large vessels to total ocean noise fields: a case study using the gerry e. studds stellwagen bank national marine sanctuary. *Environmental Management*, **42**(5):735–752, 2008.

[Heide-Jørgensen12] M. P. Heide-Jørgensen, K. L. Laidre, L. T. Quakenbush, and J. J. Citta. The northwest passage opens for bowhead whales. *Biology letters*, **8**(2):270–273, 2012.

[Heide-Jørgensen13] R. G. Heide-Jørgensen, M. P.and Hansen, K. Westdal, R. R. Reeves, and A. Mosbech. Narwhals and seismic exploration: Is seismic noise increasing the risk of ice entrapments? *Biological Conservation*, **158**:50–54, 2013.

[Henry12] G. H. R. Henry, K. A. Harper, J. R. Chen, W.and Deslippe, R. F. Grant, P. M. Lafleur *et al.* Effects of observed and experimental climate change on terrestrial ecosystems in northern canada: results from the canadian ipy program. *Climatic Change*, **115**(1):207–234, 2012.

[Hibler III79] W. D. Hibler III. A dynamic thermodynamic sea ice model. *J. Phys. Oceano.*, **9**(4):815–846, 1979.

[Hildebrand04] J. Hildebrand. *Sources of Anthropogenic Sound in the Marine Environment.* Tech. rep., Scripps Institution of Oceanography, University of California San Diego, La Jolla, CA 92093-0205, 2004.

[Hildebrand09] J. A. Hildebrand. Anthropogenic and natural sources of ambient noise in the ocean. *Marine Ecology Progress Series*, **395**(5), 2009.

[Hinzman05] L. D. Hinzman, N. D. Bettez, W. R. Bolton, F. S. Chapin, C. L. Dyurgerov, M. B.and Fastie *et al.* Evidence and implications of recent climate change in northern alaska and other arctic regions. *Climatic Change*, **72**(3):251–298, 2005.

[Hoegh-Guldberg10] O. Hoegh-Guldberg and J. F. Bruno. The impact of climate change on the world's marine ecosystems. *Science*, **328**(5985):1523–1528, 2010.

[Hong12] N. Hong. The melting arctic and its impact on china's maritime transport. *Research in transportation economics*, **35**(1):50–57, 2012.

[Huber09] P. Huber and E. Ronchetti. *Robust Statistics, second edition.* John Wiley and Sons, 2009.

[Huillery08a] J. Huillery. *Support temps-fréquence d'un signal inconnu en présence de bruit additif gaussien.* Ph.D. thesis, Institut National Polytechnique de Grenoble-INPG, 2008.

[Huillery08b] J. Huillery, F. Millioz, and N. Martin. On the description of spectrogram probabilities with a chi-squared law. *Signal Processing, IEEE Transactions on*, **56**(6):2249–2258, 2008.

[IPCC01] IPCC. Summary for policymakers. *In* Y. D. D. G. M. N. P. v. d. L. X. D. K. M. Houghton, J.T. and C. Johnson, (Eds.) *Climate Change 2001:*

The Scientific Basis. Contribution of Working Group I to the Third Assessment Report of the Intergovernmental Panel on Climate Change. Cambridge University Press, Cambridge, United Kingdom and New York, NY, USA., 2001.

[IPCC07] IPCC. Summary for policymakers. *In* D. Q. M. M. Z. C. M. M. K. A. M. Solomon, S. and H. Miller, (Eds.) *: Climate Change 2007: The Physical Science Basis. Contribution of Working Group I to the Fourth Assessment Report of the Intergovernmental Panel on Climate Change*. Cambridge University Press, Cambridge, United Kingdom and New York, NY, USA., 2007.

[Jakobsson02] M. Jakobsson. Hypsometry and volume of the arctic ocean and its constituent seas. *Geochemistry, Geophysics, Geosystems*, **3**(5):1–18, 2002.

[Jeffrey10] A. N. Jeffrey, S. E. Moore, and P. J. Stabeno. A sound budget for the southeastern bering sea: Measuring wind, rainfall, shipping, and other sources of underwater sound. *J. Acoust. Soc. Am.*, **128**(1):58–65, 2010.

[Johannessen04] O. M. Johannessen, L. Bengtsson, M. W. Miles, S. I. Kuzmina, V. A. Semenov *et al.* Arctic climate change: Observed and modelled temperature and sea-ice variability. *Tellus A*, **56**(4):328–341, 2004.

[Jones01] E. Jones. Circulation in the Arctic Ocean. *Polar Res.*, **20**(2):139–146, 2001.

[Jorgenson01] M. T. Jorgenson, C. H. Racine, J. C. Walters, and T. E. Osterkamp. Permafrost degradation and ecological changes associated with a warmingclimate in central alaska. *Climatic change*, **48**(4):551–579, 2001.

[Jorgenson10] M. T. Jorgenson, V. Romanovsky, J. Harden, Y. Shur, J. O'Donnell *et al.* Resilience and vulnerability of permafrost to climate change this article is one of a selection of papers from the dynamics of change in alaska's boreal forests: Resilience and vulnerability in response to climate warming. *Canadian Journal of Forest Research*, **40**(7):1219–1236, 2010.

[Kaleschke01] L. Kaleschke, G. Heygster, C. LÃ¼pkes, A. Bochert, J. Hartmann *et al.* SSM/I sea ice remote sensing for mesoscale ocean-atmosphere interaction analysis: Ice and icebergs. *Can. J. Rem. Sens.*, **27**(5):526–537, 2001.

[Kandia06] V. Kandia and Y. Stylianou. Detection of sperm whale clicks based on the teager–kaiser energy operator. *Applied Acoustics*, **67**(11):1144–1163, 2006.

[Kattsov10] V. M. Kattsov, V. E. Ryabinin, J. E. Overland, M. C. Serreze, M. Visbeck *et al.* Arctic sea-ice change: a grand challenge of climate science. *J. Glac.*, **56**(200):1115–1121, 2010.

[Kay98] S. M. Kay. *Fundamentals of Statistical signal processing, Volume 2: Detection theory*. Prentice Hall PTR, 1998.

[Kibblewhite76] A. C. Kibblewhite and D. A. Jones. Ambient noise under antarctic sea ice. *J. Acoust. Soc. Am.*, **59**(4):790–798, 1976.

[Kimura04] N. Kimura. Sea ice motion in response to surface wind and ocean current in the Southern Ocean. *J. Meteor. Soc. Japan*, **82**(4):1223–1231, 2004.

[Kinda13] G. B. Kinda, Y. Simard, I. J. Gervaise, C.and Mars, and L. Fortier. Under-ice ambient noise in eastern beaufort sea, canadian arctic, and its relation to environmental forcing. *J. Acoust. Soc. Am.*, **134**(1):77–87, 2013.

[Kontorovich10] A. E. Kontorovich, M. I. Epov, L. M. Burshtein, V. D. Kaminskii, A. R. Kurchikov *et al.* Geology and hydrocarbon resources of the continental shelf in russian arctic seas and the prospects of their development. *Russian Geology and Geophysics*, **51**(1):3–11, 2010.

[Koopmans74] L. H. Koopmans. *The spectral analysis of time series*, vol. 22. Academic Press Limited, 1974.

[Kwok01] R. Kwok. Deformation of the arctic ocean sea ice cover between november 1996 and april 1997: a qualitative survey. *Solid Mechanics and its Applications*, **94**:315–322, 2001.

[Kwok06] R. Kwok. Exchange of sea ice between the Arctic Ocean and the Canadian Arctic Archipelago. *Geophys. Res. Lett..*, **33**(16):L16501, 2006.

[Kwok09a] R. Kwok. Outflow of Arctic Ocean sea ice into the Greenland and Barents Seas: 1979-2007. *J. Clim.*, **22**(9):2438–2457, 2009.

[Kwok09b] R. Kwok and D. A. Rothrock. Decline in arctic sea ice thickness from submarine and icesat records: 1958–2008. *Geophys. Res. Lett..*, **36**(15), 2009.

[Kwok12] R. Kwok and G. F. Cunningham. Deformation of the arctic ocean ice cover after the 2007 record minimum in summer ice extent. *Cold Regions Science and Technology*, **76**:17–23, 2012.

[Laidre08] K. L. Laidre, I. Stirling, L. F. Lowry, Ø. Wiig, M. P. Heide-Jørgensen *et al.* Quantifying the sensitivity of arctic marine mammals to climate-induced habitat change. *Ecological Applications*, **18**(sp2):S97–S125, 2008.

[Langehaug13] H. R. Langehaug, F. Geyer, L. H. Smedsrud, and Y. Gao. Arctic sea ice decline and ice export in the cmip5 historical simulations. *Ocean Modelling*, 2013.

[Legendre98] P. Legendre and L. Legendre. *Numerical ecology. Developments in environmental modeling, 20.* Elsevier, Amsterdam, The Netherlands, 1998.

[Lewis87] J. Lewis and W. Denner. Arctic ambient noise in the Beaufort Sea: seasonal space and time scales. *J. Acoust. Soc. Am.*, **82**(3):988–997, 1987.

[Lewis88] J. Lewis and W. Denner. Arctic ambient noise in the Beaufort Sea: Seasonal relationships to sea ice kinematics. *J. Acoust. Soc. Am.*, **83**(2):549–565, 1988.

[Lindsay03] R. Lindsay, J. Zhang, and D. A. Rothrock. Sea-ice deformation rates from satellite measurements and in a model. *Atmosphere-ocean*, **41**(1):35–47, 2003.

[Lukovich09] J. V. Lukovich, M. G. Asplin, and D. G. Barber. Atmospheric forcing of the Beaufort Sea ice gyre: Surface-stratosphere coupling. *J. Geophys. Res*, **114**:C00A03, 2009.

[Ma05a] B. Ma and J. Nystuen. Passive acoustic detection and measurement of rainfall at sea. *J. Atm. Oceanic Tech.*, **22**(8):1225–1248, 2005.

[Ma05b] B. B. Ma and J. A. Nystuen. Passive acoustic detection and measurement of rainfall at sea. *J. Atm. Oceanic Tech.*, **22**(8):1225–1248, 2005.

[Ma05c] B. B. Ma, J. A. Nystuen, and R.-C. Lien. Prediction of underwater sound levels from rain and wind. *J. Acoust. Soc. Am.*, **117(6)**:3555–3565, 2005.

[Macpherson62] J. D. Macpherson. Some under-ice acoustic ambient noise measurements. *J. Acoust. Soc. Am.*, **34**:1149, 1962.

[Mahlstein12] I. Mahlstein and R. Knutti. September arctic sea ice predicted to disappear near 2 c global warming above present. *J. Geophys. Res.*, **117**(D6):D06104, 2012.

[Makris86] N. Makris and I. Dyer. Environmental correlates of pack ice noise. *J. Acoust. Soc. Am.*, **79**(5):1434–1440, 1986.

[Makris91] N. Makris and I. Dyer. Environmental correlates of Arctic ice edge noise. *J. Acoust. Soc. Am.*, **90**(6):3288–3298, 1991.

[Marques09] T. A. Marques, L. Thomas, J. Ward, N. DiMarzio, and P. L. Tyack. Estimating cetacean population density using fixed passive acoustic sensors: An example with blainville's beaked whales. *J. Acoust. Soc. Am.*, **125**:1982, 2009.

[Marsan04] D. Marsan, H. Stern, R. Lindsay, and J. Weiss. Scale dependence and localization of the deformation of Arctic sea ice. *Phys. Rev. Lett.*, **93**(17), 2004.

[Marsan12] D. Marsan, J. Weiss, E. Larose, and J. P. Metaxian. Sea-ice thickness measurement based on the dispersion of ice swell. *J. Acoust. Soc. Am.*, **131**(1):80–91, 2012. Marsan, David Weiss, Jerome Larose, Eric Metaxian, Jean-Philippe Part 1.

[Martin01a] R. Martin. Noise power spectral density estimation based on optimal smoothing and minimum statistics. *Speech and Audio Processing, IEEE Transactions on*, **9**(5):504–512, 2001.

[Martin01b] S. Martin. Polynyas. *Encyclopedia of Ocean Sciences*, **3**:2241–2247, 2001.

[Maslanik11] J. Maslanik, J. Stroeve, C. Fowler, and W. Emery. Distribution and trends in Arctic sea ice age through spring 2011. *Geophys. Res. Lett.*., **38**(13):L13502, 2011.

[Masterson13] D. Masterson. The arctic islands adventure and panarctic oils ltd. *Cold Regions Science and Technology*, **85**(0):1 – 14, 2013.

[Mathias13] D. Mathias, A. M. Thode, J. Straley, and R. D. Andrews. Acoustic tracking of sperm whales in the gulf of alaska using a two-element vertical array and tags. *J. Acoust. Soc. Am.*, **134**:2446–2461, 2013.

[McDonald06] M. A. McDonald, J. A. Hildebrand, and S. M. Wiggins. Increases in deep ocean ambient noise in the northeast pacific west of san nicolas island, california. *J. Acoust. Soc. Am.*, **120**:711, 2006.

[McKenna12] M. F. McKenna, D. Ross, S. M. Wiggins, and J. A. Hildebrand. Underwater radiated noise from modern commercial ships. *J. Acoust. Soc. Am.*, **131**:92–103, 2012.

[McPhee80] M. G. McPhee. An analysis of pack ice drift in summer. *Sea Ice Processes and Models*, 62–75, 1980.

[McPhee09] M. McPhee, A. Proshutinsky, J. H. Morison, M. Steele, and M. Alkire. Rapid change in freshwater content of the arctic ocean. *Geophys. Res. Lett.*., **36**(10):L10602, 2009.

[Mellinger07] D. K. Mellinger, K. M. Stafford, S. Moore, R. P. Dziak, and H. Matsumoto. Fixed passive acoustic observation methods for cetaceans. *Oceanography*, **20**(4):36, 2007.

[Merchant12] N. D. Merchant, M. J. Witt, P. Blondel, B. J. Godley, and G. H. Smith. Assessing sound exposure from shipping in coastal waters using a single hydrophone and automatic identification system (ais) data. *Marine pollution bulletin*, 2012.

[Millioz11] F. Millioz and N. Martin. Circularity of the stft and spectral kurtosis for time-frequency segmentation in gaussian environment. *Signal Processing, IEEE Transactions on*, **59**(2):515–524, 2011.

[Milne64] A. R. Milne and J. H. Ganton. Ambient Noise under Arctic Sea Ice. *J. Acoust. Soc. Am.*, **36**(5):855–863, 1964.

[Milne66] A. Milne. Statistical Description of Noise under Shore Fast Sea Ice in Winter. *J. Acoust. Soc. Am.*, **39(6)**:1174–1182, 1966.

[Milne67] A. R. Milne, J. H. Ganton, and D. J. McMillin. Ambient noise under sea ice and further measurements of wind and temperature dependence. *J. Acoust. Soc. Am.*, **41**:525–528, 1967.

[Moore08] S. E. Moore and H. P. Huntington. Arctic marine mammals and climate change: impacts and resilience. *Ecological Applications*, **18**(sp2):S157–S165, 2008.

[Moore12] S. E. e. a. Moore. Marine mammals and anthropogenic sound in a rapidly changing arctic. *BioScience*, **62**:289–295., 2012.

[Nakayama12] Y. Nakayama, K. Ohshima, and Y. Fukamachi. Enhancement of Sea Ice Drift due to the Dynamical Interaction between Sea Ice and a Coastal Ocean. *J. Phys. Oceanogr.*, **42**(1):179–192, 2012.

[Nassichuk83] W. W. Nassichuk. Petroleum potential in arctic north america and greenland. *Cold regions science and technology*, **7**:51–88, 1983.

[NRC03] NRC. *Ocean Noise and Marine Mammals*. National Academies Press, Washington D.C., 2003. (US).

[Nystuen86] J. Nystuen. Rainfall measurements using underwater ambient noise. *J. Acoust. Soc. Am*, **79**(4):972–982, 1986.

[Nystuen96] J. A. Nystuen. Acoustical rainfall analysis: Rainfall drop size distribution using the underwater sound field. *J. Atm. Oceanic Tech.*, **13**:74–84, 1996.

[Nystuen00] J. A. Nystuen, M. J. McPhaden, and H. P. Freitag. Surface measurements of precipitation from an ocean mooring: The underwater acoustic log from the south china sea*. *J. Appl. Meteo.*, **39**(12):2182–2197, 2000.

[Ollila11] E. Ollila, J. Eriksson, and V. Koivunen. Complex elliptically symmetric random variables–generation, characterization, and circularity tests. *Signal Processing, IEEE Transactions on*, **59**(1):58–69, 2011.

[Park05] C. Park, W. Seong, and P. Gerstoft. Geoacoustic inversion in time domain using ship of opportunity noise recorded on a horizontal towed array. *J. Acoust. Soc. Am.*, **117**:1933–1941, 2005.

[Parkinson05] A. J. Parkinson and J. C. Butler. Potential impacts of climate change on infectious diseases in the arctic. *International Journal of Circumpolar Health*, **64**(5), 2005.

[Parkinson09] A. J. Parkinson and B. Evengård. Climate change, its impact on human health in the arctic and the public health response to threats of emerging infectious diseases. *Global Health Action*, **2**, 2009.

[Parmesan06] C. Parmesan. Ecological and evolutionary responses to recent climate change. *Annual Review of Ecology, Evolution, and Systematics*, 637–669, 2006.

[Parry07] M. L. Parry. *Climate Change 2007: Impacts, Adaptation and Vulnerability: Working Group II Contribution to the Fourth Assessment Report of the IPCC Intergovernmental Panel on Climate Change*, vol. 4. Cambridge University Press, 2007.

[Payne64] F. A. Payne. Effect of ice cover on shallow-water ambient sea noise. *J. Acoust. Soc. Am.*, **36**:1943–1947, 1964.

[Peterson02] B. J. Peterson, R. M. Holmes, J. W. McClelland, C. J. Vörösmarty, R. B. Lammers *et al.* Increasing river discharge to the arctic ocean. *Science*, **298**(5601):2171–2173, 2002.

[Piggott64] C. L. Piggott. Ambient sea noise at low frequencies in shallow water of the scotian shelf. *J. Acoust. Soc. Am.*, **36**:2152–2163, 1964.

[Pijanowski11a] B. C. Pijanowski, A. Farina, S. H. Gage, S. L. Dumyahn, and B. L. Krause. What is soundscape ecology? an introduction and overview of an emerging new science. *Landscape ecology*, **26**(9):1213–1232, 2011.

[Pijanowski11b] B. C. Pijanowski, L. J. Villanueva-Rivera, S. L. Dumyahn, A. Farina, B. L. Krause *et al.* Soundscape ecology: the science of sound in the landscape. *BioScience*, **61**(3):203–216, 2011.

[Plaisant91] A. Plaisant. Modelisation de la cohérence spatiale du bruit généré par les vagues. *In Actes de Colloques, NÂ° 12*. 1991.

[Polyak10] L. Polyak, R. Alley, J. Andrews, J. Brigham-Grette, T. Cronin *et al.* History of sea ice in the Arctic. *Quaternary Sci. Revi.*, **29**(15):1757–1778, 2010.

[Popper03] A. N. Popper. Effects of anthropogenic sounds on fishes. *Fisheries*, **28**(10):24–31, 2003.

[Pritchard90] R. Pritchard. Sea ice noise generating processes. *J. Acoust. Soc. Am.*, **88**(6):2830–2842, 1990.

[Proshutinsky02] A. Proshutinsky, R. H. Bourke, and F. A. McLaughlin. The role of the beaufort gyre in arctic climate variability: Seasonal to decadal climate scales. *Geophys. Res. Lett.*., **29**(23):15–1, 2002.

[Proshutinsky05] A. Proshutinsky, J. Yang, R. Krishfield, R. Gerdes, M. Karcher *et al.* Arctic ocean study: Synthesis of model results and observations. *EOS, Transactions american geophysical union*, **86**(40):368–371, 2005.

[Prowse06] T. D. Prowse, F. J. Wrona, J. D. Reist, J. E. Hobbie, L. M. Lévesque *et al.* General features of the arctic relevant to climate change in freshwater ecosystems. *AMBIO: A Journal of the Human Environment*, **35**(7):330–338, 2006.

[Rampal08] P. Rampal, J. Weiss, D. Marsan, R. Lindsay, and H. Stern. Scaling properties of sea ice deformation from buoy dispersion analysis. *J. Geophys. Res.*, **113**(C3):C03002, 2008.

[Rampal09] P. Rampal, J. Weiss, and D. Marsan. Positive trend in the mean speed and deformation rate of Arctic sea ice, 1979 - 2007. *J. Geophys. Res.*, **114**(C5):C05013, 2009.

[Rampal11] P. Rampal, J. Weiss, C. Dubois, and J.-M. Campin. Ipcc climate models do not capture arctic sea ice drift acceleration: Consequences in terms of projected sea ice thinning and decline. *Journal of Geophysical Research*, **116**(C8):C00D07, 2011.

[Rayner03] N. A. Rayner, D. E. Parker, E. B. Horton, C. K. Folland, L. V. Alexander *et al.* Global analyses of sea surface temperature, sea ice, and night marine air temperature since the late nineteenth century. *J. Geophys. Res.: Atmospheres (1984–2012)*, **108**(D14), 2003.

[Reeder11] D. Reeder, E. Sheffield, and S. Mach. Wind-generated ambient noise in a topographically isolated basin: A pre-industrial era proxy. *J. Acoust. Soc. Am.*, **129**(1):64, 2011.

[Rice13] S. L. Rice, T. Dudley, C. Schneider, R. J. Pierce, B. Horn *et al.* Arctic seismic acquisition and processing. *The Leading Edge*, **32**(5):546–554, 2013.

[Rolland12] R. M. Rolland, K. E. Parks, S. E.and Hunt, M. Castellote, P. J. Corkeron, D. P. Nowacek *et al.* Evidence that ship noise increases stress in right whales. *Proceedings of the Royal Society B: Biological Sciences*, **279**(1737):2363–2368, 2012.

[Ross87] D. Ross. *Mechanics of Underwater Noise*. Peninsula Publising Los Atlos, California, 1987.

[Roth12] E. Roth, J. Hildebrand, S. Wiggins, and D. Ross. Underwater ambient noise on the Chukchi Sea continental slope from 2006 - 2009. *J. Acoust. Soc. Am.*, **131**(1):104–110, 2012.

[Rotschky11] G. Rotschky, T. Schuler, J. Haarpaintner, J. Kohler, and E. Isaksson. Spatio-temporal variability of snowmelt across Svalbard during the period 2000-08 derived from QuikSCAT/SeaWinds scatterometry. *Polar Res.*, **30, 5963**(0), 2011.

[Safonov10] Y. G. Safonov. Mineral potential of the russian arctic: state and efficient development. *Russian geology and geophysics*, **51**(1):112–120, 2010.

[Schulson91] E. M. Schulson and W. D. Hibler III. The fracture of ice on scales large and slllall: Arctic leads and wing cracks. *J. Glac.*, **37(127)**(127):319–322, 1991.

[Schulson04] E. M. Schulson and W. D. Hibler III. Fracture of the winter sea ice cover on the arctic ocean. *Comptes Rendus Physique*, **5**(7):753–767, 2004.

[Schulson09] E. M. Schulson, P. Duval *et al.* Creep and fracture of ice. 2009.

[Serreze00] J. E. Serreze, M. C.and Walsh, F. S. Chapin Iii, T. Osterkamp, M. Dyurgerov, V. Romanovsky *et al.* Observational evidence of recent change in the northern high-latitude environment. *Climatic Change*, **46**(1-2):159–207, 2000.

[Serreze07a] M. C. Serreze. Arctic climate change: Where reality exceeds expectations. *In American Geophysical Union Fall Meeting, San Francisco, CA*. 2007.

[Serreze07b] M. C. Serreze, M. M. Holland, and J. Stroeve. Perspectives on the arctic's shrinking sea-ice cover. *science*, **315**(5818):1533–1536, 2007.

[Siedler01] G. Siedler, J. Church, J. Gould, and S. Griffies. *Ocean circulation and climate: observing and modelling the global ocean*, vol. 77. Access Online via Elsevier, 2001.

[Simard12a] Y. Simard, B. Kinda, C. Gervaise, and L. Fortier. Annual time-series of marine mammal frequentation of eastern beaufort sea from pam methodology. *In IPY, MontrÃ©al*. 2012.

[Simard12b] Y. Simard, B. Kinda, C. Gervaise, and L. Fortier. Global warming effects on arctic and subarctic underwater soundscapes and marine mammal frequentation from an acoustic observatory. *In ArcticNet's eighth Annual Scientific Meeting (ASM2012), Vancouver, BC: Canada*. 2012.

[Simon82] T. Simon. Sur la formation et l'évolution des polynies arctiques (archipel canadien et Groenland). *Norois*, **116**(1):585–598, 1982.

[Simpson05] S. D. Simpson, M. Meekan, J. Montgomery, R. McCauley, and A. Jeffs. Homeward sound. *Science*, **308**(5719):221–221, 2005.

[Smedsrud11] L. Smedsrud, A. Sirevaag, K. Kloster, A. Sorteberg, and S. Sandven. Recent wind driven high sea ice export in the Fram Strait contributes to Arctic sea ice decline. *The Cryosphere Discuss*, **5**:1311–1334, 2011.

[Smith04] M. E. Smith, A. S. Kane, and A. N. Popper. Noise-induced stress response and hearing loss in goldfish (carassius auratus). *J. Exp. Bio.*, **207**(3):427–435, 2004.

[Socheleau12] F.-X. Socheleau, D. Pastor, and M. Duret. On symmetric alpha-stable noise after short-time fourier transformation. *Signal Processing Letters, IEEE*, **20**:455–458, 2012.

[Soja07] A. J. Soja, N. M. Tchebakova, N. H. F. French, M. D. Flannigan, H. H. Shugart *et al.* Climate-induced boreal forest change: predictions versus current observations. *Global and Planetary Change*, **56**(3):274–296, 2007.

[Sousa-Lima13] R. S. Sousa-Lima, T. F. Norris, J. N. Oswald, and D. P. Fernandes. A review and inventory of fixed autonomous recorders for passive acoustic monitoring of marine mammals. *Aquatic Mammals*, **39**(1):23–53, 2013.

[Southall08] B. L. Southall, A. E. Bowles, W. T. Ellison, J. J. Finneran, R. L. Gentry *et al.* Marine mammal noise exposure criteria: initial scientific recommendations. *Aquatic Mammals*, **33 (4)**:273–275, 2008.

[Spielhagen12] R. F. Spielhagen. History of atlantic water advection to the arctic ocean: a review of 20 years of progress since the "oden"–"polarstern" expedition arctic 91. *Polarforschung*, **82**(1):19–36, 2012.

[Spreen08] G. Spreen, L. Kaleschke, and G. Heygster. Sea ice remote sensing using AMSR-E 89-GHz channels. *J. Geophys. Res.*, **113**(C2):C02, 2008.

[Srokosz12] M. Srokosz, M. Baringer, H. Bryden, S. Cunningham, T. Delworth *et al.* Past, present, and future changes in the atlantic meridional overturning circulation. *Bulletin of the American Meteorological Society*, **93**(11):1663–1676, 2012.

[Stafford08] K. M. Stafford, S. E. Moore, K. L. Laidre, and M. P. Heide-Jørgensen. Bowhead whale springtime song off west greenland. *J. Acoust. Soc. Am.*, **124(5)**:3315–3323, 2008.

[Stein88] P. Stein. Interpretation of a few ice event transients. *J. Acoust. Soc. Am.*, **83**:617, 1988.

[Stoica97] P. Stoica and R. L. MoMoses. *Introduction to spectral analysis*, vol. 89. Prentice hall New Jersey, 1997.

[Strasberg79] M. Strasberg. Nonacoustic noise interference in measurements of infrasonic ambient noise. *J. Acoust. Soc. Am.*, **66**:1487, 1979.

[Stringer91] W. J. Stringer and J. E. Groves. Location and areal extent of polynyas in the bering and chukchi seas. *Arctic*, 164–171, 1991.

[Stroeve07] J. Stroeve, M. M. Holland, W. Meier, T. Scambos, and M. Serreze. Arctic sea ice decline: Faster than forecast. *Geophys. Res. Lett.*., **34**(9):L09501, 2007.

[Stroeve08] J. Stroeve, M. Serreze, S. Drobot, S. Gearheard, M. Holland *et al.* Arctic sea ice extent plummets in 2007. *Eos*, **89**(2):13–14, 2008.

[Stroeve12a] J. C. Stroeve and W. Meier. *Arctic Sea Ice decline, Greenhouse Gases–Emission, Measurement and Management*. InTech, 2012.

[Stroeve12b] J. C. Stroeve, M. C. Serreze, M. M. Holland, J. E. Kay, J. Malanik *et al.* The Arctic's rapidly shrinking sea ice cover: a research synthesis. *Climatic Change*, **110**(3-4):1005–1027, 2012.

[Tasker10] M. L. Tasker, M. Amundin, M. Andre, A. Hawkins, W. Lang *et al. Marine Strategy Framework Directive Task Group 11 Report Underwater noise and other forms of Marine*. Tech. rep., International Council for the Exploration of the Sea, 2010.

[Tervo11] O. M. Tervo, M. F. Christoffersen, S. E. Parks, R. M. Kristensen, and P. T. Madsen. Evidence for simultaneous sound production in the bowhead whale (balaena mysticetus). *J. Acoust. Soc. Am.*, **130(4)**:2257–2262, 2011.

[Thode00] A. M. Thode, G. D'Spain, and W. Kuperman. Matched–field processing, geoacoustic inversion, and source signature recovery of blue whale vocalizations. *J. Acoust. Soc. Am.*, **107**:1286–1300, 2000.

[Thomas10] D. N. Thomas and G. S. Dieckmann. *Sea ice (Second Edition)*. Wiley–Blackwell (A John Wiley & Sons, Ltd, Publication), 2010.

[Thorndike82] A. S. Thorndike and R. Colony. Sea ice motion in response to geostrophic winds. *J. Geophys. Res.*, **87**(C8):5845–5852, 1982.

[Thorndike86] A. S. Thorndike. Kinematics of sea ice. *The geophysics of sea ice*, **146**:489–549, 1986.

[Trevorrow08] M. V. Trevorrow, B. Vasiliev, and S. Vagle. Directionality and maneuvering effects on a surface ship underwater acoustic signature. *J. Acoust. Soc. Am.*, **124**(2):767–778, 2008.

[Tsukernik10] M. Tsukernik, C. Deser, M. Alexander, and R. Tomas. Atmospheric forcing of Fram Strait sea ice export: a closer look. *Clim. Dyn.*, **35**(7):1349–1360, 2010.

[Tyack08] P. L. Tyack. Implications for marine mammals of large-scale changes in the marine acoustic environment. *Journal of Mammalogy*, **89**(3):549–558, 2008.

[Urick71] R. Urick. The noise of melting icebergs. *J. Acoust. Soc. Am.*, **50**:337–341, 1971.

[Urick83] R. Urick. *Principles of underwater sound 3rd edition*. Peninsula Publising Los Atlos, California, 1983.

[Urick84] R. Urick. *Ambient noise in the sea*. Tech. rep., DTIC Document, 1984.

[Uscinski99] B. J. Uscinski and P. Wadhams. Ice-ocean acoustic energy transfer:: ambient noise in the ice-edge region. *Deep Sea Research Part II: Topical Studies in Oceanography*, **46**(6-7):1319–1333, 1999.

[Vallez08] S. Vallez, , C. Gervaise, A. Khenchaf, Y. Stéphan *et al.* Inversion géoacoustique d'un canal très petits fonds à partir des navires en mouvement

Traitement incohérent= Passive geoacoustic inversion of very shallow water environment with ship's noise: incoherent processing. *TS. Traitement du signal*, **25**(1-2):151–163, 2008.

[Vallez09] S. Vallez. *inversion géoacoustique passive à partir des bruits rayonnés par les navires*. Ph.D. thesis, Ecole Doctorale SICMA - ED373 Université de Bretagne Occidentale, 2009.

[Veitch85] J. G. Veitch and A. R. Wilks. A characterization of arctic undersea noise. *J. Acoust. Soc. Am.*, **77**:989–999, 1985.

[Vellinga02] M. Vellinga and R. A. Wood. Global climatic impacts of a collapse of the atlantic thermohaline circulation. *Climatic change*, **54**(3):251–267, 2002.

[Vincent12] W. F. Vincent, I. Laurion, R. Pienitz, K. M. W. Anthony, and M. Katey. Climate impacts on arctic lake ecosystems. *Climatic Change and Global Warming of Inland Waters: Impacts and Mitigation for Ecosystems and Societies.*, 27–42, 2012.

[Wadhams12] P. Wadhams. Arctic ice cover, ice thickness and tipping points. *AMBIO: A Journal of the Human Environment*, 1–11, 2012.

[Wagstaff73] R. A. Wagstaff. *RANDI: Research ambient noise directionality model*. Tech. rep., DTIC Document, 1973.

[Wales02] S. C. Wales and R. M. Heitmeyer. An ensemble source spectra model for merchant ship-radiated noise. *J. Acoust. Soc. Am.*, **111**(3):1211–1231, 2002.

[Walther02] G.-R. Walther, E. Post, P. Convey, A. Menzel, C. Parmesan *et al.* Ecological responses to recent climate change. *Nature*, **416**(6879):389–395, 2002.

[Wang12] M. Wang and J. E. Overland. A sea ice free summer arctic within 30 years: An update from cmip5 models. *Geophys. Res. Lett.*., **39**(18):L18501, 2012.

[Weiss04] J. Weiss and D. Marsan. Scale properties of sea ice deformation and fracturing. *Comptes Rendus Physique*, **5**(7):735–751, 2004.

[Weiss09a] J. Weiss, D. Marsan, and P. Rampal. Space and time scaling laws induced by the multiscale fracturing of the arctic sea ice cover. *In IUTAM Symposium on Scaling in Solid Mechanics*, 101–109. Springer, 2009.

[Weiss09b] J. Weiss, P. Rampal, and D. Marsan. Acceleration of Arctic sea ice drift and deformation over the last 30 years. *In IOP Conference Series: Earth and Environmental Science*, vol. 6, 012017. IOP Publishing, 2009.

[Wenz62] G. M. Wenz. Acoustic ambient noise in the ocean: Spectra and sources. *J. Acoust. Soc. Am.*, **34**(12):1936–1956, 1962.

[Westwood96] E. K. Westwood, C. Tindle, and N. Chapman. A normal mode model for acousto-elastic ocean environments. *J. Acoust. Soc. Am.*, **100**:3631–3645, 1996.

[Wrona06] F. J. Wrona, T. D. Prowse, J. D. Reist, J. E. Hobbie, L. M. Lévesque *et al.* Climate change effects on aquatic biota, ecosystem structure and function. *AMBIO: A Journal of the Human Environment*, **35**(7):359–369, 2006.

[Xie91] Y. Xie and D. Farmer. Acoustical radiation from thermally stressed sea ice. *J. Acoust. Soc. Am.*, **89**(5):2215–2231, 1991.

[Xie92] Y. Xie and D. Farmer. The sound of ice break up and floe interaction. *J. Acoust. Soc. Am.*, **91**(3):1423–1428, 1992.

[Xie95] Y. Xie and D. M. Farmer. The influence of pressure ridges on seismic signals due to thermal cracking of sea ice. *J. Acoust. Soc. Am.*, **97**:962–970, 1995.

[Ye95] Z. Ye. Sound generation by ice floe rubbing. *J. Acous. Soc. Am.*, **97**:2191–2198, 1995.

[Zakarauskas91] P. Zakarauskas, C. Parfitt, and J. Thorleifson. Automatic extraction of spring time Arctic ambient noise transients. *J. Acoust. Soc. Am.*, **90**:470–474, 1991.

[Zakarauskas93] P. Zakarauskas. Detection and Localization of Nondeterministic Transients in Time Series and Application to Ice-Cracking Sound. *Digital Signal Processing*, **3**(1):36–45, 1993.

[Zhang03] X. Zhang, M. Ikeda, and J. E. Walsh. Coordinated changes of sea ice over the beaufort and chukchi seas: regional and seasonal perspectives. *Polar research*, **22**(1):83–90, 2003.

[Zhang13] J. Zhang, R. Lindsay, A. Schweiger, and M. Steele. The impact of an intense summer cyclone on 2012 arctic sea ice retreat. *Geophys. Res. Lett.*., **40**:720–726, 2013.

Abstract — The Arctic sea ice melting, in the global warming context, has become a major scientific topic during the last 30 years. The Arctic Ocean plays a fundamental role in the global climate balance and requires a particular attention. The Arctic Regions are then monitored by satellite observations and *in-situ* measurements. The climatic impact of the total melting of the Arctic sea ice is not yet understood and researches are still needed for long term monitoring of Arctic Ocean, particularly the dynamics of the ice cover and its consequences on the ecosystems.

The loss of Arctic sea ice will gradually accompanied by the installation of seasonal or perennial industrial activities. As consequences, it will result a modification in the underwater soundscapes in these regions devoid of anthropogenic sound sources. The present study, focused on the Canadian Arctic and subarctic seas natural soundscapes, falls within this context through two research axes.

The first part of the present study concerns the direct consequences of the melting of sea ice on Polar Regions soundscapes. We then examined the background noise, its seasonal variations and its environmental drivers. A dedicated algorithm to estimate this ocean noise component has been developed for this purpose, in order to constitute time series from long term acoustic measurements. Through statistical analysis, we determined that the environmental variables responsible for generating the background noise depends upon the state of the ocean surface and that during the winter period, the background noise is controlled by the same environmental variables driving the large-scale Arctic Ocean circulation.

The second part of our work is to evaluate the potential of passive acoustics as a complementary means of monitoring the spatial and temporal dynamics of Arctic sea ice. To do this, we identified acoustic events related to the physical phenomena under the ice cover to improve our understanding of their generating mechanisms. We were able to bind various acoustic transients to some deformation processes of the moving ice cover.

Keywords: Arctic remote sensing, Arctic sea ice, Arctic soundscape, noise estimation, transient detection.

Résumé — La fonte rapide des glaces de l'Arctique dans le contexte actuel du réchauffement climatique est un sujet scientifique majeur de ces 30 dernières années. L'Arctique joue un rôle fondamental dans l'équilibre du climat et requiert une attention particulière. Les régions arctiques sont alors surveillées par des observations satellitaires et des mesures *in-situ*. L'impact climatique de la fonte totale de la glace arctique est encore mal connu. Des recherches sont donc nécessaires pour le suivi à long terme de l'Océan Arctique, en particulier la dynamique spatio-temporelle de la couverture de glace et ses conséquences sur les écosystèmes.

La disparition de la banquise en Arctique sera progressivement accompagnée de l'installation d'activités industrielles saisonnières ou pérennes. Ceci a pour conséquences une modification des paysages acoustiques sous-marins de ces environnements jusqu'alors préservés des sources sonores anthropiques. La présente étude, portée sur les paysages acoustiques sous-marins des régions océaniques polaires du Canada, s'inscrit dans ce contexte sous deux axes.

Le premier axe de notre étude concerne donc les conséquences directes de la disparition de la glace sur les paysages acoustiques sous-marins de l'Arctique et des mers subarctiques du Canada. Nous avons alors examiné le bruit ambiant, ses variations saisonnières ainsi ses pilotes environnementaux. Un algorithme dédié à l'estimation de cette composante du bruit océanique a été développé à cet effet, afin de constituer des séries temporelles longue durée. A travers des analyses statistiques, nous avons établi que les variables environnementaux responsables de la production du bruit de fond dépendent de l'état de la surface océanique et que pendant la période hivernale, ce bruit est piloté par les mêmes variables environnementales qui gouvernent la circulation océanique à grande échelle de l'Arctique.

Le second axe abordé au cours de ce travail de thèse vise à évaluer le potentiel de l'acoustique passive comme moyen de monitorage de la dynamique spatio-temporelle de la banquise. Pour ce faire, nous avons identifié des événements acoustiques signant de phénomènes physiques sous la glace afin d'améliorer la compréhension de leur mécanisme de production. Nous avons ainsi pu lier divers transitoires acoustiques à des processus de déformation de la banquise.

Mots clés: monitoring de l'Arctique, glace de mer, paysage sonore de l'Arctique, bruit ambiant, détection de transitoires.

Laboratoire Grenoble Image Parole Signal et Automatique
11 rue des Mathématiques, Domaine universitaire, BP46
38402 SAINT MARTIN D'HERES Cedex, France.